

8-2013

# Experimental and Analytical Investigation of the Transient Thermal Response of Air Cooled Data Centers

Hamza Salih Erden

Follow this and additional works at: <http://surface.syr.edu/etd>

 Part of the [Mechanical Engineering Commons](#)

---

## Recommended Citation

Erden, Hamza Salih, "Experimental and Analytical Investigation of the Transient Thermal Response of Air Cooled Data Centers" (2013). *Dissertations - ALL*. Paper 43.

This Dissertation is brought to you for free and open access by the SURFACE at SURFACE. It has been accepted for inclusion in Dissertations - ALL by an authorized administrator of SURFACE. For more information, please contact [surface@syr.edu](mailto:surface@syr.edu).

## Abstract

This work investigates the transient response of the thermal environment in air cooled data centers through experiments, analytical and computational tools. The key thermal characteristics of the various data center components were extracted from a set of experiments. This includes the development of practical experimental procedures for the thermal characterization of servers solely based on air temperature measurements and the transient response of the computer room air handlers. The knowledge of thermal characteristics paves the way for the physics-based lumped-capacitance models. A CFD-based transient simulation of the air temperature field, in which the transient thermal response of the servers was included via user-defined functions failed to predict the time-dependent server inlet temperature with acceptable accuracy and highlighted the need for including the thermal capacitance and heat transfer characteristics of the entire room, not just the servers. Hence, a practical faster-executing hybrid lumped capacitance-CFD/Experimental model was developed to investigate the thermal response of data centers under certain scenarios of cooling interruption, server shutdown and cooling air flow changes. Beyond the servers, the model takes into account the effect of the air volume, the building materials of the room and plenum and the CRAH units. The model is capable of predicting server inlet temperatures to within the experimental uncertainty ( $\pm 1^\circ\text{C}$ ) with inputs that are relatively easy to obtain in a production data center.

Experimental and Analytical Investigation of the Transient  
Thermal Response of Air Cooled Data Centers

By

Hamza Salih Erden

B.S. Istanbul Technical University, 2007

M.S. Syracuse University, 2009

Dissertation

Submitted in partial fulfillment of the requirements for the degree of Doctor of  
Philosophy in Mechanical and Aerospace Engineering

Syracuse University  
Syracuse, NY, U.S.A.

August 2013

Copyright © Hamza Salih Erden, 2013  
All Rights Reserved

## Acknowledgements

This dissertation is dedicated to my parents, Saban Erden and Sevincan Erden. Especially the emotional support of my family including my brothers Ibrahim and Fatih were indispensable for the continuation of my studies.

I would like to thank my advisor Dr. Khalifa for his guidance throughout my studies in Syracuse.

It has been a privilege for me to work under his supervision. My involvement in his research group not only helped me to fund my studies but also gain experience through a variety of research projects and meet many bright students and professors from different backgrounds.

Saying that, I would like to address my special thanks to my committee members Drs. Dang, Işık and Dannenhoffer for their feedback and suggestions throughout my time at Syracuse University.

I would like to thank Dr. Bogucz for his support in my research through Center of Excellence and for being part of my committee. Finally, I am thankful for the continuous support and encouragement I have received from Drs. Roger Schmidt and Madhusudan Iyengar of IBM.

The experimental part of this study requires a significant collaboration from other students. The help I have received from my current and former colleagues at Syracuse University, namely Waleed Abdelmaksoud, Dustin Demetriou, James Smith, Dan Rice, Brian Granetz, John Banas, Dale Ringham, Kevin Noble, Hua Deng, John Kotlarz and many others cannot be overlooked.

At the personal level I would like to devote special thanks to my roommates I have had over years in Syracuse; Kilic Kanat, Ilteris Sarigecili and Ozcan Yazici; and other friends Hakki Gurhan, Ramazan Cetin, Hacı Karatas, Onur Kok, Adem Bahar, Tahir Coskun and Fatih Kaburcuk, Mehmet Kaya, Mirza Tihic, Fethi Keles, Murat Baysal, Gulmammad Mammadov and members of campus community for creating the friendly environment.

# Table of Contents

<b>Acknowledgements .....</b>	<b>iv</b>
<b>Table of Contents .....</b>	<b>v</b>
<b>List of Figures.....</b>	<b>viii</b>
<b>List of Tables .....</b>	<b>xii</b>
<b>Nomenclature .....</b>	<b>xiii</b>
<b>1 Introduction .....</b>	<b>1</b>
1.1 Literature Review.....	3
1.1.1 Experimental Investigation of Data Center Dynamics.....	4
1.1.2 Reduced-Order Modeling .....	7
1.1.3 Transient CFD Modeling of Data Centers .....	12
1.1.4 Rack Modeling .....	13
1.1.5 Plenum and Tile Modeling.....	14
1.2 Research Gaps in Transient Behavior of Data Centers .....	16
1.3 Study Objectives .....	18
1.4 Thesis Organization .....	19
<b>2 Description of Experimental Facility.....</b>	<b>21</b>
2.1 Plenum .....	23
2.2 CRAH Units.....	23
2.3 Perforated Tiles .....	25
2.4 Exposed Surface Materials.....	26
2.5 Racks.....	27
2.6 Simulated Servers .....	28
2.6.1 Simulated Server Temperature Prediction .....	33
2.7 Experimental Setup and Measurement Points.....	36
<b>3 Transient Experiments.....</b>	<b>39</b>
3.1 Experiment 1: Rack Shutdown .....	43
3.2 Experiment 2: Chilled Water Interruption .....	46
3.3 Experiment 3: Sudden Change in CRAH Air Flow Rate.....	51
3.4 Experiment 4a-b-c: Server Power and CRAH Air Flow Rate Variation .....	55
3.5 Experiment 5a-b: CRAH switching Experiments .....	58

3.6	Experiment 6: CRAH Fan Failure Experiment .....	63
3.7	Uncertainty Analysis for Server Inlet Air Temperature Measurements .....	64
<b>4</b>	<b>Thermal Characterization and Modeling of Servers for Transient Simulations .....</b>	<b>68</b>
4.1	Transient Modeling of Servers.....	68
4.2	Simple Characterization of Transient Behavior of Servers.....	69
4.3	Time Constants of Simulated Servers .....	73
4.4	Thermal Conductance and Capacitance of Simulated Servers.....	76
4.5	Chapter Conclusions .....	78
<b>5</b>	<b>Room-Level Transient CFD Simulations .....</b>	<b>79</b>
5.1	Numerical Modeling Overview .....	79
5.2	Rack Shutdown Experiment for the Verification of Proposed User-Defined Function in CFD .....	83
5.3	User-Defined Function (UDF) for Transient Server Exit Air Temperature.....	87
5.4	Verification of Transient Server Boundary Conditions through CFD Results of Rack-Shutdown Experiment.....	89
5.5	Chapter Conclusions .....	95
<b>6</b>	<b>Hybrid Lumped Capacitance –CFD/EXPERIMENTAL Model .....</b>	<b>96</b>
6.1	Mathematical Model .....	99
6.2	Distribution of Thermal Mass in the Air Cooled Data Centers.....	105
6.2.1	Room Air Thermal Capacity .....	105
6.2.2	Servers.....	107
6.2.3	CRAH Units.....	107
6.2.4	Recirculation Paths .....	109
6.2.5	Plenum .....	114
6.2.6	Discussion on the Validity of Lumped Capacitance Approach .....	115
6.3	Verification of the Model Through Research Lab Experiments .....	116
6.3.1	Room Capacitance for a Single Recirculation Path .....	119
6.3.2	Multiple Paths and Transition to Real Data Centers .....	126
6.4	Large Scale Data Center Simulation .....	129
6.5	Chapter Conclusions .....	134
<b>7</b>	<b>Summary and Conclusions .....</b>	<b>136</b>
7.1	Future Work.....	138
<b>Appendix-A: Transient Experiment of IBM Blade Center.....</b>		<b>140</b>

<b>Appendix-B: UDF Source Code for Rack Shutdown Experiment .....</b>	<b>150</b>
<b>Appendix-C: Sample Journal File for UDF Setup in FLUENT .....</b>	<b>167</b>
<b>Appendix-D: MATLAB Codes for the Hybrid-Lumped Capacitance Model (Model vs. Research Lab experiments).....</b>	<b>168</b>
<b>Appendix-E: MATLAB Codes for the Hybrid-Lumped Capacitance Model (CRAH Fan Failure and CW Interruption Tests in Quadrant Data Center).....</b>	<b>186</b>
<b>Appendix-F: Method of Determining Recirculation Path Thermal Characteristics for Multiple Paths .....</b>	<b>197</b>
<b>Appendix-G: Conjugate Heat Transfer Model of the CRAH Heat Exchanger .....</b>	<b>199</b>
<b>Appendix-H: CFD as an Alternative to Conduit Approach for Room Thermal Characterization .....</b>	<b>204</b>
<b>Appendix-I: Transient Experimental Data .....</b>	<b>211</b>
<b>References .....</b>	<b>216</b>



# List of Figures

Figure 1.1: Recommended and allowable environmental conditions for electronic equipment (ASHRAE, 2012) ..... 2

Figure 2.1: RL top view (dimensions in inches) ..... 22

Figure 2.2: RL side view (dimensions in inches)..... 22

Figure 2.3: CRAH blower characteristic curve; 2400 to 3800 CFM per blower flow-rate range, or 4800 to 7600 CFM per CRAH. .... 24

Figure 2.4: Perforated tile used in the RL. .... 25

Figure 2.5: Perforated tile flow characteristic curve (Tate Access Floors, Inc.)..... 26

Figure 2.6: Rack populated with four simulated chassis (rack covers removed). (b) Schematic representation of the simulated rack front or rear doors (dimensions in inches). .... 28

Figure 2.7: Flow characteristics of a real IBM blade chassis (Total Sys: system & 2 (rack) doors). .... 29

Figure 2.8: Chassis layout: (a) Drawing (dimensions in inch); (b) Photograph from the top (cover removed). .... 31

Figure 2.9: Standalone carbon steel plate with a heater pad attached to it. .... 31

Figure 2.10: Transient temperature data obtained from the IBM Blade Center experiment (Appendix A)32

Figure 2.11: Temperature prediction along the plate in the flow direction at different heater power levels. .... 34

Figure 2.12: Predicted maximum plate temperature vs. measurements..... 35

Figure 2.13: Locations of transient air temperature measurements around the rack. .... 36

Figure 3.1: Backflow velocity measurements on top of CRAH-2. .... 42

Figure 3.2: Backflow measurements on top of CRAH-2 via TSI Flow Hood. .... 42

Figure 3.3: Flow Circuit Models for cases in which CRAH-2 is (a) sealed and (b) unsealed. .... 43

Figure 3.4: Transient server air temperature difference during rack shutdown experiment. .... 44

Figure 3.5: Natural logarithm of normalized temperature difference to estimate server time constants. ... 45

Figure 3.6: Temperature variations during chilled water interruption. .... 47

Figure 3.7: Temperature differences of air and chilled water across the CRAH unit. .... 49

Figure 3.8: Temperature variation of server inlet air temperature during chilled water interruption. .... 50

Figure 3.9: Variation of server air temperature difference during chilled water interruption.....	51
Figure 3.10: Timeline of air flow (CFM) changes during for experiment 3.....	52
Figure 3.11: Server inlet temperature and tile temperatures during variation of CRAH air flow rate.....	53
Figure 3.12: Variation of server air temperature difference in response to changing inlet air temperatures. .....	54
Figure 3.13: Timeline of events for CRAH flow (CFM) and server power (kW) changes for experiments 4 (a), (b) and (c). .....	55
Figure 3.14: Server inlet temperature and tile temperatures during experiment 4a. ....	56
Figure 3.15: Server inlet temperature and tile temperatures during experiment 4b.....	57
Figure 3.16: Server inlet temperature and tile temperatures during experiment 4c. ....	58
Figure 3.17: Timeline of events for experiment 5a.....	59
Figure 3.18: Variation of server inlet temperature for a) Rack 1, b) Rack 2 and c) Rack 3. ....	60
Figure 3.19: Timeline of events for experiment 5b.....	61
Figure 3.20: Variation of server inlet temperature for a) Rack 1, b) Rack 2 and c) Rack 3. ....	62
Figure 3.21: Server inlet temperatures for the selection of 4 servers during CRAH fan failure experiment .....	64
Figure 4.1: Simplified schematics of a transient server model. ....	68
Figure 4.2: Sample solution of transient energy balance for sudden decrease in server inlet temperature. ....	72
Figure 4.3: Natural logarithm of normalized temperature difference to estimate server time constants. ...	74
Figure 4.4: Estimated server time constants as a function of server air mass flow rate.....	75
Figure 4.5: Server exit air temperature computed based on lumped capacitance model vs. experimental data.....	76
Figure 4.6: Variation of server air temperature difference in response to changing inlet air temperatures (due to sudden increase in the CRAH air flow rate at t=300s). ....	77
Figure 5.1: $T_{inlet}-T_{tile}$ (a) Experiment; (b) Short Turbulent Length Scale (Abdelmaksoud, 2012); (c) Long Turbulent Length Scale.....	83
Figure 5.2: The 3-rack RL data center model geometry (Red: Operating CRAH, Blue: Open Tiles).....	86
Figure 5.3: Comparison of server inlet air temperature: CFD vs. experiment. a) 4 racks b) Rack1 c) Rack2 d) Rack3 .....	91

Figure 5.4: Comparison of server air temperature difference: CFD vs. experiment. a) 4 racks b) Rack1 c) Rack2 d) Rack3 .....	92
Figure 5.5: Comparison of server exit air temperature: transient CFD vs. experiment. a) 4 racks b) Rack1 c) Rack2 d) Rack3.....	93
Figure 5.6: Comparison of server inlet air temperature: Adjusted CFD vs. experiment. a) 4 racks b) Rack1 c) Rack2 d) Rack3.....	94
Figure 6.1: Simplified Hybrid-Lumped Capacitance Data Center Model .....	97
Figure 6.2: Distribution of Room Air Capacity in RL .....	106
Figure 6.3: Recirculation Flow Path Dimensions .....	110
Figure 6.4: Exposed Room Surface Covered by the Hypothetical Conduit of Recirculation Flow .....	112
Figure 6.5: Comparison of server inlet air temperature for rack shutdown experiment without room and plenum thermal masses: Model vs. experiment. a) 4 racks b) Rack1 c) Rack2 d) Rack3 .....	117
Figure 6.6: Comparison of server inlet air temperature for Chilled Water Interruption Experiment without room and plenum thermal masses: Model vs. experiment. a) 4 racks b) Rack1 c) Rack2 d) Rack3 .....	118
Figure 6.7: Comparison of server inlet air temperature for CRAH Fan Failure Experiment without room and plenum thermal masses: Model vs. experiment. a) 4 racks b) Rack1 c) Rack2 d) Rack3.....	119
Figure 6.8: Comparison of server inlet air temperature for Rack Shutdown Experiment with single path for the recirculated flow: Model vs. experiment. a) 4 racks b) Rack1 c) Rack2 d) Rack3 .....	121
Figure 6.9: Comparison of server inlet air temperature for CRAH Chilled Water Interruption Experiment with single path for the recirculated flow: Model vs. experiment. a) 4 racks b) Rack1 c) Rack2 d) Rack3 .....	122
Figure 6.10: Comparison of server inlet air temperature for CRAH Fan Failure Experiment with single path for the recirculated flow: Model vs. experiment. a) 4 racks b) Rack1 c) Rack2 d) Rack3 .....	123
Figure 6.11: Comparison of server inlet air temperature for Decreased CRAH Air Flow Rate Experiment with single path for the recirculated flow: Model vs. experiment. a) 4 racks b) Rack1 c) Rack2 d) Rack3 .....	124
Figure 6.12: Comparison of server inlet air temperature for Increased CRAH Air Flow Rate Experiment with single path for the recirculated flow: Model vs. experiment. a) 4 racks b) Rack1 c) Rack2 d) Rack3 .....	125
Figure 6.13: Comparison of server inlet air temperature for Rack Shutdown Experiment with 2 Paths (R2C4 separated) for the recirculated flow: Model vs. experiment. a) 4 racks b) Rack1 c) Rack2 d) Rack3 .....	127
Figure 6.14: Effect of surface area per rack on the model results (Rack2).....	129

Figure 6.15: Quadrant Data Center .....	130
Figure 6.16: Hybrid-Lumped Capacitance Model results for Chilled Water Interruption with shorter time constants Case a) Rack1 b) Rack3 c) Rack5 d) Rack6 e)Rack8 f)Rack10 .....	132
Figure 6.17: Hybrid-Lumped Capacitance Model results for CRAH Fan Failure with shorter time constants Case a) Rack1 b) Rack3 c) Rack5 d) Rack6 e)Rack8 f)Rack10 .....	133
Figure H.1: Comparison of server inlet air temperature for Rack Shutdown Experiment with single path for the recirculated flow and UA obtained from CFD: Model vs. experiment. a) 4 racks b) Rack1 c) Rack2 d) Rack3 .....	206

# List of Tables

Table 2-1: Summary of material properties for surfaces ..... 27

Table 3-1: CRAH Back Flow Estimates. .... 43

Table 3-2: Heating Loads and Air Flow Rates for Simulated Servers..... 45

Table 3-3: Random error of average inlet temperatures (°C) over 300 seconds of steady state operation. 66

Table 3-4: Total uncertainty of average inlet temperature over 300 seconds of steady state operation at 1 Hz..... 67

Table 5-1:Heating Loads and Air Flow Rates for Simulated Servers..... 84

Table 5-2: Extracted time constants of simulated servers and thermal capacitance assumption based on material properties ..... 85

Table 5-3: Summary of CFD model specifications and boundary conditions ..... 86

Table 5-4: Measured air flow rates through perforated tiles..... 87

Table 5-5: Temperature boundary conditions for the open perforated tiles..... 87

Table 6-1: Summary of CRAH Flow, Server Power, Room and Plenum Thermal Properties for Cases . 120

Table 6-2: Comparison of the data center room surface area per rack (RL vs. Production Data Centers)128

## Nomenclature

$Ar$	Archimedes Number (-)
$a$	area per rack ( $\text{m}^2/\text{rack}$ )
$A$	area ( $\text{m}^2$ ); inertial resistance coefficient ( $\text{Pa}\cdot\text{s}^2/\text{m}^2$ )
ACH	air changes per hour (1/h)
$b$	bias error; conduit size (m)
$B$	viscous resistance coefficient ( $\text{Pa}\cdot\text{s}/\text{m}$ )
$Bi$	Biot Number
BMS	building management system
$\dot{C}$	flow heat capacity ( $\text{kW}/\text{K}$ )
$C$	thermal capacitance ( $\text{kJ}/\text{K}$ ), chassis/server
CFD	computational fluid dynamics
CFM	cubic feet per minute
CHW	chilled water
CPU	central processing unit
CRAC	computer room air conditioner
CRAH	computer room air handler

$d$	thermal diffusion length (m)
$D$	hydraulic diameter (m)
DBN	dynamic Bayesian networks
E	energy
$f$	friction factor (-)
$Fo$	Fourier Number
$h$	convective heat transfer coefficient (W/m <sup>2</sup> K); enthalpy (J)
HDD	hard disk drive
$I$	turbulence intensity (%); current (Amps)
IBM	International Business Machines
IT	information technology
$k$	thermal conductivity (W/mK); turbulence kinetic energy (m <sup>2</sup> /s <sup>2</sup> )
$K$	overall thermal conductance (kW/K)
$L$	length (m)
MS	momentum source
MSE	mean square error
$\dot{m}$	mass flow rate (kg/s)

$NTU$	number of transfer units (-)
$Nu$	Nusselt Number (-)
$P$	power (kW)
$p$	pressure (Pa); precision error
PDU	power distribution unit
POD	proper orthogonal decomposition
$Pr$	Prandtl Number (-)
PRESTO	pressure interpolation technique
$\dot{Q}$	heat rate (kW)
R	server rack
$R$	Thermal Resistance ( $m^2K/W$ )
$R^2$	coefficient of determination (-)
$Re$	Reynolds Number (-)
RANS	Reynolds Averaged Navier Stokes
RC	resistor-capacitor
RL	Research Lab
RPM	rotation per minute



<i>s</i>	seconds
SIMPLEC	pressure-velocity coupling technique
SUGDC	Syracuse University Green Data Center
<i>t</i>	time (s)
<i>T</i>	temperature (°C or °K)
<i>u</i>	uncertainty; velocity component (m/s)
<i>U</i>	tile velocity (m/s); rack unit (1U=1.75 in=44.45 mm)
<i>UA</i>	overall thermal conductance (kW/K)
UDF	user-defined function
UPS	uninterruptable power supply
<i>V</i>	velocity (m/s), voltage (V)
$\dot{V}$	volume flow rate (m <sup>3</sup> /s)
<i>W</i>	conduit width (m)
<i>x</i>	coordinate direction (m)

## Greek Symbols

$\Delta$	difference ( $^{\circ}\text{C}$ or $^{\circ}\text{K}$ )
$\delta$	change in difference ( $^{\circ}\text{C}$ or $^{\circ}\text{K}$ )
$\varepsilon$	turbulent dissipation ( $\text{m}^2/\text{s}^3$ ); effectiveness (-)
$\rho$	density ( $\text{kg}/\text{m}^3$ )
$\theta$	normalized temperature difference
$\sigma$	porosity (-); standard deviation
$\tau$	time constant (s)
$\lambda$	leakage (-)
$\gamma$	aspect ratio (-)
$\psi$	capture index (-)
$\beta$	thermal expansion coefficient ( $1/^{\circ}\text{K}$ )
$\varphi$	power factor (-)
$\alpha$	thermal diffusivity ( $\text{m}^2/\text{s}$ )
$\eta$	compressor duty cycle (%)
$\omega$	CRAC fan speed (rpm)
$\Theta$	$\dot{Q}_s / K - T_s + T_{a-in}$ , [ $^{\circ}\text{C}$ ]

## Subscripts

a	air
c	characteristic (length); crah flow
C	crah body
chw	chilled water
D	hydraulic diameter
en	enclosure
f	server flow area
fd	fully developed
h	hydraulic
hx	heat exchanger
in	inlet
k	server block
m	mixed air
out	exit; outlet
p	pipe (thermal resistance)
P	plenum body

R recirculation path body  
r recirculation path flow  
RL research lab  
s server  
t tile  
w water; water side (thermal resistance)

# 1 Introduction

Data centers are facilities housing computers and other electronic infrastructure for data processing, storage and communications, which are indispensable for business operations (EPA, 2007). As of 2010, data centers account for about 2% of the total electricity consumption in the United States (Kooimey, 2011). Rising power demand in data centers led the industry to seek more energy efficient solutions. In addition to continuously improving data center operations, state-of-the-art designs are also needed to meet the exponentially increasing demand of the IT industry (EPA, 2007). In addition to energy, reliable operation has always been a primary design criterion for data centers. Accordingly, to sustain reliable operation, guidelines for acceptable and recommended data center thermal environment have been developed by ASHRAE (2008a) (2012). Figure 1.1 presents the recommended and allowable psychrometric operating envelopes for server inlet conditions (ASHRAE, 2012). The recommended operating envelope restricts the server inlet temperature to 27°C for continuous operation, although higher inlet temperatures up to allowable limits for different classes of equipment (A1-4) can be tolerated for short durations. Classes A3 and A4 are two new classes of equipment added In addition to Classes A1 and A2

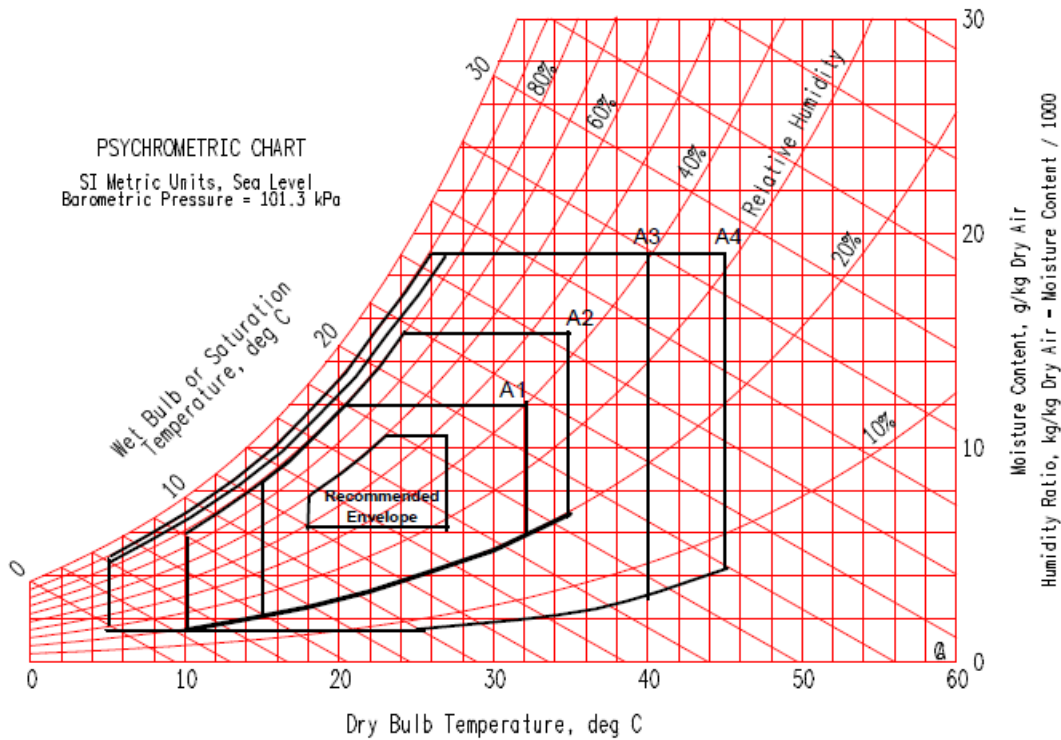


**Figure 1.1: Recommended and allowable environmental conditions for electronic equipment (ASHRAE, 2012)**

About half of the electricity used in data centers is consumed by the cooling infrastructure. Therefore, more efficient operation typically requires reduced cooling energy. Initial focus on data center research has been towards developing energy-efficient operating modes for data centers. Increasing power densities is the prevailing factor shaping the data center research since higher temperature operations become more and more common. As densely populated data centers emerge, concerns on reducing energy consumption, while maintaining the server inlet temperatures within acceptable limits under dynamically varying IT loads and coolant supply has sparked efforts on understanding the dynamic behavior of data centers.

Several transient events are anticipated in real data centers, which are primarily caused by variations in IT load, air flow rates and cooling capacity. These variations can arise from both

planned and unplanned events and may lead to the formation of undesirable hot spots. Planned events can be exemplified as routine maintenance of cooling infrastructure components and virtualization practices to relocate jobs within a data center space based on the spatial and temporal availability of cooling resources. On the other hand, interruptions in data center power supply or complete or partial failure of cooling infrastructure can have detrimental impact on the data center operations, businesses and physical hardware.

As previously introduced in Figure 1.1, tightly controlled thermal environmental conditions are recommended to sustain safe operation in data centers. Data center clients want to run data centers at higher temperatures, therefore closer to the allowable limits. However, limited transient information exists to know how close to the upper limit they can run. Due to the conservative nature of operations, testing thermal behavior of real data centers and real servers during various transient events is not feasible. Due to the restrictions on experimentation, modeling efforts have gained importance by constructing representative models that can simulate possible scenarios in data centers.

## *1.1 Literature Review*

The growing IT industry demands extensive research to improve efficiency and reliability of data center operations. There are many different approaches to address data center efficiency and reliability at various scales of data centers, from the facility to the chip level. Experimentation is usually not preferred in a real data center due to the risk for the business owner, especially in transient studies which may require testing failure scenarios. Hence, there is an extensive effort related to data center modeling, which can be classified as reduced-order and computational fluid dynamics (CFD) modeling.

### 1.1.1 Experimental Investigation of Data Center Dynamics

There are many control parameters in a data center applied to more efficiently allocate cooling resources. This led researchers to investigate the effects of changes in various parameters. As the Computer Room Air Handler (CRAH) units shifted from single speed to variable speed configurations, controls beyond server level became more viable. Variable Computer Room Air Conditioner (CRAC) supply temperature and flow rates, as well as variable opening perforated floor tiles allowed to study or develop control algorithms utilizing a stream of sensor data by Boucher et al. (2006) and Bash et al. (2006). Similarly, Chen et al. (2006a, 2006b) published two reports as a result of tests conducted in the same facility introduced by Boucher et al (2006). They statistically quantified correlation between vent opening and rack inlet temperature, which is then proposed as the basis for a local control algorithm (Boucher et al., 2006). Bash, Patel and Sharma (2006) tested a distributed sensor network to dynamically control CRAH units in an air-cooled data center and compared energy savings against the conventional data center control structure based on return air temperature into the CRAH units. Bautista and Sharma (2007) reported the influence of CRAH operation on rack inlet temperatures obtained by Principle Component Analysis which utilizes cross-correlation coefficients from a time series of sensor data. These statistical techniques are proposed as the basis for the real-time management of data centers. Amemiya et al. (2007) published time-dependent server inlet temperature data for servers of a single rack in a 1740 sq ft floor area data center. Accordingly, the results indicate that server inlet temperatures follow the disturbances in the CRAH exit temperature, which are claimed to be due to the changes in the outdoor conditions, chilled water flow rate and temperature (Amemiya et al., 2007). The data obtained in this study were applied as boundary conditions to steady state CFD models (Amemiya et al., 2007). In sum, early studies were



primarily quasi-steady analyses that were used either to find the optimum design for various operating conditions or develop sensor-based control methods with the understanding inferred from statistical investigations.

Shields (2009) conducted extensive testing aimed primarily at understanding the physics behind the transient behavior of data centers at higher levels and characterizing the thermal mass of data center components. The work can be divided into tests regarding server time constants, control volume experiments and CRAC heat exchanger responses to step change in chilled water flow. For the time constant experiments, the laboratory housing the test rack consisted of two volumes that are separated by a polyethylene sheet. While one side is cooled down to 12-15°C by a CRAC unit, the other side is heated so that it can provide an inlet temperature of 43-53°C within seconds. The sheet separating the zones allows movement of the rack between zones to mimic a scenario of sudden change at the inlet temperature. To estimate time constants, a 2U Intel server, a heating element and a legacy server at full load and idle speed are tested individually.

Accordingly, entirely different time constants were obtained (about 350 seconds for the legacy, 130 seconds for Intel and 50 seconds for the heating element). The author reported significant deviations from first order behavior, especially for the full load legacy server and Intel server due to the control algorithm that causes the server fans to ramp up after moving the rack onto the hot side. Putting aside the reliability of the time constant calculations in an uncontrolled environment, the results indicate the possible variability of thermal properties of available servers.

The second type of experiments conducted by Shields (2009) is control volume experiments where failure in CRAH fans, chilled water pumps and chillers are studied separately to develop a first order analytical model for the components of the control volume. Various thermal

capacitance values are obtained for the test bed, parametrically taking into consideration the air mass, servers, racks, body and chilled water of CRAC heat exchangers. The third experiment is to observe the transient response of the CRAC unit following a chilled water pump failure and restart. Accordingly, a time constant of 20 seconds is reported based both on chilled water and air temperature measurements.

Ghosh et al. (2011) studied air transients in a test cell of 57 m<sup>2</sup> floor area for a transient scenario of varying CRAC airflow rate. The temperature field is measured using a grid based thermocouple network, deployed in a 3-D telescopic mechanism (Nelson, 2007). For the high airflow case, the results point out the Venturi Effect at the server inlets closer to the floor, which causes hot air from the hot aisle to be entrained into the tile flow. As the CRAC air flow decreases this effect becomes less influential; instead, hot air recirculation on top of the rack is observed due to the loss of momentum in the tile flow.

Ibrahim et al. (2012) conducted tests on a server to obtain thermal mass information which is proposed to be used in CFD simulations. The study presents set of experiments to experimentally characterize the thermal mass of a 2U server. Assuming a typical range of specific heat capacity for the components inside the server, the contribution of each component is considered as the ratio of the component weight to the overall server weight. Based on the weight information and temperature measurements of each component inside the server (i.e. HDD, memory modules, power supply, CPU assembly, chassis) a unit temperature for the server can be obtained which is part of the time-dependent energy balance equation for the server. Putting aside the value of the extensive testing on the inner components of the server, this approach does not seem to be practical.

### 1.1.2 Reduced-Order Modeling

CFD is a widely used technique for modeling heat and air flow in data centers. However, the length scales in a small data center can range from tens of meters for outer walls to nanometers of transistors in chips. This corresponds to ten orders of magnitude difference in length scale, which makes it impossible to resolve each and every scale at the same time. Hence, researchers have proposed more practical models. The lower end of the scale tests were conducted at the server-level as a foundation for lumped parameter tools. For instance, the Mercury code is a simplified thermal model proposed by Heath et al. (2006) that simulates system and component temperatures in a single node or clustered systems based on simplified layouts of servers and components. Mercury is intended to serve as a thermal emergency management tool coupled with Freon, which is a system to manage component temperatures by a load balancer (Heath et al., 2006). The system execution option makes Mercury more suitable for real-time applications. However, the software requires heat flow, air flow, and hardware and utilization information along with the inlet air temperatures, fan speeds and maximum and minimum power consumption for each component (Heath et al., 2006). Sets of measurements and calibrations are required to obtain data, such as specific heat, heat transfer coefficient and air fractions within the server enclosure.

Although limited to server-level, Resistor-Capacitor (RC) thermal models were utilized by Ferreira et al. (2007) and Ayoub et al. (2010) to simulate the transient behavior of server components. Associated studies include failure scenarios investigated for a server farm to assess the temperature and load distributions as well as the quality of service (Ferreira et al., 2007). A proactive scheduling technique is proposed based on a thermal circuit model of memory modules to minimize energy consumption and react to possible performance overheads ahead of time

(Ayoub et al., 2010). Even though this approach is useful to identify hot spots inside a server, it needs to be incorporated into larger scale effects to draw more general conclusions about the transient behavior of data centers.

Another approach towards server-level modeling, optimization and control is introduced at HP Labs by Wang et al. (2009), Tolia et al. (2009) and Wang et al. (2010). The former paper is about predictive and optimal control of server fans by transient thermal modeling of HP blade servers. In conjunction with heat transfer theory and real measurements, correlation between temperatures, workloads and fan speeds were obtained. The correlated equations go through an optimization step to obtain a controller. This controller shifts the operating temperature towards the highest allowable temperature inside the server, which is 65°C in this case. In the latter publications, a model-based systems approach combines conventional server power optimization with fan power control to optimize overall energy efficiency.

The thermal models discussed so far investigate the physics of certain scales from the chip to the server-level. A significantly wider range of scales in this regard was introduced by Shah et al. (2010a-b), bridging the gap between the cooling infrastructure with the chip. The effects of changing the supply air temperature and temperature difference across the rack has been studied. In the second part, the paper extends the study to chip-level analysis and concludes that increasing the inlet air temperature is not always a very promising approach. In fact, increased fan power can hurt the overall efficiency. The results were based on simplifications such as constant and evenly distributed computing load and cooling with no recirculation. Even though multi-scale interactions are worth studying, these simplifications may have prevented learning more from this study. Additionally, transient modeling of such interactions can be part of future work.

More emphasis is given on virtualization and cost optimization in various studies. Le et al. (2010) published one of the few geographically distributed job placement studies considering energy and peak power costs and transient cooling. Dynamic Cost-Aware Distribution policies have been compared with baseline policies that are either static or do not consider the cost. Assuming that a 20-minute interval required for chiller start-up, various scenarios have been modeled using room-level CFD to develop rules for controlling large job migrations (Le et al., 2010).

Lee et al. proposed the proactive heat-imbalance based control approach against the conventional temperature-based reactive approach (2012). Reactive control is the typical approach in the thermal management of data centers. The proactive approach is intrinsically predictive in nature as it estimates the heat that will be generated in the future and adjusts the CRAC unit accordingly. The results underline the superiority of the proactive control method in terms of cooling energy, response time and equipment failure risk. The approach solves a nonlinear optimization problem controlling the CRAH fan speed,  $\omega$ , and the compressor duty cycle,  $\eta$ , based on estimated heat balance between the heat sources and sinks. The problem is solved every 50 s, which is the time window size of the air compressor duty cycle ( $T_{ON} + T_{OFF}$ ) to adjust  $\eta$  and  $\omega$ . It requires sensors at the inlet and outlet representing the temperature of the enclosure. No transient behavior is included in the CRAC model so that the supply air temperature is the return air temperature if the compressor duty cycle is off (Lee et al., 2012).

As large-scale models started to emerge, coupled management of IT workload and cooling became more important. Parolini et al. (2009) proposed a controller based on coupled thermal and computational networks, utilizing the theory of stochastic dynamic programming and, in particular, the theory of Markov Decision Process. The unified control proposed by Tolia et al.

(2009) is extended to the zone and data center levels utilizing the transient coupled thermal and computational modeling approach developed by Parolini et al. (2009) where they go beyond server-level thermal behavior. The connection between workload distribution and quality of service is handled in the computational network. In parallel, the thermal network models power consumption, heat production and the heat exchange of various thermal nodes representing CRACs, servers and the environment. The control objective is to maximize the quality of service and minimize the cost of operation utilizing changing electricity prices. The modeling and optimization is followed by the development of the controlling strategy.

As the utilization of embedded and stand-alone sensors became more common, statistical tools have been proposed to assess the correlations between various scales of data centers. Bautista and Sharma introduced a set of techniques for managing the data sets collected from data centers (2007). Temperature data sets collected from production data centers in HP Labs are used to give an insight into data mining techniques, statistical methods, exploratory data analysis techniques and principal components analysis (Bautista & Sharma, 2007). An application to a real data center in India has been introduced by Marwah et al. (2009) where chiller operation is modeled and optimized by a data mining approach. In a recent study, they assessed various statistical techniques to predict thermal anomalies so that preemptive steps can be taken to address them (Marwah et al., 2010). Of the four techniques used, Naïve Bayes performs best, with about 18% of the anomalies predicted at an average of 12 minutes before they occurred, although the false positive rate needs to be improved. In order to increase the number of anomalies predicted and reduce the false positive rate, in the future they plan to apply other machine learning techniques (e.g., dynamic Bayesian networks, or DBN). The follow-up paper to the chiller study provides an

application of DBN to extract the behavior and dependencies of a chiller system from raw sensor data (Marwah et al., 2010).

Non-CFD techniques are, as expected, computationally cheaper. They do not promise the accuracy of full scale CFD or CFD-based proper orthogonal decomposition (POD). Indeed, they are not intended to capture all the physics at the room-level; rather they rely on sensor data from key locations of the data center.

CFD-based POD is a method proposed for studying indoor airflows (Elhadidi & Khalifa, 2005). Rambo (2006) utilized the technique for compact modeling of electronics cooling. As a statistical tool, POD is used to obtain a subspace that captures the main characteristics of a data set. The flow and heat transfer equations are projected onto this subspace using various techniques (e.g., Least Squares, Collocation and Galerkin). While the Galerkin projection method is a traditional method, Rambo (2006) developed the Flux Matching Method which requires POD modes to satisfy the fluxes at the boundaries. The full CFD model neglects buoyancy effects and solves the steady incompressible Reynolds Averaged Navier Stokes (RANS) momentum and energy equations with no body forces, using second order upwinding and SIMPLEC pressure-velocity coupling with PRESTO pressure interpolation. Samadiani (2010) extended CFD-based POD studies to be multiscale, replicating room-level 3D models. Subsequently, an integrated method of POD, Galerkin projection and flux matching is presented to develop reduced order models of the temperature field in multi-scale convective systems. Compared to a full size CFD model, computational time reduced about 250 times while the results show 6% error in the temperature field (Samadiani, 2010). However, CFD-based POD techniques are thus far utilized as a steady state design and an optimization tool to determine the optimum workload distribution, the CRAC flow rate or the supply air temperature (Demetriou, 2012). Additionally, it is not a fair approach

to only compare the runtimes of CFD- based POD and CFD. Even for steady state simulations, the POD technique requires a significant number of runs of many different scenarios of interest to obtain a data set that can be used to generate new results by interpolation.

### 1.1.3 Transient CFD Modeling of Data Centers

Earlier parametric studies revealed thermal responses of servers and their effect to the surrounding environment based on changes in the server operation (Rambo and Joshi, 2003). In conjunction with this, server exhaust temperature-based workload distribution has been studied by Sharma et al. (2005) where transient thermal imbalances were investigated using a CFD model. Two cases mentioned (Sharma et al. 2005 & Bash et al. 2006) were earlier studies of room-level CFD simulations concerning CRAC failure scenarios. As sensor networks became a significant part of the data center infrastructure, the research was focused on the transient effects of each and every controllable variable in the data center infrastructure.

Large-scale CFD modeling tools are becoming more accurate in predicting steady state temperature fields inside data centers. Abdelmaksoud (2012) conducted a parametric study to draw conclusions about practical modeling techniques that can significantly decrease computational cost while keeping the accuracy within 1°C. High fidelity steady state models opened doors for more accurate transient simulations. Cooling failure in data centers (Bash et al., 2006; Marshall, 2010) and scenarios of varying heat and air flow have been studied recently (Ibrahim et al., 2010 and Gondipalli et al., 2010) through transient CFD simulations. However, absence of the thermal inertia of the computers leads to unrealistic results following sudden changes in the boundary conditions.



#### 1.1.4 Rack Modeling

Several studies proposed detailed modeling approaches at the rack level, which are limited at the rack level. Qihong (2008) integrated a thermal circuit-based Insulated Gate Bipolar Transistor module into a server enclosure many of which were intended to comprise a rack. Choi et al. (2007) used thermal properties of server component materials to construct a 3-D CFD-based thermal modeling tool, called Thermostat, for a 42U rack. The rack-level CFD-based simulator simulates fan failures and sudden inlet temperature changes to design dynamic thermal management techniques (2007). However, the tools do not go beyond being architectural tools to evaluate what-if scenarios within a rack due to the high simulation time.

A common practice in steady state modeling of racks in CFD is to use black box heat addition in models, which is proposed as a reasonable approach by Zhang et al. (2008). Utilizing blackbox heat addition models throughout his study, Abdelmaksoud (2012) also concluded that the details of racks, such as frames and rack door, are not as significant as accounting for the tile momentum.

To the best knowledge of the author, commercially available CFD packages do not offer a standard option in their heat addition models to account for the thermal mass of computing equipment. Khankari (2010) underlined the importance of thermal mass. Results of a simplified heat transfer model indicate that more than 90% of the heat is absorbed by the room air and rack enclosure during an event of cooling loss due to UPS failure, assuming that CRAH units are not on UPS. In his further study, practical recommendations, such as changing the ceiling height or the number of racks and rows are proposed as a means to manipulate the time constant of data centers (Khankari, 2011). In another study investigating the thermal inertia of data center structure and equipment, Shields (2009) conducted experiments in three steps: server time

constant experiments, control volume experiments and CRAC heat exchanger response to step change in chilled water.

At the end of his thesis, Shields (2009) proposed use of solid materials for modeling the server thermal mass in future CFD studies. Subsequently, Ibrahim et al. (2011) modeled servers as sets of plates that have a thermal capacitance comparable to real servers. However, this effort was steered towards modifying thermal boundary conditions of CFD tools to account for the thermal mass (Ibrahim et al., 2012). The same author conducted a set of experiments on a real server to extract thermal mass and conductance information which can be utilized in constructing physics-based transient thermal boundary conditions in CFD simulations (Ibrahim et al., 2012). For the experiments, a typical range of specific heat capacity for the components inside the server is assumed and the contribution of each component is computed as a function of their weight and temperatures. Knowing that the thermal mass obtained from this study is comparable to the previous one (2011), the author is hopeful to have the same thermal mass values for all servers. However, since it is required to open up servers and measure temperatures of each component, this approach appears to be of limited practical utility in transient simulations. A simpler and more practical method is needed to extract server thermal mass information.

### 1.1.5 Plenum and Tile Modeling

Pressurized under-floor plenums are common in air-cooled data centers. Cold air is supplied into the plenum and discharged via perforated tiles typically into the cold aisles. Many datacenter researchers have modeled the plenum (Schmidt et al. 2001, Schmidt et al. 2004 and Karki et al. 2003). These are considered quick prediction tools for tile flow rates which can also be used as boundary conditions for room-level CFD simulations. Abdelmaksoud (2012) bypassed plenum

modeling by specifying measured tile flow rates as tile boundary conditions. Studies about plenum modeling reported errors higher than 10 percent in predicting tile flow rates using CFD (Schmidt et al. 2001; Schmidt et al., 2004; VanGilder and Schmidt, 2005). Comparisons of CFD and measured data indicate significant flow non-uniformity through perforated tiles (Schmidt et al. 2004, VanGilder et al. 2005). They observed flow reversal in perforated tiles getting closest to the CRAC units. In order to account for flow transients due to the changes in CRAH airflow rate, Gondipalli et al. (2010) presented transient CFD results which include the modeling of a plenum. However, the flow non-uniformity has not been an issue to consider since the study was intended to show the trends rather than aiming for accuracy.

Best practices for data centers recommend the least possible obstruction in the plenum to reduce additional pressure rise across the CRAC fan units (ASHRAE 2008b, Bhopte et al. 2006, and VanGilder et al. 2005). The flow through the tile is driven by the pressure difference across the perforated tile. Considering that the pressure variations above the tile are not as significant as in the plenum, the tile flow rates are closely related to the pressure variations in the plenum. Even though more restrictive perforations increase the load on the CRAC fans, it is also desirable to decrease the pressure variations in the plenum which leads to lower non-uniformity of tile flow rates. Therefore, according to best practices, the major flow resistance is due to perforated tiles, aside from CRAH components, heat exchangers and filters.

Data center perforated tiles can have a range of 6 to 68% open area. The pressure drop due to the perforations can be modeled through a porous medium based on the relationship between the pressure drop and the flow velocity. Typically, this relationship is defined as  $\Delta p = AV^2 + BV$  which requires inertial ( $A$ ) and viscous ( $B$ ) resistance coefficients which can be obtained from experiments or manufacturer specification sheets (ANSYS Fluent, 2009).

Even though porous media can closely approximate the pressure drops across a tile, the use of porous medium has various deficiencies vis-à-vis momentum conservation and turbulence properties. The small openings of a tile behave like small individual jets at the floor-level. However, the assumption of a single large opening for a tile along with a porous medium neither provides the correct turbulence kinetic energy and dissipation nor accounts for the momentum of the jets issuing from the perforation. Since the modeling of a small opening is computationally expensive for a room-level simulation, Abdelmaksoud et al. (2010) proposed to add a volume force above the tile to compensate for the missing momentum. The CFD results showed significant improvement with the momentum body force.

Standard conservation equations are solved in a porous medium and specified tile porosity does not have any effect on the generation and dissipation rates of turbulence at the tile. However, this assumption may only be reasonable at very high porosities and turbulent eddy scales are not comparable to the tile size (Fluent, 2009). Abdelmaksoud (2012) recently conducted a parametric study about various boundary conditions for room-level data center simulations. He pointed out the sensitivity of the results to the tile turbulence boundary conditions.

## *1.2 Research Gaps in Transient Behavior of Data Centers*

Current CFD modeling tools, which are often used to study the thermal environment in data centers, are not supported with physics-based transient thermal boundary conditions. In the absence of these boundary conditions, CFD tools do not go beyond resolving air flow transients, missing significant impact of thermal masses on the thermal environment.

Computational integration of proper boundary conditions is not sufficient by itself unless proper techniques are available to measure thermal characteristics of computing equipment and other

thermal capacitances within the data center (e.g. walls, floor, PDUs, CRAHs, etc.). The thermal time-constants of the servers can be determined relatively easily through air temperature measurements based on the first-order system approximation. Since the time constant is a blend of two thermal characteristics, conductance and capacitance, at least one of these is required to construct an established physics-based server model. Current experimental techniques are not practical since they require surgery of servers to obtain thermal characteristics. Yet, one should be able to obtain the thermal characteristics of a server without the need to disassemble and weigh each and every component. Thermal characterization should be done via more feasible experiments.

Recent steady state CFD studies showed significant improvements in predicting inlet temperatures (Abdelmaksoud, 2012). However, the accuracy of transient CFD modeling is always limited by the accuracy of steady state predictions. On the other hand, faster transient tools also lack the accuracy of CFD tools due to low resolution of details at the room level (Khankari, 2010 & 2011). Considering the computational burden full scale data center CFD simulations bring about and the need to study the effects of room thermal masses with a reasonable resolution at the server inlets, computationally less expensive model based on practical rules needed to be developed.

In light of the above mentioned concerns, several areas can be listed that have not been covered in depth in the literature.

1. Current techniques for thermal characterization of servers require surgery of servers.

However, a practical experiment can be designed based on more accessible values of servers, such as air temperatures at the inlet and exit.

2. Even though examples of transient CFD simulations for data centers have been presented for about 10 years, the effect of the large thermal masses on the data center thermal environment has been overlooked and physics-based transient thermal boundary conditions for servers have never been implemented into room-level CFD simulations. In the absence of these boundary conditions CFD tools are not reliable in transient simulations.
3. The errors due to the lack of capturing the temperature field at the inlet of servers through steady state CFD simulations limit the accuracy of transient simulations along with the computational expense at full scale data center simulation. This indicates the lack of faster transient modeling tools that take thermal masses into account and promise as accurate results as those of CFD simulations.

The focus of this research is on developing practical tools capable of modeling the thermal transients driven by dynamic nature of data center operation. Specifically, the transient thermal characteristics of data centers are verified through experiments conducted in a small test cell. These characteristics comprise the parameter set required to develop adequate mathematical models. Modeling tools include transient CFD modeling at the room level with unsteady boundary conditions and faster analytical tools fed by initial conditions obtained from experiments or if available steady state CFD or real-time data.

### *1.3 Study Objectives*

The main objective of this work is to develop an experimentally validated, physics-based, practical model for predicting the time evolution of the data center thermal environment in response to load variation or equipment failure.

The specific objectives are as follows.

1. Perform transient experiments in a test cell to identify various components that significantly influence the thermal transient behavior in a typical data center and quantify the parameters that govern their time response through practical set of experiments.
2. Extract transient response parameters of key data center components from the experimental data.
3. Develop a practical, fast executing physics-based model that utilizes the component characteristics to predict data center transient thermal response and validate with the experimental data.
4. Apply the validated model to predict the transient thermal response of a typical cold aisle/hot aisle data center section.

#### *1.4 Thesis Organization*

The thesis is divided into seven chapters. Chapter 1 sets the stage for the objectives of this thesis and the work to be performed to address the gaps in previous work.

Chapter 2 gives a detailed description of the Research Lab (RL) and its features. This chapter additionally provides design information about the simulated servers that were built for the RL experiments along with the experimental capabilities of the facility.

Chapter 3 describes the transient experiments conducted in the RL. The experiments cover several of possible transient events resulting from operational disturbances of a failure or load change. The six experiments described set several stages for the upcoming chapters.

Chapter 4 describes the mathematical model governing the transient behavior of servers.

Utilizing the transient experiments in Chapter 3, the remaining sections propose techniques to extract characteristic information of servers, such as time constant, thermal capacitance and thermal conductance. These parameters are the inputs for the mathematical model developed for servers.

In Chapter 5, transient boundary conditions for servers are introduced into a commercial CFD code based on the mathematical model of Chapter 3. The transient CFD simulation of the rack shutdown is then compared to the results of the transient experiment.

Chapter 6 introduces the hybrid-lumped capacitance model and practical rules for the thermal characterization of the components beyond servers in data centers. The thesis is then closed by conclusions.

Chapter 7 summarizes the thesis underlining the importance of this study by emphasizing significant contributions, which is followed by suggested future work.



## 2 Description of Experimental Facility

Syracuse University Green Data Center (SUGDC) houses the Research Lab (RL) data center, which provides testing capability for both the steady state and transient experiments to be presented in this study. The RL has a floor area of  $480\text{ft}^2$  ( $44.6\text{ m}^2$ ) and is 12 ft (3.66 m) high, has also been utilized in the steady state experiments presented by Abdelmaksoud (2012). The layouts of the RL are shown in Figure 2.1 and 2.2.

The RL was designed to emulate the thermal environmental conditions and design features common in data centers. These features include a pressurized under-floor plenum, perforated tiles, computer room air handling (CRAH) units, and server cabinets, which are filled with simulated servers. The plenum, which has a concrete slab floor, has a linearly varying height of 2.5 to 2.8 ft (0.762 to 0.853 m). The RL is entirely isolated from the rest of SUGDC, both at the room and plenum-level. The cold air supplied by the CRAH into the plenum is discharged into the cold aisle through the perforated tiles, which are located in front of the server cabinets. The cold air is then mixed with some of the warmer recirculated air and ingested by the simulated servers inside the racks. The three racks contain a total of 12 simulated servers (4 in each rack). Each rack can generate up to 35 kW of heat. The simulated servers are designed to have comparable flow and thermal characteristics to an IBM Blade Center. Due to the heat added into the air stream by the heaters inside simulated servers, simulated servers exhaust hot air into the hot aisle. The warmer room air is then ingested by the CRAH and cooled by passing over a water-cooled heat exchanger. Having a sensible cooling capacity of 100 kW, each of the two CRAH units is capable of removing the heat output generated by all of the simulated servers at full power. The details about the RL equipment will be provided in subsequent sections.

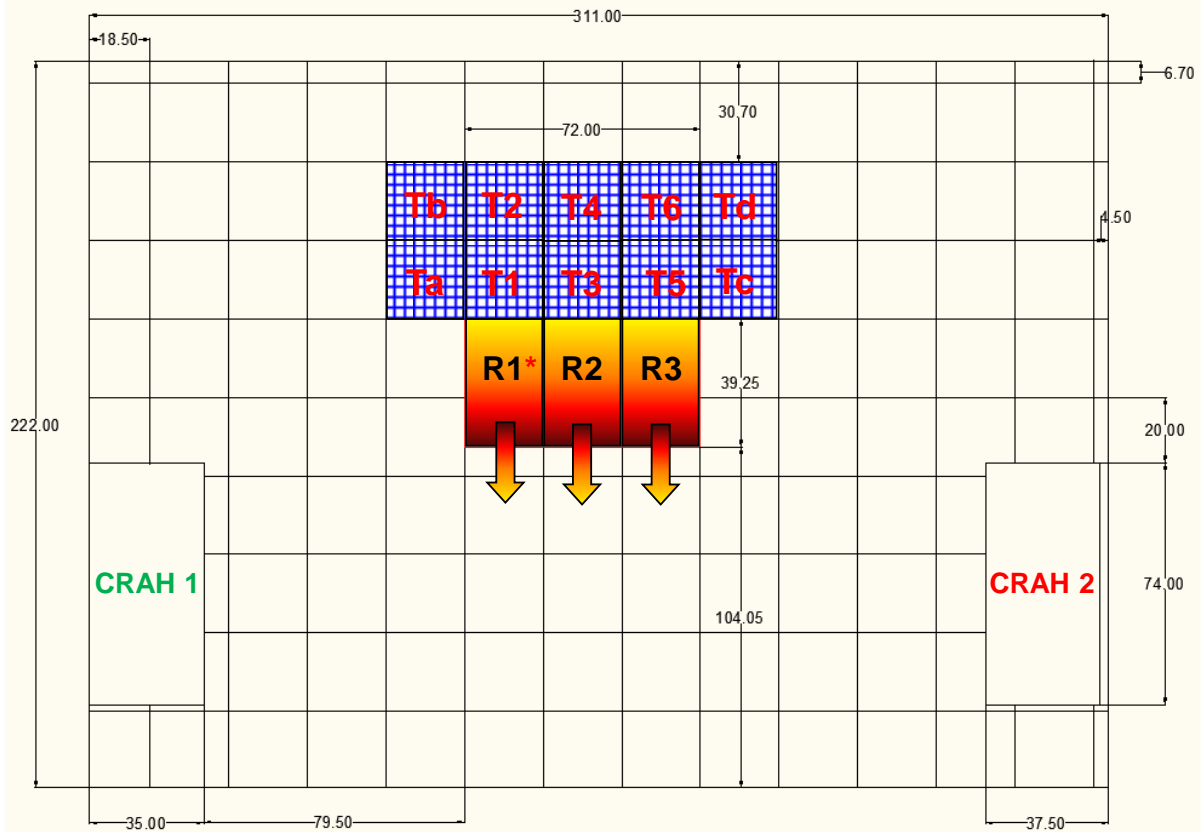


Figure 2.1: RL top view (dimensions in inches)

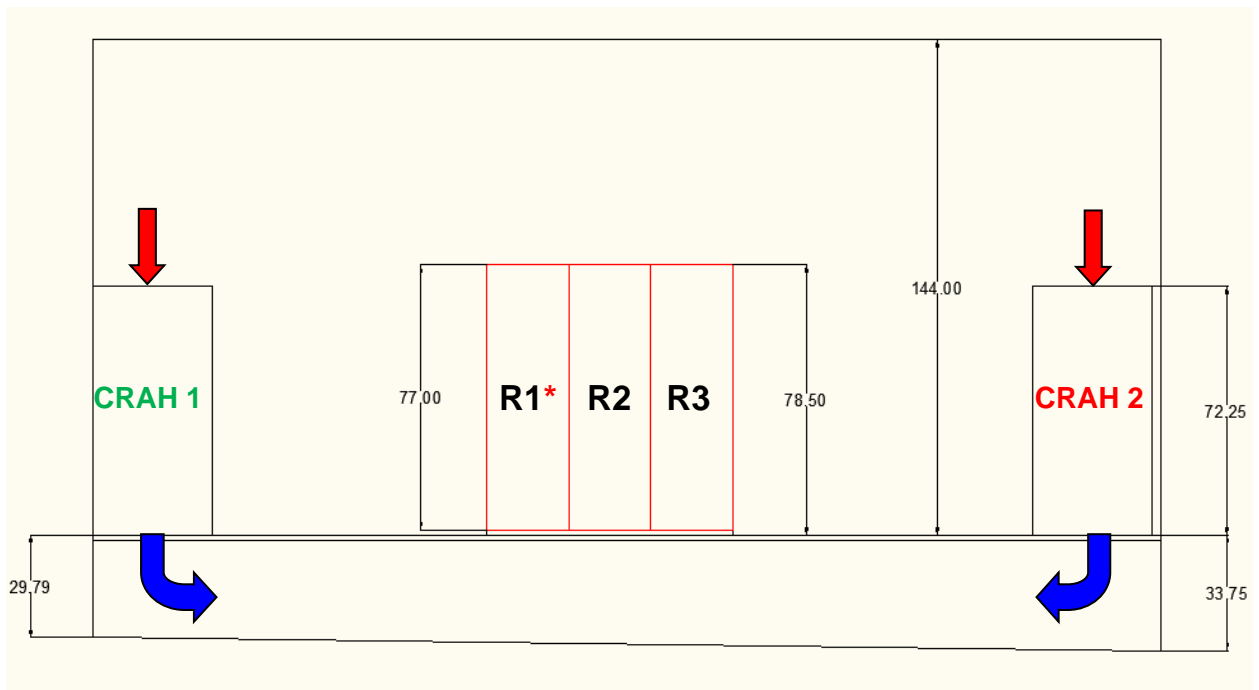


Figure 2.2: RL side view (dimensions in inches).

## *2.1 Plenum*

The RL plenum was designed to minimize the obstructions following the recommendations for the data center best practices (ASHRAE 2008b). A clean, unobstructed plenum is necessary for research work in order to diminish the uncertainties in the experimental data, which are used to CFD validation. The only obstructions in the RL plenum are the floor stanchions, power and instrument cables. The water pipes feeding the CRAH units are isolated from the plenum air space by the partitions along one side wall of the plenum and in one of the corners. In order to reduce the uncertainties associated with leakage, all the edges of the closed tiles, cable and wire cutouts, power plugs, and any other openings were sealed. No more than 2% of the CRAH air flow rate was observed as leakage during the pressurization tests of the plenum (Abdelmaksoud, 2012). A majority of the experiments in this study require single CRAH operation. In such cases, the operational CRAH is always CRAH-1 and the other unit, CRAH-2, is sealed to prevent any backflow from the pressurized plenum into the room. During the experiments that require both units in sequence, neither of the CRAH units is sealed and backflow is observed through the non-operational unit. The amount of backflow, and how it was quantified, will be discussed in the next section.

## *2.2 CRAH Units*

As previously mentioned, each of the CRAH units is capable of removing the maximum heat load the racks can generate, which is approximately 100 kW. The casing of the CRAH unit consists of a cascaded layer of filters just before the aluminum finned heat exchangers, which receive ~50 GPM (~3.15 L/s) of chilled water from the cooling plant at full capacity. Two variable-speed, forward-curved centrifugal blowers running on a single shaft overcome the

pressure drop in the entire flow path. The blower motor has a rated power of 7.5 hp (5.6 kW). Based on the tile flow rate measurements at the maximum (100% - 1050 RPM) and minimum (60% - 630 RPM) fan speeds, the intersection of the fan and system characteristic curves were obtained for a single blower (Figure 2.3). Since a single CRAH unit has two blowers, a range of 4800-to-7600 CFM (2.27-3.59 m<sup>3</sup>/s) total CRAH air-flow rate is expected from one CRAH unit.

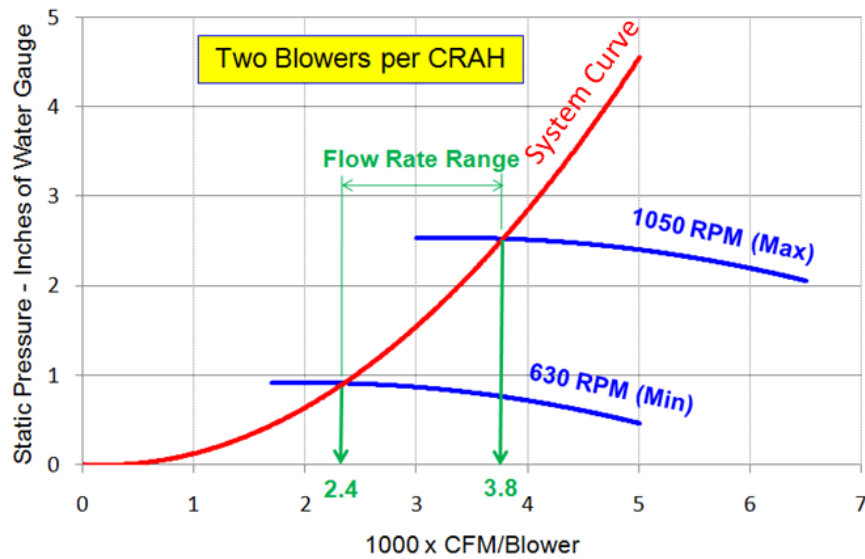


**Figure 2.3: CRAH blower characteristic curve; 2400 to 3800 CFM per blower flow-rate range, or 4800 to 7600 CFM per CRAH.**

Six thermocouples at the air inlet, and four thermocouples (two at the exit of each blower) at the air exit of each CRAH unit, provide time-dependent temperature data regarding air temperatures. Surface thermocouples are placed on each inlet and exit pipes of CRAH units to monitor the conditions of the chilled water.

While chilled water flow-rate measurements into individual CRAH units are not available, flow rate into the research lab is recorded by the building management system (BMS) with an interval of 1 minute. The data provide sufficient information about the response of the CRAH units and

how they are controlled. The control logic of a CRAH unit activates on-off modulation of the chilled water valve to keep the inlet air temperature below a certain set-point.

### *2.3 Perforated Tiles*

As seen in Figure 2.1, 10 perforated tiles are placed in front of the racks to provide cold air from the plenum to the inlets of simulated servers. Correct representation of the pressure drop across a perforated tile requires a relationship between the pressure drop and flow-rate, which can be obtained experimentally or provided by the manufacturer. The perforated tile used in the RL has 56 % open area (Figure 2.4). However, a manually adjustable damper attached at the bottom of the tile, with a maximum opening of 25 %, determines the porosity of the tile-damper combination. Flow characteristics of the perforated tiles used in the research lab are as follows (Figure 2.5).

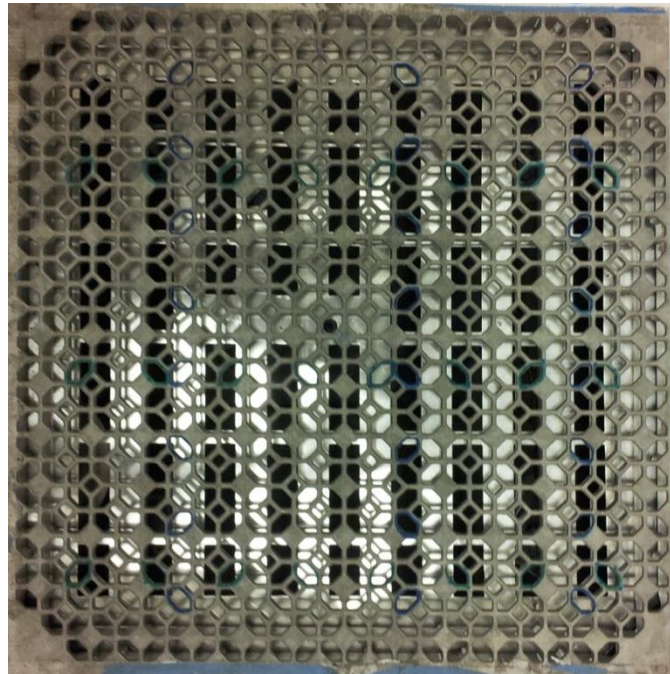


**Figure 2.4: Perforated tile used in the RL.**

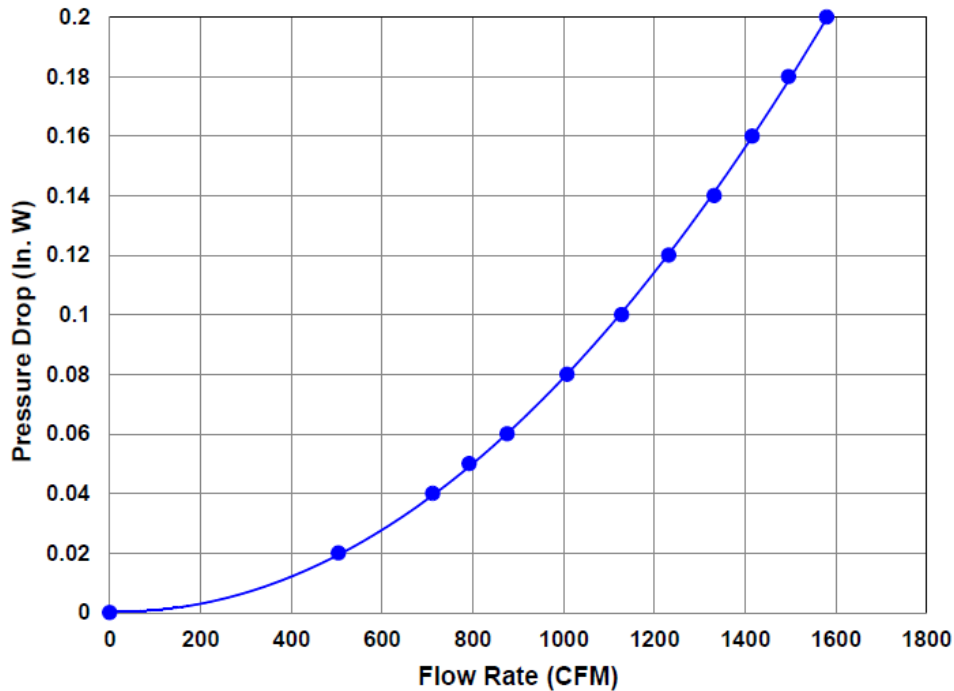


**Figure 2.5: Perforated tile flow characteristic curve (Tate Access Floors, Inc.).**

The percentage opening of the tiles with the damper was 25% for all of the experiments to be introduced in this study. Flow rates through the tiles are measured by the flow hood, and the temperature at each tile is measured via a single thermocouple in the middle of the tile attached below the damper.

#### *2.4 Exposed Surface Materials*

The RL is enclosed by three types of building materials at the room and plenum level surfaces. The closed tiles with 1/6" (4.23 mm) laminate in the RL are filled with light-weight concrete and each of them weighs 37.5 lbs (17 kg). The walls are gypsum board and the ceiling tiles are made of mineral fiber. Both the walls and the ceiling have a thickness of 16 mm. The floor of the plenum is covered by a concrete slab. Table 2.1 summarizes material properties of the surfaces in the RL.

**Table 2-1: Summary of material properties for surfaces**

<b>Material</b>	<b>Surfaces</b>	<b>Thickness (mm)</b>	<b>Specific Heat (J/kgK)</b>	<b>Density (kg/m<sup>3</sup>)</b>	<b>Thermal Cond. (W/mK)</b>
<b>Gypsum Board</b>	Walls	16	1090	950	0.17
<b>Lightweight Concrete</b>	Closed Tiles (Filling)	~35	960	2300	0.2
	Plenum Floor	N/A			
<b>Mineral Fiber</b>	Ceiling	16	800	369	0.0057
<b>Steel</b>	Rack, CRAH	~1	434	7850	60

## 2.5 Racks

Data center operations are conservative, and conducting experiments in an environment that is strictly held below certain temperatures is a significant challenge, especially during transient scenarios. The RL is designed to have an environment that is as independent as possible from the rest of the SUGDC and consists of simulated servers, which generate heat to represent high-power servers (10-30 kW/rack). The RL consists of three server cabinets/racks, each of which carries four of these high-powered simulated servers (Figure 2.6).

The server cabinets are 24 inches (0.61 m) wide (same as one tile) and approximately 6.5 feet high (2m) and 39.25 inches (1m) deep. The gaps between simulated servers in the rack were sealed by using extensions of metal sleeves to prevent recirculation of air within servers following the recommendations (Khankari, 2009) and to reduce the uncertainties in modeling. Metal sleeves were attached to the front and back of the simulated servers, and they form an isolated flow path extending from the perforated rack door at the inlet to the perforated door at

the exit. The perforations remaining outside the server flow area were neatly sealed with tape to create a designated flow path from the inlet toward the exhaust of the server.

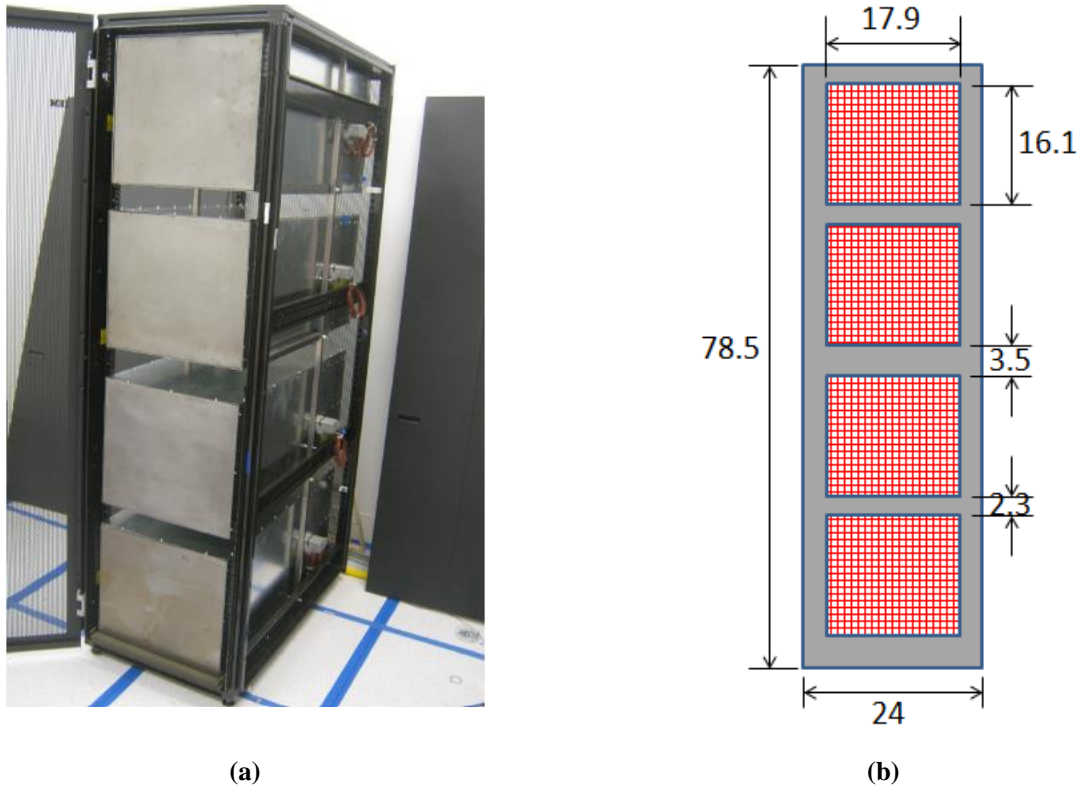


**Figure 2.6: Rack populated with four simulated chassis (rack covers removed). (b) Schematic representation of the simulated rack front or rear doors (dimensions in inches).**

## 2.6 Simulated Servers

The simulated servers were designed to mimic thermal and flow characteristics of a real server.

Figure 2.7 shows flow characteristics of an IBM Blade Center. At the normal operating

condition, a 430 CFM ( $0.2 \text{ m}^3/\text{s}$ ) air flow rate passes through the server for a pressure drop of about 300 Pa. Since six IBM servers comprise a rack, this can be interpreted as 2600 CFM/rack ( $1.23 \text{ m}^3/\text{s}/\text{rack}$ ) flow rate for a pressure drop of 300 Pa. In this study, each cabinet

accommodates four simulated servers, which are relatively higher (15.85 x 17.625 inches) ( $0.403 \times 0.448 \text{ m}$ ) compared to an IBM Blade Center (12 vs. 16 inches) ( $0.305 \times 0.406 \text{ m}$ ), and four of



the simulated servers comprise a rack comparable to a cabinet full of six IBM Blade Center servers. Based on this fact, simulated servers were designed to provide about 650 CFM (0.31 m<sup>3</sup>/s) server air-flow rate for a pressure drop of 300 Pa, which was verified by tests on a wooden chassis designed by Abdelmaksoud (2012). Screens with 23 % perforation that are used in the simulated server were installed into the wooden model along with the wooden channel-type structure, which will be replaced by eight steel plates in the real design. At the inlet and exit, the perforated rack doors were placed to account for the possible additional pressure drop. Four axial fans in parallel on four quadrants of a plate overcome the pressure drop across the server. The Type A server fans were used at the design phase, which were kept running at the full speed of 8400 RPM. The number of perforated screens is then adjusted to reach the approximate figures needed for the flow rate (~650 CFM) and the pressure drop (~300 Pa) (Abdelmaksoud ,2012).

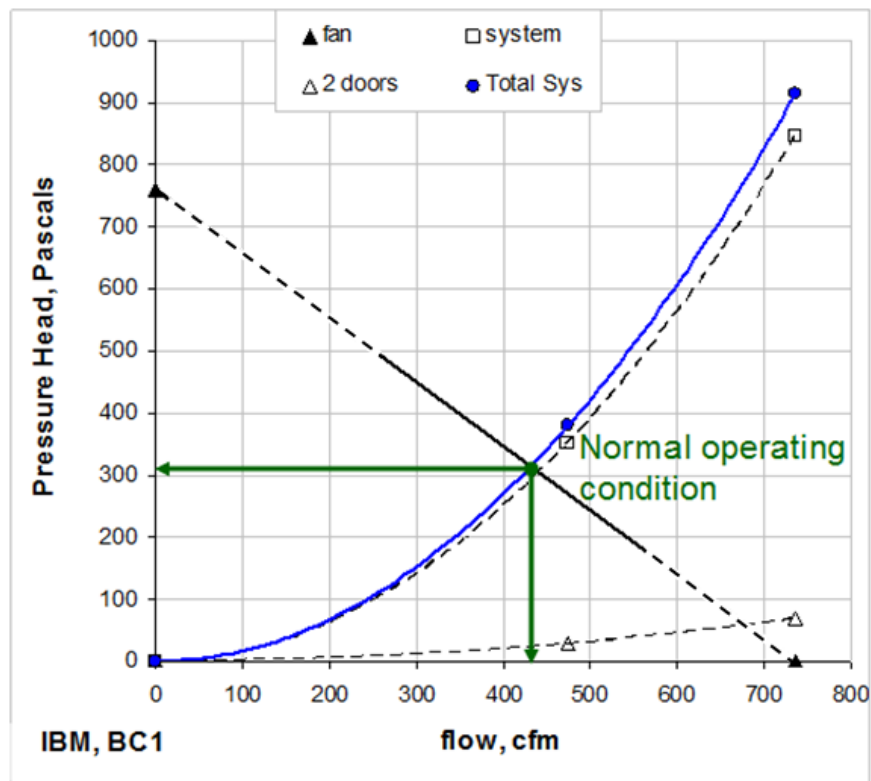
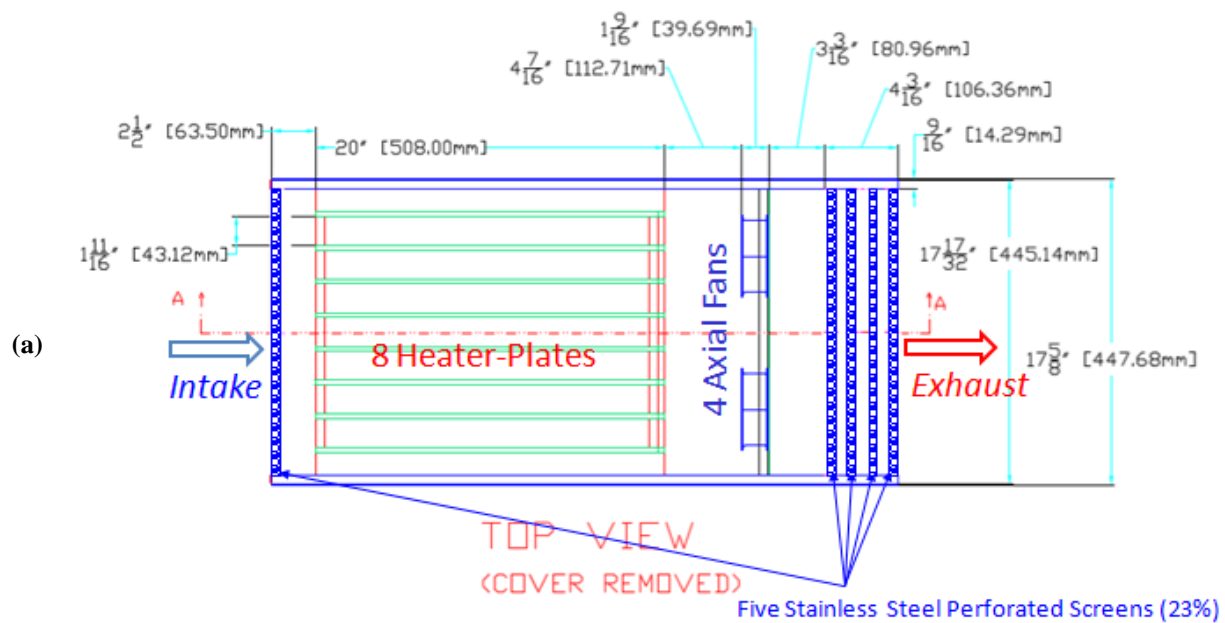


Figure 2.7: Flow characteristics of a real IBM blade chassis (Total Sys: system & 2 (rack) doors).

As a result, a total of five perforated screens were installed in the simulated server (Smith et al., 2011). The top view drawing and an image are shown in Figure 2.8. After passing the single screen at the inlet, the air flow is directed to the fan array through the heating unit. A heating unit consists of eight steel plates and silicon-rubber resistive heaters attached on the plates. Figure 2.9 shows a single 0.25" (6.35 mm) thick carbon-steel plate with a heater rated at 1080W ± 5 % heating capacity. As seen in the same figure, two thermocouples were placed between the heater and the steel, four inches away from the trailing edge. The thermocouples were intended to monitor temperatures and set up emergency controls for the system. Another step concerning safety precautions was regarding possible server fan failure scenarios. Accordingly, a pressure switch turns the heaters off if the pressure rise across the fan array is insufficient (Smith et al., 2011).





**Figure 2.8: Chassis layout: (a) Drawing (dimensions in inch); (b) Photograph from the top (cover removed).**

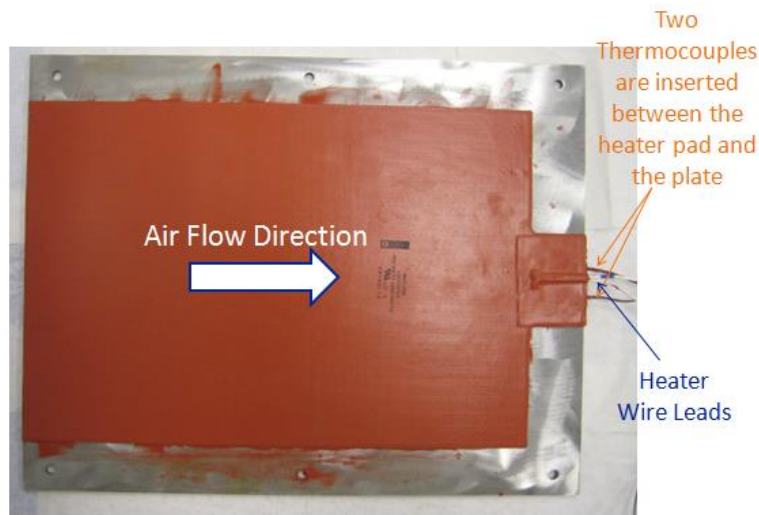


**Figure 2.9: Standalone carbon steel plate with a heater pad attached to it.**

The thermal mass of the real computer racks plays a significant role in the thermal control of data centers. Transient behavior of simulated servers needs to be considered at the design stage and monitored during the experiments. The selection for the heater plates was primarily aimed at obtaining a reasonable physical and thermal mass for the simulated servers so that it can represent a real server. An experiment was conducted in our laboratories, the details of which can be found in Appendix A. The time constant was obtained from the transient temperature data (Fig. 2.10) collected for the Blade Center. The transient measurements conducted on the IBM Blade Center revealed that the time constant for the start-up is 300 seconds (~5 min) and about 400 seconds (~6.5 min) for the shutdown. Details of time constant extraction will be provided in

the next chapters. Different time constants for start-up and shut-down was expected since the fan speed varies at different power levels, unlike the constant speed simulated chassis. At the shutdown, the server fans operate at a lower speed, which causes the heat transfer coefficient to decrease and the time constant to increase.

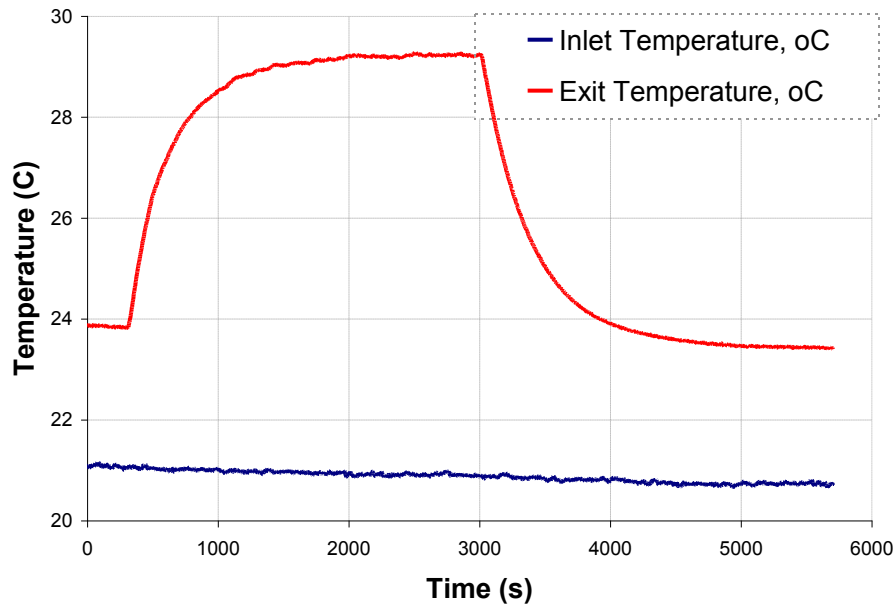


**Figure 2.10: Transient temperature data obtained from the IBM Blade Center experiment (Appendix A)**

There are two types of simulated servers designed for the RL: Type A servers, which have constant-speed fans and adjustable power, are placed in two outer racks, R1 and R3. Type B servers have adjustable fan speeds, even though fan speeds were fixed during the course of these studies. However, it needs to be noted that Type B server fans have higher rated power (90 vs. 60 W) and speed (9500 vs. 8400 RPM) compared to Type A server fans, which results in higher measured server flow rates which will be reported later.

### 2.6.1 Simulated Server Temperature Prediction

Even though simulated servers are designed to mimic the thermal behavior of IBM Blade Center, their internal components are much simpler. This helps in constructing a simple heat transfer model for the airflow that is passing through a channel.

For the channel flow between two carbon-steel plates, the Reynolds number is on the order of 10,000. For the fully turbulent flow ( $3000 < \text{Re}_D < 5 \times 10^6$ ), the Nusselt number can be computed by the Gnielinski correlation (Incropera & DeWitt, 2007),

$$Nu = \frac{f / 8 (\text{Re}_D - 1000) \text{Pr}}{1 + 127 \sqrt{f / 8 (\text{Pr}^{2/3} - 1)}}, \quad (2.1)$$

where  $Pr$  is the Prandtl number of air and the friction factor,  $f$ , for the same flow conditions is developed by Pethukhov (Incropera & DeWitt, 2007),

$$f = (0.79 \ln \text{Re}_D - 1.64)^{-2}. \quad (2.2)$$

Since the abovementioned correlations are for fully developed flow, for the developing flow region at the entry length, the local Nusselt number needs to be corrected by,

$$\frac{Nu_D}{Nu_{D,fd}} = 1 + \frac{C}{(x/D)^n}. \quad (2.3)$$

where the coefficients of  $C$  and  $n$  in our case were found to be 2.2 and 1.25, respectively (Kays et al., 2002).

The temperature variation along the heated section of the plate is computed based on the local heat transfer coefficient and air temperature as described. At the trailing edge of the heater, the one-inch long unheated section is treated like a fin, which has an adiabatic tip boundary

condition and the length of the fin is corrected accordingly. The boundary condition between the heated and unheated sections requires the axial temperature gradient to be equal. Figure 2.11 shows the temperature variation along the flow direction by solving for the temperature distribution along the heated channel and the unheated trailing edge.

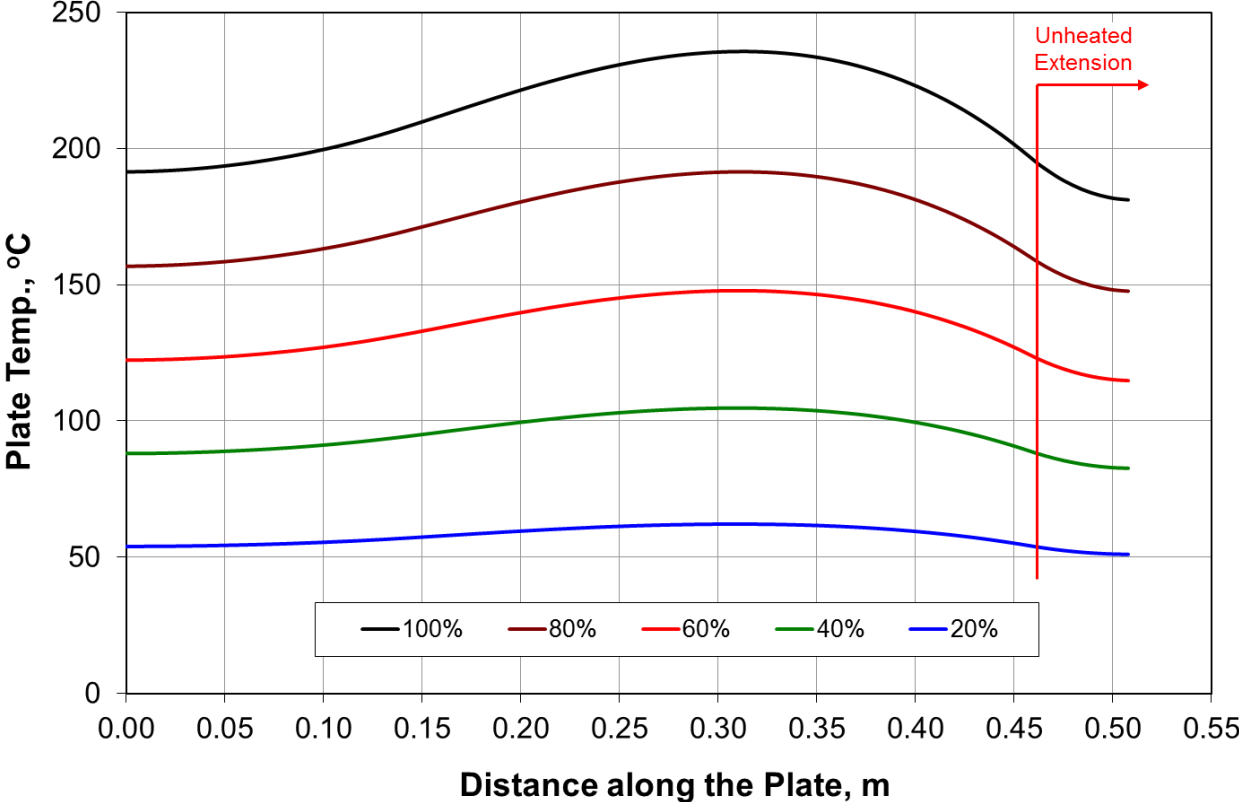


**Figure 2.11: Temperature prediction along the plate in the flow direction at different heater power levels.**

Figure 2.12 shows the maximum temperature predictions along with the measurements from two different experiments. Using this model gives a reliable prediction of the maximum temperature in the simulated servers for safe operation. The model also provides analytical estimations of the

local heat transfer coefficient, which will be revisited in verifying thermal characteristics of the simulated servers.

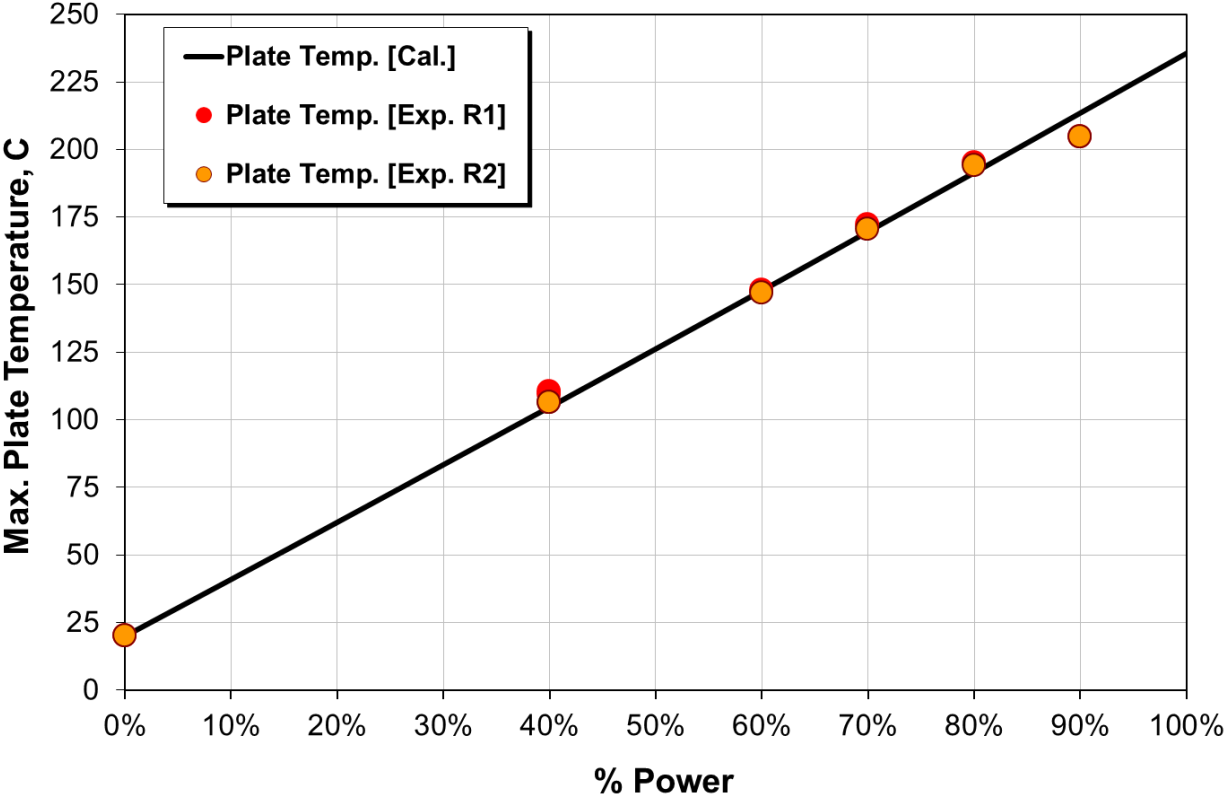


Figure 2.12: Predicted maximum plate temperature vs. measurements

In order to have higher fidelity predictions of temperature, dissipated heat inside the simulated server needs to be estimated. Simulated server power measurements were previously published in a paper by Smith et al. (2011) and Abdelmaksoud (2012) in detail. The following equation is used to compute the power based on the current ( $I$ ), voltage ( $V$ ) and power factor ( $\varphi$ ) measurements on each server,

$$P = IV \cos \varphi , \tag{2.4}$$

where power factor is assumed to be 1 due to the resistive nature of the circuit load. Device accuracies for the current and volt measurements are 5% and 0.02% respectively, which led to a power measurement accuracy of 5% (Abdelmaksoud, 2012).

## 2.7 Experimental Setup and Measurement Points

Servers comprise the heart of the data centers. Therefore, the environmental conditions at which they are operating need to be tightly controlled to avoid hotspots. The temperature measurements around the rack are of particular interest in this study as depicted in Figure 2.13. While the thermocouples attached to yellow poles monitor temperatures of 138 points – two rows in front, one row at the back, and two rows at the top of the racks – server inlet temperature measurements are dependent on thermocouples attached to the wooden frames. Each of four wooden frames consists of nine thermocouples. Since four frames are not sufficient to cover the entire surfaces of air inlet and exit, all experiments were repeated six times.

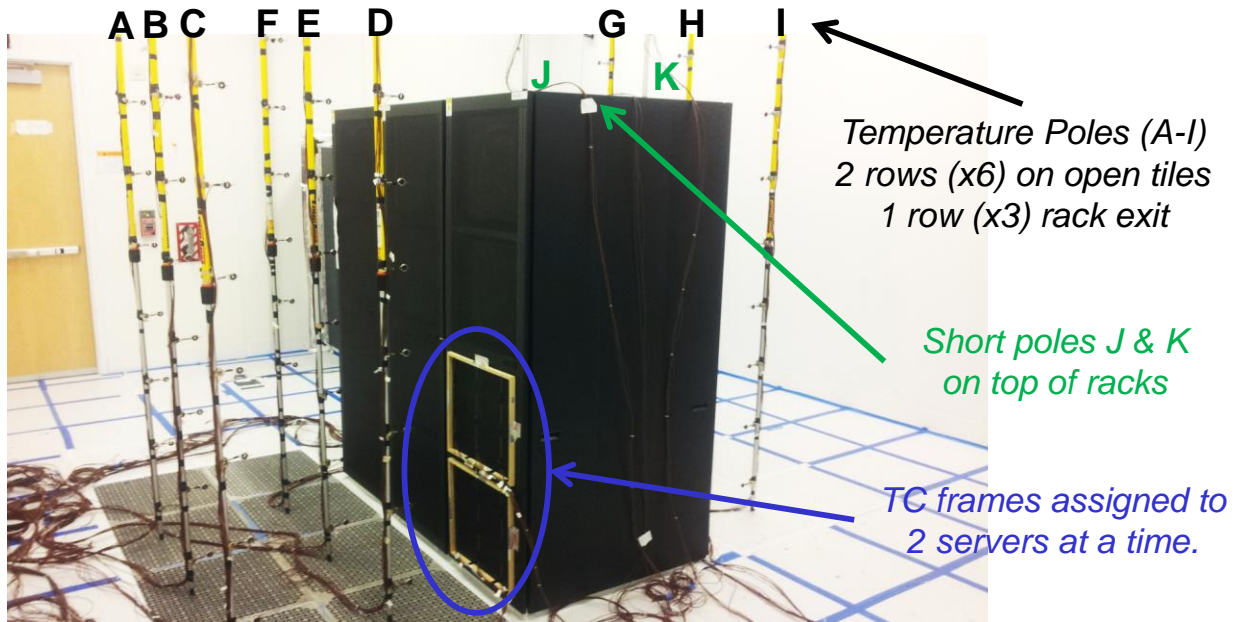


Figure 2.13: Locations of transient air temperature measurements around the rack.



In addition to the air temperature measurements around the racks, each air inlet and exit of CRAH units are equipped with a grid of six and four thermocouples, respectively. A single thermocouple is attached below each of the 10 perforated floor tiles. Chilled water temperature at the inlet and exit headers of the CRAH units, and single-point plenum concrete slab floor temperature measurements are also available for reference.

Thermocouples to measure air temperature (T-type with 24 gauge-wires) were tested in a temperature chamber (Z-Plus Chamber, model ZP(H) - 32). A statistical average of the mean square error of thermocouple readings are about  $0.05^{\circ}\text{C}$ . The uncertainty analysis primarily focused on the server inlet air temperature measurements will be discussed in a separate section at the end of Chapter 3.

Two computers connected to two data acquisition systems are placed in the data acquisition and control room. While the thermocouples measuring air and chilled water temperatures inside the room are connected to one DAQ system and computer, simulated server plate temperatures are recorded on another set to monitor to keep track of the highest temperatures in the room.

Air-flow measurements in the RL are conducted via the TSI Flow Hood (EBT721). The flow hood perfectly fits on the 2ft-by-2ft (0.61 x 0.61 m) perforated tiles. Since the RL is sealed to have a leakage no more than 2% of the CRAH air flow rate, the tile air flow measurements are also considered as CRAH air flow rate. The simulated server air flow area is smaller compared to the tiles. Therefore, the measurements at the exit of the servers require additional care to seal the excessive open area of the flow hood. Flow hood has a factory calibration with an accuracy of  $\pm 4\%$ . It was also calibrated in an IBM facility where it was found to report 6.5% higher than the

actual flow rate (Abdelmaksoud, 2012). Hence, the flow rate readings needed to be adjusted accordingly.

Additionally, chilled water-flow measurements into the research lab are provided by the building management system (BMS) for 1-minute intervals. When the chilled water valve is open, the reported chilled water flow rate is  $49.7 \pm 0.4$  GPM ( $3.14 \pm 0.025$  L/s) for CRAH-1 and  $48.3 \pm 0.3$  GPM ( $3.05 \pm 0.019$  L/s) for CRAH-2.

### 3 Transient Experiments

There are various parameters causing the temperature and flow field to change dynamically in a data center thermal environment. Change in the server power, CRAH fan speed, CRAH chilled water flow rate, and operating CRAH can be listed as several of many major parameters, individually or combinations of which were tested in the research lab (RL).

The first group of experiments, 1-4, can be called “Single CRAH Experiments” where one of the two CRAH units, called CRAH-2, was kept non-operational and sealed to prevent reversed flow from the pressurized plenum into the room.

Servers are the major heat generating components of data centers. Aside from being the major heat-generating equipment, servers also constitute a significant part of the thermal mass in a data center. The first experiment is aimed to understand the transient response of servers through a step change in power level. Servers in three racks were allowed to operate for an hour at approximately 45 kW of total power to reach a steady state before simulated server heating power was turned off. The server fans were kept running during the cool-down period. Similarly, the CRAH chilled water valve was also forced to stay open via an extremely low (10°C) return air set-point temperature, so any cycling in the chilled water supply into the CRAH was prevented over the course of the experiment. The results of the test were primarily used to demonstrate the extraction of time constants from the temperature difference across the servers. However, the results also indicate significant contribution of the thermal masses of several other components that will be discussed later.

The second experiment aimed to emulate a chilled water interruption scenario, which could result from pump or valve failure or physical damage to the piping. The test was designed on the knowledge that setting a high return air set-point temperature forces the chilled water valve to close and a low set-point forces the valve to open. The energy storing capacity of the CRAH heat exchanger and water mass were the primary focus along with the transient behavior of the simulated server thermal mass. There were also indications that the thermal mass associated with the plenum affects the transient response in such a failure mode.

The first two experiments did not cause a major disruption to the flow field in the RL, assuming the temperature variations were not as drastic to let the buoyancy effects dominate the characteristically high momentum flow in the space. A sudden change of CRAH flow was investigated in the third experiment. Unlike the first two experiments this case was the first case that was subject to a significant disturbance in the flow field. The transient response was expected to be indicative of the relatively fast time constants of the air space in the research lab; however, the results also set the ground for a technique to extract heat capacitance of servers, which will be discussed later.

The fourth experiment consisted of three subsequent tests, which were inspired by the transient CFD study presented by Gondipalli et al. (2010). The goal of this test was to show how the lack of thermal mass could deteriorate the accuracy of the CFD results if the tools do not take thermal mass effects of the equipment into consideration.

The last set of experiments is listed as 2-CRAH experiments, which required both CRAH units to be ready to operate. Experiment 5 consists of two experiments where the operating CRAH unit was turned off and the other CRAH was turned on. The nuance between subsequent tests is

related to the waiting time until the second CRAH turns on. The reason for different delay times can be two-fold: the indicators of a CRAH failure in a data center are the result of either the pressure drop in the plenum or locally emerging hotspot. Pressure drop caused by a CRAH failure is a very fast event since the pressure wave travels at the speed of sound. However, the rise of the temperature at the inlets of the server is a function of relatively longer time constants. The first test regarding a CRAH-switching experiment presents an instantaneously activated CRAH response. The delays were primarily due to the inertia of the fans; however, the response of the chilled water valve is a significant factor that needs to be taken into account, since chilled water valve response is not as quick as fan response. The subsequent test emulated the absence of CRAH air flow for a 30 second period until one of the servers experience an air inlet temperature of 35°C, which is highest allowable server inlet temperature in data centers (see Class A1, A2 in Figure 1.1).

Experiment 5 requires sequential operation of CRAH units. Unlike other experiments, the sealing on CRAH 2 needed to be removed to have the unit ready for operation. This caused a backflow stream to establish from the pressurized plenum into the room space through the non-operational unit, which was quantified by a set of flow measurements on CRAH-2. The first test was based on velocity measurements via hot sphere anemometers at 15 points along two lines on two levels of filters.

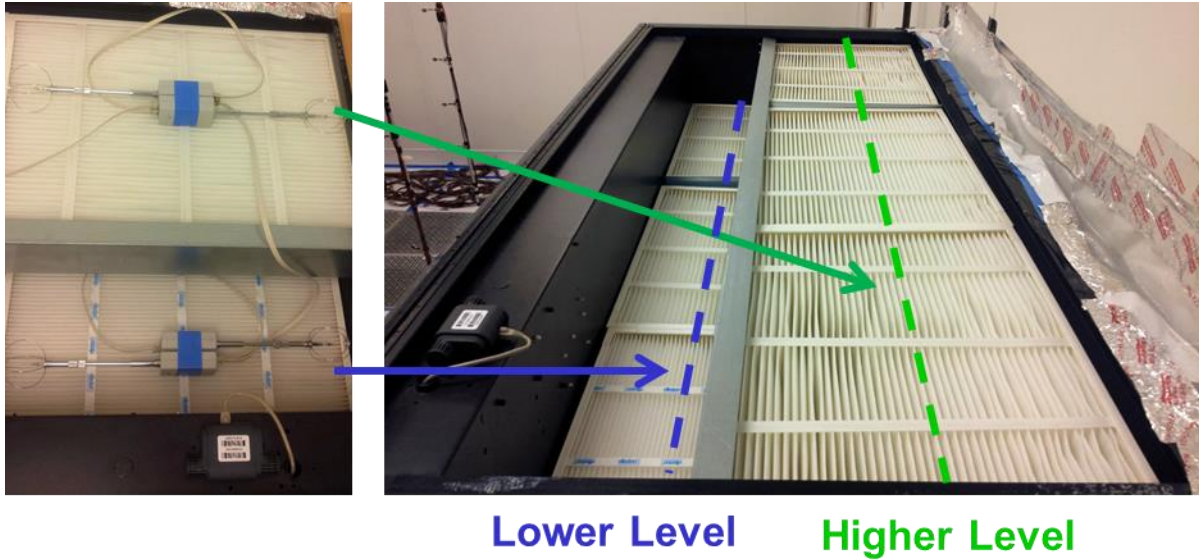


**Figure 3.1: Backflow velocity measurements on top of CRAH-2.**

The velocity measurements were repeated for two different tile-flow rates, and the backflow was calculated based on the assumption that the measured velocities were uniform along the width of the filter level and had only perpendicular components to the CRAH inlet.

The second test consisted of measurements via the TSI Flow Hood in three parts over the top of the unit. The slightly larger width of the inlet compared to the TSI Flow Hood was blocked to direct the local flow through the flow hood (Figure 3.2).

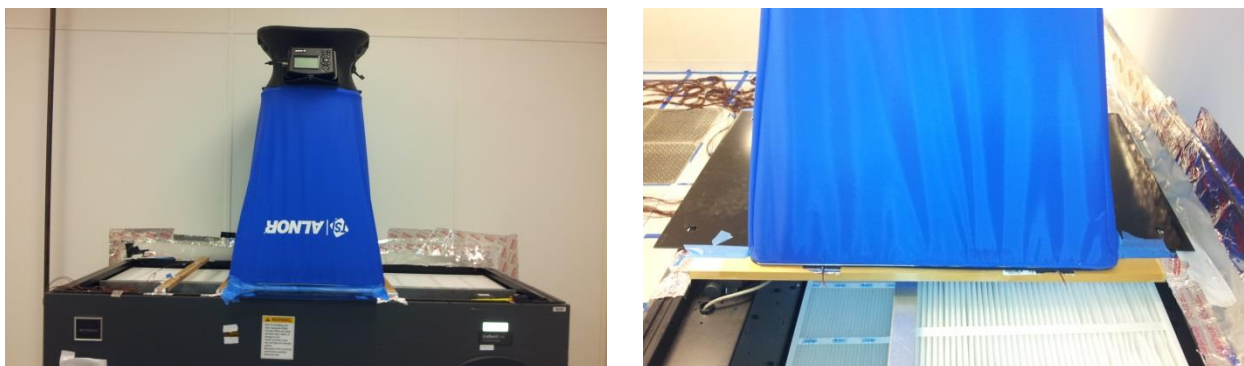


**Figure 3.2: Backflow measurements on top of CRAH-2 via TSI Flow Hood.**

In addition to the two tests described above, backflow results were also verified through a flow-circuit model based on the assumption that the resistance coefficient of the CRAH unit is applicable to the backflow. The resistance coefficients of the tile and CRAH units were obtained respectively from Figure 2.5 and Figure 2.7.

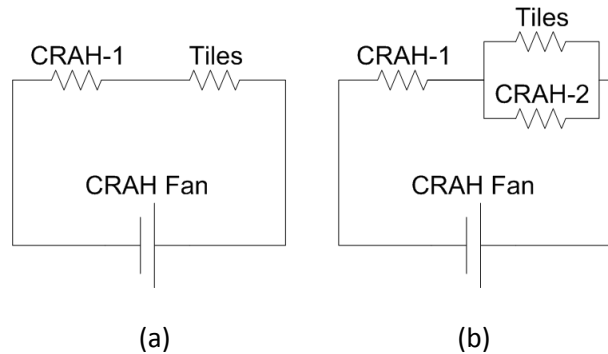


**Figure 3.3: Flow Circuit Models for cases in which CRAH-2 is (a) sealed and (b) unsealed.**

Table 3.1 provides a summary of the results of the three methods. Considering the error in assuming uniform distribution of velocity measurements over the surface, flow hood measurements were considered a more reliable approximation of the backflow rate. Accordingly, the results indicate that the amount of backflow can be approximated as 11% of the tile flow rate.

**Table 3-1: CRAH Back Flow Estimates.**

Tile Flow Rate (CFM)	CRAH Back Flow Rate (CFM)		
	Hydraulic Circuit	Test 1: Hot Sphere	Test 2: Flow Hood
5570	743	770	651
4020	536	560	454

### 3.1 Experiment 1: Rack Shutdown

The time constant of the server is a function of thermal capacitance of the constituent material and heat transfer conductance (UA) resulting from the physical characteristics of the flow path. The servers tested as part of this study ran at a constant speed. Hence, a single time constant can

be obtained for each server. The rack shutdown experiment was also a demonstration of time constant extraction for servers without removing them out of the racks. Keeping track of inlet and exit air temperatures of the server was sufficient to estimate a time constant, which can be used in modeling the server as a first-order system.

Figure 3.4 shows the experimental data for the change in server air temperature difference in time after heating power of about 45 kW in all racks is turned off at time=0s. Due to the heat addition by the constantly running server fans, the temperature difference of the server as it approaches a steady state value varies between 0.7 to 0.85°C. These heating power and temperature-rise values can be verified by the initial and idle power listed server-by-server in Table 3.2 along with the measured server air flow rates.

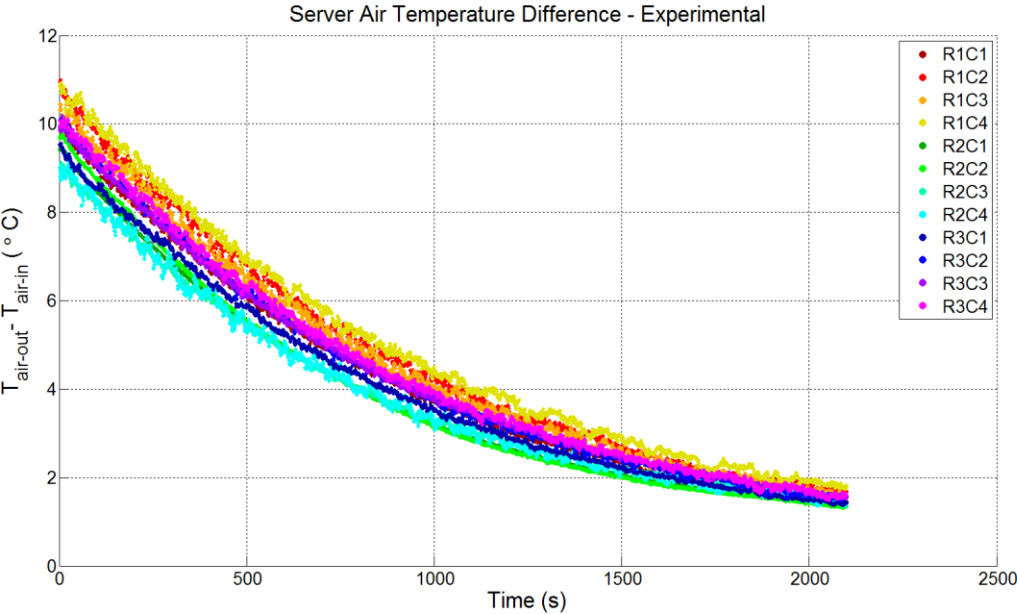


**Figure 3.4: Transient server air temperature difference during rack shutdown experiment.**



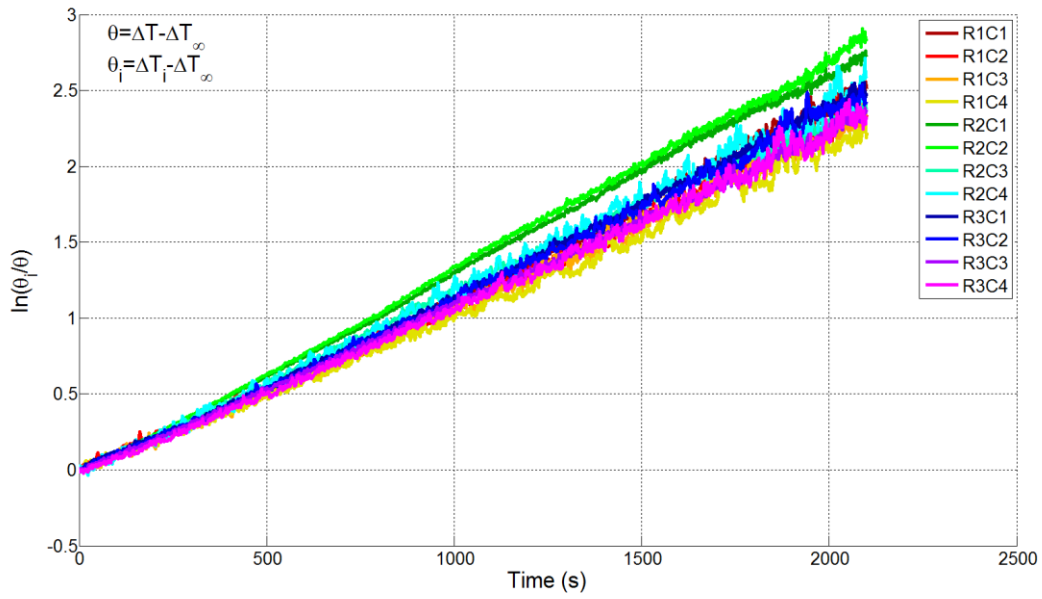


Figure 3.5: Natural logarithm of normalized temperature difference to estimate server time constants.

Table 3-2: Heating Loads and Air Flow Rates for Simulated Servers

Server	Initial Load (W)	Idle Load (W)	Air Flow Rate (CFM)
R1C1	3715	259	664
R1C2	3680	253	664
R1C3	3688	251	673
R1C4	3700	253	660
R2C1	3826	360	748
R2C2	3813	348	748
R2C3	3820	354	785
R2C4	3785	348	790
R3C1	3679	261	678
R3C2	3690	272	664
R3C3	3657	259	673
R3C4	3636	248	655

\* R1C1 is the bottom server of Rack 1

\* Rack 1 is closer to the operational CRAH unit, CRAH 1

Figure 3.5 confirms that servers exhibit typical first-order system behavior where  $\theta_i$  is the difference between initial and steady state air temperature rise and  $\theta$  is the instantaneous difference between and steady state air temperature rise. In other words, the transient behavior of the server air temperature difference observed in Figure 3.4 can be modeled by a single time constant as long as initial and steady state conditions are known. The extraction of a thermal time constant will be discussed in the next chapter when thermal characterization techniques for the servers are introduced.

### *3.2 Experiment 2: Chilled Water Interruption*

Pump failure is one of the many failure events that can be observed in a data center. A test representing CRAC unit response following a pump restart was conducted by Shields (2009). Based on the transient air temperature data, the time constant for the CRAC unit was extracted as 20 seconds. The time constant obtained in that study was based solely on the period after the pump was restarted. Due to the moving air and chilled water, the thermal resistance due to convection was relatively low, which leads to a higher thermal conductance. However, in cases of a failure, the chilled water is likely to be trapped in the heat exchanger. Therefore, the bulk of water and heat exchanger body should be the determining thermal mass following a failure. A corresponding time constant indicates available cooling in case of chilled-water interruption.

This experiment was conducted at a lower power level (20%), which corresponded to approximately 24 kW of heat dissipation from all servers. As previously mentioned, the event of chilled water interruption was represented by a sudden enforcement of higher return air set-point temperature. As soon as a high set-point for return air was assigned at the time  $t=60$  seconds, the modulating valve at the chilled water return pipe started to shutdown. It took about a minute to

entirely shutdown the chilled water valve, which could be monitored from the control panel of the unit. Figure 3.6 shows the variation of average CRAH air temperatures, chilled water temperatures, average tile temperature, and heater-plate surface temperature of one of the simulated servers, R1C3. The qualitative difference in temperature response following the changes to the chilled water valve position verifies that there are two distinct time constants for the CRAH units that can be obtained from this test.

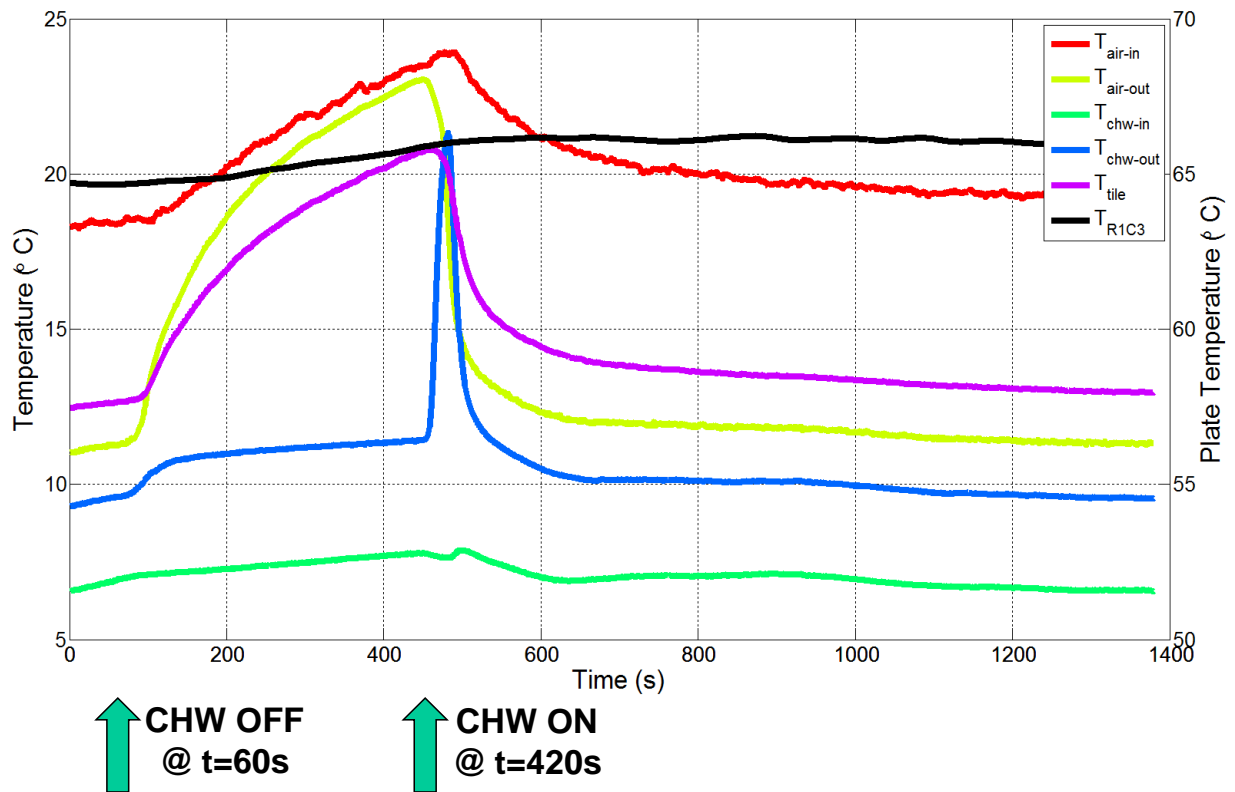
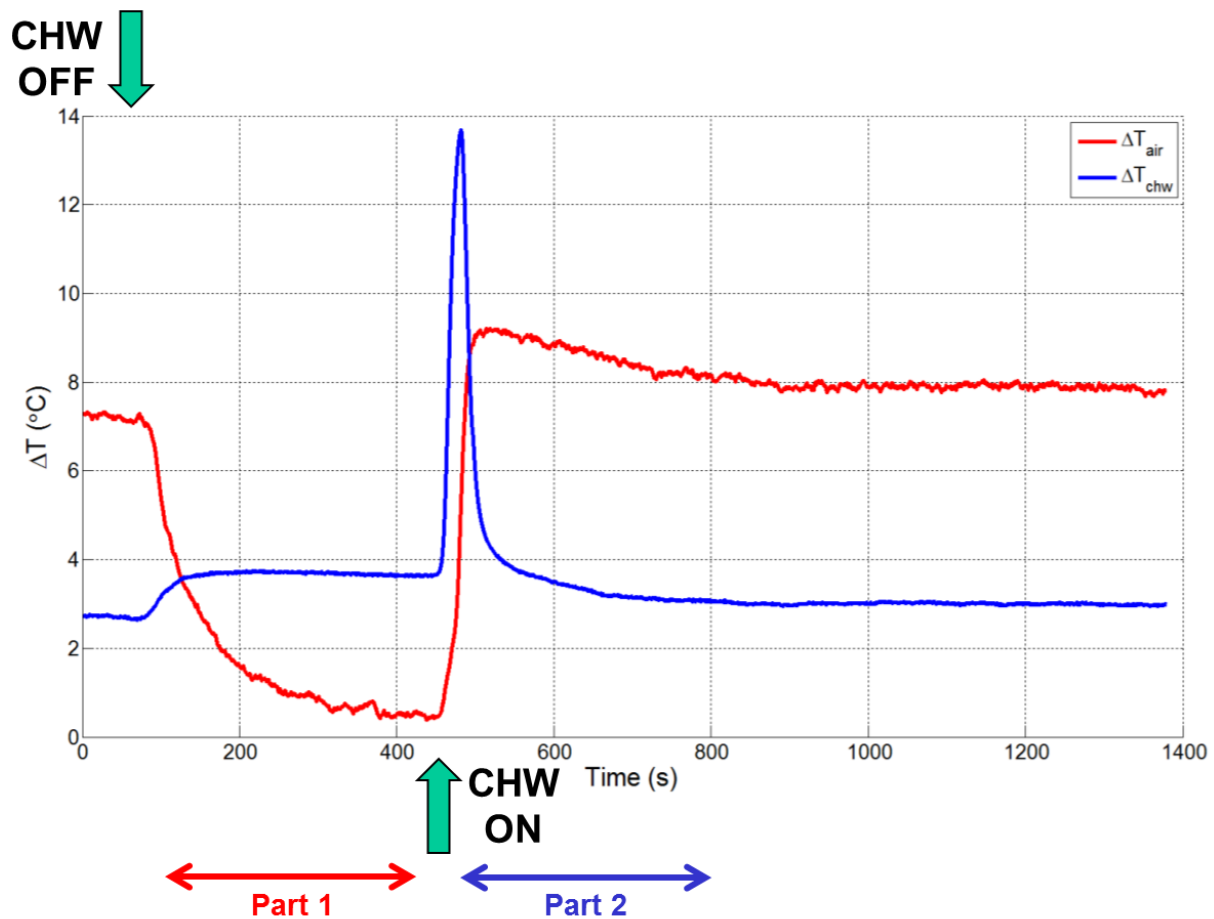


Figure 3.6: Temperature variations during chilled water interruption.

The temperature rise in the room air temperature, which is represented by the CRAH inlet air temperature, the red line labeled  $T_{air-in}$ , was due to the absence of chilled water supply into the CRAH unit. A couple minutes after the chilled water valve closed, the average CRAH exit air temperature approached the average inlet temperature of air into the CRAH units. This indicated

the loss of cooling, meaning that the body of the heat exchanger and non-moving water could no longer remove heat from the air stream. The time constant for the period after which the chilled water valve shuts down is obviously longer since the water trapped in the heat exchanger has a lower heat transfer coefficient, which increases the thermal resistance and decreases the overall heat conductance of the heat exchanger leading to a longer time constant. Figure 3.7 displays the temperature difference of the air and water stream of the CRAH unit. For Part 1, considering that the CRAH is bulk mass of aluminum and non-moving water representing a first order system behavior, the time constant can be approximated from the air temperature difference, which was about 70 seconds. Conversely, Part 2 led to a time constant of 15 seconds, which is comparable to the results obtained by Shields (2009). The sudden rise in temperature reading at the exit pipe of the CRAH unit caused the spike at the beginning of Part 2. This sudden temperature rise was caused by the trapped water inside the heat exchanger during Part 1. After the chilled-water valve opens, the warmed water passed by the thermocouple attached on the exit pipe which led to a sudden rise in the temperature readings.

Another observation was the crossover of CRAH exit air temperature and the tile temperature shortly after the chilled water interruption in Figure 3.6. During the travel of air from the CRAH units to the perforated tiles, the plenum cools the warmer air flow exiting the CRAH. In case of a loss of chilled water supply, the air temperature rises much faster than the temperature of building materials such as the concrete floor, side walls and floor tiles surrounding the plenum. As the air temperature rises, these have a damping effect on the temperature response by their large and cooler thermal masses.



**Figure 3.7: Temperature differences of air and chilled water across the CRAH unit.**

Since the CRAH fans operated at the same speed throughout the experiment, there was not a major change in the room flow field. However, the temperature field was directly affected by the gradually increasing CRAH exit air temperatures due to the lack of cooling after chilled water was interrupted. As seen in Figure 3.8, servers started to experience increasing inlet temperatures.

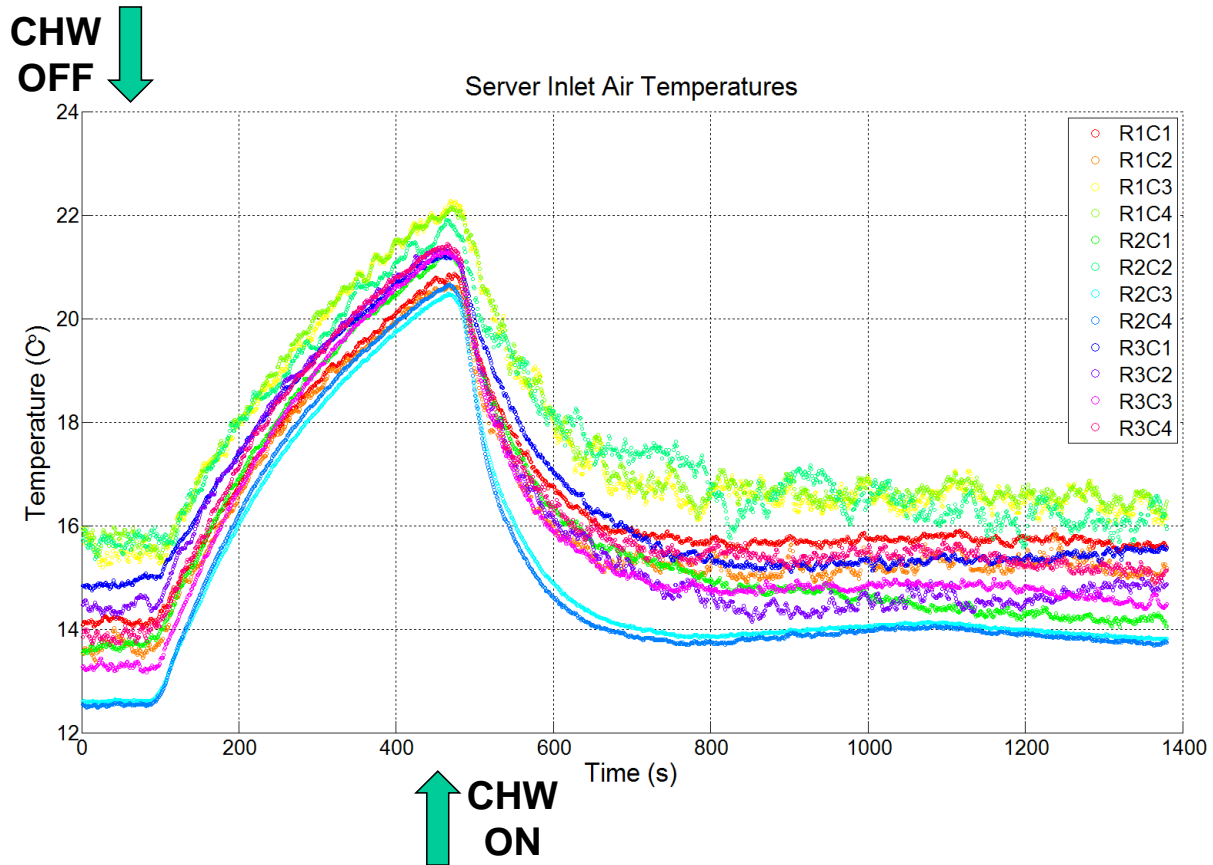


**Figure 3.8: Temperature variation of server inlet air temperature during chilled water interruption.**

The sudden decrease or increase in the server inlet temperature caused simulated servers to release or store heat, respectively, to adjust to the new thermal environmental conditions. Figure 3.9 shows the time series data for the temperature difference across the server based on the sequence of events during this test.

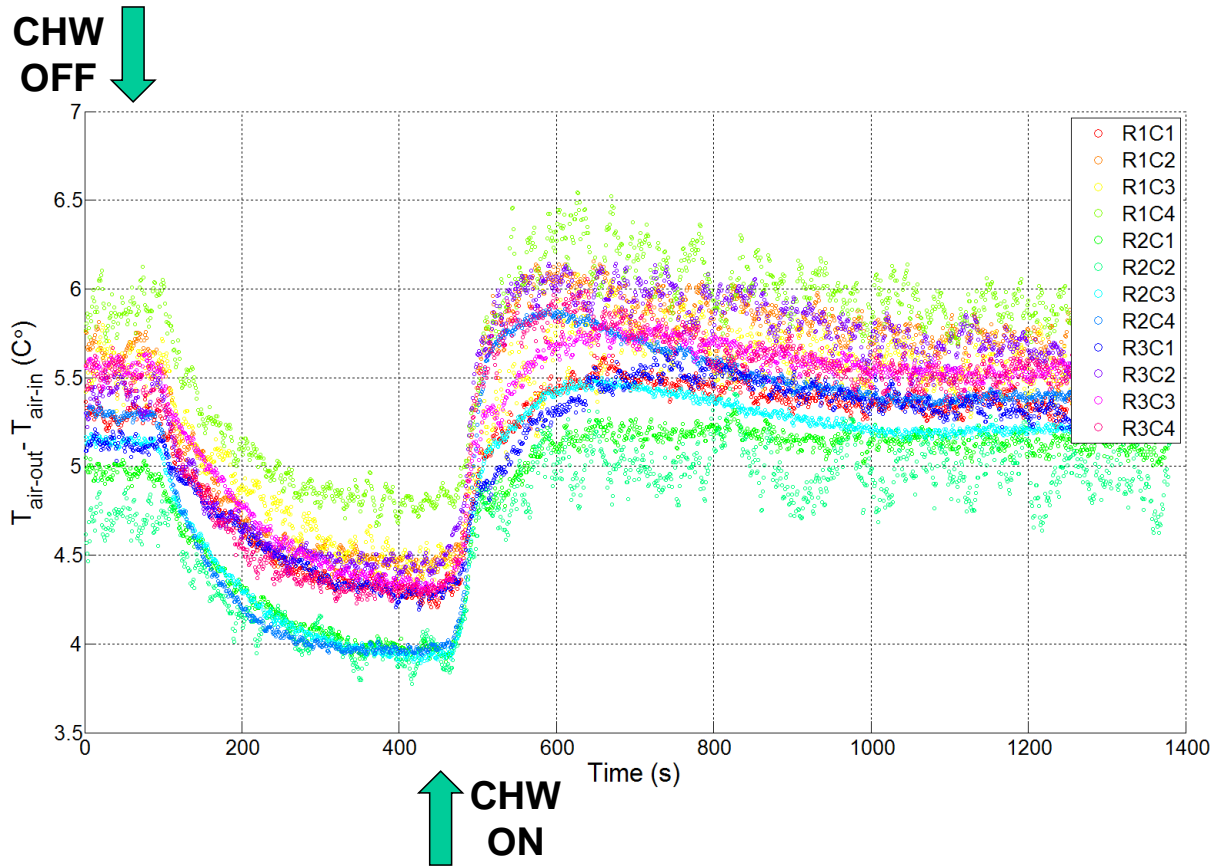


**Figure 3.9: Variation of server air temperature difference during chilled water interruption.**

### 3.3 Experiment 3: Sudden Change in CRAH Air Flow Rate

Data center air space is dominated by the high momentum air flow through perforated tiles and servers, which results in high number of air changes per hour (~1 air changes per minute).

Hence, air flow transients are expected to be fast ( $\tau \sim 60\text{s}$ ). Figure 3.10 shows the sequence of events during the experiment in which the only parameter varied was CRAH air flow rate.

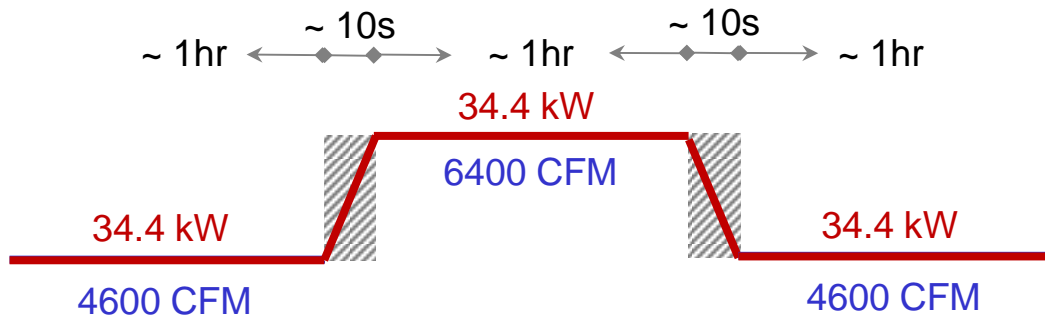
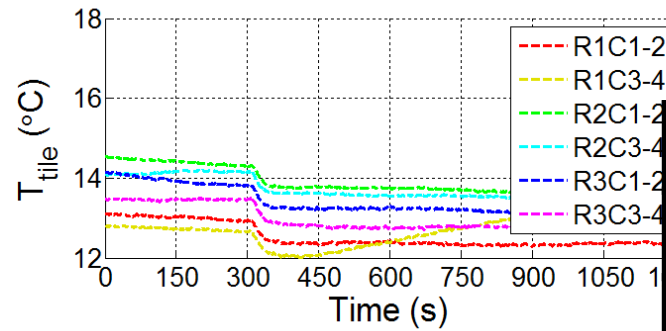
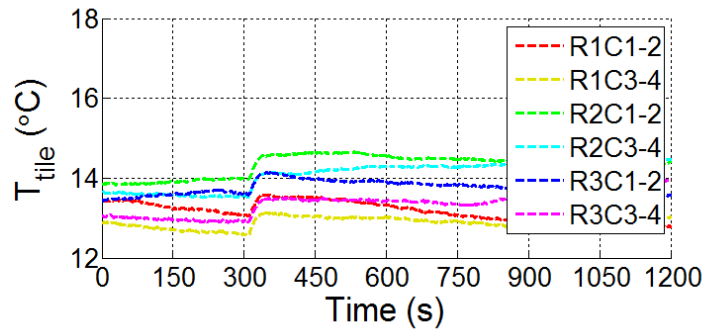


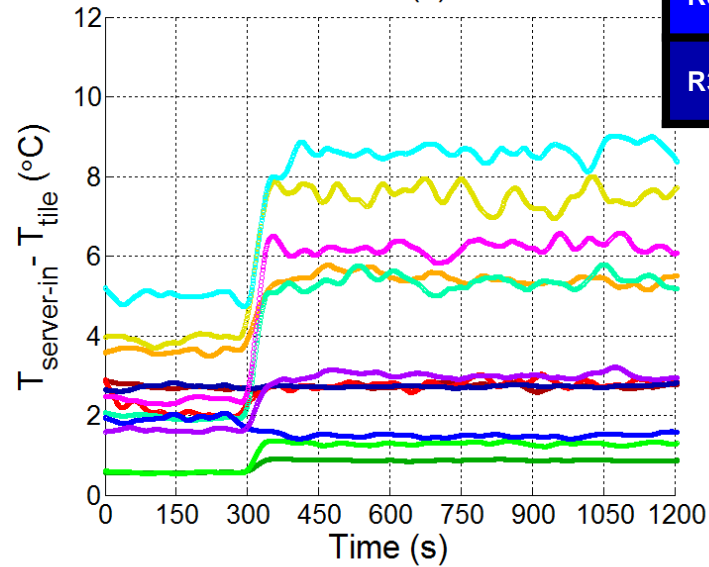
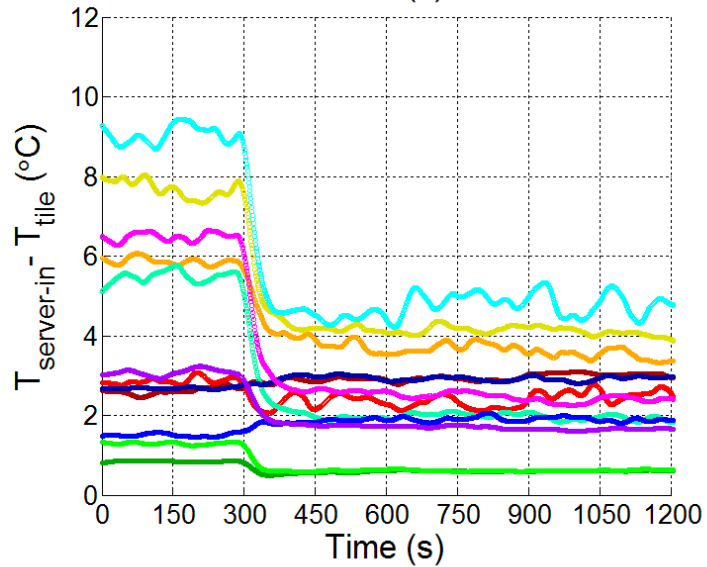
**Figure 3.10: Timeline of air flow (CFM) changes during for experiment 3.**

Total rack power remained constant at 34.4 kW throughout the experiment. The system was allowed to run about an hour to reach the steady state conditions each time before air flow was changed from low flow (4600 CFM) to high flow (6400 CFM) and vice versa. Figure 3.11 shows the temperature difference between the server inlet temperatures and tile average temperature for the transition between high and low flow cases.





R3C4	R2C4	R1C4
R3C3	R2C3	R1C3
R3C2	R2C2	R1C2
R3C1	R2C1	R1C1



Increased CRAH Air Flow Rate  
4600 → 6400 CFM  
@ t=300s

Decreased CRAH Air Flow Rate  
6400 → 4600 CFM  
@ t=300s

Figure 3.11: Server inlet temperature and tile temperatures during variation of CRAH air flow rate.

A time constant of about 40 to 45 seconds was extracted from server inlet temperatures, which represents the time-dependent response characteristics of air space. Another important observation was related to the transient server air temperature rise. The top servers (R1C4, R2C4, R3C4) were exposed to sudden temperature changes after CRAH flow rate is changed. As seen in Figure 3.11, after switching from high to low CRAH air flow, top servers started to receive inlet air at higher temperatures. Similarly, after switching from low to high CRAH air flow, top servers started to receive inlet air at lower temperatures. The transient temperature difference across servers in Figure 3.12 indicates that top servers were forced to a newer equilibrium state. The height of the spike in the air temperature difference is a characteristic thermal property of the server. Built upon this, a technique will be introduced in the next chapter to extract thermal capacitance and conductance of servers.

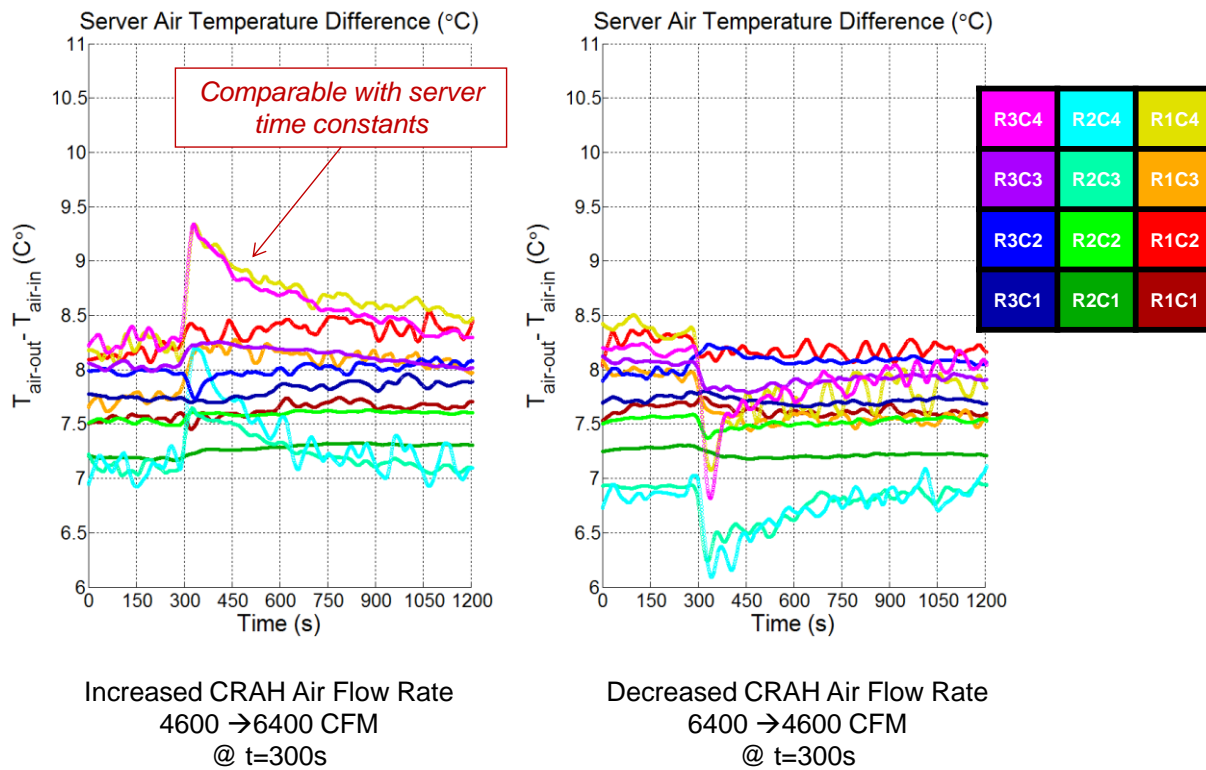


**Figure 3.12: Variation of server air temperature difference in response to changing inlet air temperatures.**

### 3.4 Experiment 4a-b-c: Server Power and CRAH Air Flow Rate Variation

Varying rack power and air flow rate scenarios were presented in a CFD study by Gondipalli et al. (2011). Three of the following tests were inspired by that work, and aimed to present inaccuracies of transient CFD calculations in the absence of server thermal masses. Figure 3.13 shows the procedure followed in three subsequent tests in which the changes of server power and CRAH air flow occurred (a) instantaneously, (b) led by either CRAH air flow, or (c) server power. The first experiment, 4a, represents a case in which changes were imposed concurrently. In 4b, rack power change was followed by CRAH air flow change 150 seconds behind; lastly, in 4c, rack power was changed 150 seconds after the CRAH air flow rate was changed.

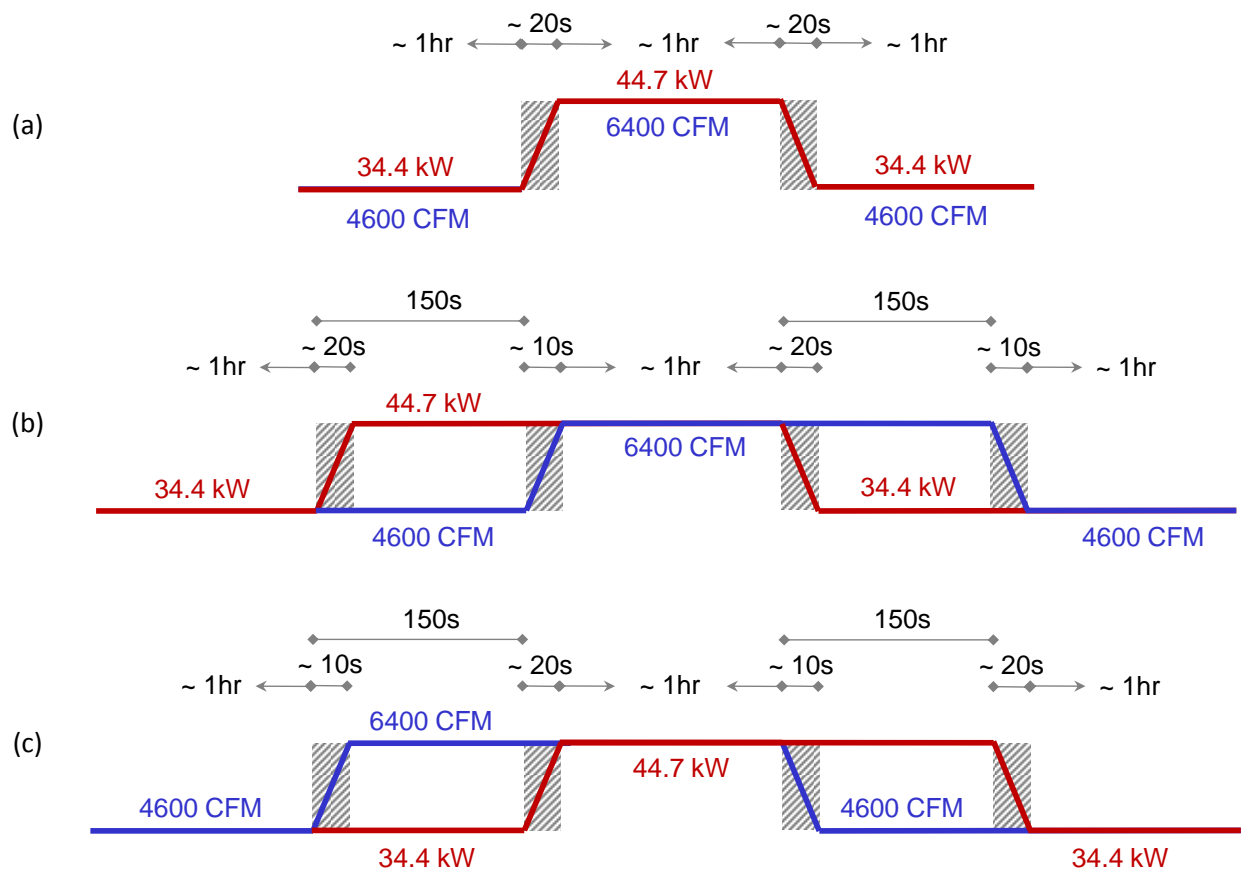
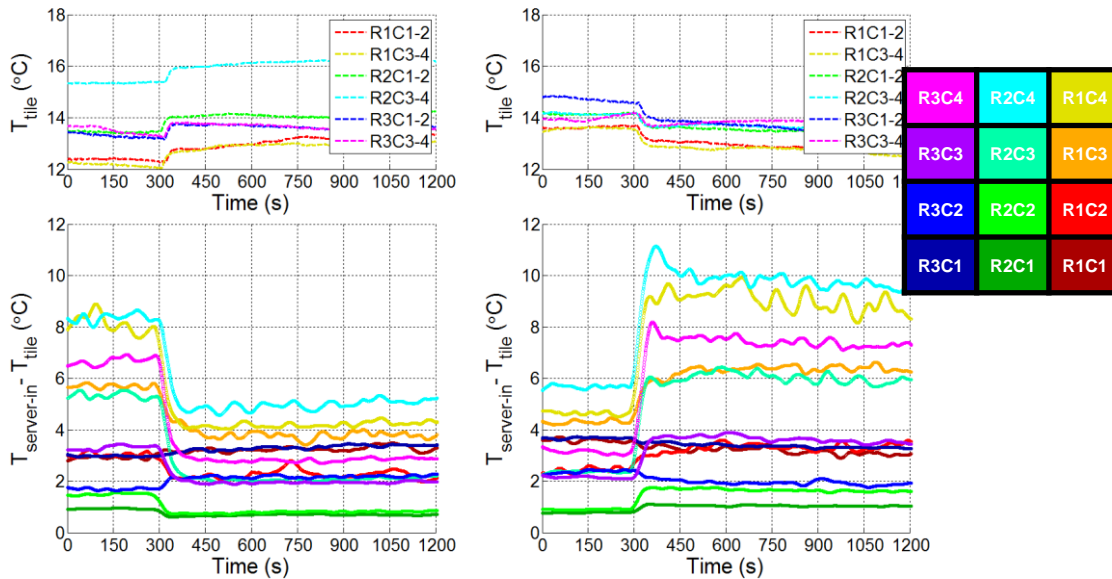


**Figure 3.13: Timeline of events for CRAH flow (CFM) and server power (kW) changes for experiments 4 (a), (b) and (c).**

Figure 3.14 shows the variation of server inlet air temperature difference and tile average temperatures for the concurrent variation of server power and CRAH air flow rate. The main observation was the traces of relatively longer time constants regarding servers compared to the air transients. Accordingly, after decreasing and increasing the air flow rate, any sudden rise and drop in server inlet temperatures is driven by air transients, which is more than an order of magnitude faster than server transients. The slower server response can be observed, respectively, as a gradual increase and decrease in temperatures until steady state temperatures are reached.



Increased CRAH Air Flow Rate and Rack Power  
4600 CFM & 34 kW → 6400 CFM & 45 kW  
@ t=300s

Decreased CRAH Air Flow Rate and Rack Power  
6400 CFM & 45 kW → 4600 CFM & 34 kW  
@ t=300s

**Figure 3.14: Server inlet temperature and tile temperatures during experiment 4a.**

The presence of thermal mass is more pronounced in the results of experiment b and c. Figure 3.15 shows the results for experiment b where rack server power is decreased or increased at t=300 seconds, which is followed by the decreased or increased CRAH air flow rate change after 150 seconds. Within the 150 seconds, neither tile temperatures nor inlet air temperature indicate

a significant change in the operating conditions. This is primarily because of the time constants of the servers, which are on the order of 10 minutes.

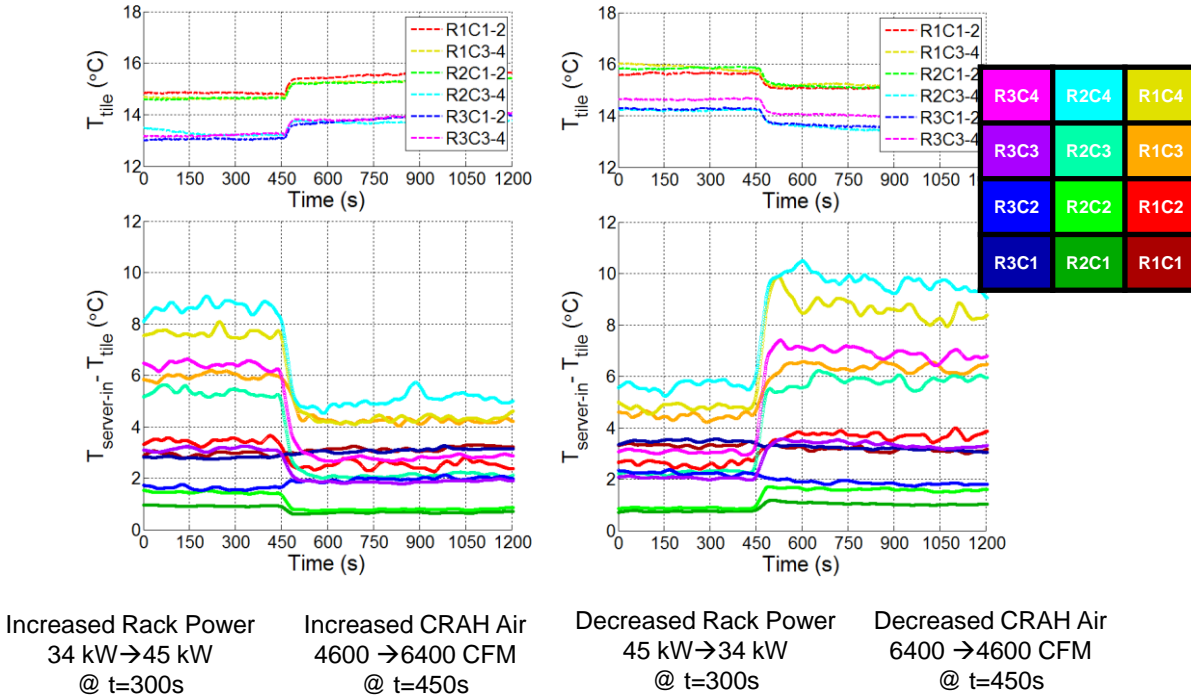


**Figure 3.15: Server inlet temperature and tile temperatures during experiment 4b.**

The slower response of the servers can be clearly observed in the results of experiment 4c. Since CRAH flow rate is changed at t=300 seconds, significant change in the flow field is shown at this time. In the next 150 seconds, the system runs either at high flow and low power or low flow with high power. In a CFD simulation that is blind to server thermal mass, the temperature field would experience a faster response after the change of server power level. However, Figure 3.16 shows a much slower response.

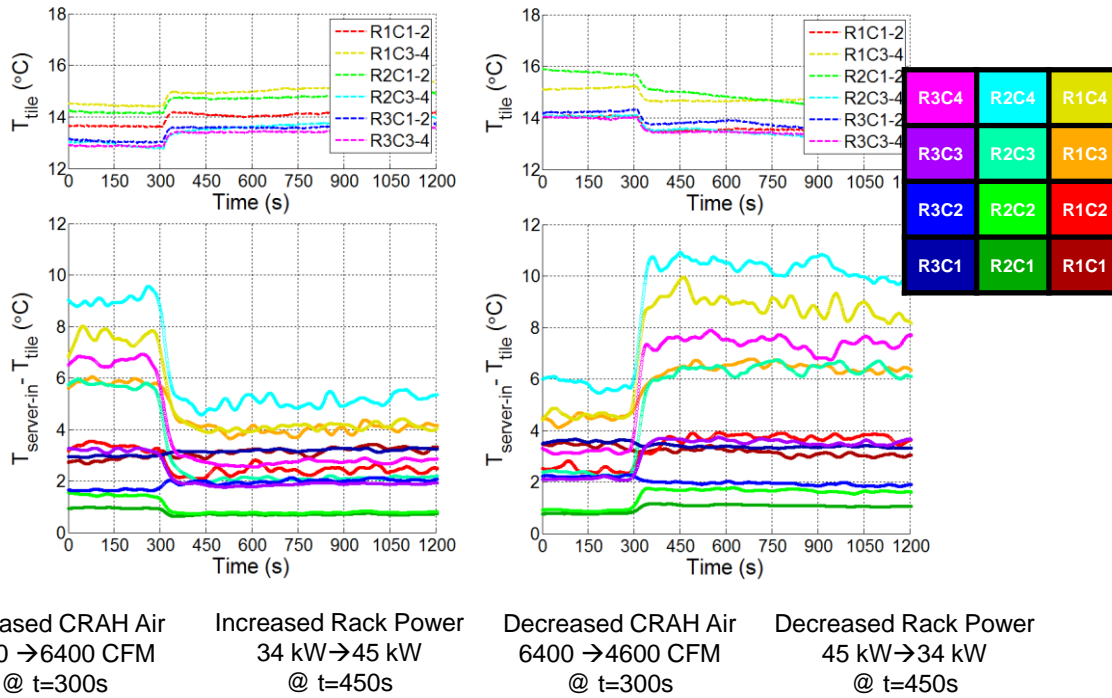


Figure 3.16: Server inlet temperature and tile temperatures during experiment 4c.

### 3.5 Experiment 5a-b: CRAH switching Experiments

Another failure scenario experienced in data centers is the complete loss of a CRAH unit.

Indications of CRAH unit failure can include a loss of pressure in the plenum or emerging hot spots at key locations in the space, which are typically server inlet temperatures in data centers.

Two experiments were designed based on these two indicators. The first experiment represents CRAH units envisioned to respond to a loss of plenum pressure. Since the pressure waves travel at the speed of sound, the experiment was designed so a nonoperational CRAH unit was instantaneously switched on at the moment an operational CRAH was turned off. Both experiments in this section were conducted under constant total rack power of 45 kW, and both CRAH units were set to provide approximately the same tile air flow rate of 6000 CFM when they were active.

Figure 3.17 shows the timeline of events for experiment 5a, in which the non-operational CRAH unit is turned on at the moment when the operational CRAH unit is turned off.

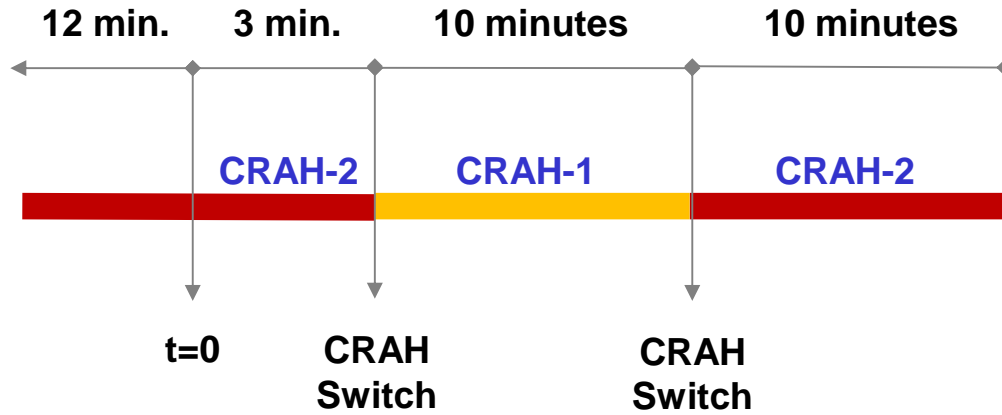


**Figure 3.17: Timeline of events for experiment 5a.**

CRAH-2 remained operational for 25 minutes until switching to CRAH-1 took place. After switching to CRAH-1, the unit was kept operational for 10 minutes and eventually operators switched to CRAH-2 again to prepare for the next set. Similar to previous experiments, this experiment was also repeated six times to have a full coverage of server inlet and exit temperatures.

Recovering the flow field in the RL after CRAH switching took about 30 seconds. This was expected due to the transients related to the CRAH fan ramp-up/down schedule; however, another observation about the CRAH operation was a 85-seconds delayed-response of chilled water valve. Consequently, the servers encountered two waves of rising temperatures, caused by the lack of CRAH air flow supply within the first 30 seconds and chilled water flow delay in first 90 seconds, respectively. Figure 3.18 shows temperature rise at the server inlet of about 5°C. This can be translated that the temperature would hit class A1 limit of 32°C (Figure 1.1) if the highest temperature was at 27°C.

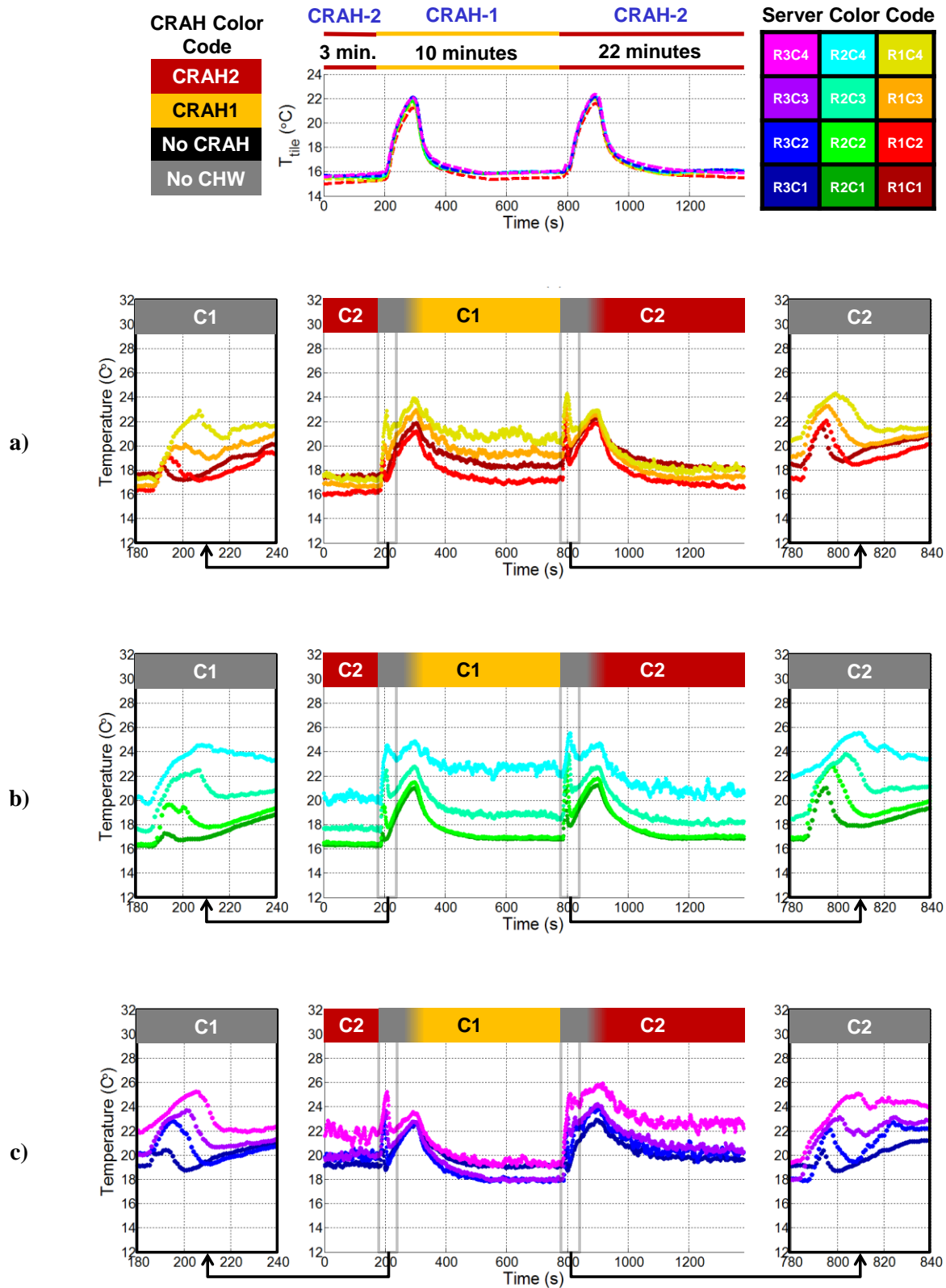


Figure 3.18: Variation of server inlet temperature for a) Rack 1, b) Rack 2 and c) Rack 3.



Figure 3.19 shows the sequence of events during Experiment 5b. Unlike part b, where CRAH switching takes place instantaneously, there is a period of 30 seconds without any CRAH operation. Also, for each of six consecutive sets of the experiment, CRAH-2 and CRAH-1 were operational for a total of 30 and 10 minutes, respectively.

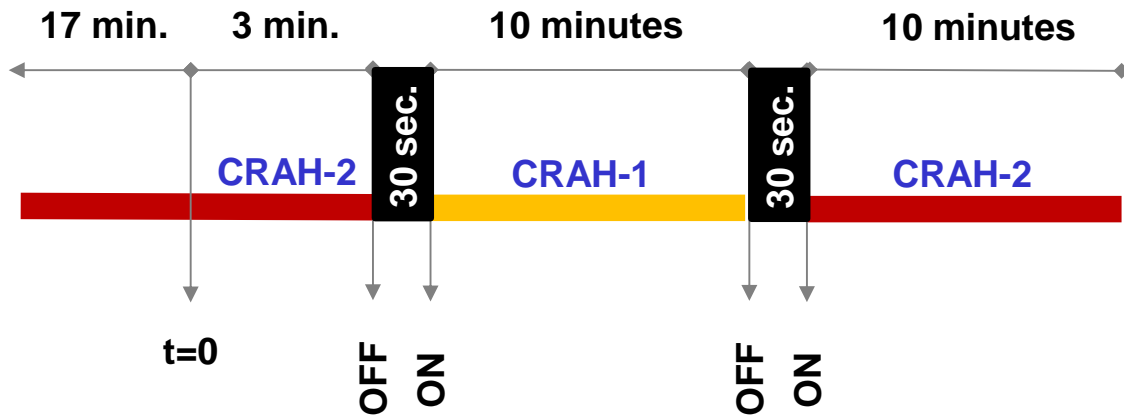


Figure 3.19: Timeline of events for experiment 5b.

As noted in the results of Experiment 5a, the delay of chilled water valve operation plays an important role in the transients of CRAH units. However, as the operation of the CRAH unit was delayed for 30 seconds, the temperature rise caused by the lack of CRAH air flow was pronounced in the results in Figure 3.20. During 30 second period, servers received the hot air they exhausted into the room, so the temperatures kept rising. After about 30 seconds of switching the CRAH, the wildly rising trend of the temperatures was disrupted, and the temperatures dropped to a lower level before they started to rise at a slower pace until the chilled water valves started to open. Figure 3.20 shows temperature rise at the server inlet of about 8°C. This means that the temperature would hit the class A2 limit of 35°C (Figure 1.1) if the highest temperature was at the recommended maximum of 27°C. Beyond 35°C, alarms would be activated in a data center of class A2 (Fig. 1.1), which would be a serious operational emergency.

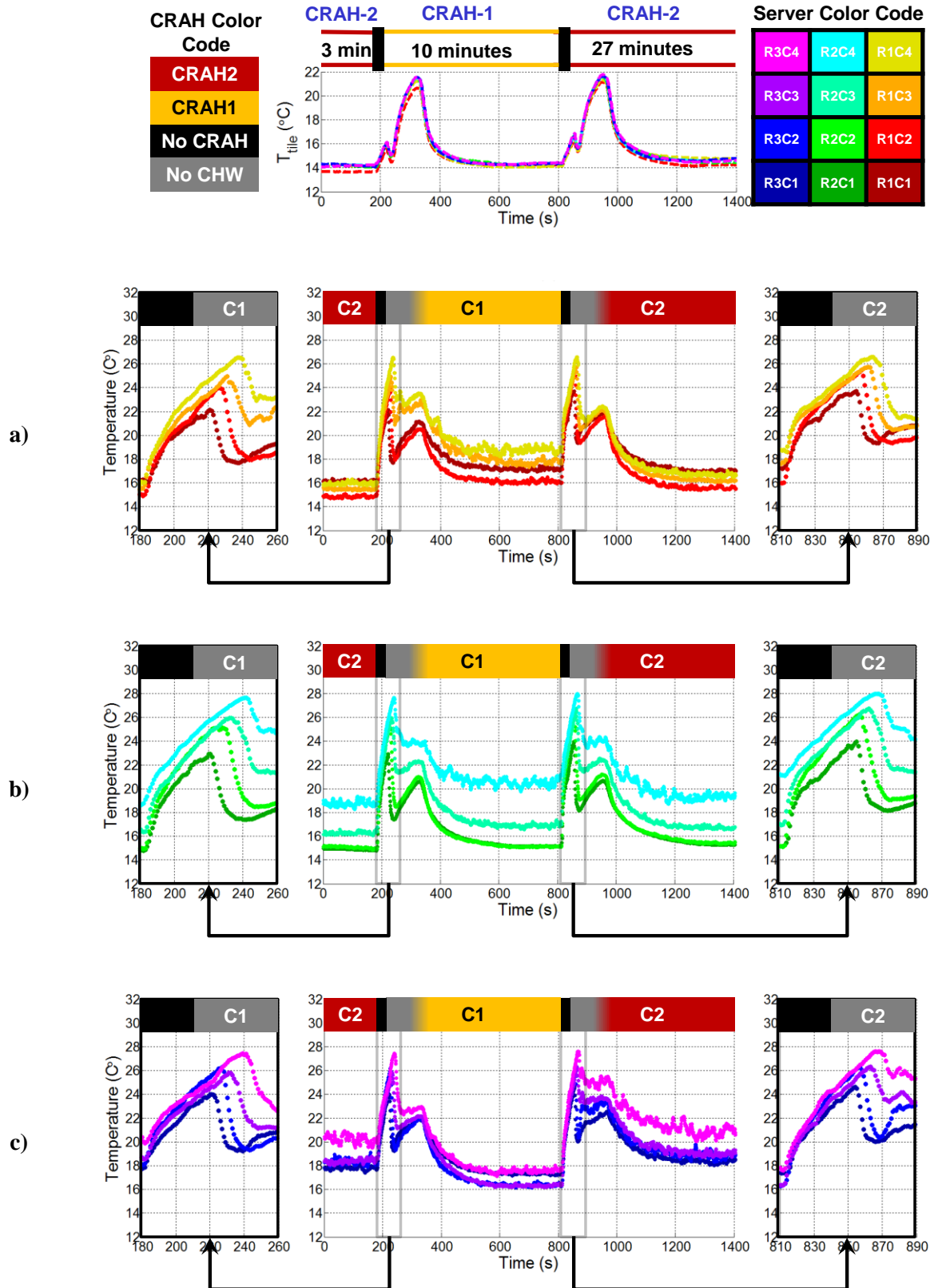


Figure 3.20: Variation of server inlet temperature for a) Rack 1, b) Rack 2 and c) Rack 3.

Experiments 5a and 5b were sufficient to demonstrate a case in which allowable limits of server inlet temperatures were already hit. While the experiment in part a exemplified the significance of the delay in the chilled water valve response, part b showed the severity of the lack of operational CRAH unit in which 90 seconds was sufficient to hit the allowable limits when the data center is operated at the recommended upper limit.

### *3.6 Experiment 6: CRAH Fan Failure Experiment*

Even though the period of operation without CRAH air flow was limited in section 3.5 the allowable temperature limits were exceeded. However, a longer data set is required for a solid verification case for our modeling tools. This experiment was conducted as a single set as opposed to the others which had 6 sets to cover the entire inlet and exit surfaces of the servers due to the limited number of thermocouple frames. In the single set of the experiment, all four of the thermocouple frames were attached to the inlets of R1C3, R1C4, R2C4 and R3C4.

The experiment is conducted at 30% power level (~34.5 kW – 11.5 kW/rack) to allow a longer time for data collection. Figure 3.21 shows the data for 6 minutes during which the CRAH was turned off and the servers did not receive air besides their own exhaust in the room. A temperature rise of 8°C is achieved in about 90 seconds.

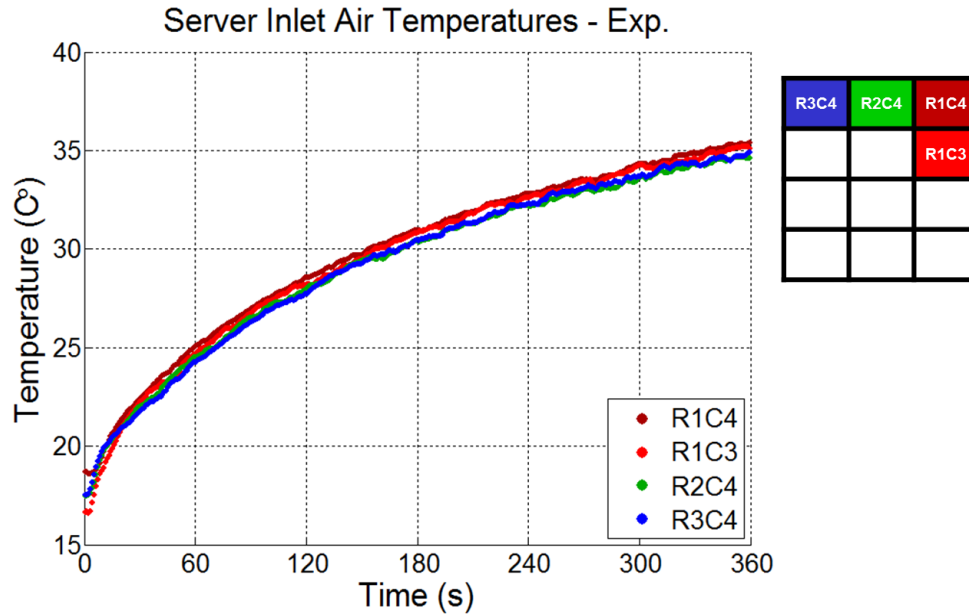


Figure 3.21: Server inlet temperatures for the selection of 4 servers during CRAH fan failure experiment

### 3.7 Uncertainty Analysis for Server Inlet Air Temperature Measurements

Inlet air temperatures into simulated servers were measured by 9 equally spaced thermocouples attached to a wooden frame. The temperatures of interest over the course of this study were the average values of temperature over the surface of the inlet and exit of the servers. Hence, an uncertainty analysis is aimed to quantify the systematic and random error in the reported experimental temperature data of the area-weighted average temperature data over the surface of server inlet and exit.

All of the thermocouples used in the set of experiments to be presented were tested in a chamber (Z-Plus Chamber, model ZP(H) – 32) (Abdelmaksoud, 2012). The majority (212) of 220 thermocouples in the research lab were found to have a mean square error (MSE) of less than  $0.1^{\circ}\text{C}$ , while the remaining 8 thermocouples have a MSE between  $0.1$  and  $0.2^{\circ}\text{C}$  (Abdelmaksoud, 2012). The individual thermocouples that are allocated for the inlet and exit air

temperature measurements of the servers have an average MSE of 0.1°C. Average MSE of the inlet temperatures (0.1°C), data acquisition error of (~0.025°C) and the error due to the possible location error due to misaligned thermocouple frames are taken into account in determining the systematic error. The anticipated maximum horizontal and vertical location errors are 1 inch and 2 inches respectively. Experimental data indicates that maximum horizontal and vertical temperature gradients are 0.91°C/in and 0.375°C/in. Even though some of the servers with negligible recirculation air do not experience these temperature gradients a conservative approach is used and the location errors are assumed to be the same for all servers and experiments.

For each thermocouple bias error can be computed as 1.19°C by using the following equation.

$$b = \sqrt{\sum_1^j b_j} . \quad (2.4)$$

The bias error of the 9-point average server inlet air temperature measurements is then 0.4 by

$$b_{avg} = \frac{b}{\sqrt{n}} , \quad (2.5)$$

where n is the number of thermocouples.

Transient experiments involve controlled changes in the operation of the data center. However, the research lab is not entirely isolated from the rest of the data center. In fact, the same cooling infrastructure of the SUGDC provides the chilled water to the CRAH units in the research lab.

During the experiments, uncontrolled fluctuations in the chilled water temperature were observed that translate into variations in the entire room air temperature field. In order to account for uncertainties of this nature, standard deviation  $\sigma$  of the experimental data is computed based on

steady state data over 300 seconds at a sampling rate of 1 Hz. The data for the periods of steady state operation during transient experiments were collected just before the controlled transient experiments begin. These are periods before which the lab ran under certain air flow and heating power level for at least an hour. Random errors were obtained for all of the experiments that were compared against model results to be discussed in the next chapters. Table 3-3 gives the summary of the maximum random error,  $2\sigma$  (~95% confidence interval) for the readings of the thermocouple frames at the inlet of each simulated server.

**Table 3-3: Random error of average inlet temperatures (°C) over 300 seconds of steady state operation.**

	R1C1	R1C2	R1C3	R1C4	R2C1	R2C2	R2C3	R2C4	R3C1	R3C2	R3C3	R3C4
1	0.25	0.58	0.57	0.37	0.05	0.08	0.18	0.67	0.15	0.19	0.16	0.24
2	0.24	0.34	0.50	0.36	0.03	0.04	0.18	0.62	0.34	0.35	0.40	0.48
3	0.16	0.49	0.37	0.32	0.03	0.06	0.17	0.49	0.18	0.30	0.13	0.24
4	0.26	0.40	0.45	0.82	0.11	0.16	0.52	0.70	0.18	0.20	0.24	0.52
5			0.21	0.36				0.36				0.36

- 1) Exp.1: Rack Shutdown
- 2) Exp.2: Chilled Water Interruption
- 3) Exp.3: CRAH Air Flow Change – High Flow
- 4) Exp.3: CRAH Air Flow Change – Low Flow
- 5) Exp.7: Repeated CRAH Fan Failure

The error analysis can be concluded by calculating the total uncertainty by

$$u = \sqrt{b^2 + p^2} , \tag{2.6}$$

where b stands for systematic (bias) error and p for random (precision) error (Tavoularis, 2005).

The total uncertainty values are tabulated similarly in Table 3-4.

**Table 3-4: Total uncertainty of average inlet temperature over 300 seconds of steady state operation at 1 Hz.**

	R1C1	R1C2	R1C3	R1C4	R2C1	R2C2	R2C3	R2C4	R3C1	R3C2	R3C3	R3C4
1	0.47	0.70	0.69	0.54	0.40	0.40	0.44	0.78	0.42	0.44	0.43	0.46
2	0.46	0.52	0.64	0.53	0.40	0.40	0.43	0.74	0.52	0.53	0.56	0.62
3	0.43	0.63	0.54	0.51	0.40	0.40	0.43	0.63	0.43	0.49	0.42	0.46
4	0.48	0.57	0.60	0.91	0.41	0.43	0.65	0.80	0.43	0.44	0.46	0.65
5			0.45	0.53				0.54				0.53

- 1) Exp.1: Rack Shutdown
- 2) Exp.2: Chilled Water Interruption
- 3) Exp.3: CRAH Air Flow Change – High Flow
- 4) Exp.3: CRAH Air Flow Change – Low Flow
- 5) Exp.7: Repeated CRAH Fan Failure

## 4 Thermal Characterization and Modeling of Servers for Transient Simulations

Thermal transient behavior of a server can be approximated by a lumped parameter system approach. This chapter introduces a single black-box model representing a server and how to obtain the associated parameters to have a working thermal model of a server. In order to utilize the model, appropriate characteristic parameters - time constants, thermal conductance and thermal capacitance - need to be obtained. Later subsections of this chapter propose a set of practical experiments to estimate these parameters that govern the characteristic behavior of servers under unsteady operating conditions. Finally, parameters specific to the simulated servers will be obtained using the techniques introduced.

### 4.1 Transient Modeling of Servers

Figure 4.1 shows schematics of the black-box model for a server that is cooled by a stream of air flow. Assuming that thermal capacitance of the servers can be defined as  $C_s$ , first-order transient system behavior is governed by the equation in 4.1.

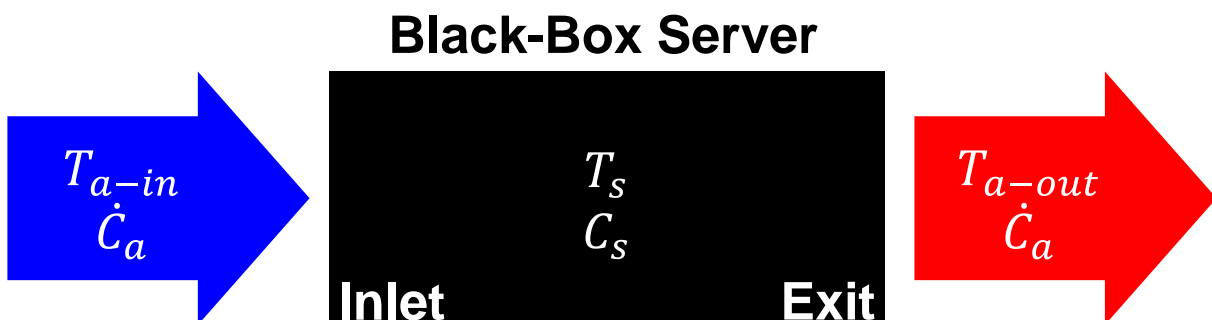


Figure 4.1: Simplified schematics of a transient server model.



Time-dependent exit air temperature of a server can be computed based on the solution of the lumped parameter transient energy balance equation. The governing equations for the unsteady energy balance of the server and air stream are

$$C_s \frac{dT_s}{dt} = \dot{Q}_s - \dot{C}_a (T_{a-out} - T_{a-in}), \quad (4.1)$$

$$\dot{C}_a (T_{a-in} - T_{a-out}) = \varepsilon \dot{C}_a (T_{a-in} - T_s), \quad (4.2)$$

where  $\varepsilon = 1 - e^{-NTU}$ .

After simplifications, the first order differential equation takes the form of

$$C_s \frac{dT_s}{dt} = \dot{Q}_s - K(T_s - T_{a-in}), \quad (4.3)$$

where

$$K = \varepsilon \dot{C}_a. \quad (4.4)$$

The time constants for the first order differential equation given in Equation 4.3 is defined as,

$$\tau = \frac{C_s}{K}. \quad (4.5)$$

The next sections discuss practical experimental techniques to extract these parameters for servers.

## 4.2 Simple Characterization of Transient Behavior of Servers

Equation 4.3 is solved to obtain the transient temperature of the lumped thermal mass of the server, which is required to compute the heat transfer between the air stream and server.

Subsequently, resultant heat transfer between the server thermal mass and air stream is used to determine the transient temperature rise leading to the exit air temperature of the server.

The rack shutdown experiment is proposed to extract the time constants of servers. The heater power was turned off at  $t = 0$  while the server fans are kept running at a constant speed. Defining  $\Theta = \dot{Q}_s / K - T_s + T_{a-in}$ , the differential equation in 4.3 has the exact solution of

$$\Theta(t) = \Theta(0) \exp(-t / \tau). \quad (4.6)$$

The air residence time inside the server is short ( $\sim 1$ s). Therefore, the air transients are negligible.

The convective heat transfer equation dictates that

$$K(T_s - T_{a-in}) = \dot{C}_a (T_{a-out} - T_{a-in}). \quad (4.7)$$

The air temperature difference across the server,

$$\Delta T_a = (T_{a-out} - T_{a-in}), \quad (4.8)$$

can be shown to follow the same first-order behavior governed by the same time constant,  $\tau$ , as in the case when the server inlet temperature is constant. Therefore, the time constant can be obtained experimentally from the inverse of the slope of the following expression

$$\ln \frac{\Delta T_a(0) - \Delta T_a(\infty)}{\Delta T_a(t) - \Delta T_a(\infty)} = \ln \frac{\theta_i}{\theta} = t / \tau. \quad (4.9)$$

Whether the system exhibits a first-order behavior can be ascertained from the linearity of the  $\ln(\theta_i/\theta)$  vs.  $t$  data (Figure 3.5). Another justification for the lumped capacitance approach for the simulated servers can be shown through Biot number for the heater plates ( $\sim 10^{-3} \ll 0.1$ ) according to,

$$Bi = \frac{hL_c}{k}, \quad (4.10)$$

where  $h$  can be estimated (as  $\sim 18.5 \text{ W/m}^2\text{K}$ ) by the channel flow heat transfer calculations provided in Section 2.5.1. Characteristic length  $L_c$  is the half of the plate thickness ( $L_c=3.175 \text{ mm}$ ) and  $k$  is the thermal conductivity of carbon steel ( $49.8 \text{ W/mK}$ ). The time constant (Eq. 4.5) for the first order differential equation (Eq. 4.3) is given in terms of thermal conductance and thermal capacitance. Obviously, the time constant by itself is not sufficient to solve the governing equations. Two of the three parameters ( $\tau$ ,  $C_s$  and  $K$  in equation 4.5) are required to construct a working mathematical model of Equations 4.3 and 4.7 for the time-dependent server behavior.  $K$  requires the knowledge of the average surface temperatures inside the server, which is not available. Similarly, the server thermal capacitance  $C_s$  cannot be determined without weighing and measuring the temperature of components and knowing their specific heats, which is clearly impractical. Inlet and exit air temperatures are easily measured and can be employed to estimate the server heat capacity or thermal conductance as described below.

The proposed technique of extracting thermal conductance or capacitance is based on a case where server inlet air temperature is decreased almost instantaneously. The governing equations were solved for this case, and Figure 4.2 shows the transient response of server air temperature rise  $\Delta T_a$ , following the sudden drop in the inlet air temperature. The change in the inlet air temperature is equal to the change in the server thermal mass temperature (assumed to be uniform in lumped capacitance formulation) after it reaches a steady state ( $\Delta T_{a-in}=\Delta T_s$ ). Meanwhile, the spike in the server air temperature difference is indicative of the transient release of heat from the thermal mass of the server into the air stream.

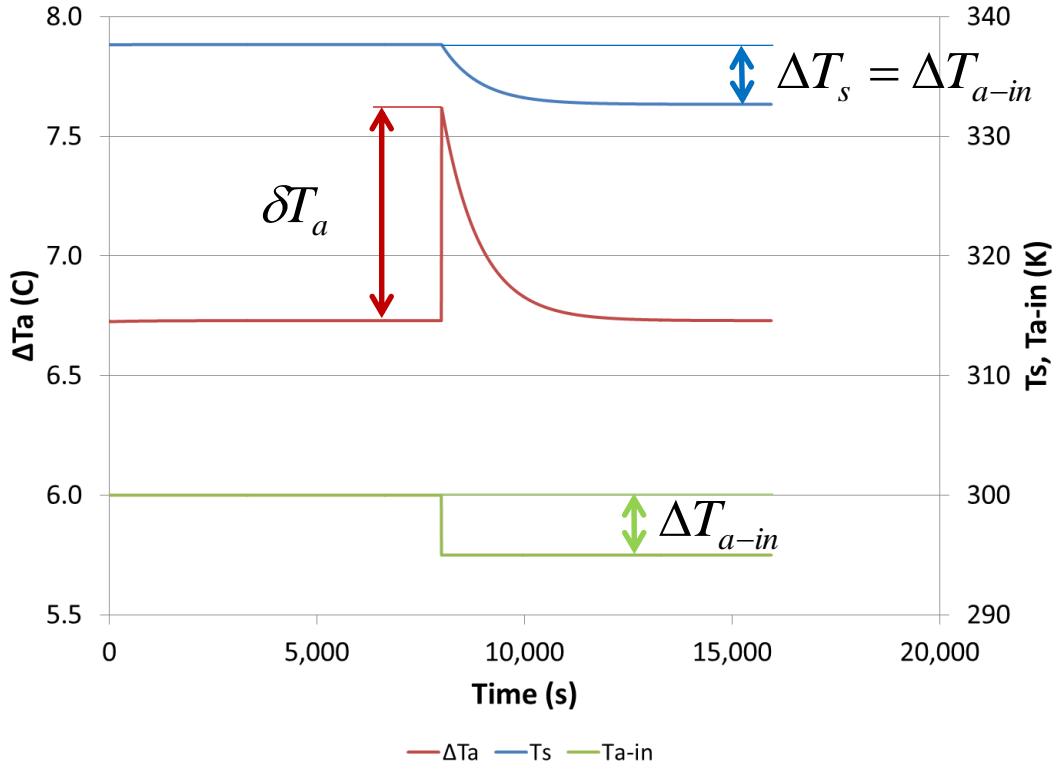


**Figure 4.2: Sample solution of transient energy balance for sudden decrease in server inlet temperature.**

The loss of internal energy of the server is equal to the total heat transferred owing to the increased temperature difference between the server and the air stream until new equilibrium temperatures are reached. The total amount of heat transfer beyond the generated heat is the integrated area under the  $\delta T_a$  vs.  $t$  curve after the spike  $\delta T_a$  occurs in  $\Delta T_a$ , viz.

$$C_s \Delta T_{a-in} = \int_0^{\infty} \dot{C}_a \delta T_a e^{-t/\tau} dt. \quad (4.11)$$

By solving Equation 4.11, the thermal capacity of the server can be defined as

$$C_s = \frac{\tau \dot{C}_a \delta T_a}{\Delta T_{a-in}}. \quad (4.12)$$

While this expression can be used to calculate the thermal capacitance of the servers, by replacing the definition of time constants in Equation 4.5, a prediction equation for the thermal conductance  $K$  can be obtained as

$$K = \dot{C}_a \varepsilon = \frac{\dot{C}_a \delta T_a}{\Delta T_{a-in}}. \quad (4.13)$$

which can be used to estimate the thermal conductance  $UA$  for servers,

$$UA = -\dot{C}_a \ln \left( 1 - \frac{\delta T_a}{\Delta T_{a-in}} \right). \quad (4.14)$$

This equation is independent of estimated quantities, such as time constants. Therefore, it is a direct measure of thermal conductance of the server.

As indicated in the results of Experiment 3, “Reduction in CRAH Air Flow Rate”, the height of the spike,  $\delta T_a$ , observed in the server air temperature difference  $\Delta T_a$  for the top servers, represents a similar behavior. Utilization of the method proposed leads to thermal capacitance values for the simulated servers which are comparable to the estimates based on the weight and specific heats of the material content. Relevant discussion will be provided in later sections of this chapter.

### 4.3 Time Constants of Simulated Servers

Experimental data to extract time constants originates from the transient temperature difference of server air during the rack shutdown experiment introduced in Figure 3.4 of Chapter 3. The time constants are obtained in accordance with Eq. 4.9 from the slopes of the straight lines displayed in Figure 4.3. The difference between the initial air temperature rise at high power

levels and steady state air temperature rise at idle power levels is defined as  $\theta_i$ . Being a function of time,  $\theta$  is defined as the difference between the steady state and instantaneous air temperature differences.

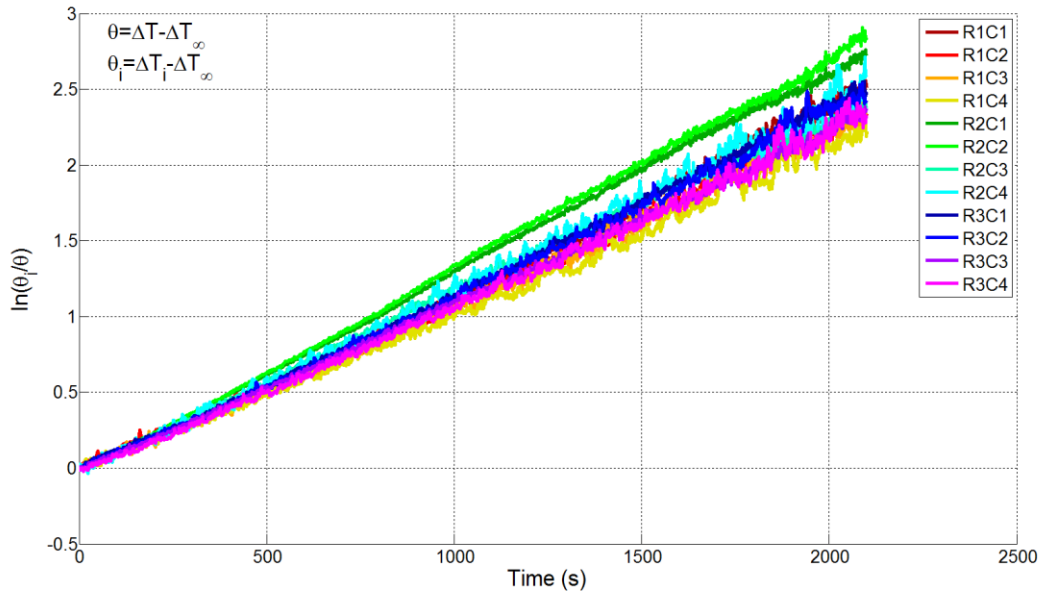


**Figure 4.3: Natural logarithm of normalized temperature difference to estimate server time constants.**

Using a logarithmic form of the time constant equation provides trends which are linear over a long time span, which is the characteristic of the exponential first-order behavior. Departure from the exponential behavior becomes more pronounced as the steady state is approached due to the high uncertainty as temperature difference approaches zero. The time constant values depend on the slope of the relatively linear portion of the graph, where the coefficient of determination,  $R^2$ , for the linear fit is higher than 0.99. The extracted time constant for the given data in Figure 4.3 is approximately 13 minutes. Figure 4.4 shows extracted time constants as a function of measured server flow rates. Overall, shorter time constants due to slightly higher flow rates of Type B servers (R2) can be observed even though R2C3 and R2C4 seem to be closer to the Type A servers (See Chapter 2.6 for Type A and B servers). At the same time, it is

notable to mention that extracted time constants are relatively higher compared to that of IBM Blade Center, after which simulated servers have been designed. The BladeCenter time constant was obtained as about 5 minutes which is relatively shorter than the time constants of the simulated servers. This is most likely due to the simple structure inside the simulated servers as opposed to the packed flow path in BladeCenter where the thermal conductance are expected to be higher.

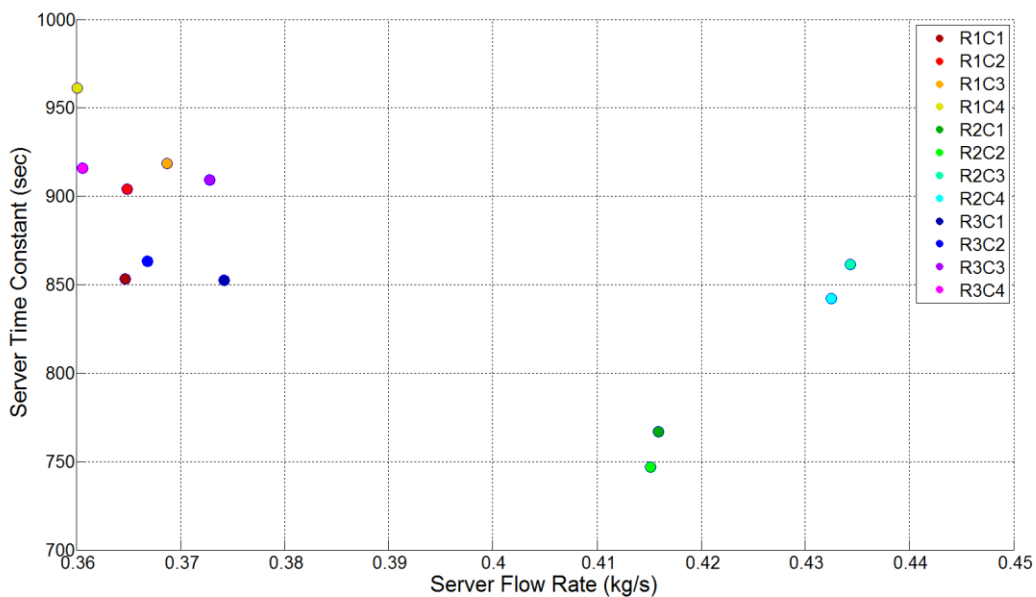


**Figure 4.4: Estimated server time constants as a function of server air mass flow rate.**

Extracted time constants are useful in combination with the known initial conditions, transient inlet air temperatures and estimated steady state values. Based on Equation 4.9 the entire transient trend of air temperatures at the exit of the servers can be predicted. Figure 4.5 shows an excellent agreement between the first-order lumped parameter model prediction and the experimental results as expected. This verifies the accuracy of the first-order system assumption for the thermal behavior of the servers.

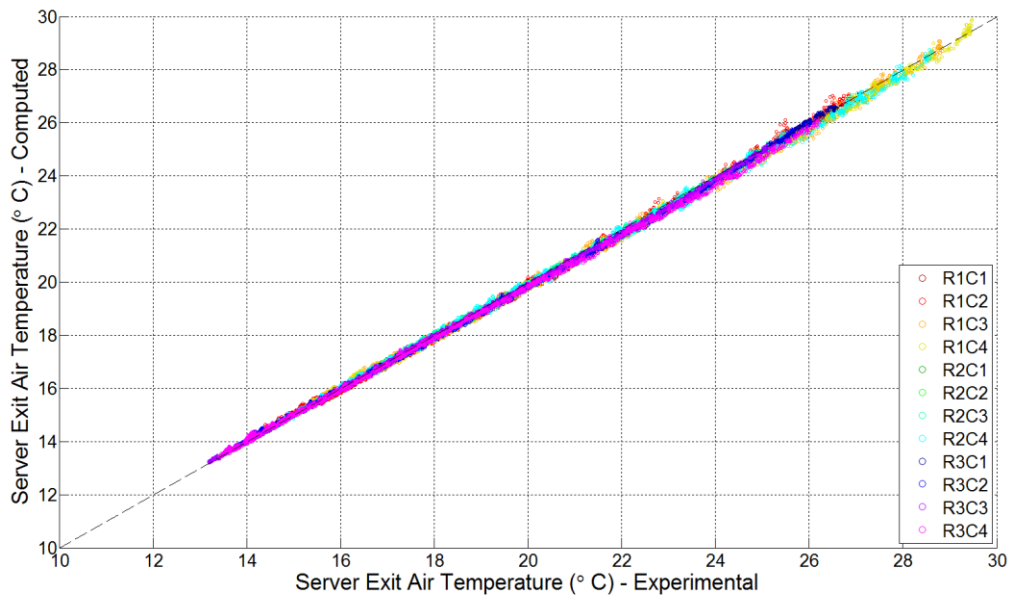


**Figure 4.5: Server exit air temperature computed based on lumped capacitance model vs. experimental data.**

#### 4.4 Thermal Conductance and Capacitance of Simulated Servers

Data center air space is dominated by the high momentum air flow through perforated tiles and servers, which results in a high number of air changes per hour (ACH). Typical air change rate in data centers is of the order of 60 ACH. Hence, air transients are expected to be fast and primarily a function of the number of air changes in the data center space. The following experiment is part of the experiment described in Chapter 3.3, titled “Sudden Change in CRAH Air Flow Rate”.

There we focus on the transient event where CRAH air flow rate is suddenly increased in the RL. Rack power was kept constant at 34.4 kW (the total for 3 racks) throughout the experiment.

Before air flow was changed from low (4600 CFM) to high (6400 CFM), the system ran about an hour to reach the steady state conditions. Figure 4.6 shows the air temperature difference across the server and inlet air temperature measurements for the top chassis side by side, following a sudden increase in the CRAH air flow rate.



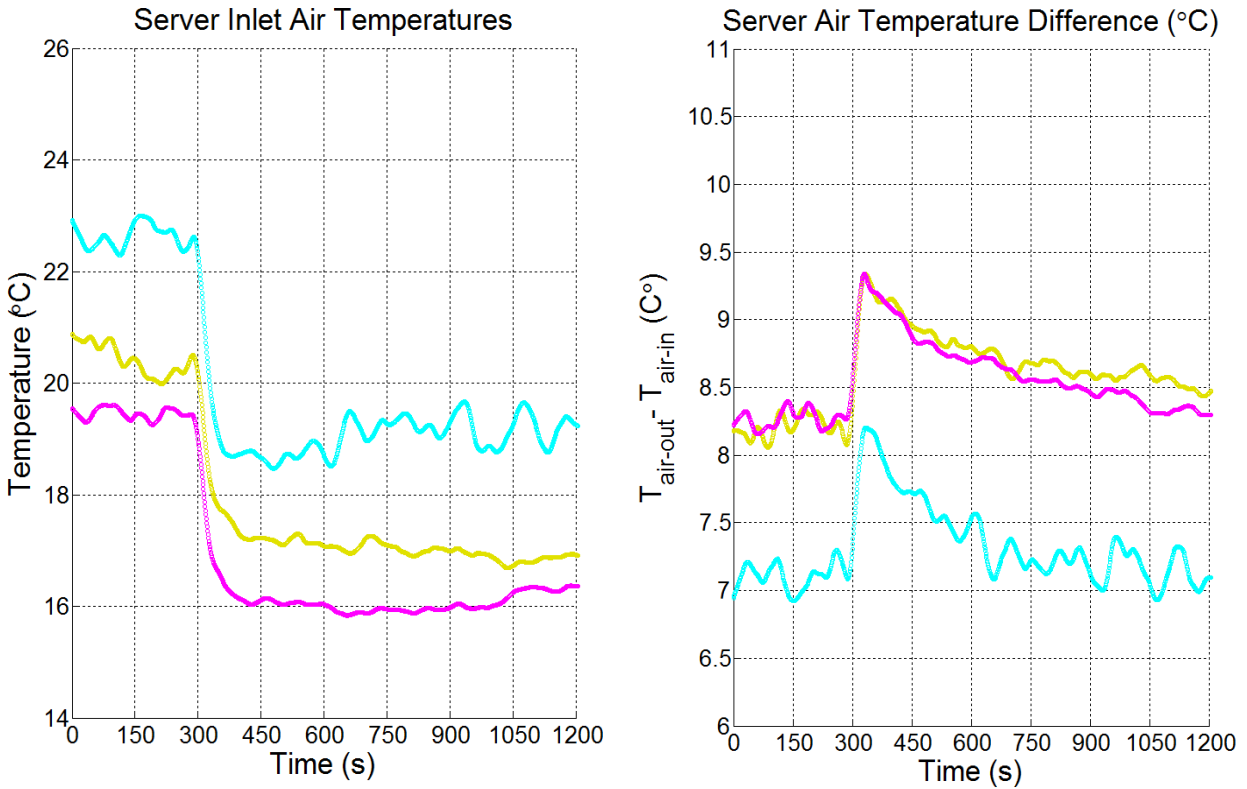


**Figure 4.6: Variation of server air temperature difference in response to changing inlet air temperatures (due to sudden increase in the CRAH air flow rate at  $t=300s$ ).**

The height of the spike in the air temperature difference is indicative of the characteristic thermal capacitance of the server as explained above. Estimation of thermal capacitance of the simulated server without the rack doors at the back and front is approximately 70 kJ/K based on the properties of the material content. Adding the rack doors leads to a thermal capacitance of approximately 85 kJ/K. Application of the method on the top 3 chassis leads to thermal capacitances of 95 kJ/K, which are comparable. The difference can be attributed to the frames, rails and other interior parts the servers are in contact with inside the rack enclosure. On the other hand, the experimental results can also be used to directly estimate  $UA$  through Eq. 4.14 which leads to values of approximately 120 W/K for servers (R1C4 and R3C4) relatively lower flow rates and 140 W/K for higher flow server (R2C4).

## 4.5 Chapter Conclusions

This chapter introduces two practical experiments to extract the thermal characteristics of servers. Simulated servers tested in this study operated at constant fan speeds. In our recent paper (Smith et al., 2011) about the design of the simulated servers indicated that there is a negligible variation in the time constant at different power levels. On the other hand, fan speeds of real servers are likely to be controlled by algorithms depending on workload or temperature measurements. In such cases, servers would require testing at various controlled flow conditions, so that a map of time constants can be obtained for a range of server operation.

Server time constant can be obtained through rack shutdown experiment. However, a time constant is not the only parameter required to enable the solution of the unsteady heat balance equation for a black-box servers. One of the major contributions of this study is the development of a method to extract thermal capacitance of the server through air temperature measurements at the inlet and exit. The verification of the method is conducted based on the assumption that air transients are fast. Additionally, low temperature variations,  $\sim 4^{\circ}\text{C}$ , observed here could have contributed to the observed deviation between the experimentally determined capacitance and that determined directly from the mass and specific heat of the simulated servers. We expect that better test environments with faster and larger inlet temperature variations may be provided in better controlled test tunnels at the manufacturers' facilities.

## 5 Room-Level Transient CFD Simulations

CFD simulations are commonly used to investigate data center thermal environments. However, boundary conditions for transient simulations must account for the thermal capacitance and time response of embedded black box servers. Transient boundary conditions for computing equipment are not represented in commercial CFD packages. Hence, transient CFD simulations are not reliable when the thermal transients of large masses are as important as they are in data centers. This chapter discusses the implementation of the transient black box server model, introduced in Chapter 4, into a commercial CFD code via user-defined functions. The simulations herein were performed using several versions (12.1 and 14.0, 14.5) of ANSYS FLUENT on the grids generated via Gambit 2.4.6.

### 5.1 Numerical Modeling Overview

Data center thermal environmental conditions are governed by conservation equations of mass, momentum and energy along with appropriate turbulence models. ANSYS FLUENT provides the platform to solve these equations for a given geometry using the Finite Volume Method.

The mass conservation equation for unsteady compressible flow is,

$$\frac{\partial \rho}{\partial t} + \frac{\partial(\rho u_i)}{\partial x_i} = 0. \quad (5.1)$$

Air flow in data centers can be assumed incompressible for typical velocities of 1 m/s. For incompressible flow continuity, the equation reduces to,

$$\frac{\partial u_i}{\partial x_i} = 0. \quad (5.2)$$

By applying Reynolds decomposition to the Navier-Stokes equation, Reynolds Averaged Navier Stokes (RANS) equations can be obtained,

$$\frac{\partial(\rho u_i)}{\partial t} + \frac{\partial(\rho u_i u_j)}{\partial x_j} = -\frac{\partial p}{\partial x_i} + \frac{\partial}{\partial x_j} \left[ \mu \left( \frac{\partial u_i}{\partial x_j} + \frac{\partial u_j}{\partial x_i} - \frac{2}{3} \delta_{ij} \frac{\partial u_l}{\partial x_l} \right) \right] + \frac{\partial}{\partial x_j} (-\rho u'_i u'_j), \quad (5.3)$$

which is solved in FLUENT. The last term on the right-hand side is called Reynolds Stresses, which consists of the fluctuating components,  $u'$ , of the velocity components. This term requires an appropriate turbulence modeling for a closure. The standard, two-equation, k- $\epsilon$  model is one of the turbulence models that were used in this study.

The ANSYS FLUENT solves the energy conservation equation

$$\frac{\partial(\rho E)}{\partial t} + \frac{\partial(u_i(\rho E + p))}{\partial x_i} = \frac{\partial}{\partial x_j} \left[ k_{eff} \frac{\partial T}{\partial x_j} + u_i (\tau_{ij})_{eff} \right] + S_h, \quad (5.3)$$

where the first term on the right-hand side represents the energy transfer by conduction via the effective conductivity  $k_{eff}$ , representing the sum of the molecular and turbulent thermal conductivity. The second term represents the energy transfer through viscous dissipation. Any volumetric heat generation is accounted for in the source term  $S_h$ .

The total energy E is defined as a function of static enthalpy, the kinetic energy and pressure work.

$$E = h - \frac{p}{\rho} + \frac{V^2}{2}. \quad (5.3)$$

For an incompressible flow, kinetic energy and pressure work terms are negligible such that pressure-based solver, by default, does not consider these terms. The density and pressure are functions of temperature for an ideal gas. If the temperature variations in the domain are no longer negligible, buoyancy effects become important and the energy equation needs to be solved simultaneously with the momentum equation.

In data centers where the flows are primarily momentum-driven, buoyancy effects are not as significant as they are in an office environment. Abdelmaksoud (2012) defined an Archimedes number for data centers to quantify the importance of buoyancy,

$$Ar = \frac{\beta g L \Delta T}{U^2}, \quad (5.3)$$

where  $\beta=1/T$  is thermal expansion coefficient for the tile air in this case, L is the characteristic length scale, which is assumed to be the height of the rack as 2 m;  $\Delta T$  is the temperature rise across the servers, and U is the characteristic (tile) velocity. An Archimedes number of unity implies comparable contribution of inertial and buoyancy forces. The initial conditions of rack shutdown experiment correspond to a case where  $Ar \sim 1$ . After the power is turned off, the buoyancy effect will gradually decrease over the course of the experiment. The failure scenarios are conducted at lower power levels, which are initially primarily momentum-driven flows. As the air temperature rises, following a failure in the room, buoyancy effects may become important.

Data center simulations require many simplifications to reduce the range of length scale of the problem. For instance, the server can be modeled as black-box heat addition models to avoid modeling the details inside a server. Similarly, it is not practical to model the small openings of the tiles. Instead, the common practice is to introduce tiles as fully open surfaces. However, this approach lacks the ability to account for the momentum that has been lost by smearing out the small jets of an actual tile. Abdelmaksoud (2012) proposed a body force model to account for the deficit in momentum in a volume just above the tile,

$$F = \frac{1}{V} \rho \dot{V} \left( \frac{\dot{V}}{\sigma A_{tile}} - \frac{\dot{V}}{A_{tile}} \right). \quad (5.4)$$

Here  $V$  represents the volume,  $\dot{V}$  is the volume flow rate,  $A_{tile}$ , and  $\sigma$  is the porosity of the tile.

As a result of the parametric study conducted by Abdelmaksoud (2012), reasonable agreement in the coarse grid (4") CFD simulations are obtained. The effect of tile turbulence boundary conditions on the overall temperature distribution at the inlet of the servers was mentioned previously. Figure 5-1b shows one of the coarse grid cases (as noted as Case 9 in the reference) obtained by Abdelmaksoud, compared to the experimental data in Figure 5-1a. In this simulation, another step is introduced beyond Abdelmaksoud (2012): namely, using a turbulent length scale that is a fraction of the tile size rather than a fraction of the small perforations in the tile. The results in this chapter are based on this new, longer turbulence length scale boundary condition. The server inlet temperature contours for that case are depicted in Figure 5-1c. The results are noticeably different. However, the major observation is that the entrainment of warm air at the lower edges of the aisles still requires additional work.

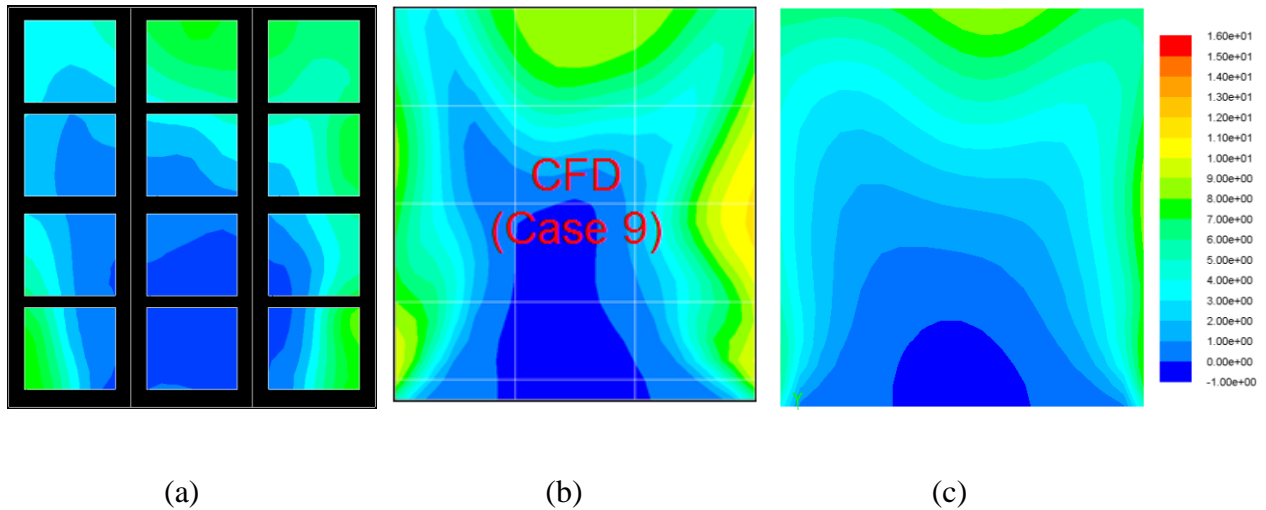


**Figure 5.1:  $T_{inlet}-T_{tile}$  (a) Experiment; (b) Short Turbulent Length Scale (Abdelmaksoud, 2012); (c) Long Turbulent Length Scale**

The scope of this study did not extend to improving the current steady-state data center CFD simulations. Instead, the primary contribution regarding CFD is to introduce a physics-based transient server exit boundary condition. Hence, the accuracy of the results is limited by the capabilities of the current steady-state CFD practices.

## *5.2 Rack Shutdown Experiment for the Verification of Proposed User-Defined Function in CFD*

The rack shutdown experiment is designed to investigate transient behavior of the data center test cell between two operating modes at two server power levels. Many types of virtualization techniques can be considered as similar realistic scenarios in real data centers. Large variation in the power level is expected to lead to larger temperature differences, which are significantly larger than the experimental accuracy.

According to the experimental procedure, all servers were switched to the idle mode at time=0, after running at a total heat load of about 45 kW for about an hour. Idling servers typically

consume about 300 W just due to the constantly spinning fans. The initial and idling power values and the air flow rates for simulated servers are given in Table 5-1.

**Table 5-1: Heating Loads and Air Flow Rates for Simulated Servers**

Server	Initial Load (W)	Idle Load (W)	Air Flow Rate (CFM)
R1C1	3715	259	664
R1C2	3680	253	664
R1C3	3688	251	673
R1C4	3700	253	660
R2C1	3826	360	748
R2C2	3813	348	748
R2C3	3820	354	785
R2C4	3785	348	790
R3C1	3679	261	678
R3C2	3690	272	664
R3C3	3657	259	673
R3C4	3636	248	655

**\* R1C1 is the bottom server of Rack 1**

**\* Rack 1 is closer to the operational CRAH unit, CRAH 1**

CRAH 1 was operational for the entire experiment, and CRAH 2 was sealed to prevent any backflow from the pressurized plenum into the room space. The fans in CRAH 1 as well as the simulated server fans were kept at constant speeds. That is, the flow pattern in the room was disturbed as little as possible. The chilled water valve in the CRAH unit was forced to remain open throughout the experiment by setting a low CRAH return air set point temperature of 10°C, which was never reached during the test.

As discussed in Chapter 4, the simple lumped capacitance model requires that two of the three parameters (i.e. Time Constant, Thermal Conductance and Thermal Capacitance) be known in order to solve the first order differential equation. While the time constant obtained in this study is obtained through the experimental data of the rack shutdown experiment and given in Table 5-2, thermal capacitance is 95 kJ/K as it was obtained in Chapter 4.4.



**Table 5-2: Extracted time constants of simulated servers and thermal capacitance assumption based on material properties**

Simulated Server	Time Constant, $\tau$ (s)
R1C1	817
R1C2	887
R1C3	889
R1C4	930
R2C1	752
R2C2	729
R2C3	865
R2C4	821
R3C1	830
R3C2	838
R3C3	895
R3C4	879
Thermal Capacitance, $C_s$ (J/K)	95,000

The transient rack shutdown experiment is simulated using the commercial CFD software, ANSYS FLUENT, and the 3 dimensional geometry of the 3-rack RL data center without the plenum as shown in Figure 5.2.

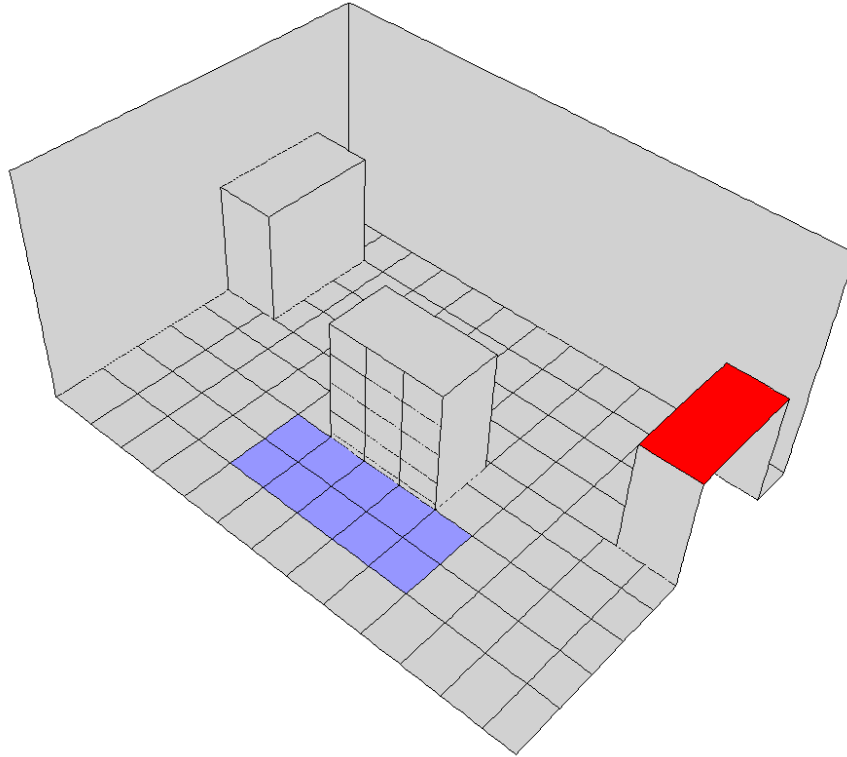


**Figure 5.2: The 3-rack RL data center model geometry (Red: Operating CRAH, Blue: Open Tiles)**

Model specifications and key boundary conditions are given in Table 5-3. The CFD model of interest in this study does not include the plenum. Instead, the measured air flow rates and temperatures are specified at the tile as they are given in Tables 5-4 and 5-5.

**Table 5-3: Summary of CFD model specifications and boundary conditions**

Grid Size	~150,000 cells		
Buoyancy	Yes (Incompressible Ideal Gas Model)		
Turbulence	Length Scale (mm)	Tile	60
		Server Exit	55
	Kinetic Energy ( $m^2/s^2$ ) $\times 10^2$	Tile	110
		Server Exit	9
Model	Standard k- $\epsilon$		
Floor, Ceiling and Wall BCs	Adiabatic		
Momentum Source Model (Abdelmaksoud, 2012)	Tile	Yes	
	Server Exit	Yes	

**Table 5-4: Measured air flow rates through perforated tiles**

a	b	1	2	3	4	5	6	C	d
500	612	584	659	678	697	673	687	659	683

**Table 5-5: Temperature boundary conditions for the open perforated tiles**

a	b	1	2	3	4	5	6	c	d
14.3	14.2	13.8	14.0	13.1	13.7	13.8	13.7	13.6	13.3

### *5.3 User-Defined Function (UDF) for Transient Server Exit Air Temperature*

This section elaborates on the structure and setup of the user-defined function (UDF) to incorporate the transient air temperature boundary condition at the exit of the servers. Written in C language, UDFs allow users to modify FLUENT boundary conditions to address specific requirements of the problem. FLUENT provides access to special macros and functions through several header files. The default UDF library is named `udf.h`, and it has to be included to access many available macros in FLUENT. The users can read certain variables at various cells and faces. Aside from the general UDF library, `unsteady` (`unsteady.h`) and parallel computing (`para.h`) functions were also required as part of this study. These header files need to be called at the beginning of the UDF files. The UDF file used in this study can be found in the Appendix B.

The general structure of the UDF can be divided into four parts; Inputs, Monitors, Calculations and Data Saving. For each server, the user needs to specify inlet and exit surface ID, mass flow rate, flow area, thermal capacitance, time constant, and the time of the transient event. Since the transient event in this study is rack shutdown, initial and new heat loads were also specified.

Given the surface IDs of respective server inlet surfaces and handled by the `DEFINE_ADJUST` macro, area weighted average of the inlet and exit air temperatures are computed here. These

values are then passed into the calculations of lumped capacitance model for each server, which takes place in the `DEFINE_PROFILE` macro to impose the transient air temperature at the exit of each server.

This UDF computes three temperatures internally: the temperatures at the inlet and exit of each server and the temperature of the lumped body. The values corresponding to these variables need to be available during the compilation process or anytime when the compiled FLUENT case is being loaded. Hence, text files needed to be located in the same directory of the case file for each server, which gives access to values for the three corresponding temperatures. A successful compilation or loading of a CFD case with compiled UDF requires these inputs to be accessible. `DEFINE_EXECUTE_ON_LOADING` is another of many macros provided by the FLUENT UDF library, which is executed when the case is loading. Aforementioned text files are read through this macro. The data files can be arranged in a way that they consist of the actual inlet and exit temperatures of the case. Lumped body temperature can also be computed externally to ensure that the model starts at a certain condition if needed. On the other hand, the UDF allows a user-defined period of steady state calculations before switching into transient calculations. That is, the model can be arranged to conduct the calculations in the steady state mode, which is equivalent to quasi-steady black-box heat addition models available commercially (Zhang et al., 2008). The transient calculations can be started at a specified time where the transient event starts, which in our case is the rack shutdown.

The internally computed variables can be saved in text files when exiting by utilizing the `DEFINE_EXECUTE_AT_EXIT` macro. These files can be loaded again through the `DEFINE_EXECUTE_ON_LOADING` macro when the user needs to continue the simulation from the point where it was stopped. As a reference, how the case is set up and compiled, a

sample journal file is included in Appendix C, which provides FLUENT text user interface commands to compile the UDF file and run transient simulations.

#### *5.4 Verification of Transient Server Boundary Conditions through CFD Results of Rack-Shutdown Experiment*

The results provided herein include comparison of experimental data and CFD simulation results for the inlet and exit temperatures and temperature differences of servers. Figure 5.3 shows the comparison of the transient inlet temperature variation after server heaters are turned off. The large dots in the Figure 5.3a represent initial inlet air temperature of the server. The mismatch of the inlet conditions here is due to errors in the steady state CFD predictions. As the time progresses the data approach the 45 degree line due to the decreasing temperature variation in the room.

The CFD simulations predict warmer inlet temperatures, especially at the inlets of top side servers (R1&R3), in Figure 5.3b and Figure 5.3d. As steady state experiments showed in Figure 5.1, regions of warm air are observed on the outer sides of the edge racks (R1 & R3) closer to the tile level. The relatively higher inlet air temperatures for the bottom servers (R1C1 & R3C1) are due to the fact that all coarse CFD models have difficulties in capturing the rapid entrainment just above the tile.

Figure 5.4 shows a similar comparison set for the transient air temperature difference. Governing transient heat transfer equations are solved internally to calculate transient server exit air temperature. The results show maximum error of about 1°C in predicting the server air temperature difference.

Exit air temperature predictions primarily rely on the accuracy of the inlet air temperature predictions since the errors at the inlet are carried over to exit temperatures, which can be seen in Figure 5.5.

One important observation about the general trend in inlet air temperatures given in Figure 5.3 is that the decay rate of the inlet temperatures in CFD is higher than that of the experiment. This is possibly an indication of overlooked additional thermal masses, which needs further investigation. Hence, the next chapter is dedicated to the possible thermal masses beyond computing equipment.

Since the computed temperatures are initially relatively higher compared to the experimental data, and they asymptote to the steady state values lower than experimental data, the rapid decrease of the computed inlet temperature can be difficult to realize. In order to have the fast decay of the CFD results stand out compared to the experimental data, CFD results are adjusted to have the same initial condition explicitly, and Figure 5.6 shows a magnified version of the results indicating unaccounted for thermal masses in the data centers.

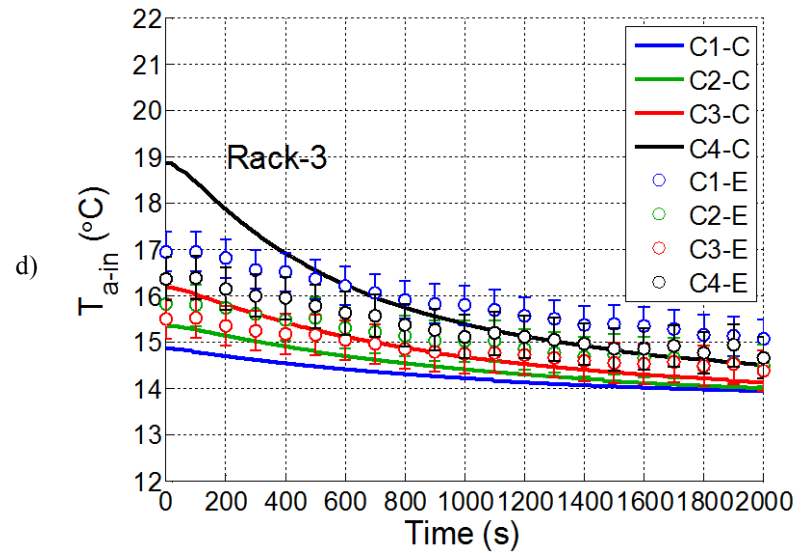
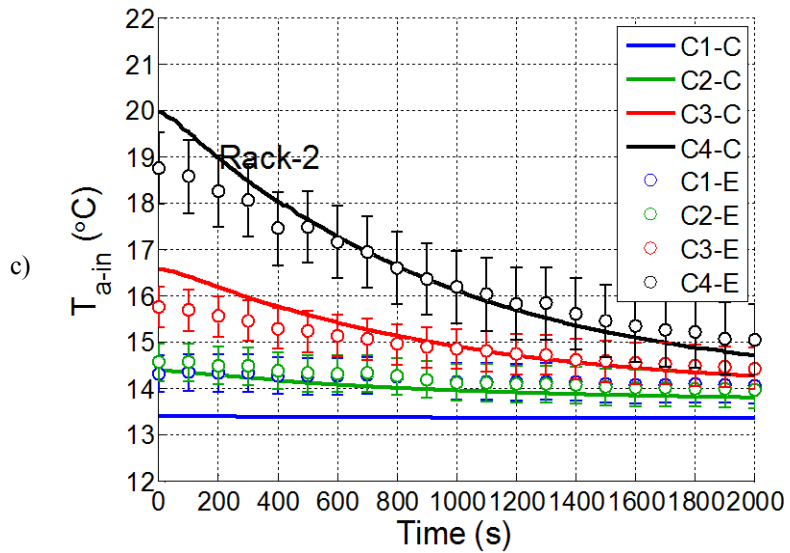
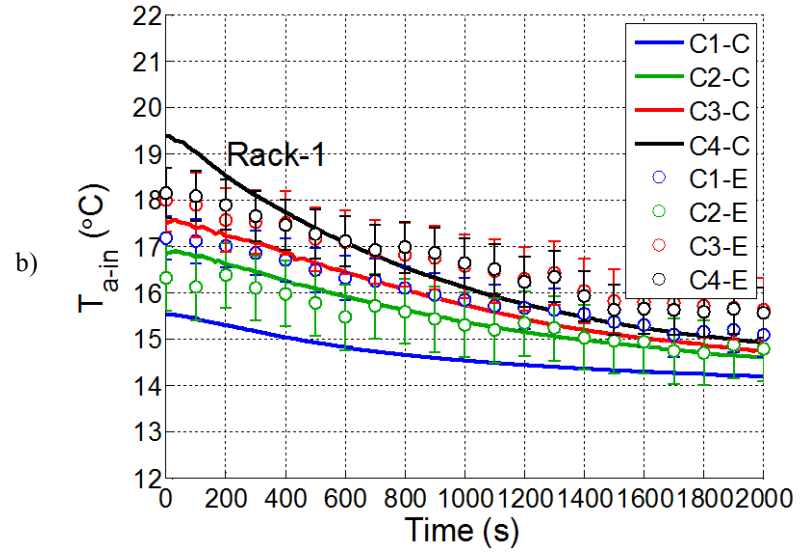
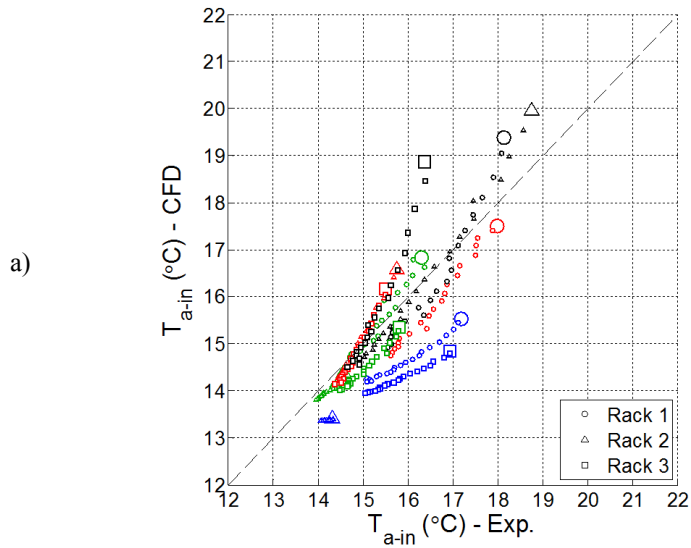


Figure 5.3: Comparison of server inlet air temperature: CFD vs. experiment. a) 4 racks b) Rack1 c) Rack2 d) Rack3

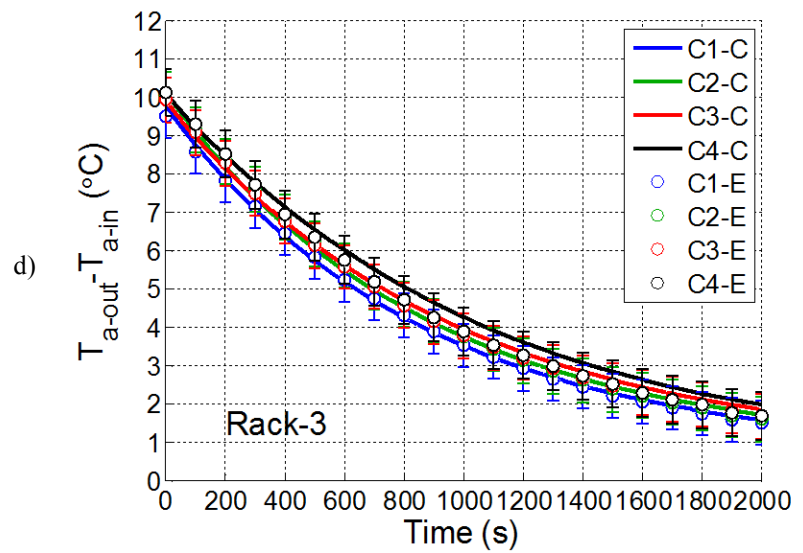
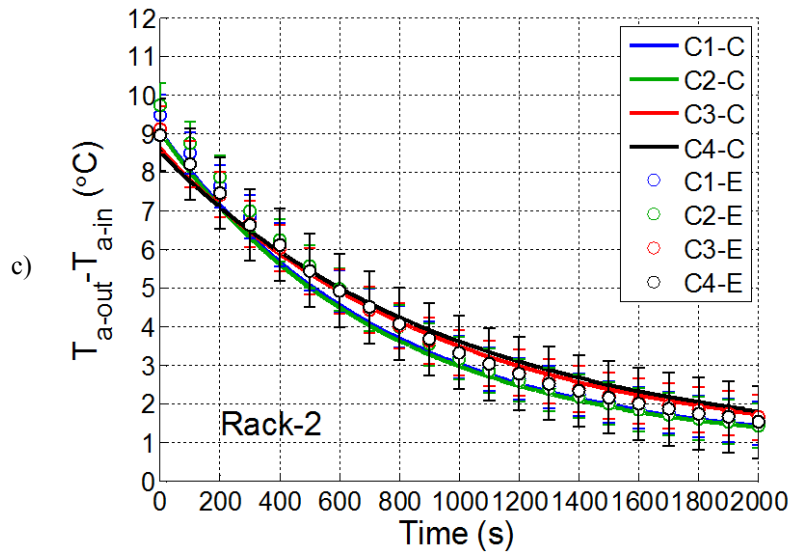
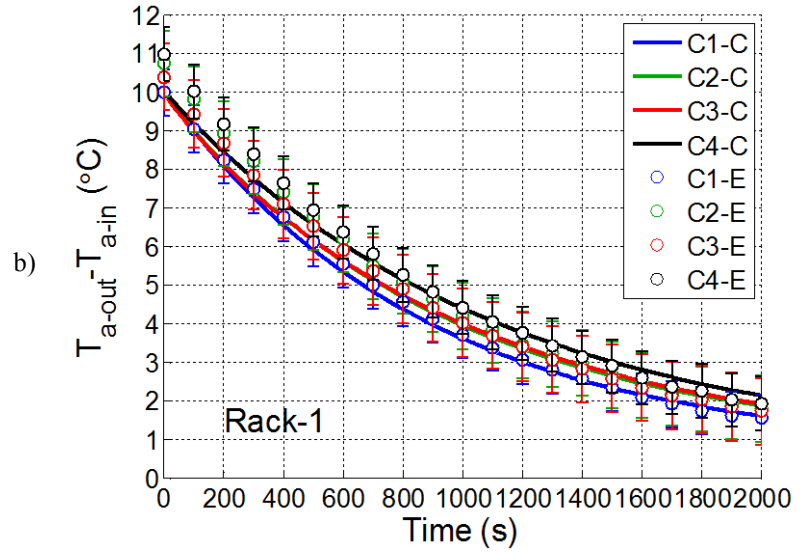
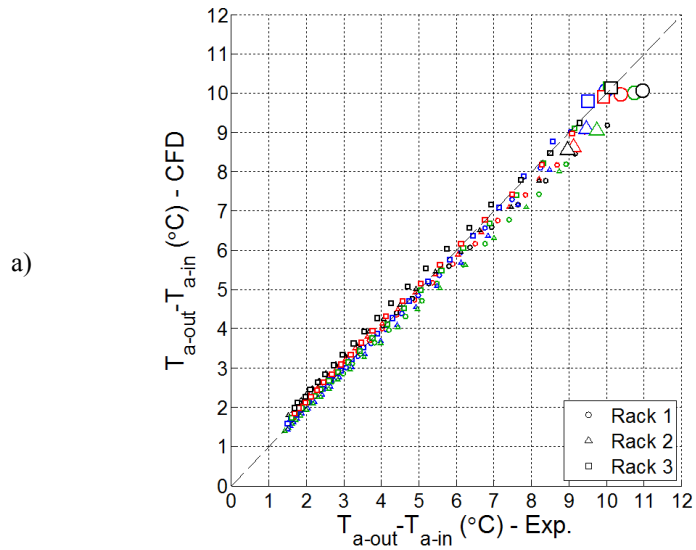


Figure 5.4: Comparison of server air temperature difference: CFD vs. experiment. a) 4 racks b) Rack1 c) Rack2 d) Rack3



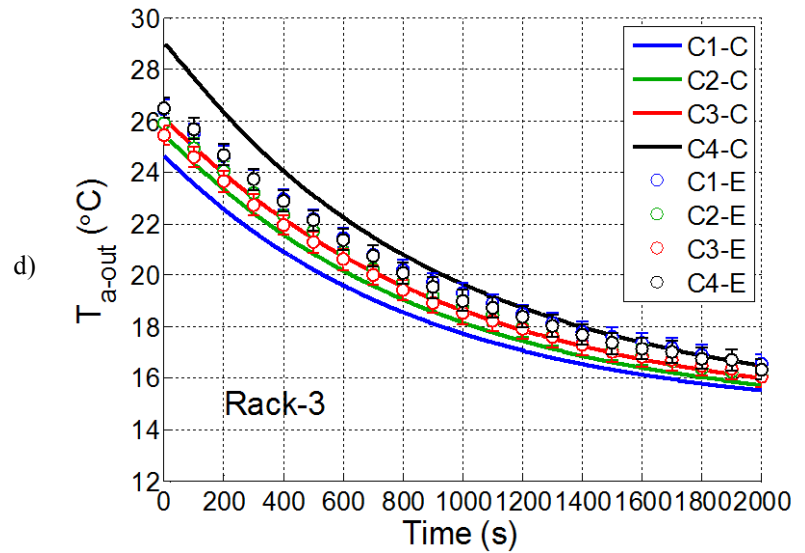
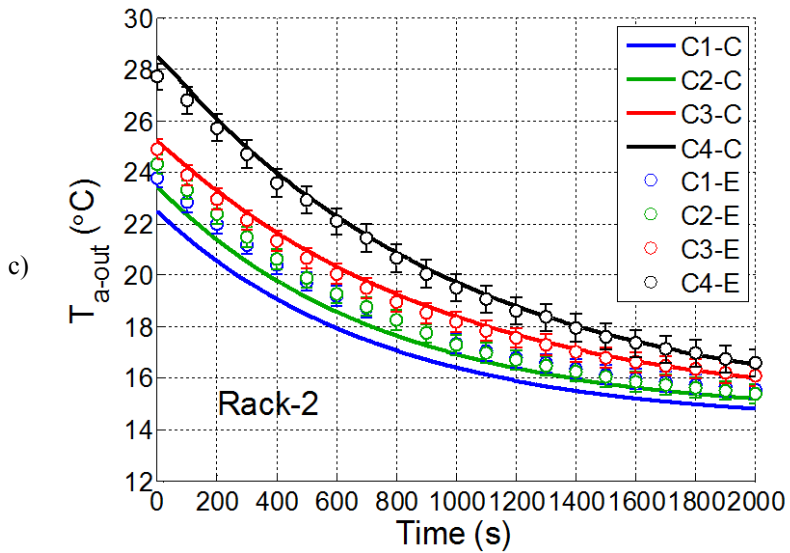
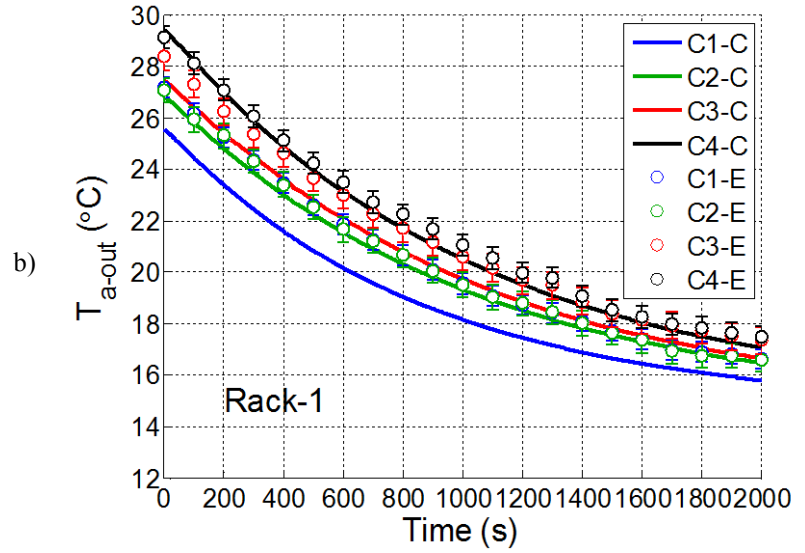
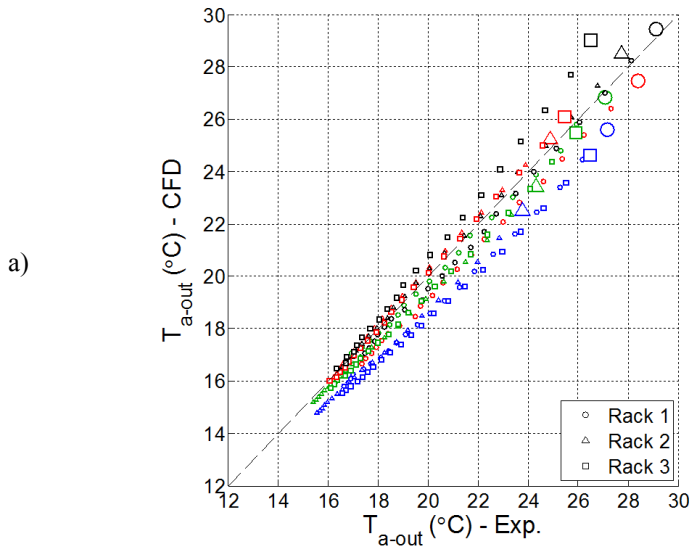


Figure 5.5: Comparison of server exit air temperature: transient CFD vs. experiment. a) 4 racks b) Rack1 c) Rack2 d) Rack3

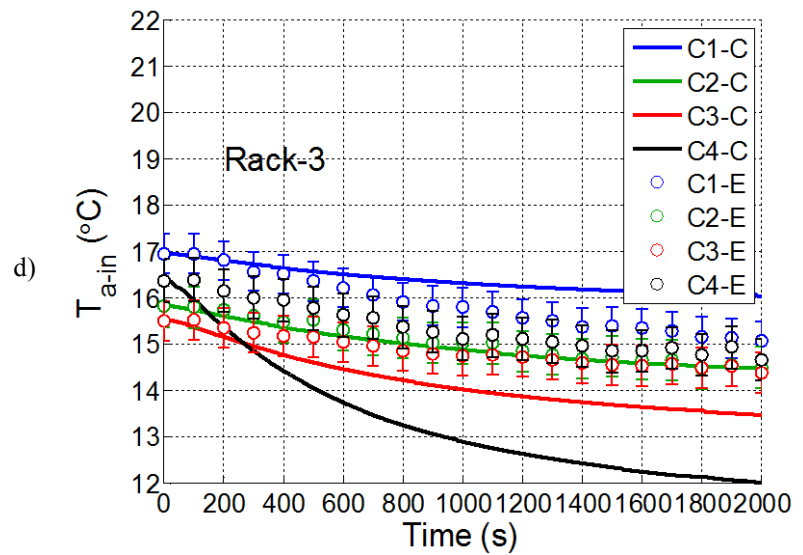
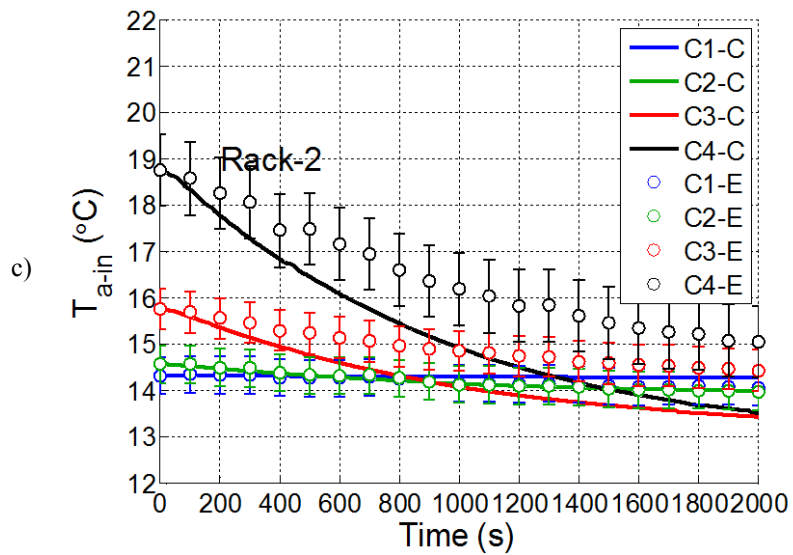
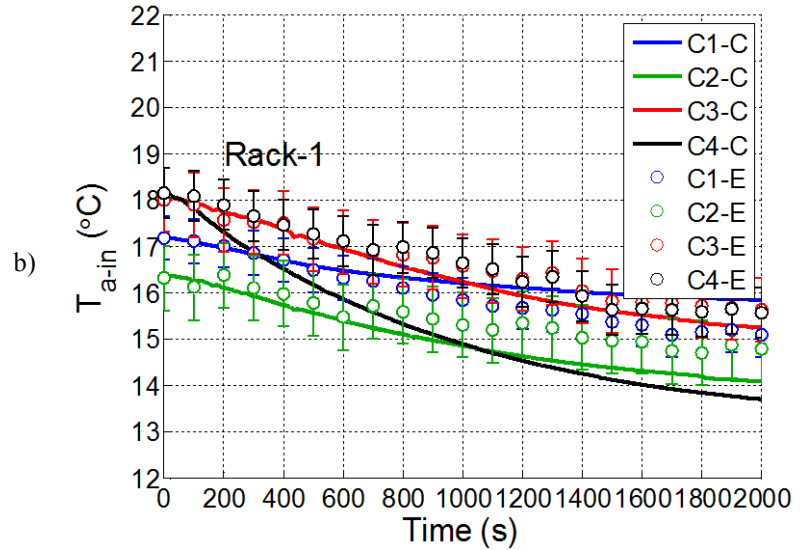
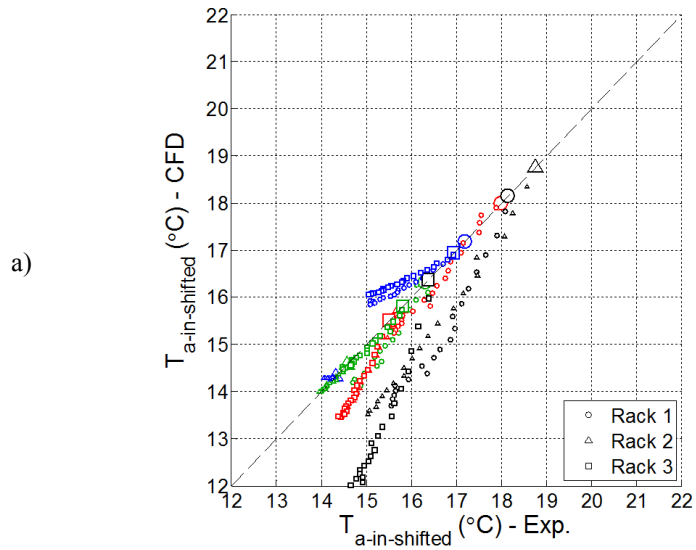


Figure 5.6: Comparison of server inlet air temperature: Adjusted CFD vs. experiment. a) 4 racks b) Rack1 c) Rack2 d) Rack3

## 5.5 Chapter Conclusions

CFD is a mainstream modeling tool that works toward achieving a better understanding of physics governing the thermal environment in air cooled data centers. However, the tools based on quasi-steady boundary conditions lack the ability to resolve the effects of massive equipment in the data center space. As studies indicate, thermal masses are significant to the dynamic nature of data centers. This chapter introduced an initial attempt to conduct a room-level transient simulation of rack shutdown experiment with unsteady server exit temperature boundary conditions. The results are promising since the largest errors at the inlet of the servers are primarily due to the initial conditions, and these errors are translated to the exit of the servers. This is also an indication of the decent work by the unsteady server model in predicting transient temperature difference across the server.

On the other hand, results are also encouraging for future work since the faster decay of room temperature in CFD compared to the experimental results is indicative of the unexplored data center dynamics. In order to study the effects of thermal masses in a data center environment, an analytical model will be introduced in the next chapter as a fast executing tool.

## 6 Hybrid Lumped Capacitance –CFD/EXPERIMENTAL Model

The inclusion of the thermal masses of the server by itself showed significant improvement in CFD results. However, addressing many different thermal masses that contribute to the transient thermal behavior of data centers is not as obvious or easy to incorporate in CFD simulations as it is for servers. Here we develop and test a time-dependent enhancement of the data center simplified model proposed by Khalifa and Demetriou (2011). Many details have been added to the previous steady-state model to account for the transient effects, which include but are not limited to the servers.

Consider an air-cooled data center cooled by a CRAH unit through an under-floor plenum as depicted in the simplified block diagram in Figure 6.1. The data center has many servers,  $j=1, S$  (only 3 servers are shown in Figure 6.1), each of which is simplified as three (3) blocks unlike single black-box model introduced previously. While this can still be converted to a single box, the model has the flexibility to account for multiple of thermal masses inside the including heated and unheated sections, which may have different thermal characteristics. The cooling air flows in series over the blocks. Each block is characterized by a thermal capacitance, a convective conductance, and a heat generation rate that can be turned on or off.

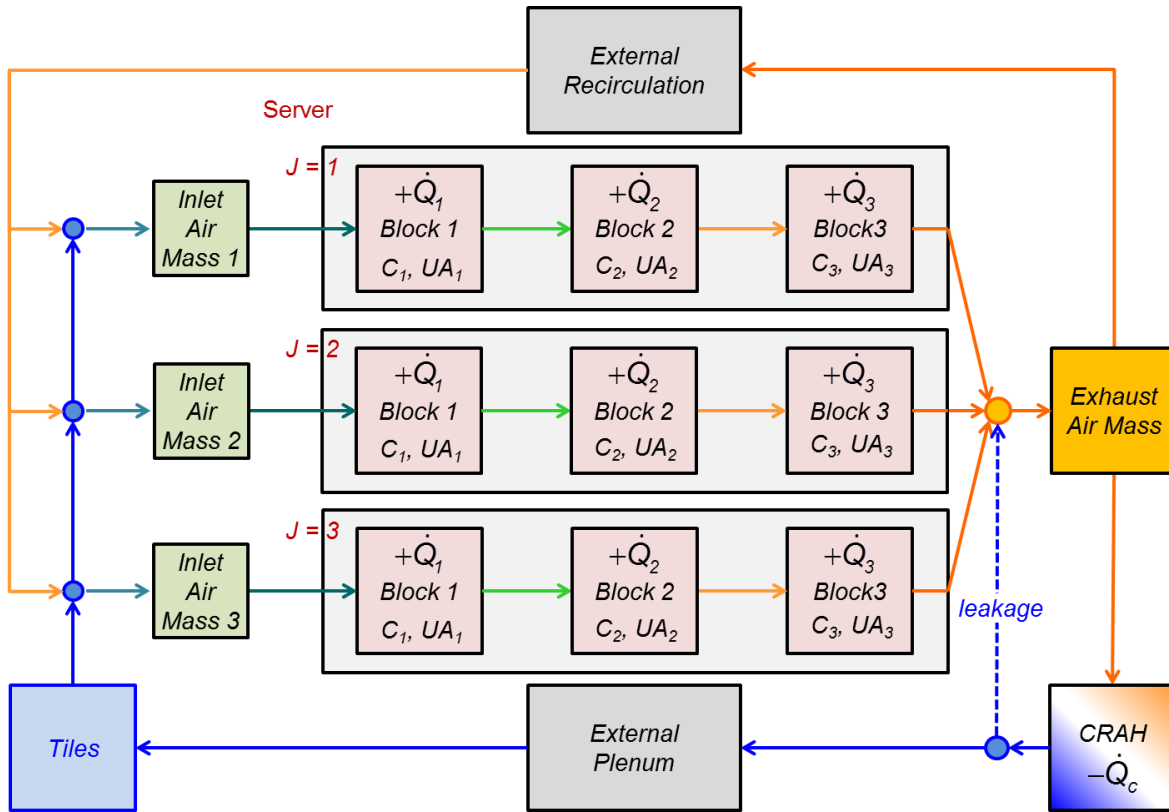


**Figure 6.1: Simplified Hybrid-Lumped Capacitance Data Center Model**

The CRAH is also characterized by a thermal capacitance, a convective conductance and a heat removal rate that can be increased or decreased in a step fashion. As we will show later, the CRAH does not exhibit a 1<sup>st</sup> order behavior and needs to be represented by two thermal masses. The hot exhaust from all the servers sharing a hot aisle is assumed to mix to a uniform temperature in the hot aisles, and blends with cold air leaked from the under-floor plenum. A fraction of the mixed warm air passes through the CRAH, where it is cooled, and is blown into the under-floor plenum. Some of CRAH discharge leaks back into the data center space, where it mixes with the hot air exhausted from the servers, and the remainder passes through the plenum where it exchanges heat with the plenum thermal mass through a plenum convective conductance before it issues from the perforated tiles into the data center cold aisles.

After mixing with the leakage air, the remaining hot exhaust air is recirculated back to the inlet of the servers in the cold aisles, where it mixes with varying fractions of the cold air emanating from the perforated tiles before it enters the servers. The recirculation path varies from server to server depending on the location of the rack within the data center and the location of the server within the rack. For example, servers placed near the bottom of a rack in the middle of a bank of racks are not likely to receive much, if any, hot recirculated air, while those located near the top of a rack at either end of a bank of racks are likely to receive a considerable amount of recirculated air. Servers located near the top of a rack in the middle of a bank of racks also receive a considerable amount of recirculated hot air from the adjacent hot aisle. The path traveled by the hot circulated air also depends on the location of the server within the rack and the rack within the data center aisles. In any of these recirculation paths the air may exchange heat during a transient event with various thermal masses (blocks) located within the room, each of which may be characterized in this simplified model by a heat capacitance and a convective conductance. As a consequence, each server may have a different inlet temperature based on its location within the rack and the location of the rack within the data center, which determine the percentage of recirculated air blended into the air drawn into each server, as well as the contribution of heat exchange with the recirculation path thermal mass to the time-dependence of the server inlet temperature. The fraction of cold tile air in the inlet of server  $j$  is known as the capture index,  $\psi_j$  (VanGilder & Shrivastava, 2007), whose value depends on the complex flow-field in the room. It should be noted here that in this simplified model, any air emanating from the under-floor plenum that does not enter the servers is treated as leakage; i.e., no distinction is made between air that leaks through tile gaps and cable cut-outs and air from the perforated tiles that bypasses the cold aisles and the racks arranged in them.

The heat capacitance and the convective conductance values of the various components of this simplified data center (the server blocks, the room blocks, the CRAH and the plenum), the thermal capacity of the air volume, the air-flow rate and the capture index for each of the servers, and the heat generation rates in each server block, as well as the heat removal rate of the CRAH are external inputs that must be assigned a priori.

Transient events may be associated with step changes in the heat generation rates in the blocks of the servers, changes in the CRAH heat removal rate (e.g., loss of chilled water, loss or change of air flow rate). In both types of transients, it is assumed that the flow rates through the servers remain constant. Under constant CRAH flow conditions the flow-field within the data center remains essentially unchanged, and consequently the capture index for all the servers also remains unchanged except for buoyancy effects, which are assumed to change little during transient events. In case of an interruption or change in the CRAH air flow rate the flow field in the data center is expected to change which results in new values of capture index corresponding to the new flow field. Capture index values for all the servers may be obtained from steady state CFD or from steady-state experimental data describing the prevailing server inlet, tile air supply temperatures and data center heat load before the onset of the transient. It is assumed that adjustments of the flow field occur much more rapidly than other transients (server & room). This is borne out by the fact that the air change rate in data centers (air volume divided by total server flow rate is typically faster than 1 air changes per minute).

## *6.1 Mathematical Model*

We developed a mathematical model for a single server, which was then generalized for any number of different servers in a data center with distinct recirculation loops, a CRAH and an

under-floor plenum. Capture index,  $\psi_j$ , indicates the amount of tile flow a server  $j$  receives.

Accordingly, steady state inlet temperature into the server  $j$  is defined as

$$T_{1,j} = \psi_j T_t + (1 - \psi_j) T_{r,j}, \quad (6.1)$$

where  $T_t$  and  $T_{r,j}$  are average tile temperature and recirculated air temperature of server  $j$ . For the initial conditions under steady state the capture index,  $\psi_j$ , can be computed as

$$\psi_j = 1 - \frac{T_{1,j} - T_t}{T_m - T_t} = 1 - \frac{T_{1,j} - T_t}{\dot{Q} / \dot{C}_c}, \quad (6.2)$$

where  $\dot{Q}$  is the total heat load during steady state and  $\dot{C}_c$  is the CRAH flow capacity. For server  $j$ , the transient temperature of the air entering the first block is obtained by solving the unsteady heat balance equation for the air mass at the cold aisle of each server:

$$C_{in,j} \frac{dT_{1,j}}{dt} = \dot{C}_{a,j} \psi_j T_t + \dot{C}_{a,j} (1 - \psi_j) T_{r,j} - \dot{C}_{a,j} T_{1,j} \quad (6.3)$$

$C_{in,j}$  represents the thermal capacity of the air volume dedicated to the inlet of the server  $j$ ,  $\dot{C}_{a,j}$  is the thermal capacity rate of the server  $j$  air flow. A heat balance of the air stream passing through block  $k$  yields:

$$T_{k+1,j} - T_{k,j}^b = (T_{k,j} - T_{k,j}^b) e^{-NTU_{k,j}}, \quad (6.4)$$

where the superscript b stands for the block and number of transfer units (NTU) is defined as,

$$NTU = \frac{UA}{\dot{C}}. \quad (6.5)$$



$UA$  is the thermal conductance of the heat exchanger. The air temperature change across block  $k$  of server  $j$  is given by:

$$T_{k,j} - T_{k+1,j} = (T_{k,j} - T_{k,j}^b) \left(1 - e^{-NTU_{k,j}}\right) = (T_{k,j} - T_{k,j}^b) \varepsilon_{k,j}. \quad (6.6)$$

where  $\varepsilon_{k,j}$  is the heat exchange effectiveness, i.e.,

$$\varepsilon_{k,j} = \left(1 - e^{-NTU_{k,j}}\right). \quad (6.7)$$

The exhaust temperature of server  $j$  (exit of the 3rd block) is given by

$$T_{e,j} - T_{3,j}^b = (T_{3,j} - T_{3,j}^b) e^{-NTU_{3,j}} = (T_{3,j} - T_{3,j}^b) (1 - \varepsilon_{3,j}). \quad (6.8)$$

and the mixed exhaust temperature in the hot aisle is obtained from,

$$T_x = \frac{\sum_{j=1}^S \dot{C}_j T_{e,j}}{\dot{C}_s}; \text{ where } \dot{C}_s = \sum_{j=1}^S \dot{C}_j, \quad (6.9)$$

where  $\dot{C}_s$  is the total server air heat capacity rate for the given hot aisle. The exhaust air from the servers mixes in the hot aisle with the cold leakage air from the floor, therefore for a certain hot aisle air mass a mixed air temperature,  $T_m$ , can be computed as follows,

$$C_m \frac{dT_m}{dt} = \dot{C}_s T_x + \dot{C}_\lambda (T_c + T_t) / 2 - (\dot{C}_s + \dot{C}_\lambda) T_m, \quad (6.10)$$

in which  $\lambda$  refers to the leakage, which is assumed to enter the data center space at the average temperature of CRAH exit and the tile exit. Excluding the cold tile air that is not captured by the servers, which we treat as an airstream bypassing the cold aisle and entering the hot aisle air

space, the heat capacity rate of the cooling air issuing from the perforated tiles and entering the servers is:

$$\dot{C}_t = \sum_{j=1}^S \psi_j \dot{C}_j. \quad (6.11)$$

The heat capacity rate of the cooling air discharged from the CRAH is given by,

$$\dot{C}_c = \dot{C}_t / (1 - \lambda), \quad (6.12)$$

where  $\lambda$  is the fraction of CRAH flow that leaks. Therefore, the heat capacity rate of the recirculated air is:

$$\dot{C}_r = \dot{C}_s - \dot{C}_t. \quad (6.13)$$

Under transient conditions, the lumped-capacitance energy equation for the blocks of the server takes the first-order form,

$$C_{k,j} \frac{dT_{k,j}^b}{dt} = \dot{Q}_{k,j} + \dot{C}_j (T_{k,j} - T_{k+1,j}) = \dot{Q}_{k,j} + \dot{C}_j (T_{k,j} - T_{k,j}^b) \epsilon_{k,j}, \quad (6.14)$$

which is subject to the previously prevailing steady-state initial conditions, including the server inlet temperatures (or, alternatively, the capture indices). Therefore, the initial condition is described by,

$$T_{k,j}^{b,0} = T_{k,j}^0 + \frac{\dot{Q}_{k,j}^0}{\dot{C}_j \epsilon_{k,j}}, \quad (6.15)$$

$$T_{k+1,j}^0 = T_{k,j}^0 + \frac{\dot{Q}_{k,j}^0}{\dot{C}_j}, \text{ and } T_{e,j}^0 = T_{1,j}^0 + \frac{\sum_{k=1}^3 \dot{Q}_{k,j}^0}{\dot{C}_j}. \quad (6.16)$$

A time constant inspired for block k of server j by the lumped capacitance model may be defined by

$$\tau_{k,j} = \frac{C_{k,j}}{\varepsilon_{k,j} \dot{C}_j}, \quad (6.17)$$

which will prove useful in interpreting the results of this model (or any first-order model), as we will show later.

Integrating Equation 6.14 over the time interval from  $t - \delta t$  to  $t$ , we obtain:

$$T_{k,j}^b(t) - T_{k,j}^b(t - \delta t) = \frac{\delta t}{C_{k,j}} \left[ \bar{\dot{Q}}_{k,j} + \varepsilon_{k,j} \dot{C}_j (\bar{T}_{k,j} - \bar{T}_{k,j}^b) \right], \quad (6.18)$$

in which the top bar designates time-averaging over the short time interval  $\delta t$ , viz.,

$$\bar{T}_{k,j} = [T_{k,j}(t - \delta t) + T_{k,j}(t)]/2; \text{ and } \bar{T}_{k,j}^b = [T_{k,j}^b(t - \delta t) + T_{k,j}^b(t)]/2. \quad (6.19)$$

Equation 6.18 can be rearranged to yield:

$$T_{k,j}^b(t) = \frac{T_{k,j}^b(t - \delta t) \left[ 1 - \frac{\delta t}{2\tau_{k,j}} \right] + \left[ \frac{\delta t \bar{\dot{Q}}_{k,j}}{C_{k,j}} + \frac{\delta t}{\tau_{k,j}} \bar{T}_{k,j} \right]}{\left[ 1 + \frac{\delta t}{2\tau_{k,j}} \right]}, \quad (6.20)$$

with the heat generation rate representing the average value over the interval  $\delta t$ .

To complete the model, we need to account for the transient behavior of the room, the CRAH and the plenum. These will also be treated as lumped capacitances in this model. Therefore, the heat capacitance and the convective conductance in each of these components must be known, as well as the heat removal rate of the CRAH, whose steady-state value must be equal to the sum of the heat generated by the servers and other equipment in the data center-space. Equations similar to those derived for the servers as described above may be used for that purpose. For example we may write for the recirculated room air

$$T_m - T_r = (T_m - T_R^b)\epsilon_R, \quad (6.21)$$

and for each of the room lumped capacitances we write,

$$T_R^b(t) = \frac{T_R^b(t - \delta t) \left[ 1 - \frac{\delta t}{2\tau_R} \right] + \left[ \frac{\delta t \bar{Q}_R}{C_R} + \frac{\delta t \bar{T}_m}{\tau_R} \right]}{\left[ 1 + \frac{\delta t}{2\tau_R} \right]}, \quad (6.22)$$

with the subscript  $R = R1, R2, \dots$  representing the various room recirculation path blocks if more than one path is needed. We may also write analogous equations for the plenum and for the CRAH, which will link the CRAH inlet temperature,  $T_m$ , to the plenum exit temperature (the tile air temperature),  $T_t$ , through the CRAH exit temperature,  $T_c$ . However, the CRAH is an actively modulated component that is dynamically controlled to maintain the temperature of the air entering or leaving the CRAH at a pre-set value, or to deliver cold air at a pre-set temperature. This is achieved by continuously changing the flow rate of the chilled water via a feedback controller to maintain the desired conditions. The control signal is provided by sensing the CRAH entering or leaving air temperature. This is equivalent to imposing a constraint on the value of  $T_m$  or  $T_c$  and changing the CRAH heat removal rate to satisfy this constraint. Under this

scenario, a simple control algorithm must be employed that will change  $T_c$  so that  $T_m$  is within a small error (e.g.  $0.5^\circ\text{C}$ ) of the pre-set value, or alternatively, maintain the CRAH air discharge temperature,  $T_c$ , at its pre-set value  $T_c^*$ .

The above set of equations, along with the initial conditions constitutes a complete implicit set of linear equations that can be solved numerically by inverting a matrix at each time step. The time marching solution yields to the time variations of the time-dependent air temperatures at the inlet and outlet of each server, at the inlet and outlet of the CRAH, the plenum and the recirculation path, as well as the uniform, time-dependent temperatures of the various lumped capacitances. This will be illustrated in the examples described in the next section, including the experimental validation of the model.

## *6.2 Distribution of Thermal Mass in the Air Cooled Data Centers*

The solution of the abovementioned set of equations requires a set of inputs regarding thermal characteristics of the data center components. The bases of the parameters and how they are quantified are discussed in the following subsections.

### *6.2.1 Room Air Thermal Capacity*

Hot and cold aisle configuration is a common arrangement in air-cooled data centers, which is also the case for the RL. In order to account for the mixing process of the air within the data center, air space is divided into two parts. The hot aisle air mass is related to the typical volume of the air in the hot aisle (Figure 6.2). The remainder of the room volume is equally distributed among the number of servers as inlet mixing zones.

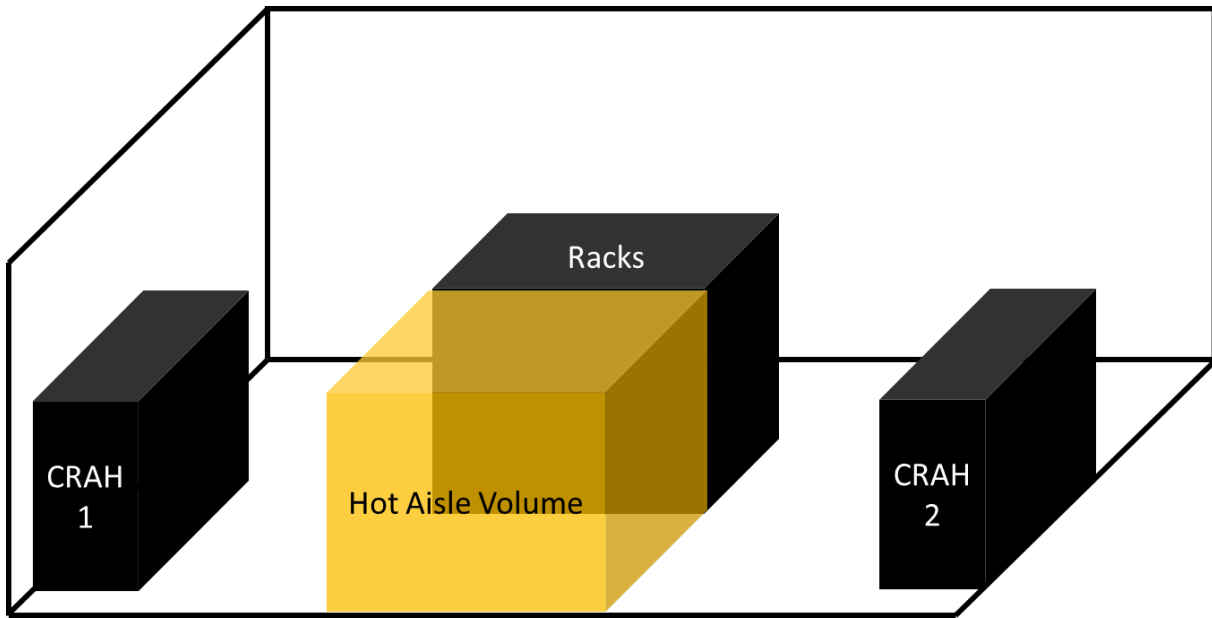


**Figure 6.2: Distribution of Room Air Capacity in RL**

Air thermal capacity in the RL is approximately 190 kJ/K excluding the volume occupied by the racks and CRAH units. The air mass behind the racks constitutes 6.5% of the total air volume. 93.5% of the volume is uniformly divided into twelve volumes, each of which is assigned to the inlet of a server.

As indicated in Equation 6.3, certain proportions of tile and recirculated air streams mix in the inlet air volume of each server according to the capture index, which gives the sense of server location in the model. The assignment of hot aisle volume as exhaust air mass allows a larger volume for the inlet air masses, so that air transients of the warm recirculated air at the exhaust can be captured. If instead, the inlet air volume was restricted to the cold aisle, the air transients would be almost instantaneous due to the limited volume at the server inlets. Hence, exhaust air volume should be rather confined to a volume representative of the hot aisle.

## 6.2.2 Servers

The techniques introduced in Chapter 4 to extract server thermal characteristics treat a server as a single lumped capacitance. The present lumped capacitance model provides an option to treat each server as a set of three blocks. This option adds the flexibility to explicitly account for heated or unheated thermal masses in a server, depending on the knowledge of the server architectural information. This option can be omitted by lumping the entire thermal mass and heat generation into a single capacitance and assigning negligible amount of thermal mass and little or no heat generation to the others.

Simulated server thermal capacitance was obtained experimentally (See Chapter 4) and was found to be approximately 95 kJ/K. Thermal conductance values vary between 120 W/K to 140 W/K as a function of the measured server air flow rate. The heated section of the simulated server constitutes 45% of the thermal mass of the entire simulated server and it is represented by the second of the three blocks representing the server. It is the only block in the group with heat generation. The thermal mass of the server frame, single perforated screen at the inlet and the inlet door of the rack are assigned to the first block which does not have any heat generation. The third block only consists of the rack door at the back and the screens at the exit of the server box. Before the last block the heat generated by the fan array is represented explicitly.

## 6.2.3 CRAH Units

A CRAH unit has an enclosure which consists of filters, heat exchangers and fans. During an interruption of chilled water (e.g. pump failure), the CRAH thermal mass is defined as the collection of the heat exchanger, the water trapped inside the heat exchanger, other components (e.g. fans, motor etc.) and structural elements. The effectiveness for the entire CRAH body is

$$\varepsilon_C = 1 - \exp(-NTU_C), \quad (6.23)$$

where

$$NTU_C = UA_C / \dot{C}_c. \quad (6.24)$$

Calculation of NTU requires UA values for the combination of various components listed above, which can vary at least an order of magnitude across the CRAH enclosure. The UA for the heat exchanger during normal operation  $UA_{hx}$  (active chilled water) can be obtained by solving  $\varepsilon$ -NTU relations for which the effectiveness can be obtained experimentally by,

$$\varepsilon = \frac{(T_{a-in} - T_{a-out})}{(T_{a-in} - T_{w-in})}. \quad (6.25)$$

The resultant UA is that for the heat exchanger during normal operation since the heat transfer into passive components will cease at steady state. UA value on the air side of the heat exchanger can be obtained by subtracting the estimated thermal resistances for the internal chilled water flow and the pipe thickness,

$$UA_a = \left( \frac{1}{UA_{hx}} - R_w - R_p \right)^{-1}, \quad (6.26)$$

where the thermal resistance of the pipe,  $R_p$ , is negligible and the resistance on the water side,  $R_w$ , can be computed for the water flow inside the tube using the Gnielinski correlation for the turbulent internal flows (Incropera & DeWitt, 2007),

$$Nu = \frac{f / 8(\text{Re}_D - 1000) \text{Pr}}{1 + 127 \sqrt{f / 8} (\text{Pr}^{2/3} - 1)}, \quad (6.27)$$



It is assumed that the air-side UA will not change even if water flow is interrupted so long as the air flow is unchanged.

This analysis leads to a thermal conductance of approximately 3800 W/K on the air side of the heat exchanger for the RL. On the other hand, the heat transfer relations for the internal flow for the rest of the mass inside the CRAH, assuming that CRAH is a duct conveying air from the inlet area to the fan exit area based on the estimated enclosure surface area, leads to a thermal conductance of about several hundreds. Hence, the CRAH unit can be considered as the succession of two bodies (heat exchanger with high UA and cooling rate during normal operation, the rest of the CRAH with lower UA and no cooling rate).

CRAH heat exchanger in the RL has a compact cross-flow heat exchanger with 32 circuits of copper tubes carrying chilled water, each of which has 4 passes. Based on the dimensions of the heat exchanger pipes and fins, the thermal capacitance of the heat exchanger and the water body is estimated to be ~235 kJ/K, which is subject to a high UA of ~3800W/K. Installed mass of each CRAH units in RL is 516 kg. Assuming the rest of the CRAH content made of steel, this corresponds to a thermal capacitance of about ~150kJ/K, which is exposed to lower UA values ~150 W/K. The UA value for the second block is estimated based on the heat transfer relations for a duct and an estimated surface area inside the CRAH enclosure excluding the heat exchanger.

#### 6.2.4 Recirculation Paths

Consider a server of face area  $A_f$  with an average face velocity  $V_f$ . If we visualize a conduit of the same cross-sectional area conveying the recirculated air flow to the inlet of the servers emanating from the exhaust, the velocity of the recirculated air in this conduit,  $V_r$ , can be approximated by

$$\bar{V}_r = \sum_j V_{f,j} (1 - \psi_j). \quad (6.28)$$

Assuming that the conduit has a constant rectangular cross section area but allowed to distort at a certain aspect ratio,  $\gamma$ , as defined in Figure 6.3.

$$b/W = \gamma. \quad (6.29)$$

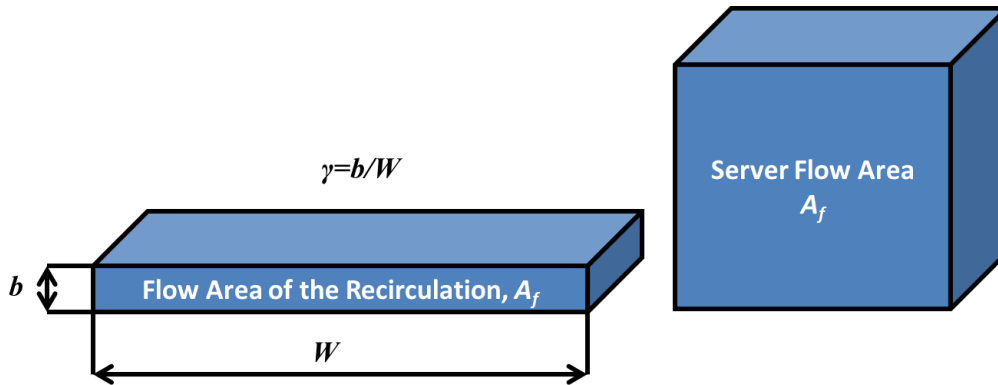


**Figure 6.3: Recirculation Flow Path Dimensions**

Assume that the entire flow of recirculated air will pass over the exposed surface of the room (walls, ceiling and floor) whose total area is  $A_R$ . The wetted perimeter for the distorted conduit is

$$W = \sqrt{A_R}, \quad (6.30)$$

and therefore,

$$b = A_f / W. \quad (6.31)$$

The hydraulic diameter,  $D_h$ , can be defined as

$$D_h = 4A_f / P = 2A_f / (\sqrt{A_R} + A_f / \sqrt{A_R}) = \frac{2A_f \sqrt{A_R}}{A_R + A_f}, \quad (6.32)$$

where  $P$  is the perimeter. For  $A_R \gg A_f$  Equation 6.32 can be simplified as

$$D_h \approx \frac{2A_f}{\sqrt{A_R}} \approx 2b, \quad (6.33)$$

Along this conduit, energy transfer between the room thermal mass and the recirculated air is assumed to happen along the width,  $W$ , of the cross-section area. The thermal conductance of the heat transfer surface can be related to the conduit dimensions by,

$$UA = UWL, \quad (6.34)$$

where  $L$  is the length of the conduit, and  $U$  is the heat transfer coefficient. Overall heat transfer coefficient  $U$  can be approximated by a relationship of the form (Incropera & DeWitt, 2007),

$$U = \frac{kNu}{D_h} = 0.023 \frac{k}{D_h} \text{Re}^{0.8} \text{Pr}^{1/3}. \quad (6.35)$$

There are two dimensions, conduit length,  $L$ , and width,  $W$ , that need to be determined to make a closure for this approach. For a data center with the exposed surface area,  $A_R$ , a practical rule for the characteristic length can be as follows,

$$L = \sqrt{A_R}. \quad (6.36)$$

The exposed surface area,  $A_R$ , of the data center is in contact with the room air. Therefore a hypothetical conduit conveying the recirculated air is also assumed to cover the entire exposed surface of the data center (Figure 6.4). Since the cross-section area for the hypothetical recirculation flow conduit is assumed to be constant, the conduit width,  $W$ , will expand or shrink to the extent that the entire exposed surface is covered by one side of the conduit cross-section area of  $A_f$ .

The approach to calculate the thermal conductance,  $UA_r$ , for the recirculation path can be further simplified by the calculation of a baseline thermal conductance value  $UA_{en}$  for the entire enclosure. The baseline  $UA_{en}$  can be defined as an extreme case of the recirculation flow path conveying the entire server flow rate in the absence of tile flow rate. The resultant  $UA_{en}$  gives the maximum possible  $UA_r$ . The subsequent  $UA_r$  values for various recirculation flow rates can be approximated by apportioning the baseline value  $UA_{en}$  by the ratio of actual recirculation flow capacity  $\dot{C}_r$  to the sum of server flow capacity  $\dot{C}_s$ ,

$$UA_r = UA_{en} \frac{\dot{C}_r}{\dot{C}_s}. \quad (6.37)$$

An alternative to the hypothetical conduit approach to estimate  $UA_r$  is also developed based on steady state CFD simulations, details of which can be found in Appendix H.

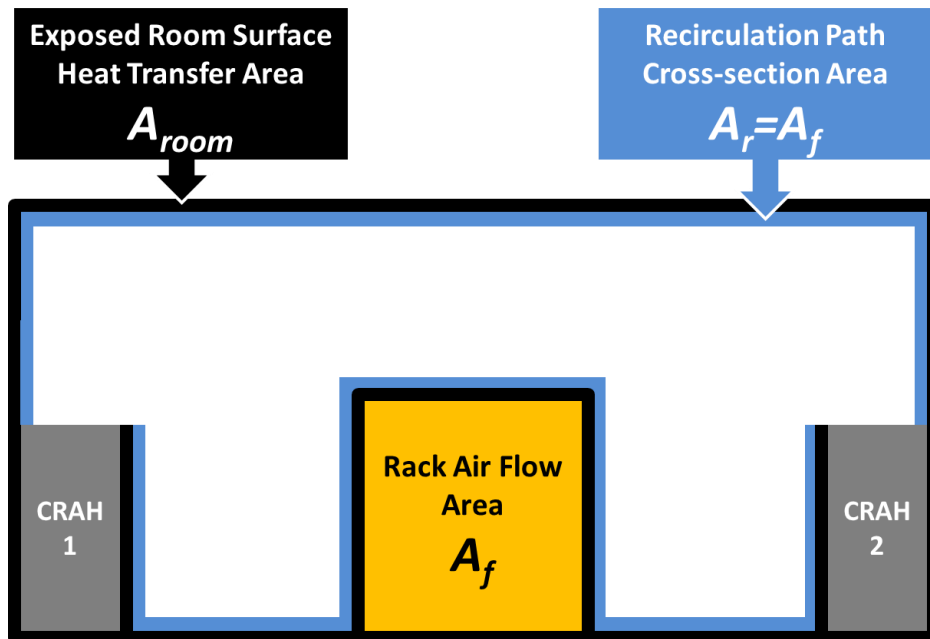


Figure 6.4: Exposed Room Surface Covered by the Hypothetical Conduit of Recirculation Flow

The hypothetical conduit approach also helps in estimating the contributing room thermal mass by assigning a certain thickness of a building material for the entire heat transfer surface. Three major types of building materials constitute the surfaces of the data center, material for the tiles, walls and the ceiling. For the research lab the tile material is primarily concrete, the walls are gypsum board with a thickness of 16 mm and the ceiling is made of mineral fiber with the same thickness. The volumetric heat capacity of the concrete, gypsum board and mineral fiber are 2.21, 1.04 and 0.29 kJ/m<sup>3</sup> respectively. Based on the exposed surface area for each material, an area weighted average leads approximately the same properties of the gypsum board for the research lab. Similar distribution of building materials is also expected to lead to similar conclusion in a production data center. Therefore for this analysis the material of the conduit for the recirculation air is considered to be gypsum board for the entire room.

The thermal diffusion depth for semi-infinite solid can be estimated as

$$d \sim \sqrt{\alpha t}, \quad (6.38)$$

where  $\alpha$  is the thermal diffusivity of the building material and  $t$  is the time of interest. The time of interest is assumed to be about 10 minutes considering required actions will be taken no later than that especially during a failure scenario. This leads to a thermal diffusion length of 10.5 mm for gypsum board. Since this is comparable to the thickness gypsum board (16 mm), the entire thickness of the wall is attributed to the conduit wall thickness at the heat transfer surface.

This approach leads to the room thermal capacitance of about 2500 kJ/K for the research lab and various thermal conductance values depending on the amount of the recirculated air. For the fan failure case in which entire server flow is recirculated, the thermal conductance is calculated to

be about 900 W/K. For the cases with lower recirculation (higher tile flow) it can be as low as 260 W/K.

### 6.2.5 Plenum

The approach introduced for determining thermal conductance and capacitance of the recirculation path can be applied to the plenum with two adjustments. The first adjustment depends on determining the conduit cross-section area. In the data center space the recirculated air was introduced and ingested by the same areas. Also, the recirculated air velocities are relatively small compared to those in the plenum, where air velocities can vary significantly from CRAH discharge to the tile. UA values were computed for two cases, where conduit cross section area was assumed to be equal to the tile area and to CRAH air discharge area. An average of the two values is assumed to be the actual thermal conductance of the plenum thermal mass. This can be interpreted as half of the plenum surface area is subject to heat transfer due to lower velocities and the other half is due to higher velocities.

The total surface area of the plenum is known. When determining the thermal capacitance of the conduit covering the entire surface of the plenum, a material and a thickness needs to be assigned for the surface. Since the floor of the plenum and the filling of the raised floor tiles are made of concrete, the primary material can be considered to be concrete. However, the effective thickness for the floor concrete slab must be estimated based on the diffusion length over the time period of interest (Eq. 6.38). The time of interest for the CRAH chilled water interruption experiment is about 10 minutes. For this time of interest the diffusion length is about 7 mm for the concrete conduit surfaces in the plenum. Accordingly, thermal capacitance and conductance for the

research lab at a typical CRAH flow rate of 6400 CFM were found to be approximately 1500 kJ/K and 900 W/K respectively.

### 6.2.6 Discussion on the Validity of Lumped Capacitance Approach

The application of lumped capacitance model is justified for values of Biot number less than 0.1. For the server we have justified the use of the lumped capacitance model in Chapter 4. For the typical average heat transfer coefficients of about 1 W/m<sup>2</sup>K (higher tile flow) to 5 W/m<sup>2</sup>K (no tile flow) for the recirculation path and assumed conduit wall material, gypsum board, for the known thickness of 16 mm gives a Biot number range of 0.1-0.5, which is typically larger than 0.1. These numbers even got worse for the thick concrete slab and heat transfer coefficient of ~10 W/m<sup>2</sup>K for the plenum, as well as the insulating (mineral fiber) ceiling material.

Based on the Biot number, coarse assumption of lumped capacitance is arguable. On the other hand, the analytical one term solution to the transient conduction problem leads to the dimensionless temperature as follows (Cengel and Ghajar, 2010)

$$\theta = A_1 e^{-\lambda_1^2 Fo} \cos(\lambda_1 x / L), \quad (6.39)$$

which is also exponential in nature. In fact, the cosine term is the factor representing the spatial temperature variation and for the center plane (x=0) of the wall (of the thickness of 2L) the time-dependent temperature is entirely exponential. Considering the proximity of the Biot number for the wall material to 0.1 and even for higher Biot numbers the solution being a “polluted” exponential, purely exponential lumped capacitance approach may be justified within the accuracy of heat transfer relations and experiments.

### *6.3 Verification of the Model Through Research Lab Experiments*

Conclusions of Chapter 5 pointed out that there must be unaccounted thermal masses beyond the servers that account for the slower decay in the experiment. This observation can be verified by the Hybrid Lumped Capacitance model through disabling the thermal masses beyond servers. Figure 6.5 shows the results for the rack shutdown experiment obtained from the hybrid model without room capacitance compared to the experimental data. These results are comparable to the ones discussed in Chapter 5 for the same experiment. The air mass defined in the hybrid model is implicitly taken into account by the CFD models. With the exception of the Rack 2 results, the absence of the room capacitance leads to a faster decay of the server inlet temperature than exhibited in the experimental data. The better agreement with the experiment for Rack 2 indicates that the recirculation for the top server in this rack is short-circuited, i.e, probably does not exchange much heat with the room thermal mass.



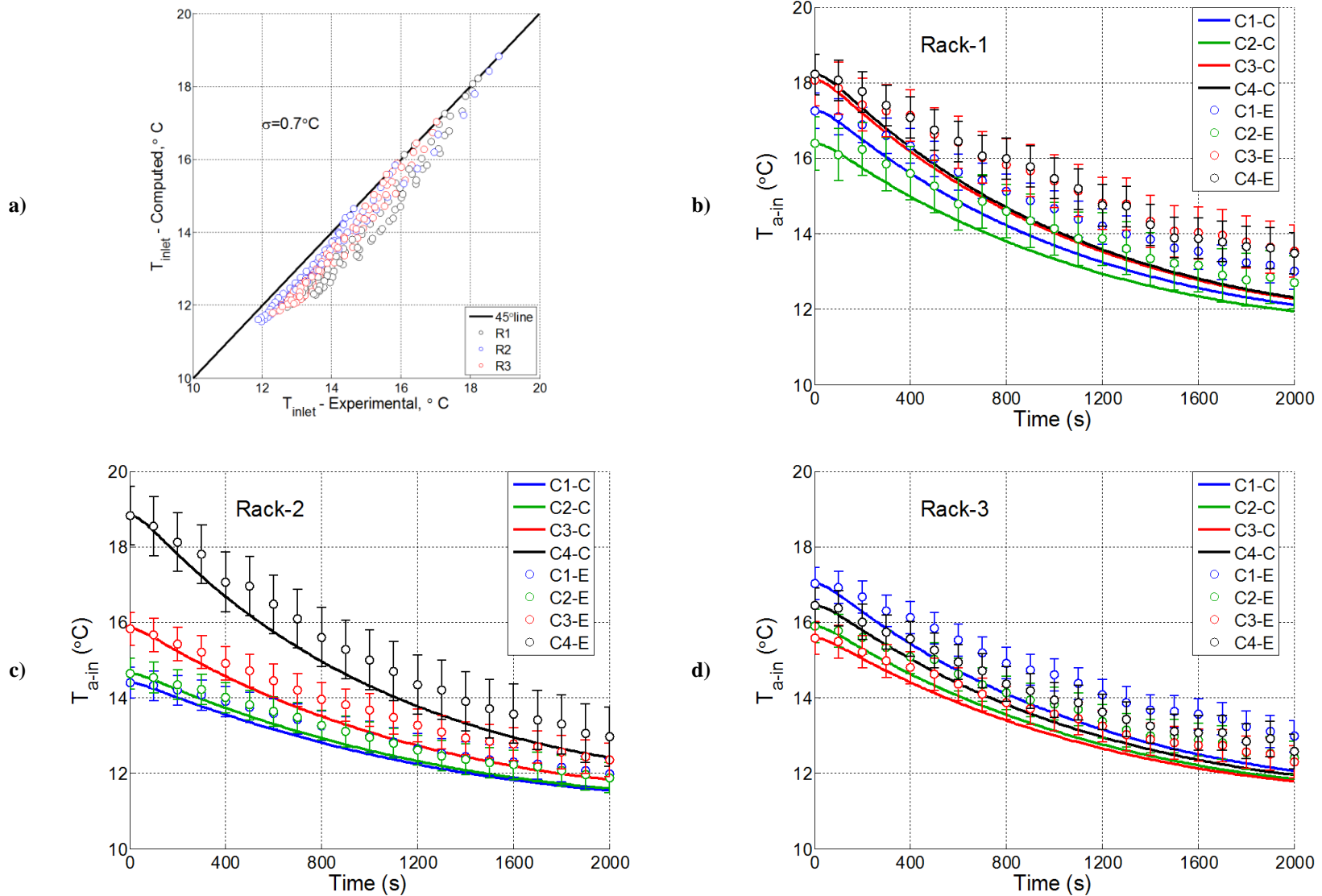


**Figure 6.5: Comparison of server inlet air temperature for rack shutdown experiment without room and plenum thermal masses: Model vs. experiment. a) 4 racks b) Rack1 c) Rack2 d) Rack3**

The rack shutdown experiment is a safe scenario where initial and steady state operating conditions are within the allowable region of the data center thermal environment. The impact of thermal masses and the accuracy of the model become even more significant under cooling failure scenarios. Figure 6.6 and Figure 6.7 show the computed inlet air temperature in case of a chilled water interruption and CRAH fan failure assuming negligible building thermal mass. Ignoring the building thermal masses in such critical conditions lead to large errors and they can lead to considerably conservative actions than necessary.

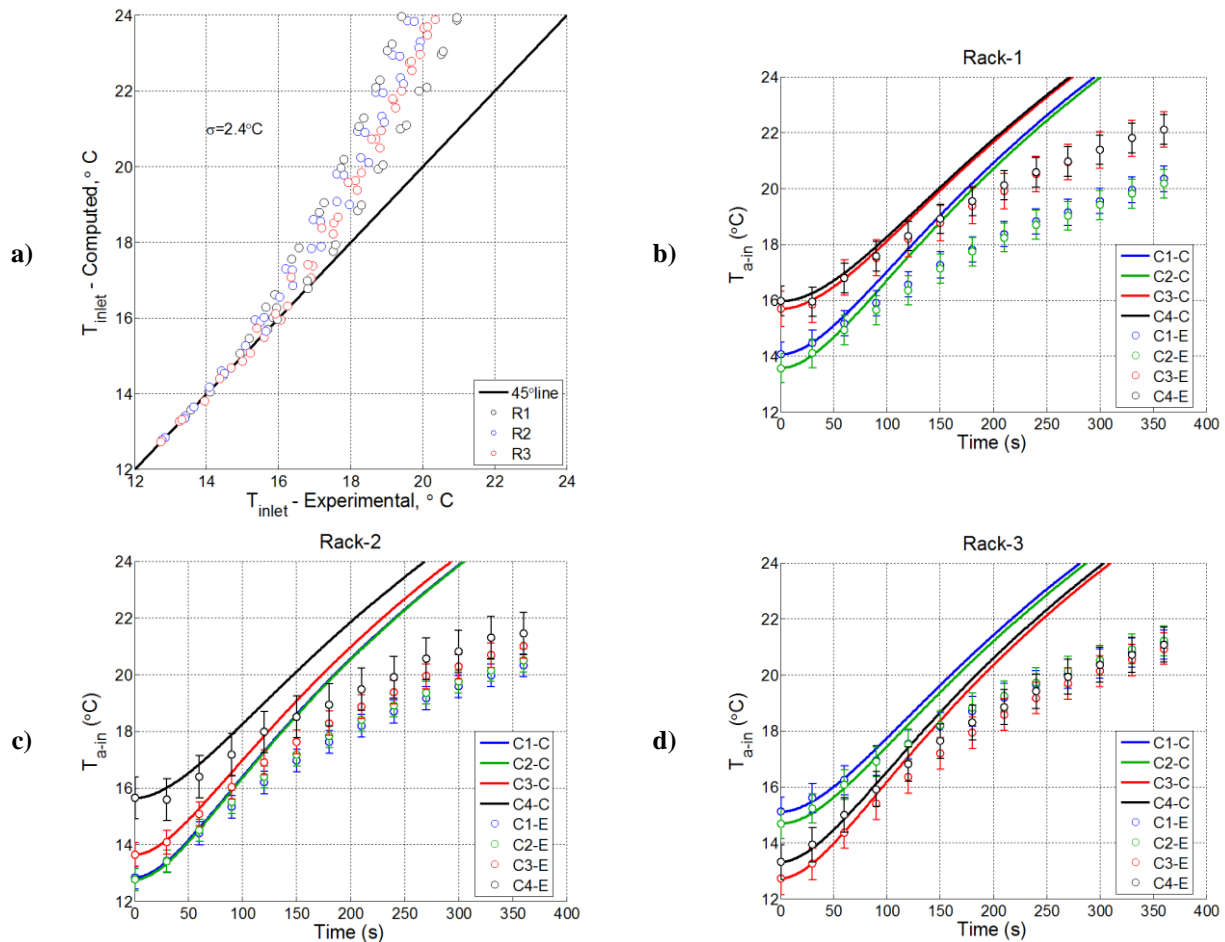


**Figure 6.6: Comparison of server inlet air temperature for Chilled Water Interruption Experiment without room and plenum thermal masses: Model vs. experiment. a) 4 racks b) Rack1 c) Rack2 d) Rack3**

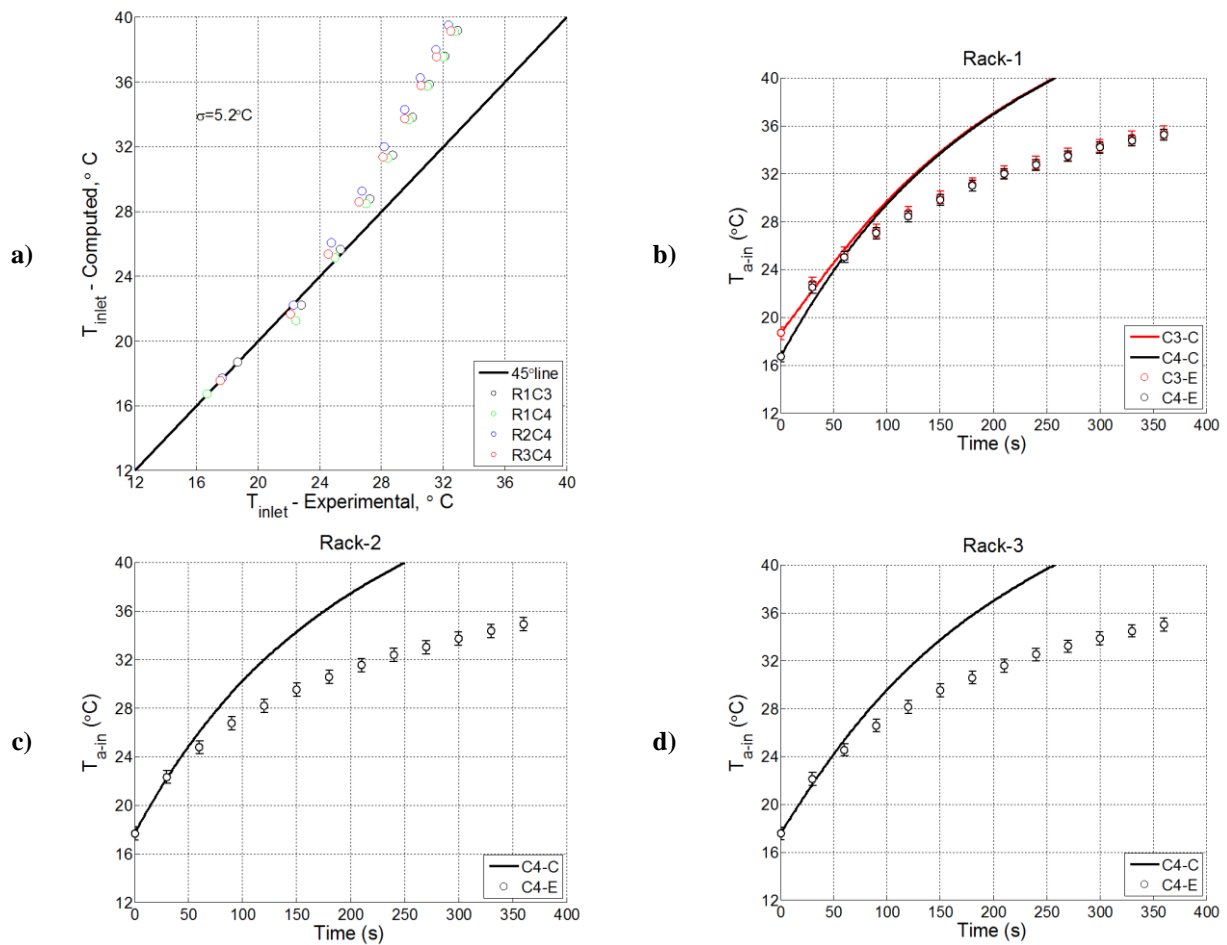


**Figure 6.7: Comparison of server inlet air temperature for CRAH Fan Failure Experiment without room and plenum thermal masses: Model vs. experiment. a) 4 racks b) Rack1 c) Rack2 d) Rack3**

### 6.3.1 Room Capacitance for a Single Recirculation Path

The simplest and most practical approach to take into account the room contributors is to assume that the entire recirculated air flow passes over a single thermal capacity. The Table 6-1 gives a summary of CRAH air flow and server power for different cases along with the room and plenum thermal characteristic inputs for the single path simulations of research lab.

**Table 6-1: Summary of CRAH Flow, Server Power, Room and Plenum Thermal Properties for Cases**

	<b>Server Power Level (kW/rack)</b>		<b>CRAH Flow Rate (CFM)</b>		<b>Thermal Mass (<math>10^6</math> J/K)</b>		<b>UA (W/K)</b>	
	<u>Initial</u>	<u>t&gt;0</u>	<u>Initial</u>	<u>t&gt;0</u>	<u>Room</u>	<u>Plenum</u>	<u>Room</u>	<u>Plenum</u>
	Rack Shutdown	15	1.2	6400	6400	2.7	1.5	214
Chilled Water Failure	8	8	6400	6400	2.7	1.5	214	904
CRAH Fan Failure	11.5	11.5	6600	0	2.7	1.5	937	927
CRAH Air Flow Decrease	11.5	11.5	4600	6400	2.7	1.5	295	694
CRAH Air Flow Increase	11.5	11.5	6400	4600	2.7	1.5	214	904

The following Figures 6.8 through Figure 6.12 show the results for the research lab for various cases corresponding to the experiments performed. Computed inlet temperature for the top server of Rack 2 (R2C4) is exposed to a larger thermal mass than the experiments indicate here. As mentioned before this is an indication of the server having a short-circuit path, which can be fixed by using two paths.

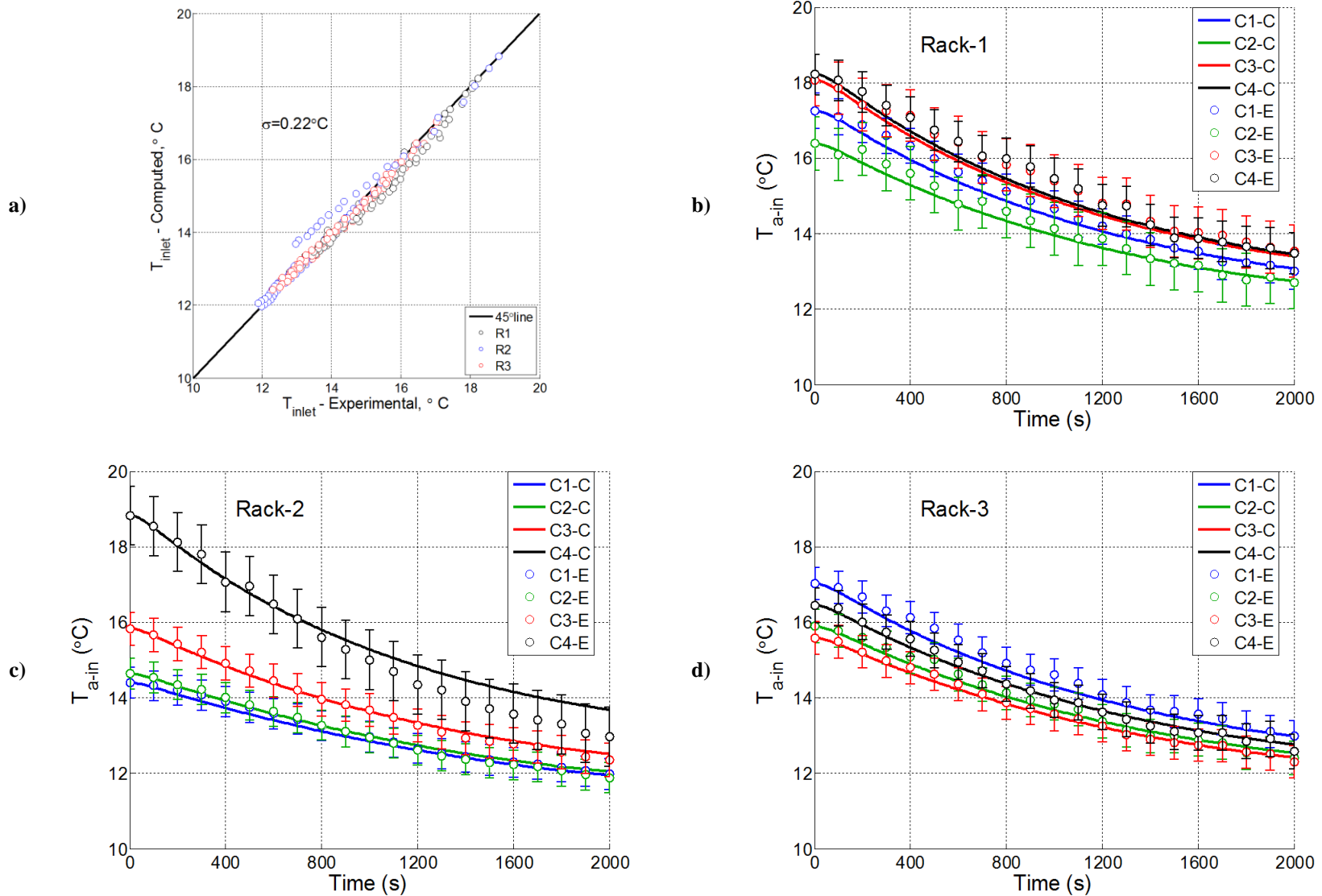


**Figure 6.8: Comparison of server inlet air temperature for Rack Shutdown Experiment with single path for the recirculated flow: Model vs. experiment. a) 4 racks b) Rack1 c) Rack2 d) Rack3**

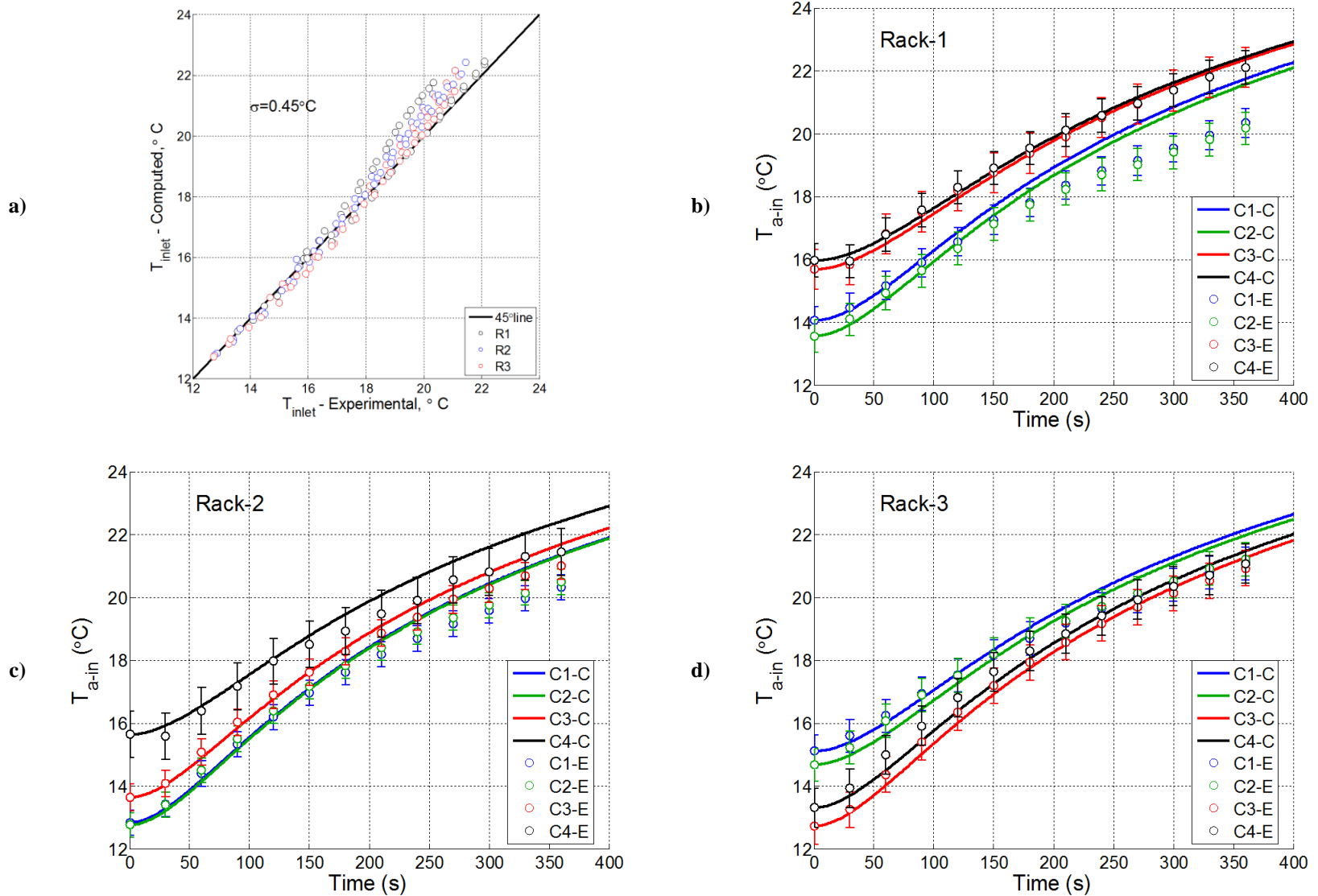


**Figure 6.9: Comparison of server inlet air temperature for CRAH Chilled Water Interruption Experiment with single path for the recirculated flow:**

**Model vs. experiment. a) 4 racks b) Rack1 c) Rack2 d) Rack3**

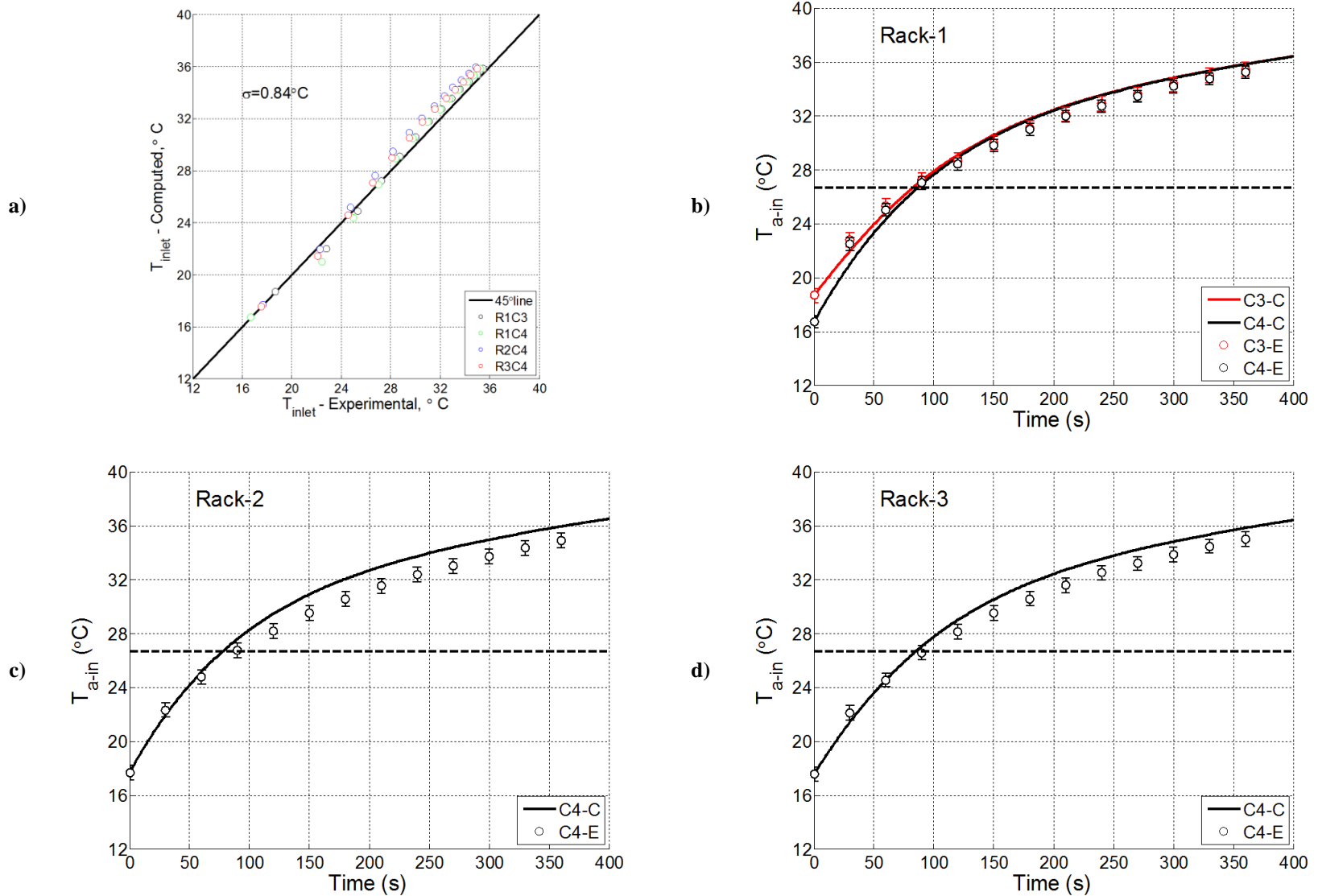


**Figure 6.10: Comparison of server inlet air temperature for CRAH Fan Failure Experiment with single path for the recirculated flow: Model vs. experiment. a) 4 racks b) Rack1 c) Rack2 d) Rack3**

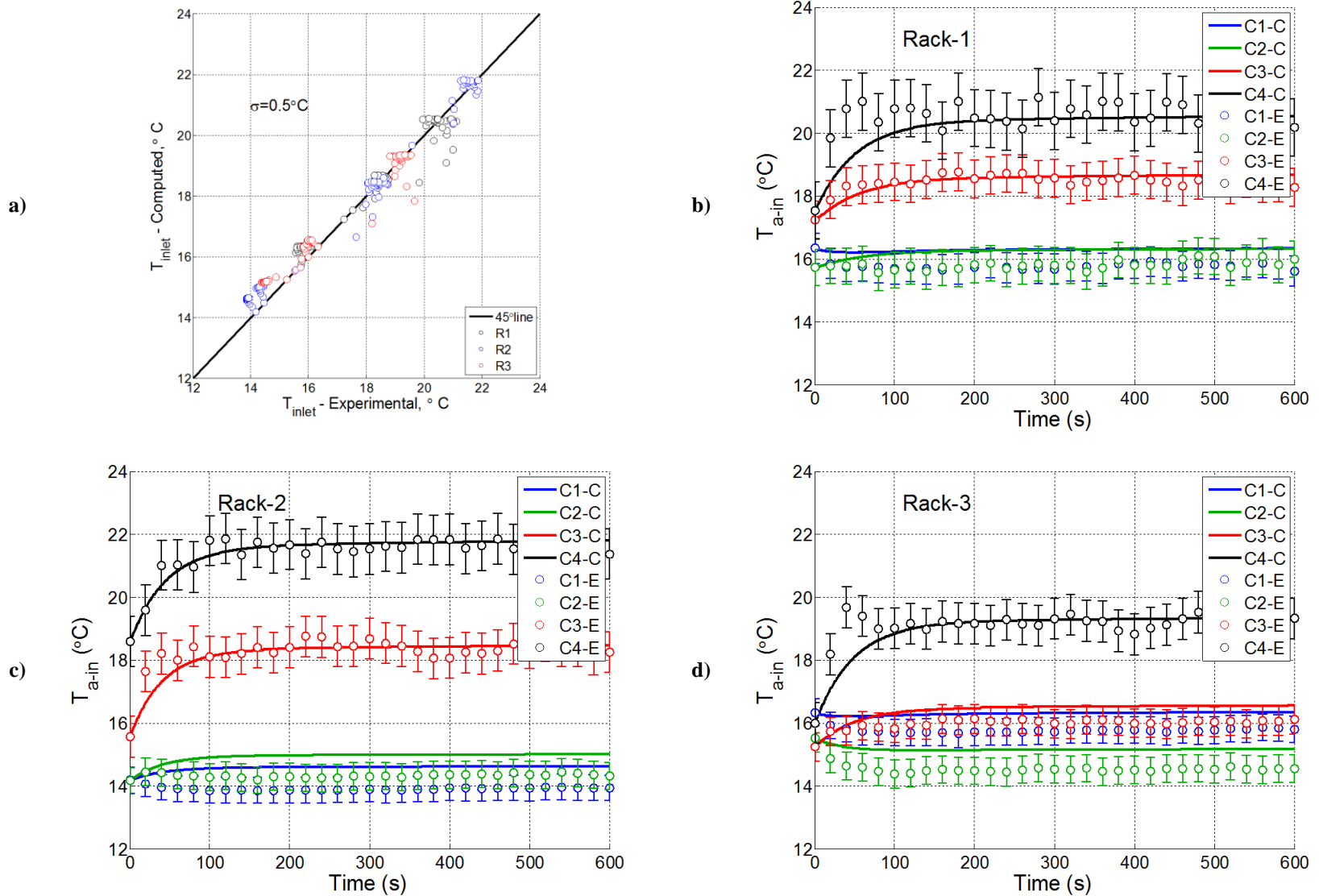


**Figure 6.11: Comparison of server inlet air temperature for Decreased CRAH Air Flow Rate Experiment with single path for the recirculated flow:**

**Model vs. experiment. a) 4 racks b) Rack1 c) Rack2 d) Rack3**



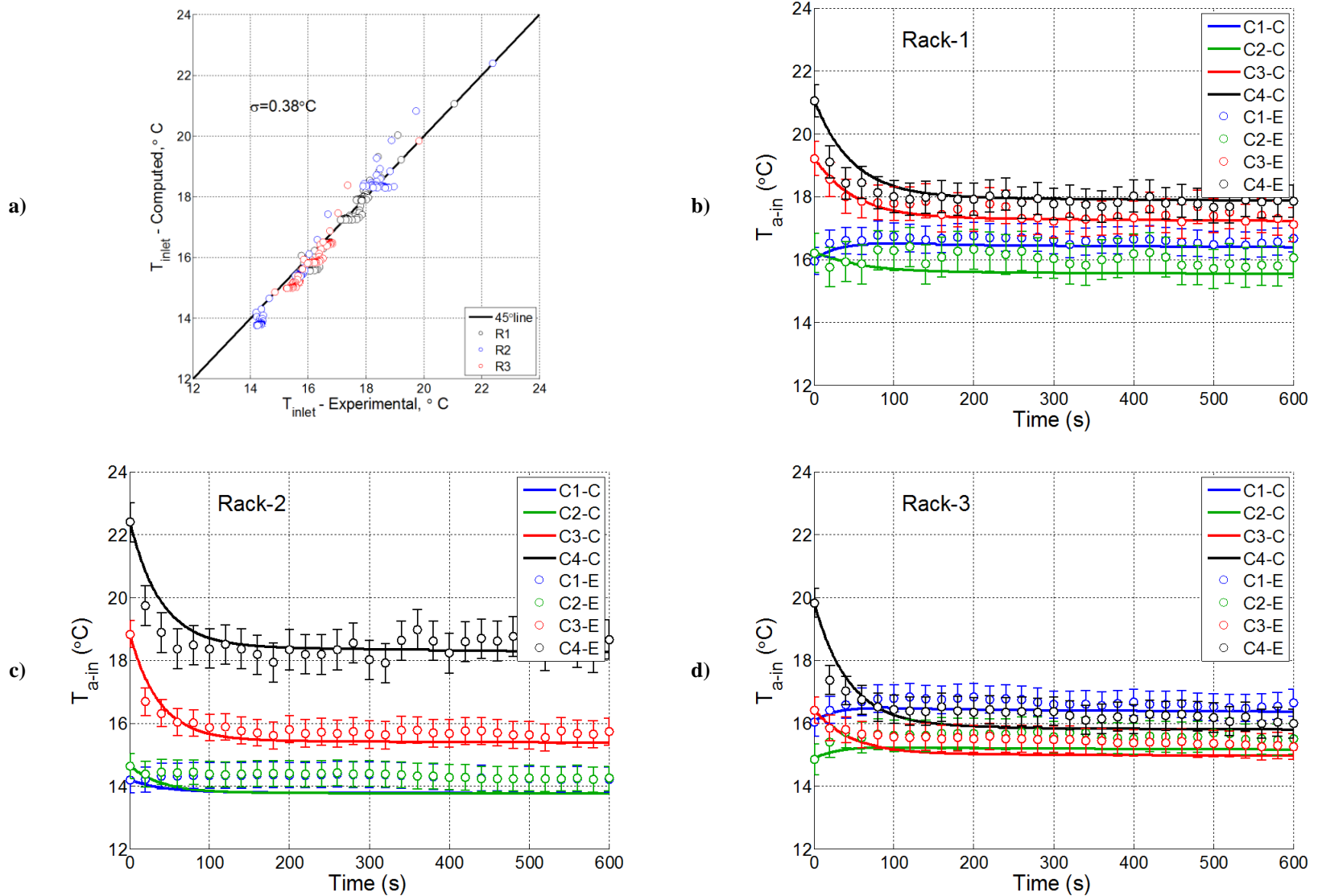


**Figure 6.12: Comparison of server inlet air temperature for Increased CRAH Air Flow Rate Experiment with single path for the recirculated flow: Model vs. experiment. a) 4 racks b) Rack1 c) Rack2 d) Rack3**

### 6.3.2 Multiple Paths and Transition to Real Data Centers

The results for a single path approach showed reasonable agreement for most of the cases. An observation in the results of Case 1, the computed temperature decay for the server R2C4 (the top server in the middle rack) seemed to be noticeably slower indicating an exposure to a larger thermal capacitance than it actually sees. The R2C4 server is representative of the top middle servers in a typical data center aisle, which receive significant amount of recirculated air but primarily over the top as a short circuit. If we separate the flow path of R2C4 from the rest and assign to it a shorter length (the distance from the back wall to front wall instead of the square root of the exposed surface area of the entire room) the results can be improved even further (Figure 6.13). The method described in Section 6.3.1 is only applicable to single recirculation path. In order to account for multiple paths with different lengths the approach can be modified as it is provided in the Appendix-F.

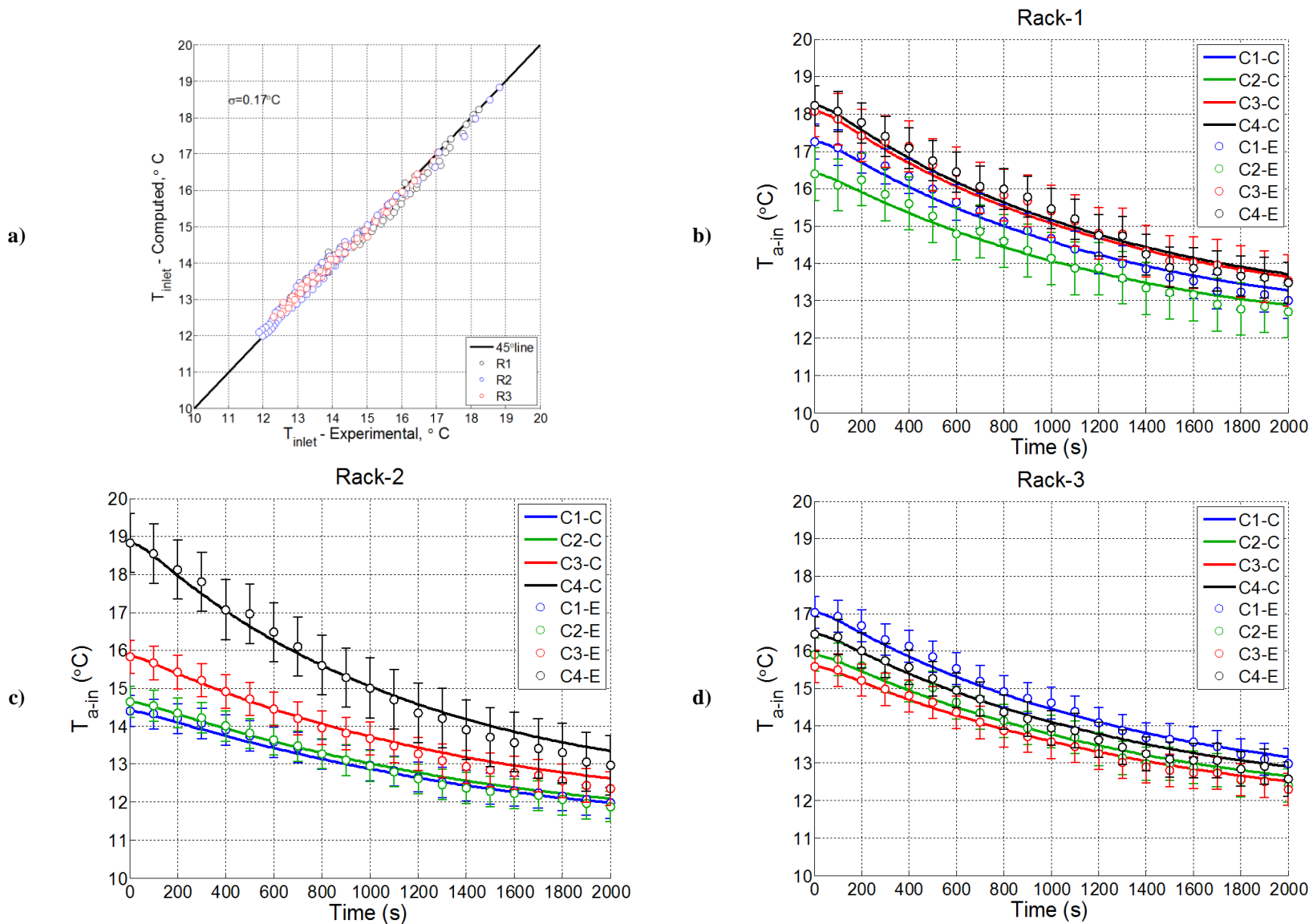


**Figure 6.13: Comparison of server inlet air temperature for Rack Shutdown Experiment with 2 Paths (R2C4 separated) for the recirculated flow:**

**Model vs. experiment. a) 4 racks b) Rack1 c) Rack2 d) Rack3**

However, at this point we need to note the uniqueness of our research lab, which has a much more complex circulation pattern than in a higher density production data center. It is a relatively difficult “data center” case to verify a model. As can be seen in Table 6.2, RL has about 5 times the room surface area per server than typical production data centers.

**Table 6-2: Comparison of the data center room surface area per rack (RL vs. Production Data Centers)**

	RL[1]	NCEPn[2]	IBM1 [3]	IBM2 [4]	IBM3 [5]	Livermore [6]	QDC [7]
Area/Rack ( $a_r$ :m <sup>2</sup> /rack)	62.7	12.8	12.4	14.8	15.7	8.5	14.0
$a_{RL} / a_r$	1	4.9	5.1	4.2	4.0	7.4	4.5

[1] RL: Research Lab

[2] NCEPn: (Fig 2.1 in ASHRAE, 2008b)

[3] IBM1: IBM Poughkeepsie (Fig 2.10 in ASHRAE, 2008b)

[4] IBM2: IBM Poughkeepsie – Region A (Fig 2.32 in ASHRAE, 2008b)

[5] IBM3: IBM Poughkeepsie – Region B (Fig 2.33 in ASHRAE, 2008b)

[6] Livermore: (Fig 2.35 in ASHRAE, 2008b)

[7] Quadrant Data Center (Large Scale Data Center Model, see Ch.6.4)

This indicates higher contribution of the room thermal mass in the thermal environment of the RL compared with a production data center. Even though Figure 6.13 shows possible improvements by using different path definitions and lengths, the reduced contribution of the room thermal mass promises better results in a production data center with only a single recirculation path definition. This argument is tested by running the rack shutdown experiment case for a room which has a surface area 4 times smaller than the actual exposed surface area. Figure 6.14 shows a comparison of these model results.

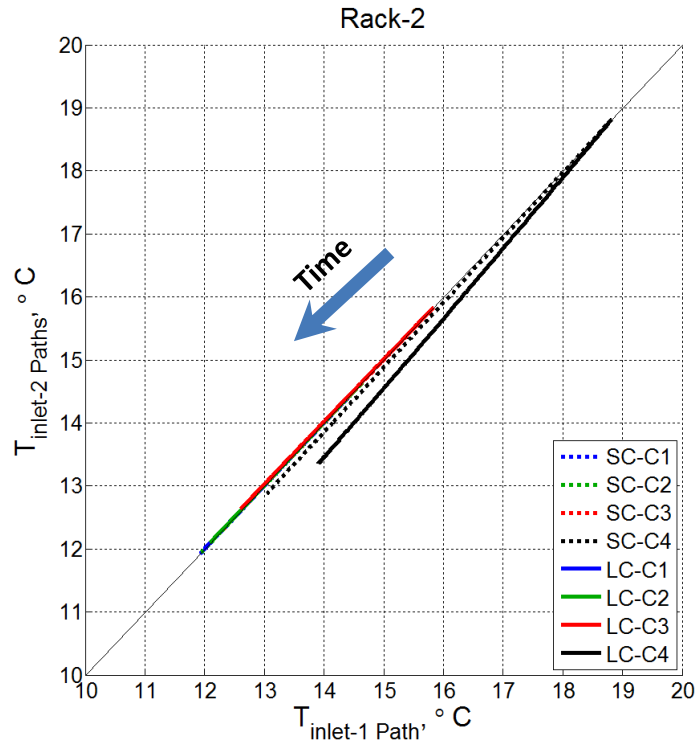


**Figure 6.14: Effect of surface area per rack on the model results (Rack2).**

The inlet temperatures obtained through 2 path definitions are read at the vertical axis and single path results are on the horizontal axis. SC and LC in the legends stand for the “small capacitance” for 4 times smaller surface area per rack and “large capacitance” for the actual surface area per rack in our RL. While going from 2 paths to 1 path noticeably changes the results for R2C4 with the LC, the difference is about a tenth of a degree C for the case of the data center with smaller surface area per rack (SC).

#### 6.4 Large Scale Data Center Simulation

The Hybrid Lumped Capacitance Model procedure that was introduced can be extended to a more realistic data center setting as shown in Figure 6.15. The figure shows the layout of the quadrant of a data center which has symmetry boundary conditions along the sides given without

walls. The domain consists of a total number of 60 servers in 10 racks. The 2 kW server heat load causes a temperature rise of 10°C across each server. Two full CRAH units (one and two halves) serve this quadrant of the data center providing a tile flow rate, which is 75% of the entire air flow rate of the pushed through the racks. The remainder of the rack air flow (25%) is compensated by the recirculated air.

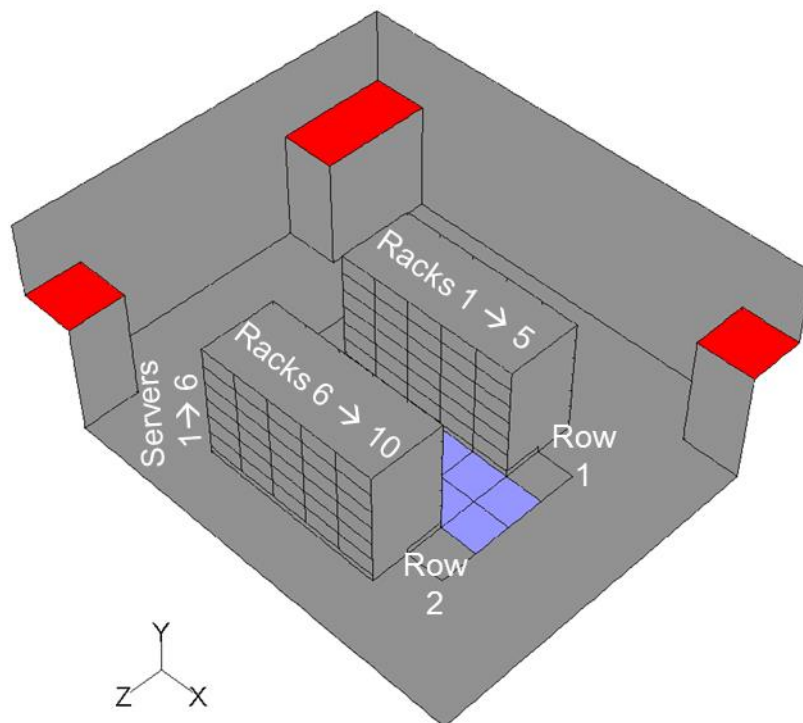


**Figure 6.15: Quadrant Data Center**

It was shown in the previous section that the demand for multiple path definitions diminishes for production data centers, which have at least factor of 4 less surface area per rack compared to our research lab. Hence, the analysis in this part will be based on the single path for the entire recirculated air flow. The inlet air temperature data is obtained through a steady state CFD simulation as provided as an input. The racks in the CFD model were assumed to have comparable thermal characteristics compared to the simulated servers in the research lab.

Two critical cases where the temperatures exceed allowable limits, scenarios of CRAH fan failure and chilled water interruption, were exercised in the model based on the quadrant data center. Figure 6.16 and 6.17 show computed inlet temperatures of certain racks respectively for the cases of chilled water interruption and CRAH fan failure.

The maximum operating temperature recommended for the continuous operation of servers is 27°C. For a maximum allowable temperature of 35°C, in case of a failure scenario the time of interest can be interpreted as the time for the inlet temperature of the hottest server to increase 8°C. The dashed black line in the figures represents the temperature 8°C higher than the maximum inlet temperature at the initial condition. For the given load and operating conditions and type of the data center, the data center operator would have a time of about a minute following a complete failure of all CRAH fans. Similarly, after a failure of chilled water pump, the temperatures are expected to exceed the allowable limits in about 250 seconds. These results are for racks populated with servers that have time constants of about 6 minutes and thermal capacitance comparable to simulated servers.

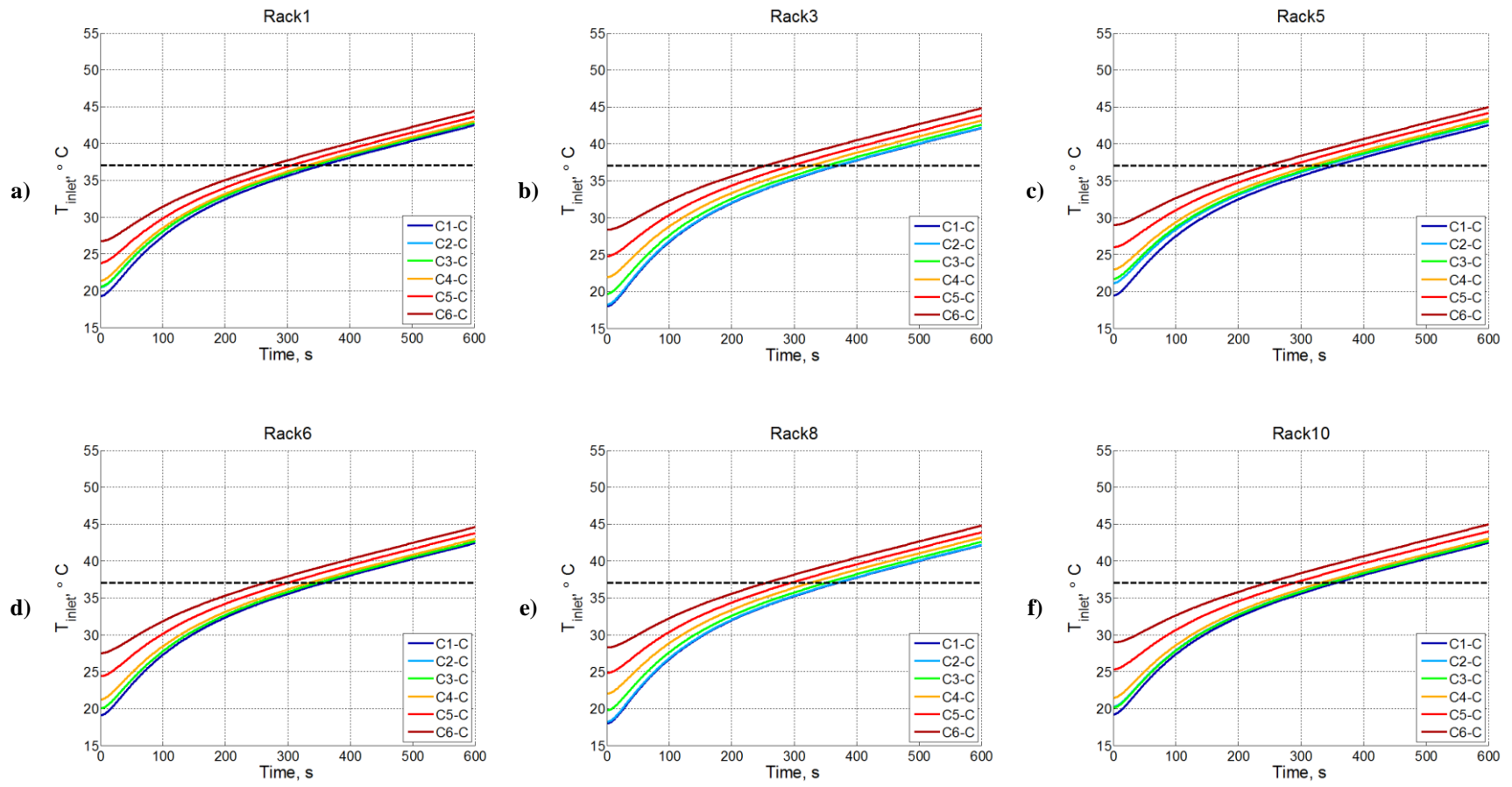


**Figure 6.16: Hybrid-Lumped Capacitance Model results for Chilled Water Interruption with shorter time constants Case a) Rack1 b) Rack3 c) Rack5 d) Rack6 e) Rack8 f) Rack10**



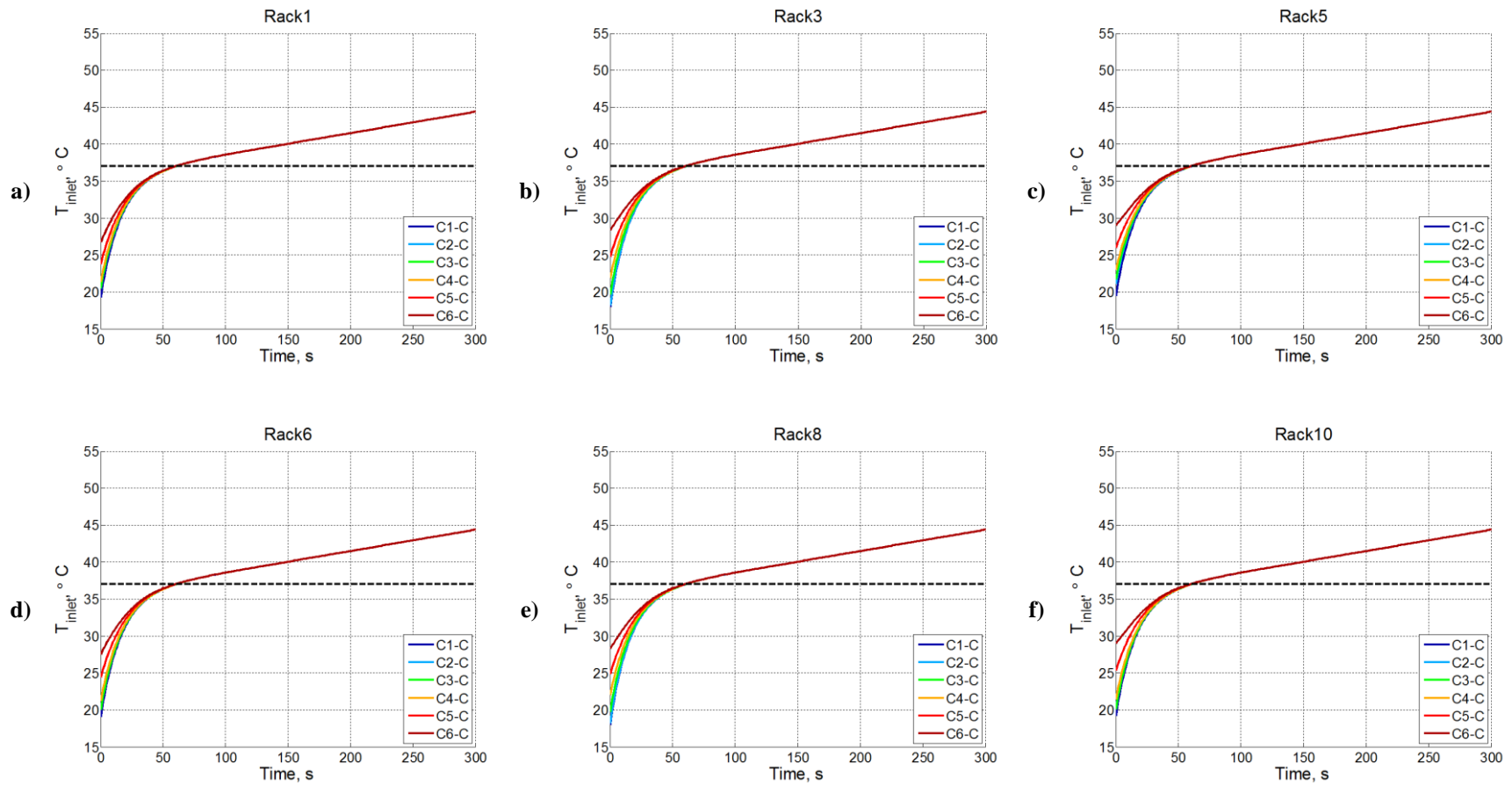


Figure 6.17: Hybrid-Lumped Capacitance Model results for CRAH Fan Failure with shorter time constants Case a) Rack1 b) Rack3 c) Rack5 d) Rack6 e) Rack8 f) Rack10

## 6.5 Chapter Conclusions

The effect of thermal masses in a data center was studied through a novel hybrid lumped capacitance model comprising a fast executing transient modeling tool. As indicated at the conclusion of Chapter 5, there is a significant contribution from the thermal masses in the room beyond those of the servers. In addition to the servers, air mass transients, thermal masses of the CRAH units, the room and plenum are introduced as components of the model. The room air transients are handled by volumes of air at either face of the rack. Even though the model is a collection of lumped capacitance models, experimental or computed (e.g., CFD) server inlet temperature data provides the resolution to capture the non-uniformity at the rack inlet face. These temperatures along with the concept of capture index,  $\psi$ , are used to define the amount of warm air conveyed through recirculated paths and cold air through the tiles. For cases of constant CRAH flow rate, the flow field in the room is assumed to be unchanged throughout the simulations. On the other hand, the model can also simulate scenarios involving change in the room flow field.

Hypothetical conduits carrying the recirculated air flow are an easy-to-model technique to characterize the thermal capacitance and thermal conductance of the room as well as the plenum. Robust and simple rules for the dimensions of the conduit increase the practicality of the proposed approach.

The inputs and various parameters that need to be obtained to setup a case are listed as follows.

1. Operational data based on steady state operation
  - a. Steady state server inlet and tile temperatures (Experiments or CFD)
2. Server characteristics

- a. Flow Rate
  - b. Heat Generation
  - c. Thermal Capacitance & Thermal Conductance
3. CRAH characteristics
- a. Flow Rate
  - b. Fan Power
  - c. Thermal Capacitance & Thermal Conductance
    - i. Number of CRAH units
4. Room characteristics
- a. Thermal Capacitance & Thermal Conductance
    - i. Room Dimensions
      - 1. Exposed Surface Area
      - 2. Room volume vs. hot aisle volume
    - ii. Surface Material
  - b. Air Thermal Capacity
5. Plenum characteristics
- a. Thermal Capacitance & Thermal Conductance
    - i. Plenum dimensions
    - ii. Plenum Surface Area
    - iii. Surface Material
    - iv. Area of Open Tiles
    - v. Area of CRAH Discharge

## 7 Summary and Conclusions

The main objectives of this study are experimental and analytical investigation of the transient thermal response of air-cooled data centers. Series of the transient experiments were conducted as explained in detail in Chapter 3. These were intended to provide insight into prominent elements that contribute to the transient thermal behavior of the data centers.

Servers are the primary heat sources in a data center and they constitute a significant part of the entire data center thermal mass. Simulated servers in this study have the typical thermal mass of a real server but a relatively higher time constant due to the lower UA compared to the real servers. However, considering the higher density of server racks per area in a real data center the server's contribution would remain as significant as it was during the experiments in the RL.

Regarding thermal characterization of the servers two practical experiments have been proposed in Chapter 4, which only require readily measurable air temperature at the inlet and exit of a server. Following a sudden change in the power the air temperatures reveal the characteristic time constant of a server. In order to complete server characterization required for the modeling of the server, one needs to find either the thermal conductance or the thermal capacitance of the server. A new approach based on a sudden change in the server inlet temperature has been shown to yield a reasonably accurate estimate of the server thermal capacitance and the thermal capacitance.

CFD inherently captures the transients of air flow and air temperature. However, other thermal masses cannot be easily incorporated in practical CFD simulations of data centers. Hence, utilization of CFD for transient analysis does not capture the full transients in a data center. This

study provides a physics-based transient exit temperature boundary condition for servers, which is implemented in a room-level transient simulation in Chapter 5.

As indicated by the CFD results of the rack shutdown, which consider the rack/server thermal mass, there are unaccounted thermal masses beyond the server that require a more flexible and faster tool to study the effects of these thermal masses on the data center. Chapter 6 introduced a simple practical model that includes lumped capacitances and convective conductances for various components of a data center. Steady state experimental data or CFD simulation results are required to establish the initial conditions of the transient simulations and to capture the temperature variations over an inlet face of racks. The thermal mass of the room air, the room and the plenum and the CRAH units, and estimates of their convective conductances are needed for the hybrid model. A methodology and practical rules for estimating these values are proposed and tested against experimental measurements. Practical rules are proposed for the CRAH and the plenum.

The capacitance of the room enclosure that plays a role in the transient events is determined through the estimated penetration depth of the building material for both of the room and plenum. Due to the thinner building materials (gypsum board) at the room level and their higher thermal diffusivity the entire thickness of those materials are estimated to be as the contributing thermal masses. On the other hand, plenum typically has a thicker concrete slab which has even lower thermal diffusivity. Therefore the calculations of the thermal capacitance for the plenum requires a time of interest for the type of event that needs to be tested.

The CRAH unit along with the plenum becomes an important factor during a failure of chilled water supply. Even if the available cooling in the thermal mass of the CRAH heat exchanger is

important, high thermal conductance of the CRAH heat exchanger causes the cooling core to have faster response compared to the rest of the mass of the CRAH unit. The measurements indicated that about 65% of the CRAH thermal mass is attributed to the heat exchanger with high thermal conductance. However, the thermal conductance for the remainder of the thermal mass is estimated to be less than 10% of the typical air side thermal conductance of the heat exchanger. This leads to a composite structure with two distinct time constants. The hybrid lumped capacitance model takes the two-structure approach of the CRAH unit into account.

As a results of this study, a practical and fast executing physics-based hybrid lumped-capacitance model has been developed and experimentally validated to predict data center transient thermal response following typical disturbances. Subsequent effort demonstrated the importance of server, room, plenum, CRAH unit and air thermal masses in transient simulations of data centers. The model developed showed an RMS error typically less than 1°C. Results of the model application to a representative section of a data center indicated very rapid rise of the temperature at key locations to rise beyond allowable limits within a minute following a complete fan failure scenario. The time for the temperatures to hit the limits following a chilled water interruption is relatively longer (~250 seconds) for the given rack density and server thermal characteristics.

### *7.1 Future Work*

In parallel to the objectives, this study introduced tools with reasonable accuracy based on practical rules. There are several items that needs to be addressed as part of the future work. The results herein are verified in a room, the RL, that has several key features of typical data centers. However, in a production data center of the same size, more than ten racks can be easily

accommodated rather than as few as three. The results indicated increasing influence of the room thermal mass on the transient thermal environment for sparsely populated data centers. A single path approach was shown to be applicable in larger production data centers due to the diminishing improvement of multiple paths in case of higher rack density per data center surface area. Using the single path approach, verifying the set of practical rules in setting up the hybrid thermal capacitance model for a real data center can be a valuable extension to this work. The model can be exercised for more complex scenarios.

The methods that have been proposed to obtain the time constant, thermal conductance and thermal capacitance of servers were tested on the simulated servers. In order to identify possible deficiencies or to verify the concepts, a set of real servers can be tested based on a more systematic experimental procedure. In addition to the experiments for the servers, practical transient experiments for the CRAH units can be designed similarly. The thermal capacitance of the CRAH unit in this study is verified by the dimensional information. As the conclusions indicated CRAH thermal response is a function of two distinct thermal masses. The new experiments as well as the existing experiments can possibly reveal techniques to extract thermal characteristics of the CRAH units as a second layer of verification.

Transient temperature boundary condition for the servers increased the reliability of the future room level transient CFD simulations even though room level transients need to be possibly carried out through conjugate heat transfer models. Regarding the server boundary condition, the generated UDF is a useful starting point for the CFD software developers to implement the tool into commercial codes as a default boundary condition, which does not require the hassle of UDF compilations and substitutes the not user-friendly C coding with a fancy and easy to use graphical user interface.

## Appendix-A: Transient Experiment of IBM Blade Center

Note: This experiment is conducted and documented by a former member of our lab, Dustin Demetriou, PhD.

The transient thermal behavior of the blade chassis can be determined by measuring the inlet and exit temperatures, air flow rate and power input to the chassis. To perform this experiment, an experimental facility, pictured in Figure A-1, was constructed using the already constructed Syracuse University fan tunnel. The fan tunnel was designed according to ASHRAE Standard 51 using a 5" ASME flow nozzle (MFC-3M). A measurement of the differential pressure across the nozzle is done which is related to the flow rate through the nozzle. Since the system is well sealed, this also represents the flow rate through the chassis. The differential pressure measurement is done using a 2" IW ASHCROFT CXL differential pressure transducer with an accuracy of  $\pm 0.4\%$  FS or  $\pm 0.064$  mA. The chassis is housed in a well-sealed and insulated box to minimize leakage air and heat transfer. The chassis under investigation is a 7U IBM BladeCenter E, pictured in Figure A-2, which houses 14 HS20 blade servers, 4-2000W power supply modules, 2 centrifugal blowers, a IBM Advanced Management Module (AMM), 2-Gigabit Ethernet switches, floppy disk drive and a CD-Rom drive. The chassis is rated for a maximum heat output of 5,478 W and air flow rates of 250 CFM @ 25oC and 455 CFM @ 32oC or greater. Each server contains 2 Intel Xeon processors, can support up to 16 GB of RAM and supports 2 SAS HDDs.



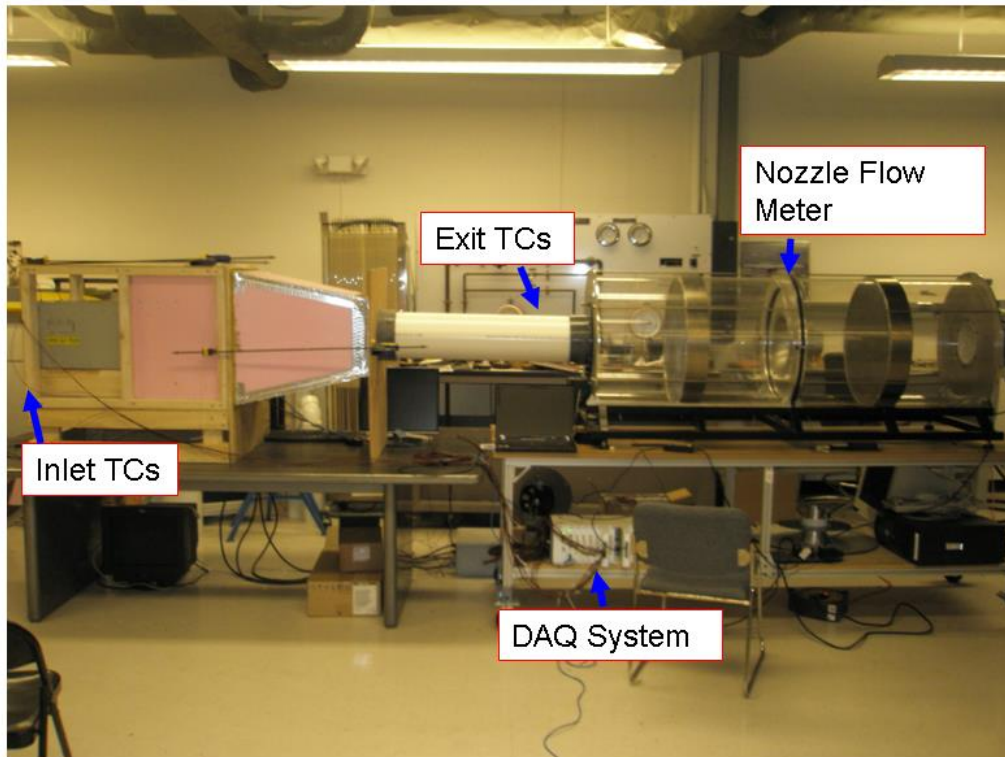
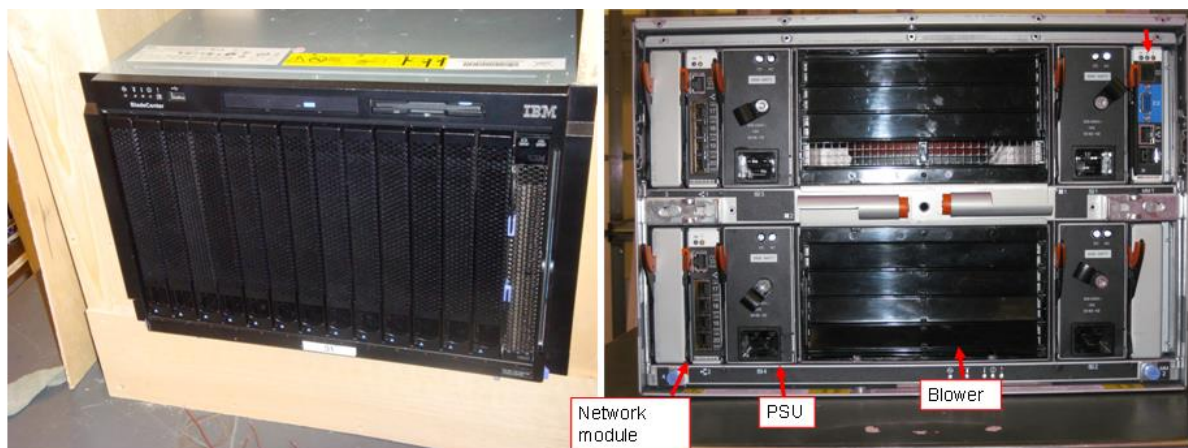


**Figure A.1 – Syracuse University Experimental Setup**



*Front*

*Rear*

**Figure A.2 – IBM Bladecenter E chassis**

The chassis housing is connected to the fan tunnel through a converging section and an 8" PVC duct. The converging section was added to increase mixing before the air enters the duct. The inlet and exit temperatures are measured using calibrated Type-T thermocouples. The thermocouples are calibrated in a temperature controlled chamber housed at Syracuse University. Individual calibration curves are created for each thermocouple with an accuracy of  $\pm 0.1^\circ\text{C}$ . The inlet temperature is measured across the front of the chassis using 6 thermocouples, as specified in the ASHRAE High-density Data Centers Best Practices (2008b). The exit temperature is measured at 5 locations around the duct, four locations around an 7" circumference and a single point at the center of the duct. Temperature measurements of the chassis outside surface temperature are also done at 4 locations (2 top, 1 right and 1 left). These measurements are done with Type-T surface mount thermocouples.

Power measurements are done using Fluke i410 current clamps with a useable AC current range of 0.5 to 400 Amps with an AC accuracy of 3.5% + 0.5 Amps. The output voltage signal of the clamp is connected to a DAQ system using shielded banana jacks. The output scale of the clamp is 1mV per amp. In order to capture the RMS value of the current signal, the DAQ system samples at 1 kHz to avoid any aliasing and allow for RMS signal conditioning. Currently, this procedure is done in software, but results in unnecessary data collection on all channels. The voltage is measured at the wall input socket using a digital multimeter. In order to quantify the power consumption of the chassis at different levels of CPU usage, the software Stress was used to load the CPUs to 100% usage. The Stress software can also be used to read/write data to hard disk and load memory.

All data is collected using a National Instruments SCXI-1600 USB data acquisition and control module system. The SCXI chassis uses two types of signal conditioning terminal modules. For

thermocouple data collection, the SCXI-1102 thermocouple input module is used. This card offers built-in cold junction sensors, 2 Hz lowpass filtering and amplification on each channel and onboard calibration reference. For collection of voltage signals out of either the differential pressure transducer or the current measurement clamps, the SCXI-1102C input module is used. This module has similar characteristics as the 1102C however can also be used to acquire millivolt, volt, 0 to 20 mA and 4 to 20 mA current input signals. In combination with the SCXI-1600 module, these cards analog input channels can be scanned at rates up to 333 kS/s (3  $\mu$ s per channel). The DAQ system has an accuracy of  $\pm 0.2$  mV accuracy with an auto-selected gain. The DAQ system is interfaced to a PC which uses VDAQ (Variable Data Acquisition System) V 4.0 software. This software is designed to acquire, log and export data collected by National Instruments DAQ cards. The software consists of two modules, the recorded and calibrator. The recorded is used to view real-time data, record data, playback previously recorded data and export data. The calibration is used to provide simultaneous channel-specific signal calibration (Viewpoint, 2009).

The thermal characteristics of the chassis are determined for both start-up and shut-down conditions. These tests were performed in series with the entire testing period lasting 2 hours.

The methodology of the test is as follows:

1. The chassis is supplied power from the rated 208 V source. The AMM, fans, floppy disk drive, and CD-Rom are allowed to come to steady state. Data is collected for 15 minutes.
2. For the start-up test, the blade servers are simultaneously turned on without any CPU loading using the web-interface to the AMM. Data is collected for 45 minutes.
3. Upon completion of the start-up test, the blade serves are simultaneously turned off using the web-interface to the AMM. Data is again collected for 45 minutes.

4. Finally, the chassis is allowed to return to steady state as in step 1. Data is collected for another 15 minutes.
5. Data is post-processed to extract the thermal time constant of the chassis with appropriate checks done on the data using energy balance.

Figure A-3 shows the results for a transient start-up test for the inlet and exit air temperature. The results showed uniform distribution across the thermocouples and therefore, the 6 inlet thermocouples are averaged as well as the 5 exit thermocouples. An important item to notice is that the inlet temperature remains constant throughout the test. This is important since the fan speed control is based on the inlet air temperature sensor located on the chassis. This constant inlet temperature will result in constant fan speed and therefore flow rate. The exit air temperature profile exhibits that of a first-order system as anticipated. The chassis takes around 25 minutes to reach steady-state conditions upon start-up. Figure A-4 shows the surface mounted thermocouples temperature profiles. TC 27 and 28 are placed on the left and right side of the chassis and show good symmetry with in the chassis. TC 29 is place on the top in the front and TC 26 is placed to the top towards the back. Interestingly, the top, back thermocouple has the highest temperature as it is place over the chassis power supply units. Consistent with the air temperature measurements, the metal temperature also reaches steady-state conditions within about 25 minutes. Figure A-5 and A-6 show the results for the transient air conditions and metal conditions during the shut-down test. The shut-down test behavior is similar to that of the start-up test with a steady-state time of around 25 minutes.

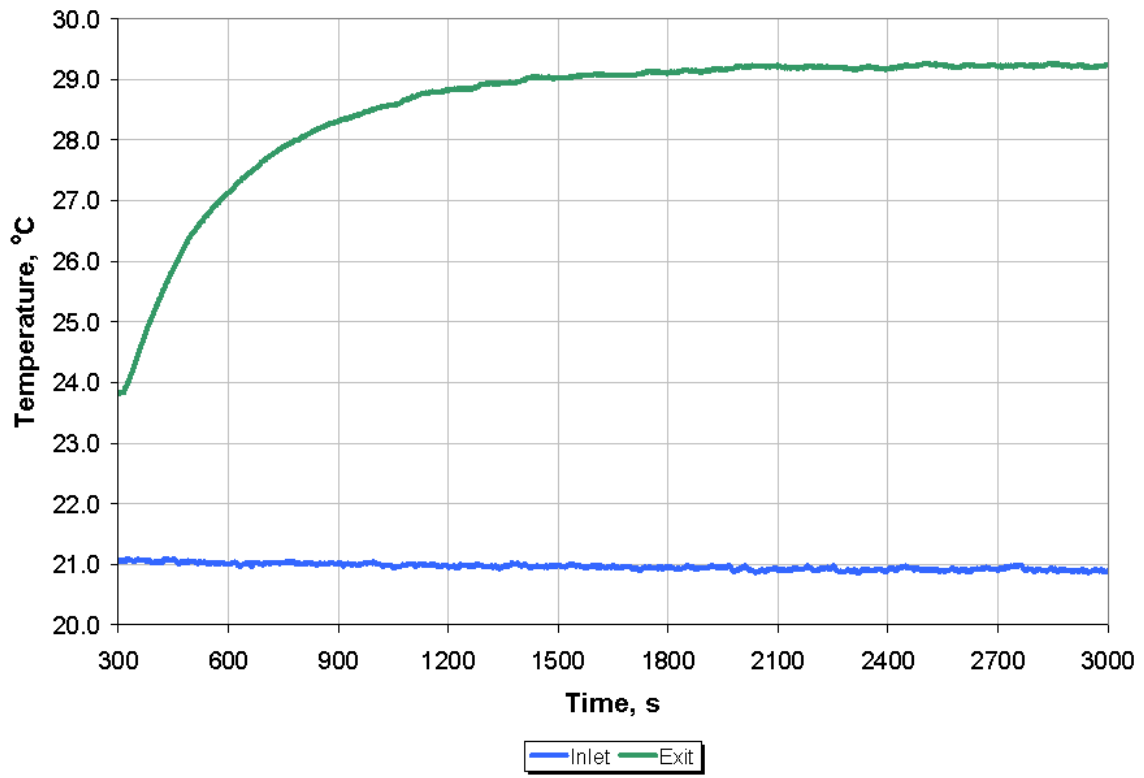


**Figure A.3 – Start-up Test Air Temperature Measurements**

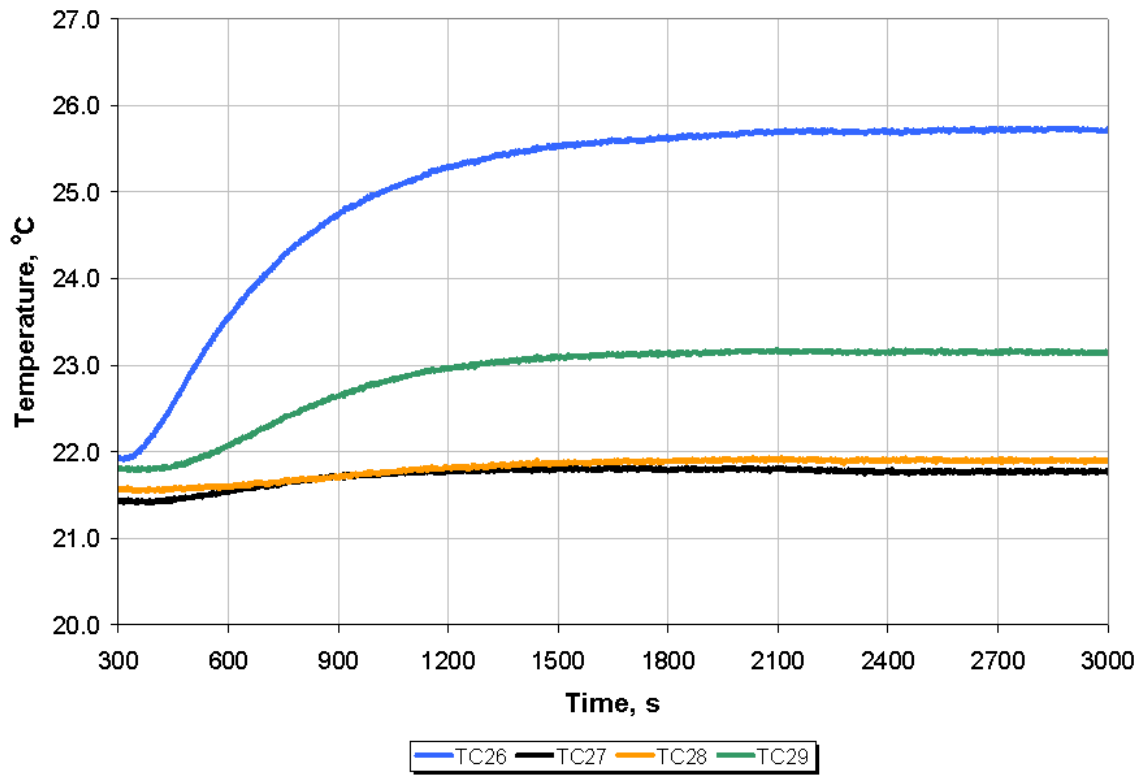


**Figure A.4 – Start-up Test Metal Temperatures**

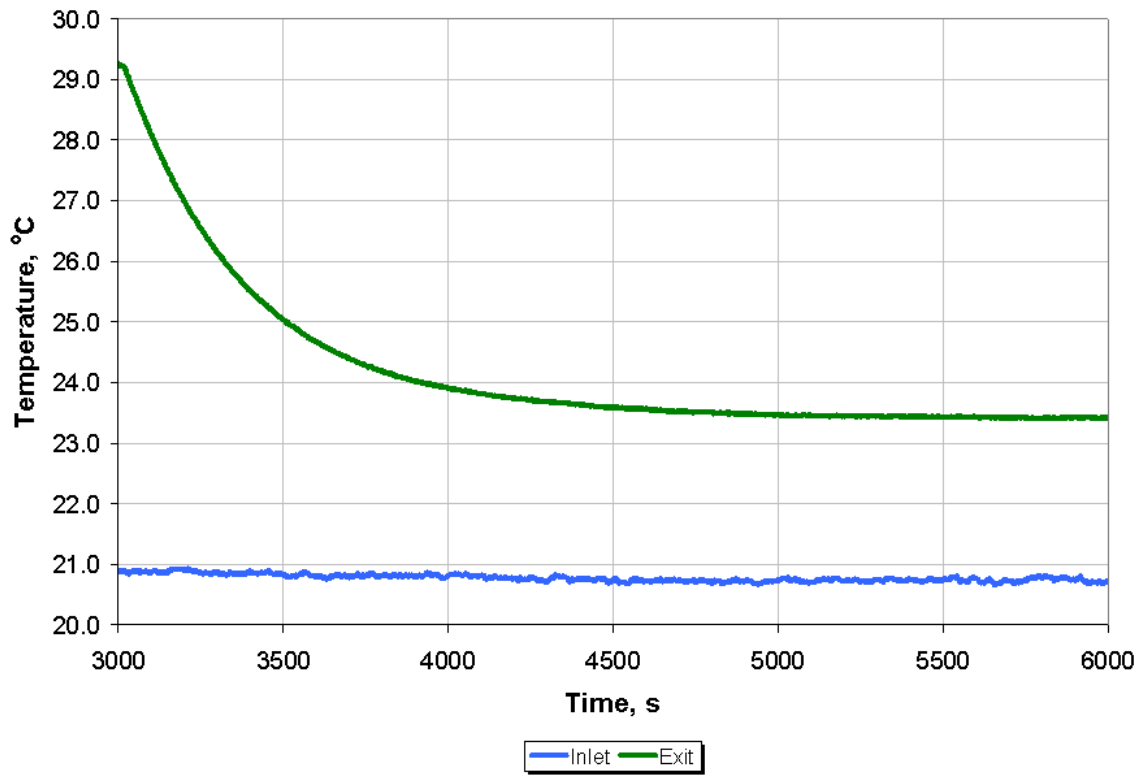


**Figure A.5 – Shut-down Test Air Temperature Measurements**

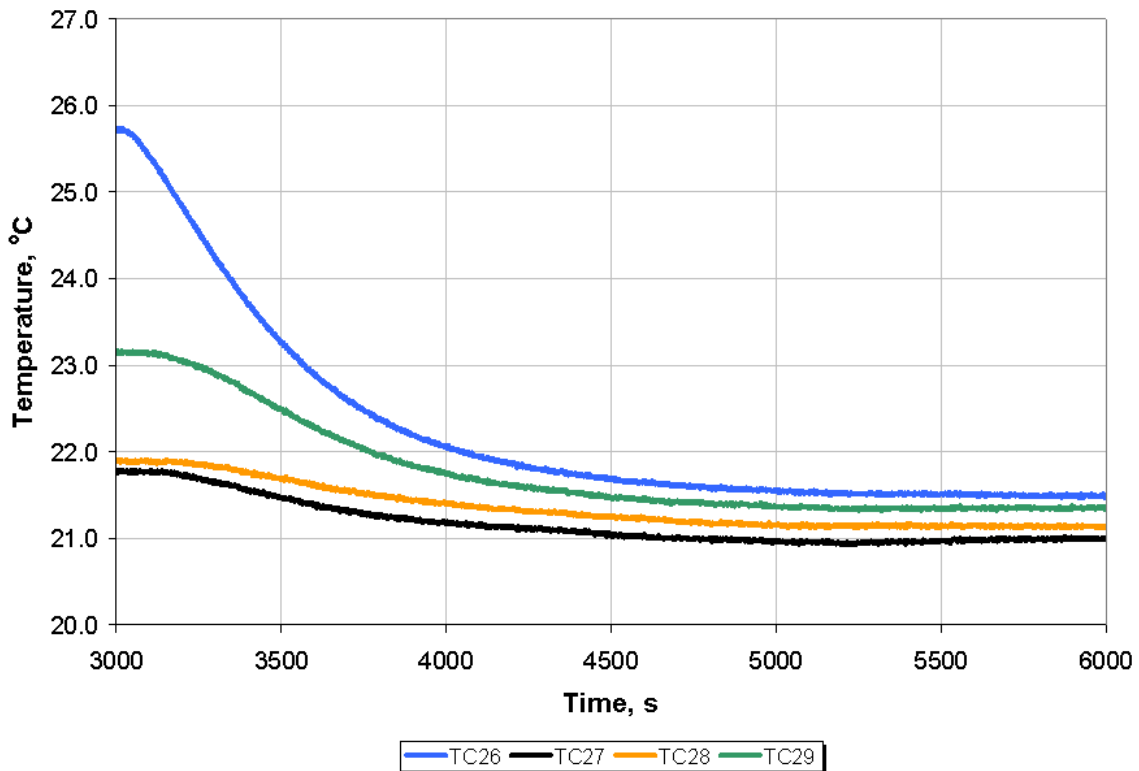


**Figure A.6 – Shut-down Test Metal Temperatures**

In each of the test, the CPUs were not loaded beyond any idle processes the operating system has. To justify this procedure a test was done that measured the power consumption for different CPU usage levels. The BladeCenter contains 28 CPUs across the 14 servers. For this test, a different number of CPUs were loaded to 100% usage and the power consumption was measured. Figure A-7 shows a plot of power consumption vs. CPU usage. The idle state of the chassis, that at which all servers are on at 0% usage, is around 1225 W. The addition of the 28 CPUs running at 100% usage adds about 200 W or about 15% power consumption.



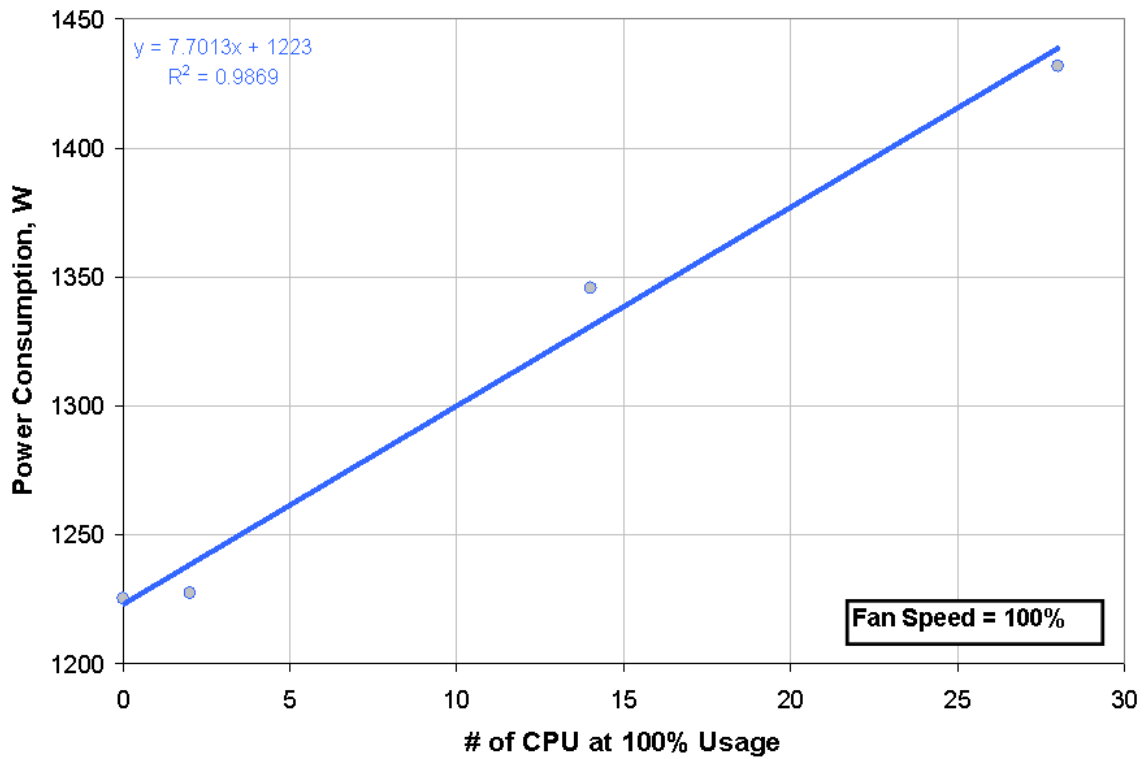


**Figure A.7– Chassis Power Consumption vs. CPU Usage**

As anticipated, the chassis exhibits the behavior of a first-order lumped capacitance thermal system. The similar behavior of both start-up and shut-down facilitates the extraction of a single time constant.

## Appendix-B: UDF Source Code for Rack Shutdown Experiment

```

/*****
This UDF computes transient exit air temperature of the server
following a sudden change in the server power.
*****/
/*****
Initial part of the udf consists of the input parameters
*****/
#include "udf.h"
#include "unsteady.h"
#include "para.h"
#define n 15          /***Number of servers partitions***/
int id_i[n] = {132,166,165,164,163,131,162,161,160,159,130,158,157,156,155};    /***Inlet
boundary ID of the server***/
int id_o[n] = {129,154,153,152,151,128,150,149,148,147,127,146,145,144,143};    /***outlet
boundary ID of the server***/
int ns;              /*** counter for number of servers ***/
real mdot[n] =
{0.074574,0.292426,0.366,0.368,0.366,0.085141,0.33386,0.419,0.44,0.44,0.076,0.298,0.362,0.367,0.3
57};    /***Mass flow rate for server partitions (kg/s)***/
real T_in;          /*** Air Temperature over the face cells of the server inlet ***/
real T_inavg[n];    /*** Average Server Inlet Air Temperature ***/
real T_inavg_old[n]; /*** Average Server Inlet Air Temperature at the previous time step***/
real T_out;         /*** Air Temperature over the face cells of the server exit ***/
real T_outavg[n];   /*** Average Server Exit Air Temperature ***/
real area[n] =
{0.06193537,0.2428647,0.3048,0.3048,0.30302,0.06193537,0.2428647,0.3048,0.3048,0.30302,0.06193537
,0.2428647,0.3048,0.3048,0.30302};    /*** Server Flow Area ***/
real Tnext[n];     /*** The lumped temperature of the server at the current time step ***/
real Tprev[n];     /*** The lumped temperature of the server at the previous time step ***/
real tcheck[n];    /*** The current time saved at the beginning of each time step.
***/
real uson;         /***unsteady calculation is ON when uson=1; OFF when uson=0. ***/
real Cs[n] =
{19304,75696,95000,95000,95000,19304,75696,95000,95000,95000,19304,75696,95000,95000,95000};
    /***Server Thermal Capacity - J/K***/
real Qs1[n] =
{754.8,2959.9,3680.3,3687.7,3699.5,777.4,3048.6,3813.3,3819.6,3784.5,747.5,2931.1,3689.8,3657.1,3
636.3}; /***Initial Server Power - W***/
real Qs2[n] =
{52.6,206.1,253.1,250.9,253.1,73.2,287.2,347.7,354.0,347.7,53.0,207.9,272.2,258.7,247.5};
    /***Server Power after transient event happens at the time of tswitch - w***/
real tswitch[n] = {300,300,300,300,300,300,300,300,300,300,300,300,300,300,300};
    /***Flow Time to Switch Server Power - s***/
real tau[n] = {817,817,887,889,930,752,752,729,865,821,830,830,838,895,879};
    /***Server Time Constants - s***/
FILE *fp;

DEFINE_EXECUTE_ON_LOADING(loaddata, lib3d)
{
/*Loading the temperature data during startup.*/

for (ns=0; ns<n; ns++)

{

if (ns==0)
{fp = fopen("tnext_last 1.csv","r+");
fscanf (fp,"%lf,%lf,%lf\n",&Tprev[ns],&T_inavg[ns],&T_outavg[ns]);
fclose(fp);
host_to_node_real_3(Tprev[ns],T_inavg[ns],T_outavg[ns]);}

else if (ns==1)
{fp = fopen("tnext_last 2.csv","r+");
fscanf (fp,"%lf,%lf,%lf\n",&Tprev[ns],&T_inavg[ns],&T_outavg[ns]);
fclose(fp);
host_to_node_real_3(Tprev[ns],T_inavg[ns],T_outavg[ns]);}

}

}

```

```

else if (ns==2)
{fp = fopen("tnext_last_3.csv","r+");
fscanf (fp,"%lf,%lf,%lf\n",&Tprev[ns],&T_inavg[ns],&T_outavg[ns]);
fclose(fp);
host_to_node_real_3(Tprev[ns],T_inavg[ns],T_outavg[ns]);}

else if (ns==3)
{fp = fopen("tnext_last_4.csv","r+");
fscanf (fp,"%lf,%lf,%lf\n",&Tprev[ns],&T_inavg[ns],&T_outavg[ns]);
fclose(fp);
host_to_node_real_3(Tprev[ns],T_inavg[ns],T_outavg[ns]);}

else if (ns==4)
{fp = fopen("tnext_last_5.csv","r+");
fscanf (fp,"%lf,%lf,%lf\n",&Tprev[ns],&T_inavg[ns],&T_outavg[ns]);
fclose(fp);
host_to_node_real_3(Tprev[ns],T_inavg[ns],T_outavg[ns]);}

else if (ns==5)
{fp = fopen("tnext_last_6.csv","r+");
fscanf (fp,"%lf,%lf,%lf\n",&Tprev[ns],&T_inavg[ns],&T_outavg[ns]);
fclose(fp);
host_to_node_real_3(Tprev[ns],T_inavg[ns],T_outavg[ns]);}

else if (ns==6)
{fp = fopen("tnext_last_7.csv","r+");
fscanf (fp,"%lf,%lf,%lf\n",&Tprev[ns],&T_inavg[ns],&T_outavg[ns]);
fclose(fp);
host_to_node_real_3(Tprev[ns],T_inavg[ns],T_outavg[ns]);}

else if (ns==7)
{fp = fopen("tnext_last_8.csv","r+");
fscanf (fp,"%lf,%lf,%lf\n",&Tprev[ns],&T_inavg[ns],&T_outavg[ns]);
fclose(fp);
host_to_node_real_3(Tprev[ns],T_inavg[ns],T_outavg[ns]);}

else if (ns==8)
{fp = fopen("tnext_last_9.csv","r+");
fscanf (fp,"%lf,%lf,%lf\n",&Tprev[ns],&T_inavg[ns],&T_outavg[ns]);
fclose(fp);
host_to_node_real_3(Tprev[ns],T_inavg[ns],T_outavg[ns]);}

else if (ns==9)
{fp = fopen("tnext_last_10.csv","r+");
fscanf (fp,"%lf,%lf,%lf\n",&Tprev[ns],&T_inavg[ns],&T_outavg[ns]);
fclose(fp);
host_to_node_real_3(Tprev[ns],T_inavg[ns],T_outavg[ns]);}

else if (ns==10)
{fp = fopen("tnext_last_11.csv","r+");
fscanf (fp,"%lf,%lf,%lf\n",&Tprev[ns],&T_inavg[ns],&T_outavg[ns]);
fclose(fp);
host_to_node_real_3(Tprev[ns],T_inavg[ns],T_outavg[ns]);}

else if (ns==11)
{fp = fopen("tnext_last_12.csv","r+");
fscanf (fp,"%lf,%lf,%lf\n",&Tprev[ns],&T_inavg[ns],&T_outavg[ns]);
fclose(fp);
host_to_node_real_3(Tprev[ns],T_inavg[ns],T_outavg[ns]);}

else if (ns==12)
{fp = fopen("tnext_last_13.csv","r+");
fscanf (fp,"%lf,%lf,%lf\n",&Tprev[ns],&T_inavg[ns],&T_outavg[ns]);
fclose(fp);
host_to_node_real_3(Tprev[ns],T_inavg[ns],T_outavg[ns]);}

else if (ns==13)
{fp = fopen("tnext_last_14.csv","r+");
fscanf (fp,"%lf,%lf,%lf\n",&Tprev[ns],&T_inavg[ns],&T_outavg[ns]);
fclose(fp);
host_to_node_real_3(Tprev[ns],T_inavg[ns],T_outavg[ns]);}

```

```

else if (ns==14)
{fp = fopen("tnext_last_15.csv","r+");
fscanf (fp,"%lf,%lf,%lf\n",&Tprev[ns],&T_inavg[ns],&T_outavg[ns]);
fclose(fp);
host_to_node_real_3(Tprev[ns],T_inavg[ns],T_outavg[ns]);}

}

}

/*****
Internally computed variables (Server Mass Temperature, Inlet and Exit Air Temperatures)
are saved in data files (.csv) when exiting (see DEFINE_EXECUTE_AT_EXIT).
The program gives error on loading, in case Excel files
for the servers are not available in the same directory with the case and data files.
If the simulation is started from scratch, data files are still required to be able to load the
case.
If the simulation starts with unsteady mode (uson=1) the inputs of the data files need to be
computed externally. Otherwise, correct values can be calculated during steady mode (uson=0) of
the
calculations.
DEFINE_EXECUTE_AT_EXIT saves the internally computed variables for each server
partition in a ".csv" file that can be loaded when the case is loaded again to
continue the simulation from the point where it was stopped.
*****/
DEFINE_EXECUTE_AT_EXIT(savedata)
{
/*Saving the temperature data at the exit.*/

for (ns=0; ns<n; ns++)

{

if (ns==0)
{fp = fopen("tnext_last_1.csv","w+");
fprintf (fp,"%lf,%lf,%lf\n",Tprev[ns],T_inavg[ns],T_outavg[ns]);
fclose(fp);}

else if (ns==1)
{fp = fopen("tnext_last_2.csv","w+");
fprintf (fp,"%lf,%lf,%lf\n",Tprev[ns],T_inavg[ns],T_outavg[ns]);
fclose(fp);}

else if (ns==2)
{fp = fopen("tnext_last_3.csv","w+");
fprintf (fp,"%lf,%lf,%lf\n",Tprev[ns],T_inavg[ns],T_outavg[ns]);
fclose(fp);}

else if (ns==3)
{fp = fopen("tnext_last_4.csv","w+");
fprintf (fp,"%lf,%lf,%lf\n",Tprev[ns],T_inavg[ns],T_outavg[ns]);
fclose(fp);}

else if (ns==4)
{fp = fopen("tnext_last_5.csv","w+");
fprintf (fp,"%lf,%lf,%lf\n",Tprev[ns],T_inavg[ns],T_outavg[ns]);
fclose(fp);}

else if (ns==5)
{fp = fopen("tnext_last_6.csv","w+");
fprintf (fp,"%lf,%lf,%lf\n",Tprev[ns],T_inavg[ns],T_outavg[ns]);
fclose(fp);}

else if (ns==6)
{fp = fopen("tnext_last_7.csv","w+");
fprintf (fp,"%lf,%lf,%lf\n",Tprev[ns],T_inavg[ns],T_outavg[ns]);
fclose(fp);}

else if (ns==7)

```

```

{fp = fopen("tnext_last_8.csv","w+");
fprintf (fp,"%lf,%lf,%lf\n",Tprev[ns],T_inavg[ns],T_outavg[ns]);
fclose(fp);}

else if (ns==8)
{fp = fopen("tnext_last_9.csv","w+");
fprintf (fp,"%lf,%lf,%lf\n",Tprev[ns],T_inavg[ns],T_outavg[ns]);
fclose(fp);}

else if (ns==9)
{fp = fopen("tnext_last_10.csv","w+");
fprintf (fp,"%lf,%lf,%lf\n",Tprev[ns],T_inavg[ns],T_outavg[ns]);
fclose(fp);}

else if (ns==10)
{fp = fopen("tnext_last_11.csv","w+");
fprintf (fp,"%lf,%lf,%lf\n",Tprev[ns],T_inavg[ns],T_outavg[ns]);
fclose(fp);}

else if (ns==11)
{fp = fopen("tnext_last_12.csv","w+");
fprintf (fp,"%lf,%lf,%lf\n",Tprev[ns],T_inavg[ns],T_outavg[ns]);
fclose(fp);}

else if (ns==12)
{fp = fopen("tnext_last_13.csv","w+");
fprintf (fp,"%lf,%lf,%lf\n",Tprev[ns],T_inavg[ns],T_outavg[ns]);
fclose(fp);}

else if (ns==13)
{fp = fopen("tnext_last_14.csv","w+");
fprintf (fp,"%lf,%lf,%lf\n",Tprev[ns],T_inavg[ns],T_outavg[ns]);
fclose(fp);}

else if (ns==14)
{fp = fopen("tnext_last_15.csv","w+");
fprintf (fp,"%lf,%lf,%lf\n",Tprev[ns],T_inavg[ns],T_outavg[ns]);
fclose(fp);}

}

}

/*****
DEFINE_ADJUST read air temperatures of the server at the inlet and exit faces
and computes area weighted average values. The computed values are passed into
DEFINE_PROFILE modules to calculate current lumped body temperature of the servers.
*****/
DEFINE_ADJUST(serverinout,d)
{
/*Reading the mass flow rate and temperature at the inlet.*/

#if !RP_HOST                               /**PARALLELIZATION***/
Thread *t;
real area_t;
real A[ND_ND];
face_t f;
#endif /* !RP_HOST */                       /**PARALLELIZATION***/

d = Get_Domain(1);

for (ns=0; ns<n; ns++)

{

host_to_node_int_1(id_i[ns]);               /**PARALLELIZATION***/

#if !RP_HOST                               /**PARALLELIZATION***/

t= Lookup_Thread(d,id_i[ns]);

```

```

if (CURRENT_TIME>tcheck[ns])
{Tprev[ns] = Tnext[ns];}

tcheck[ns]= CURRENT_TIME;

area[ns]=0.0;
T_in=0.0;

begin_f_loop(f,t)
if (PRINCIPAL_FACE_P(f,t))          /****PARALLELIZATION****/
{
    F_AREA(A,f,t);
    area_t = NV_MAG(A);
    area[ns] += area_t;
    T_in += F_T(f,t)*area_t;
}
end_f_loop(f,t)
#if RP_NODE                          /****PARALLELIZATION****/
area[ns] = PRF_GRSUM1(area[ns]);
T_in = PRF_GRSUM1(T_in);
T_inavg[ns] = T_in/fabs(area[ns]);
#endif /* RP_NODE*/                  /****PARALLELIZATION****/
#endif /* !RP_HOST */                /****PARALLELIZATION****/

host_to_node_int_1(id_o[ns]);
#if !RP_HOST                          /****PARALLELIZATION****/
t= Lookup_Thread(d,id_o[ns]);
area[ns]=0.0;
T_out=0.0;

begin_f_loop(f,t)
if (PRINCIPAL_FACE_P(f,t))          /****PARALLELIZATION****/
{
    F_AREA(A,f,t);
    area_t = NV_MAG(A);
    area[ns] += area_t;
    T_out += F_T(f,t)*area_t;
}
end_f_loop(f,t)
#if RP_NODE                          /****PARALLELIZATION****/
area[ns] = PRF_GRSUM1(area[ns]);
T_out = PRF_GRSUM1(T_out);
T_outavg[ns] = T_out/fabs(area[ns]);
#endif /* RP_NODE*/                  /****PARALLELIZATION****/
#endif /* !RP_HOST */                /****PARALLELIZATION****/

}
}

/*****
Remaining DEFINE_PROFILE functions are required for each server to compute
the current body temperature and the transient exit air temperature.
Each of these need to be hooked at the temperature of exit velocity boundary condition.
See journal file for instructions to setup this UDF.
Until transient events start (CURRENT_TIME<tswitch[ns]), the calculations are steady (uson=0).
After transient events start (CURRENT_TIME>tswitch[ns]), the calculations are unsteady (uson=1).
*****/

/*****
UDF for SERVER EXIT TEMPERATURE - 1
*****/
DEFINE_PROFILE(exittemp1,t,i)
{
/*Compute transient server exit air temperature.*/
#if !RP_HOST                          /****PARALLELIZATION****/
face_t f;

real Qs;
real cp = 1005; /*J/kg/K*/
real UA;

```

```

real Ca;
real K;
real dt = CURRENT_TIMESTEP;
real A_1;
real B_1;
real C_1;
real NTU;

ns=0;
Ca = mdot[ns]*cp;
K = Cs[ns]/tau[ns];
if (K/Ca<1)
{NTU = -log(1-K/(Ca+0.0000001));}
else
{NTU = 30;}
UA = Ca*NTU;

if (CURRENT_TIME<tswitch[ns])
{Qs = Qs1[ns];
uson = 0.0;}
else
{Qs = Qs2[ns];
uson = 1.0;}

A_1=(1-dt*Ca*(1-exp(-NTU))/2/Cs[ns])/(1+dt*Ca*(1-exp(-NTU))/2/Cs[ns]);
B_1=(dt*Ca*(1-exp(-NTU))/Cs[ns])/(1+dt*Ca*(1-exp(-NTU))/2/Cs[ns]);
C_1=Qs*dt/Cs[ns]/(1+dt*Ca*(1-exp(-NTU))/2/Cs[ns]);

begin_f_loop(f,t)
if (PRINCIPAL_FACE_P(f,t) /****PARALLELIZATION****/
{
F_PROFILE(f,t,i) = (1-uson)*(T_inavg[ns]+Qs/Ca)+uson*(T_inavg[ns]*exp(-
NTU)+(A_1*Tprev[ns]+B_1*T_inavg[ns]+C_1)*(1-exp(-NTU)));
}
end_f_loop(f,t)
#endif RP_NODE /****PARALLELIZATION****/
Tnext[ns]=(1-uson)*(T_inavg[ns]+Qs/Ca/(1-exp(-NTU)))+uson*(A_1*Tprev[ns]+B_1*T_inavg[ns]+C_1);
#endif /* RP_NODE*/ /****PARALLELIZATION****/

#endif /* !RP_HOST*/ /****PARALLELIZATION****/

}

/*****
UDF for SERVER EXIT TEMPERATURE - 2
*****/
DEFINE_PROFILE(exittemp2,t,i)
{
/*Compute transient server exit air temperature.*/
#ifdef RP_HOST /****PARALLELIZATION****/
face_t f;

real Qs;
real cp = 1005; /*J/kg/K*/
real UA;
real Ca;
real K;
real dt = CURRENT_TIMESTEP;
real A_1;
real B_1;
real C_1;
real NTU;

ns=1;
Ca = mdot[ns]*cp;
K = Cs[ns]/tau[ns];
if (K/Ca<1)
{NTU = -log(1-K/(Ca+0.0000001));}
else
{NTU = 30;}
UA = Ca*NTU;

```

```

if (CURRENT_TIME<tswitch[ns])
{Qs = Qs1[ns];
uson = 0.0;}
else
{Qs = Qs2[ns];
uson = 1.0;}

A_1=(1-dt*Ca*(1-exp(-NTU))/2/Cs[ns])/(1+dt*Ca*(1-exp(-NTU))/2/Cs[ns]);
B_1=(dt*Ca*(1-exp(-NTU))/Cs[ns])/(1+dt*Ca*(1-exp(-NTU))/2/Cs[ns]);
C_1=Qs*dt/Cs[ns]/(1+dt*Ca*(1-exp(-NTU))/2/Cs[ns]);

begin_f_loop(f,t)
if(PRINCIPAL_FACE_P(f,t)) /***PARALLELIZATION***/
{
F_PROFILE(f,t,i) = (1-uson)*(T_inavg[ns]+Qs/Ca)+uson*(T_inavg[ns]*exp(-
NTU)+(A_1*Tprev[ns]+B_1*T_inavg[ns]+C_1)*(1-exp(-NTU)));
}
end_f_loop(f,t)
#ifdef RP_NODE /***PARALLELIZATION***/
Tnext[ns]=(1-uson)*(T_inavg[ns]+Qs/Ca/(1-exp(-NTU)))+uson*(A_1*Tprev[ns]+B_1*T_inavg[ns]+C_1);
#endif /* RP_NODE*/ /***PARALLELIZATION***/

#endif /* !RP_HOST*/ /***PARALLELIZATION***/

}

/*****
UDF for SERVER EXIT TEMPERATURE - 3
*****/
DEFINE_PROFILE(exittemp3,t,i)
{
/*Compute transient server exit air temperature.*/
#ifdef !RP_HOST /***PARALLELIZATION***/
face_t f;

real Qs;
real cp = 1005; /*J/kg/K*/
real UA;
real Ca;
real K;
real dt = CURRENT_TIMESTEP;
real A_1;
real B_1;
real C_1;
real NTU;

ns=2;
Ca = mdot[ns]*cp;
K = Cs[ns]/tau[ns];
if (K/Ca<1)
{NTU = -log(1-K/(Ca+0.0000001));}
else
{NTU = 30;}
UA = Ca*NTU;

if (CURRENT_TIME<tswitch[ns])
{Qs = Qs1[ns];
uson = 0.0;}
else
{Qs = Qs2[ns];
uson = 1.0;}

A_1=(1-dt*Ca*(1-exp(-NTU))/2/Cs[ns])/(1+dt*Ca*(1-exp(-NTU))/2/Cs[ns]);
B_1=(dt*Ca*(1-exp(-NTU))/Cs[ns])/(1+dt*Ca*(1-exp(-NTU))/2/Cs[ns]);
C_1=Qs*dt/Cs[ns]/(1+dt*Ca*(1-exp(-NTU))/2/Cs[ns]);

begin_f_loop(f,t)
if(PRINCIPAL_FACE_P(f,t)) /***PARALLELIZATION***/
{

```



```

        F_PROFILE(f,t,i) = (1-uson)*(T_inavg[ns]+Qs/Ca)+uson*(T_inavg[ns]*exp(-
NTU)+(A_1*Tprev[ns]+B_1*T_inavg[ns]+C_1)*(1-exp(-NTU)));
    }
    end_f_loop(f,t)
# if RP_NODE_                                /**PARALLELIZATION***/
Tnext[ns]=(1-uson)*(T_inavg[ns]+Qs/Ca/(1-exp(-NTU)))+uson*(A_1*Tprev[ns]+B_1*T_inavg[ns]+C_1);
# endif /* RP_NODE*/                          /**PARALLELIZATION***/

# endif /* !RP_HOST*/                          /**PARALLELIZATION***/
}

/*****
UDF for SERVER EXIT TEMPERATURE - 4
*****/
DEFINE_PROFILE(exittemp4,t,i)
{
/*Compute transient server exit air temperature.*/
# if !RP_HOST                                /**PARALLELIZATION***/
face_t f;

real Qs;
real cp = 1005; /*J/kg/K*/
real UA;
real Ca;
real K;
real dt = CURRENT_TIMESTEP;
real A_1;
real B_1;
real C_1;
real NTU;

ns=3;
Ca = mdot[ns]*cp;
K = Cs[ns]/tau[ns];
if (K/Ca<1)
{NTU = -log(1-K/(Ca+0.00000001));}
else
{NTU = 30;}
UA = Ca*NTU;

if (CURRENT_TIME<tswitch[ns])
{Qs = Qs1[ns];
uson = 0.0;}
else
{Qs = Qs2[ns];
uson = 1.0;}

A_1=(1-dt*Ca*(1-exp(-NTU))/2/Cs[ns])/(1+dt*Ca*(1-exp(-NTU))/2/Cs[ns]);
B_1=(dt*Ca*(1-exp(-NTU))/Cs[ns])/(1+dt*Ca*(1-exp(-NTU))/2/Cs[ns]);
C_1=Qs*dt/Cs[ns]/(1+dt*Ca*(1-exp(-NTU))/2/Cs[ns]);

    begin_f_loop(f,t)
if(PRINCIPAL_FACE_P(f,t))                    /**PARALLELIZATION***/
{
        F_PROFILE(f,t,i) = (1-uson)*(T_inavg[ns]+Qs/Ca)+uson*(T_inavg[ns]*exp(-
NTU)+(A_1*Tprev[ns]+B_1*T_inavg[ns]+C_1)*(1-exp(-NTU)));
    }
    end_f_loop(f,t)
# if RP_NODE_                                /**PARALLELIZATION***/
Tnext[ns]=(1-uson)*(T_inavg[ns]+Qs/Ca/(1-exp(-NTU)))+uson*(A_1*Tprev[ns]+B_1*T_inavg[ns]+C_1);
# endif /* RP_NODE*/                          /**PARALLELIZATION***/

# endif /* !RP_HOST*/                          /**PARALLELIZATION***/
}

/*****
UDF for SERVER EXIT TEMPERATURE - 5
*****/
DEFINE_PROFILE(exittemp5,t,i)

```

```

{
/*Compute transient server exit air temperature.*/
#if !RP_HOST                                     /**PARALLELIZATION***/
face_t f;

real Qs;
real cp = 1005; /*J/kg/K*/
real UA;
real Ca;
real K;
real dt = CURRENT_TIMESTEP;
real A_1;
real B_1;
real C_1;
real NTU;

ns=4;
Ca = mdot[ns]*cp;
K = Cs[ns]/tau[ns];
if (K/Ca<1)
{NTU = -log(1-K/(Ca+0.0000001));}
else
{NTU = 30;}
UA = Ca*NTU;

if (CURRENT_TIME<tswitch[ns])
{Qs = Qs1[ns];
uson = 0.0;}
else
{Qs = Qs2[ns];
uson = 1.0;}

A_1=(1-dt*Ca*(1-exp(-NTU))/2/Cs[ns])/(1+dt*Ca*(1-exp(-NTU))/2/Cs[ns]);
B_1=(dt*Ca*(1-exp(-NTU))/Cs[ns])/(1+dt*Ca*(1-exp(-NTU))/2/Cs[ns]);
C_1=Qs*dt/Cs[ns]/(1+dt*Ca*(1-exp(-NTU))/2/Cs[ns]);

begin_f_loop(f,t)
if(PRINCIPAL_FACE_P(f,t))                       /**PARALLELIZATION***/
{
F_PROFILE(f,t,i) = (1-uson)*(T_inavg[ns]+Qs/Ca)+uson*(T_inavg[ns]*exp(-
NTU)+(A_1*Tprev[ns]+B_1*T_inavg[ns]+C_1)*(1-exp(-NTU)));
}
end_f_loop(f,t)
#if RP_NODE                                     /**PARALLELIZATION***/
Tnext[ns]=(1-uson)*(T_inavg[ns]+Qs/Ca/(1-exp(-NTU)))+uson*(A_1*Tprev[ns]+B_1*T_inavg[ns]+C_1);
#endif /* RP_NODE*/                           /**PARALLELIZATION***/

#endif /* !RP_HOST*/                           /**PARALLELIZATION***/
}

/*****
UDF for SERVER EXIT TEMPERATURE - 6
*****/
DEFINE_PROFILE(exittemp6,t,i)
{
/*Compute transient server exit air temperature.*/
#if !RP_HOST                                     /**PARALLELIZATION***/
face_t f;

real Qs;
real cp = 1005; /*J/kg/K*/
real UA;
real Ca;
real K;
real dt = CURRENT_TIMESTEP;
real A_1;
real B_1;
real C_1;
real NTU;

```

```

ns=5;
Ca = mdot[ns]*cp;
K = Cs[ns]/tau[ns];
if (K/Ca<1)
{NTU = -log(1-K/(Ca+0.0000001));}
else
{NTU = 30;}
UA = Ca*NTU;

if (CURRENT_TIME<tswitch[ns])
{Qs = Qs1[ns];
uson = 0.0;}
else
{Qs = Qs2[ns];
uson = 1.0;}

A_1=(1-dt*Ca*(1-exp(-NTU))/2/Cs[ns])/(1+dt*Ca*(1-exp(-NTU))/2/Cs[ns]);
B_1=(dt*Ca*(1-exp(-NTU))/Cs[ns])/(1+dt*Ca*(1-exp(-NTU))/2/Cs[ns]);
C_1=Qs*dt/Cs[ns]/(1+dt*Ca*(1-exp(-NTU))/2/Cs[ns]);

begin_f_loop(f,t)
if(PRINCIPAL_FACE_P(f,t)) /****PARALLELIZATION****/
{
F_PROFILE(f,t,i) = (1-uson)*(T_inavg[ns]+Qs/Ca)+uson*(T_inavg[ns]*exp(-
NTU)+(A_1*Tprev[ns]+B_1*T_inavg[ns]+C_1)*(1-exp(-NTU)));
}
end_f_loop(f,t)
#if RP_NODE /****PARALLELIZATION****/
Tnext[ns]=(1-uson)*(T_inavg[ns]+Qs/Ca/(1-exp(-NTU)))+uson*(A_1*Tprev[ns]+B_1*T_inavg[ns]+C_1);
#endif /* RP_NODE*/ /****PARALLELIZATION****/

#endif /* !RP_HOST*/ /****PARALLELIZATION****/
}

/*****
UDF for SERVER EXIT TEMPERATURE - 7
*****/
DEFINE_PROFILE(exittemp7,t,i)
{
/*Compute transient server exit air temperature.*/
#if !RP_HOST /****PARALLELIZATION****/
face_t f;

real Qs;
real cp = 1005; /*J/kg/K*/
real UA;
real Ca;
real K;
real dt = CURRENT_TIMESTEP;
real A_1;
real B_1;
real C_1;
real NTU;

ns=6;
Ca = mdot[ns]*cp;
K = Cs[ns]/tau[ns];
if (K/Ca<1)
{NTU = -log(1-K/(Ca+0.0000001));}
else
{NTU = 30;}
UA = Ca*NTU;

if (CURRENT_TIME<tswitch[ns])
{Qs = Qs1[ns];
uson = 0.0;}
else
{Qs = Qs2[ns];
uson = 1.0;}

```

```

A_1=(1-dt*Ca*(1-exp(-NTU))/2/Cs[ns])/(1+dt*Ca*(1-exp(-NTU))/2/Cs[ns]);
B_1=(dt*Ca*(1-exp(-NTU))/Cs[ns])/(1+dt*Ca*(1-exp(-NTU))/2/Cs[ns]);
C_1=Qs*dt/Cs[ns]/(1+dt*Ca*(1-exp(-NTU))/2/Cs[ns]);

begin_f_loop(f,t)
if(PRINCIPAL_FACE_P(f,t)) /***PARALLELIZATION***/
{
F_PROFILE(f,t,i) = (1-uson)*(T_inavg[ns]+Qs/Ca)+uson*(T_inavg[ns]*exp(-
NTU)+(A_1*Tprev[ns]+B_1*T_inavg[ns]+C_1)*(1-exp(-NTU)));
}
end_f_loop(f,t)
#endif RP_NODE /***PARALLELIZATION***/
Tnext[ns]=(1-uson)*(T_inavg[ns]+Qs/Ca/(1-exp(-NTU)))+uson*(A_1*Tprev[ns]+B_1*T_inavg[ns]+C_1);
#endif /* RP_NODE*/ /***PARALLELIZATION***/

#endif /* !RP_HOST*/ /***PARALLELIZATION***/

}

/*****
UDF for SERVER EXIT TEMPERATURE - 8
*****/
DEFINE_PROFILE(exittemp8,t,i)
{
/*Compute transient server exit air temperature.*/
#ifdef RP_HOST /***PARALLELIZATION***/
face_t f;

real Qs;
real cp = 1005; /*J/kg/K*/
real UA;
real Ca;
real K;
real dt = CURRENT_TIMESTEP;
real A_1;
real B_1;
real C_1;
real NTU;

ns=7;
Ca = mdot[ns]*cp;
K = Cs[ns]/tau[ns];
if (K/Ca<1)
{NTU = -log(1-K/(Ca+0.0000001));}
else
{NTU = 30;}
UA = Ca*NTU;

if (CURRENT_TIME<tswitch[ns])
{Qs = Qs1[ns];
uson = 0.0;}
else
{Qs = Qs2[ns];
uson = 1.0;}

A_1=(1-dt*Ca*(1-exp(-NTU))/2/Cs[ns])/(1+dt*Ca*(1-exp(-NTU))/2/Cs[ns]);
B_1=(dt*Ca*(1-exp(-NTU))/Cs[ns])/(1+dt*Ca*(1-exp(-NTU))/2/Cs[ns]);
C_1=Qs*dt/Cs[ns]/(1+dt*Ca*(1-exp(-NTU))/2/Cs[ns]);

begin_f_loop(f,t)
if(PRINCIPAL_FACE_P(f,t)) /***PARALLELIZATION***/
{
F_PROFILE(f,t,i) = (1-uson)*(T_inavg[ns]+Qs/Ca)+uson*(T_inavg[ns]*exp(-
NTU)+(A_1*Tprev[ns]+B_1*T_inavg[ns]+C_1)*(1-exp(-NTU)));
}
end_f_loop(f,t)
#endif RP_NODE /***PARALLELIZATION***/
Tnext[ns]=(1-uson)*(T_inavg[ns]+Qs/Ca/(1-exp(-NTU)))+uson*(A_1*Tprev[ns]+B_1*T_inavg[ns]+C_1);
#endif /* RP_NODE*/ /***PARALLELIZATION***/

#endif /* !RP_HOST*/ /***PARALLELIZATION***/

```

```

}

/*****
UDF for SERVER EXIT TEMPERATURE - 9
*****/
DEFINE_PROFILE(exittemp9,t,i)
{
/*Compute transient server exit air temperature.*/
#if !RP_HOST                               /**PARALLELIZATION***/
face_t f;

real Qs;
real cp = 1005; /*J/kg/K*/
real UA;
real Ca;
real K;
real dt = CURRENT_TIMESTEP;
real A_1;
real B_1;
real C_1;
real NTU;

ns=8;
Ca = mdot[ns]*cp;
K = Cs[ns]/tau[ns];
if (K/Ca<1)
{NTU = -log(1-K/(Ca+0.0000001));}
else
{NTU = 30;}
UA = Ca*NTU;

if (CURRENT_TIME<tswitch[ns])
{Qs = Qs1[ns];
uson = 0.0;}
else
{Qs = Qs2[ns];
uson = 1.0;}

A_1=(1-dt*Ca*(1-exp(-NTU))/2/Cs[ns])/(1+dt*Ca*(1-exp(-NTU))/2/Cs[ns]);
B_1=(dt*Ca*(1-exp(-NTU))/Cs[ns])/(1+dt*Ca*(1-exp(-NTU))/2/Cs[ns]);
C_1=Qs*dt/Cs[ns]/(1+dt*Ca*(1-exp(-NTU))/2/Cs[ns]);

begin_f_loop(f,t)
if(PRINCIPAL_FACE_P(f,t))                /**PARALLELIZATION***/
{
F_PROFILE(f,t,i) = (1-uson)*(T_inavg[ns]+Qs/Ca)+uson*(T_inavg[ns]*exp(-
NTU)+(A_1*Tprev[ns]+B_1*T_inavg[ns]+C_1)*(1-exp(-NTU)));
}
end_f_loop(f,t)
#if RP_NODE                               /**PARALLELIZATION***/
Tnext[ns]=(1-uson)*(T_inavg[ns]+Qs/Ca/(1-exp(-NTU)))+uson*(A_1*Tprev[ns]+B_1*T_inavg[ns]+C_1);
#endif /* RP_NODE*/                       /**PARALLELIZATION***/
#endif /* !RP_HOST*/                       /**PARALLELIZATION***/
}

/*****
UDF for SERVER EXIT TEMPERATURE - 10
*****/
DEFINE_PROFILE(exittemp10,t,i)
{
/*Compute transient server exit air temperature.*/
#if !RP_HOST                               /**PARALLELIZATION***/
face_t f;

real Qs;
real cp = 1005; /*J/kg/K*/
real UA;

```

```

real Ca;
real K;
real dt = CURRENT_TIMESTEP;
real A_1;
real B_1;
real C_1;
real NTU;

ns=9;
Ca = mdot[ns]*cp;
K = Cs[ns]/tau[ns];
if (K/Ca<1)
{NTU = -log(1-K/(Ca+0.0000001));}
else
{NTU = 30;}
UA = Ca*NTU;

if (CURRENT_TIME<tswitch[ns])
{Qs = Qs1[ns];
uson = 0.0;}
else
{Qs = Qs2[ns];
uson = 1.0;}

A_1=(1-dt*Ca*(1-exp(-NTU))/2/Cs[ns])/(1+dt*Ca*(1-exp(-NTU))/2/Cs[ns]);
B_1=(dt*Ca*(1-exp(-NTU))/Cs[ns])/(1+dt*Ca*(1-exp(-NTU))/2/Cs[ns]);
C_1=Qs*dt/Cs[ns]/(1+dt*Ca*(1-exp(-NTU))/2/Cs[ns]);

begin_f_loop(f,t)
if (PRINCIPAL_FACE_P(f,t) /****PARALLELIZATION****/
{
F_PROFILE(f,t,i) = (1-uson)*(T_inavg[ns]+Qs/Ca)+uson*(T_inavg[ns]*exp(-
NTU)+(A_1*Tprev[ns]+B_1*T_inavg[ns]+C_1)*(1-exp(-NTU)));
}
end_f_loop(f,t)
#endif RP_NODE /****PARALLELIZATION****/
Tnext[ns]=(1-uson)*(T_inavg[ns]+Qs/Ca/(1-exp(-NTU)))+uson*(A_1*Tprev[ns]+B_1*T_inavg[ns]+C_1);
#endif /* RP_NODE*/ /****PARALLELIZATION****/

#endif /* !RP_HOST*/ /****PARALLELIZATION****/

}

/*****
UDF for SERVER EXIT TEMPERATURE - 11
*****/
DEFINE_PROFILE(exittemp11,t,i)
{
/*Compute transient server exit air temperature.*/
#ifdef RP_HOST /****PARALLELIZATION****/
face_t f;

real Qs;
real cp = 1005; /*J/kg/K*/
real UA;
real Ca;
real K;
real dt = CURRENT_TIMESTEP;
real A_1;
real B_1;
real C_1;
real NTU;

ns=10;
Ca = mdot[ns]*cp;
K = Cs[ns]/tau[ns];
if (K/Ca<1)
{NTU = -log(1-K/(Ca+0.0000001));}
else
{NTU = 30;}
UA = Ca*NTU;

```

```

if (CURRENT_TIME<tswitch[ns])
{Qs = Qs1[ns];
uson = 0.0;}
else
{Qs = Qs2[ns];
uson = 1.0;}

A_1=(1-dt*Ca*(1-exp(-NTU))/2/Cs[ns])/(1+dt*Ca*(1-exp(-NTU))/2/Cs[ns]);
B_1=(dt*Ca*(1-exp(-NTU))/Cs[ns])/(1+dt*Ca*(1-exp(-NTU))/2/Cs[ns]);
C_1=Qs*dt/Cs[ns]/(1+dt*Ca*(1-exp(-NTU))/2/Cs[ns]);

begin_f_loop(f,t)
if(PRINCIPAL_FACE_P(f,t)) /***PARALLELIZATION***/
{
F_PROFILE(f,t,i) = (1-uson)*(T_inavg[ns]+Qs/Ca)+uson*(T_inavg[ns]*exp(-
NTU)+(A_1*Tprev[ns]+B_1*T_inavg[ns]+C_1)*(1-exp(-NTU)));
}
end_f_loop(f,t)
#ifdef RP_NODE /***PARALLELIZATION***/
Tnext[ns]=(1-uson)*(T_inavg[ns]+Qs/Ca/(1-exp(-NTU)))+uson*(A_1*Tprev[ns]+B_1*T_inavg[ns]+C_1);
#endif /* RP_NODE*/ /***PARALLELIZATION***/

#endif /* !RP_HOST*/ /***PARALLELIZATION***/

}

/*****
UDF for SERVER EXIT TEMPERATURE - 12
*****/
DEFINE_PROFILE(exittempl2,t,i)
{
/*Compute transient server exit air temperature.*/
#ifdef !RP_HOST /***PARALLELIZATION***/
face_t f;

real Qs;
real cp = 1005; /*J/kg/K*/
real UA;
real Ca;
real K;
real dt = CURRENT_TIMESTEP;
real A_1;
real B_1;
real C_1;
real NTU;

ns=11;
Ca = mdot[ns]*cp;
K = Cs[ns]/tau[ns];
if (K/Ca<1)
{NTU = -log(1-K/(Ca+0.0000001));}
else
{NTU = 30;}
UA = Ca*NTU;

if (CURRENT_TIME<tswitch[ns])
{Qs = Qs1[ns];
uson = 0.0;}
else
{Qs = Qs2[ns];
uson = 1.0;}

A_1=(1-dt*Ca*(1-exp(-NTU))/2/Cs[ns])/(1+dt*Ca*(1-exp(-NTU))/2/Cs[ns]);
B_1=(dt*Ca*(1-exp(-NTU))/Cs[ns])/(1+dt*Ca*(1-exp(-NTU))/2/Cs[ns]);
C_1=Qs*dt/Cs[ns]/(1+dt*Ca*(1-exp(-NTU))/2/Cs[ns]);

begin_f_loop(f,t)
if(PRINCIPAL_FACE_P(f,t)) /***PARALLELIZATION***/
{

```

```

        F_PROFILE(f,t,i) = (1-uson)*(T_inavg[ns]+Qs/Ca)+uson*(T_inavg[ns]*exp(-
NTU)+(A_1*Tprev[ns]+B_1*T_inavg[ns]+C_1)*(1-exp(-NTU)));
    }
    end_f_loop(f,t)
# if RP_NODE_                                /**PARALLELIZATION***/
Tnext[ns]=(1-uson)*(T_inavg[ns]+Qs/Ca/(1-exp(-NTU)))+uson*(A_1*Tprev[ns]+B_1*T_inavg[ns]+C_1);
# endif /* RP_NODE*/                        /**PARALLELIZATION***/

# endif /* !RP_HOST*/                        /**PARALLELIZATION***/
}

/*****
UDF for SERVER EXIT TEMPERATURE - 13
*****/
DEFINE_PROFILE(exittemp13,t,i)
{
/*Compute transient server exit air temperature.*/
# if !RP_HOST                                /**PARALLELIZATION***/
face_t f;

real Qs;
real cp = 1005; /*J/kg/K*/
real UA;
real Ca;
real K;
real dt = CURRENT_TIMESTEP;
real A_1;
real B_1;
real C_1;
real NTU;

ns=12;
Ca = mdot[ns]*cp;
K = Cs[ns]/tau[ns];
if (K/Ca<1)
{NTU = -log(1-K/(Ca+0.00000001));}
else
{NTU = 30;}
UA = Ca*NTU;

if (CURRENT_TIME<tswitch[ns])
{Qs = Qs1[ns];
uson = 0.0;}
else
{Qs = Qs2[ns];
uson = 1.0;}

A_1=(1-dt*Ca*(1-exp(-NTU))/2/Cs[ns])/(1+dt*Ca*(1-exp(-NTU))/2/Cs[ns]);
B_1=(dt*Ca*(1-exp(-NTU))/Cs[ns])/(1+dt*Ca*(1-exp(-NTU))/2/Cs[ns]);
C_1=Qs*dt/Cs[ns]/(1+dt*Ca*(1-exp(-NTU))/2/Cs[ns]);

    begin_f_loop(f,t)
if(PRINCIPAL_FACE_P(f,t))                    /**PARALLELIZATION***/
{
        F_PROFILE(f,t,i) = (1-uson)*(T_inavg[ns]+Qs/Ca)+uson*(T_inavg[ns]*exp(-
NTU)+(A_1*Tprev[ns]+B_1*T_inavg[ns]+C_1)*(1-exp(-NTU)));
    }
    end_f_loop(f,t)
# if RP_NODE_                                /**PARALLELIZATION***/
Tnext[ns]=(1-uson)*(T_inavg[ns]+Qs/Ca/(1-exp(-NTU)))+uson*(A_1*Tprev[ns]+B_1*T_inavg[ns]+C_1);
# endif /* RP_NODE*/                        /**PARALLELIZATION***/

# endif /* !RP_HOST*/                        /**PARALLELIZATION***/
}

/*****
UDF for SERVER EXIT TEMPERATURE - 14
*****/
DEFINE_PROFILE(exittemp14,t,i)

```



```

{
/*Compute transient server exit air temperature.*/
#if !RP_HOST                                     /**PARALLELIZATION***/
face_t f;

real Qs;
real cp = 1005; /*J/kg/K*/
real UA;
real Ca;
real K;
real dt = CURRENT_TIMESTEP;
real A_1;
real B_1;
real C_1;
real NTU;

ns=13;
Ca = mdot[ns]*cp;
K = Cs[ns]/tau[ns];
if (K/Ca<1)
{NTU = -log(1-K/(Ca+0.0000001));}
else
{NTU = 30;}
UA = Ca*NTU;

if (CURRENT_TIME<tswitch[ns])
{Qs = Qs1[ns];
uson = 0.0;}
else
{Qs = Qs2[ns];
uson = 1.0;}

A_1=(1-dt*Ca*(1-exp(-NTU))/2/Cs[ns])/(1+dt*Ca*(1-exp(-NTU))/2/Cs[ns]);
B_1=(dt*Ca*(1-exp(-NTU))/Cs[ns])/(1+dt*Ca*(1-exp(-NTU))/2/Cs[ns]);
C_1=Qs*dt/Cs[ns]/(1+dt*Ca*(1-exp(-NTU))/2/Cs[ns]);

begin_f_loop(f,t)
if(PRINCIPAL_FACE_P(f,t))                       /**PARALLELIZATION***/
{
F_PROFILE(f,t,i) = (1-uson)*(T_inavg[ns]+Qs/Ca)+uson*(T_inavg[ns]*exp(-
NTU)+(A_1*Tprev[ns]+B_1*T_inavg[ns]+C_1)*(1-exp(-NTU)));
}
end_f_loop(f,t)
#if RP_NODE                                     /**PARALLELIZATION***/
Tnext[ns]=(1-uson)*(T_inavg[ns]+Qs/Ca/(1-exp(-NTU)))+uson*(A_1*Tprev[ns]+B_1*T_inavg[ns]+C_1);
#endif /* RP_NODE*/                             /**PARALLELIZATION***/

#endif /* !RP_HOST*/                             /**PARALLELIZATION***/
}

/*****
UDF for SERVER EXIT TEMPERATURE - 15
*****/
DEFINE_PROFILE(exittemp15,t,i)
{
/*Compute transient server exit air temperature.*/
#if !RP_HOST                                     /**PARALLELIZATION***/
face_t f;

real Qs;
real cp = 1005; /*J/kg/K*/
real UA;
real Ca;
real K;
real dt = CURRENT_TIMESTEP;
real A_1;
real B_1;
real C_1;
real NTU;

```

```

ns=14;
Ca = mdot[ns]*cp;
K = Cs[ns]/tau[ns];
if (K/Ca<1)
{NTU = -log(1-K/(Ca+0.0000001));}
else
{NTU = 30;}
UA = Ca*NTU;

if (CURRENT_TIME<tswitch[ns])
{Qs = Qs1[ns];
uson = 0.0;}
else
{Qs = Qs2[ns];
uson = 1.0;}

A_1=(1-dt*Ca*(1-exp(-NTU))/2/Cs[ns])/(1+dt*Ca*(1-exp(-NTU))/2/Cs[ns]);
B_1=(dt*Ca*(1-exp(-NTU))/Cs[ns])/(1+dt*Ca*(1-exp(-NTU))/2/Cs[ns]);
C_1=Qs*dt/Cs[ns]/(1+dt*Ca*(1-exp(-NTU))/2/Cs[ns]);

begin_f_loop(f,t)
if(PRINCIPAL_FACE_P(f,t)) /***PARALLELIZATION***/
{
F_PROFILE(f,t,i) = (1-uson)*(T_inavg[ns]+Qs/Ca)+uson*(T_inavg[ns]*exp(-
NTU)+(A_1*Tprev[ns]+B_1*T_inavg[ns]+C_1)*(1-exp(-NTU)));
}
end_f_loop(f,t)
#if RP_NODE /***PARALLELIZATION***/
Tnext[ns]=(1-uson)*(T_inavg[ns]+Qs/Ca/(1-exp(-NTU)))+uson*(A_1*Tprev[ns]+B_1*T_inavg[ns]+C_1);
#endif /* RP_NODE*/ /***PARALLELIZATION***/

#endif /* !RP_HOST*/ /***PARALLELIZATION***/
}

```

## Appendix-C: Sample Journal File for UDF Setup in FLUENT

```
rcd casename.cas
;*****
; activate 2nd order transient solver
def mod un2 y
;*****
; UDF Compilation
def us cf com "libraryname" y "UDFname.c" "" "" cf load "libraryname"
; Function hooked up to Fluent
def us f a "serverinout::libraryname" ""
def us f eaexit "savedata::libraryname" ""
;*****
; Define user defined transient temperature of the server exit velocity boundary condition.
; Requires Surface ID (129)
; Requires Face velocity (1.028)
; Requires UDF and library name (exittemp1::libraryname)
; Requires Turbulence Boundary Conditions
def bc zt 129 vi vi 129 n n y y n 1.028 n 0.0 y y "udf" "exittemp1::libraryname" y n 0.09 n 0.08
def bc zt 154 vi vi 154 n n y y n 1.028 n 0.0 y y "udf" "exittemp2::libraryname" y n 0.09 n 0.08
def bc zt 153 vi vi 153 n n y y n 1.028 n 0.0 y y "udf" "exittemp3::libraryname" y n 0.09 n 0.08
def bc zt 152 vi vi 152 n n y y n 1.042 n 0.0 y y "udf" "exittemp4::libraryname" y n 0.09 n 0.08
def bc zt 151 vi vi 151 n n y y n 1.028 n 0.0 y y "udf" "exittemp5::libraryname" y n 0.09 n 0.08
def bc zt 128 vi vi 128 n n y y n 1.158 n 0.0 y y "udf" "exittemp6::libraryname" y n 0.09 n 0.08
def bc zt 150 vi vi 150 n n y y n 1.158 n 0.0 y y "udf" "exittemp7::libraryname" y n 0.09 n 0.08
def bc zt 149 vi vi 149 n n y y n 1.158 n 0.0 y y "udf" "exittemp8::libraryname" y n 0.09 n 0.08
def bc zt 148 vi vi 148 n n y y n 1.216 n 0.0 y y "udf" "exittemp9::libraryname" y n 0.09 n 0.08
def bc zt 147 vi vi 147 n n y y n 1.231 n 0.0 y y "udf" "exittemp10::libraryname" y n 0.09 n 0.08
def bc zt 127 vi vi 127 n n y y n 1.050 n 0.0 y y "udf" "exittemp11::libraryname" y n 0.09 n 0.08
def bc zt 146 vi vi 146 n n y y n 1.050 n 0.0 y y "udf" "exittemp12::libraryname" y n 0.09 n 0.08
def bc zt 145 vi vi 145 n n y y n 1.028 n 0.0 y y "udf" "exittemp13::libraryname" y n 0.09 n 0.08
def bc zt 144 vi vi 144 n n y y n 1.042 n 0.0 y y "udf" "exittemp14::libraryname" y n 0.09 n 0.08
def bc zt 143 vi vi 143 n n y y n 1.020 n 0.0 y y "udf" "exittemp15::libraryname" y n 0.09 n 0.08
;*****
; Solver settings
; Solve / Set / Time Step Size / Report Interval /
sol s t 0.1 rep 25
; Start transient calculation
; Solve / dual-time-iterate / # ts / # it per ts /
sol d 24000 50
;
```

# Appendix-D: MATLAB Codes for the Hybrid-Lumped Capacitance

## Model (Model vs. Research Lab experiments)

```
clear all; close all; clc;
CASE=1;      % (1) Rack Shutdown
             % (2) Chilled Water Shutdown
             % (3) Fan Failure
             % (4) Decreased Air Flow
             % (5) Increased Air Flow
savefigures=0; % (0) Does not save figures
             % (1) Saves figures to the directory
% Physical properties of the Room and Racks %%%%%%%%%%%%%%%%%%%%%%%%%%%%%%%
b=3;        % number of blocks in the server
s=12;       % number of servers
rz=1;       % number of recirculation zones
sr=4;       % number of servers per rack
nr=s/sr;    % number of racks
%%%%%%%%%%%%%%%%%%%%%%%%%%%%%%%%%%%%%%%%%%%%%%%%%%%%%%%%%%%%%%%%%%%%%%%%%%%%%%

% Assignment of recirculation path/zone to server j %%%%%%%%%%%%%%%%%%%%%%%%%
rzassign(1,1)=1; % R1C1
rzassign(2,1)=1; % R1C2
rzassign(3,1)=1; % R1C3
rzassign(4,1)=1; % R1C4
rzassign(5,1)=1; % R2C1
rzassign(6,1)=1; % R2C2
rzassign(7,1)=1; % R2C3
rzassign(8,1)=1; % R2C4
rzassign(9,1)=1; % R3C1
rzassign(10,1)=1; % R3C2
rzassign(11,1)=1; % R3C3
rzassign(12,1)=1; % R3C4

% if RS(j,k)=1 Server j is part of recirculation zone k
% Based on the numbering of servers assign servers to recirculation zones
for j=1:s
    for r=1:rz
        if r==rzassign(j,1)
            RS(j,r)=1;
        else
            RS(j,r)=0;
        end
    end
end
%%%%%%%%%%%%%%%%%%%%%%%%%%%%%%%%%%%%%%%%%%%%%%%%%%%%%%%%%%%%%%%%%%%%%%%%%%%%%%

% This function loads the experimental data and the plotting
% parameters specific to various cases depending on the definition of CASE
[Ttold,DT1t,Ttnew,DT1tnew,cc,imsize_x,imsize_y,DTexp,Ttile_exp,err,CRAHCFMold,...
    CRAHCFMnew,ymin,ymax,ytick,xmin,xmax,xtick,dt_exp,ndt_exp,tstamp_exp,dt,ndt,tstamp]...
    = readdata(CASE,s);

% Model Inputs for Servers and CRAH Controls %%%%%%%%%%%%%%%%%%%%%%%%%%%%%%%
% This function loads case dependent model inputs for servers and CRAH controls
[CW,CWnew,CRC,Tmc,time_redline,t_flow,RF,Cs,UAs,Ca,Qfold,Qf,a1,a2,Qold,Q] ...
    = inputs(CASE,s,b,dt);

for j=1:s
    for k=1:b
        E(j,k)=1-exp(-UAs(j,k)/Ca(j)); % Effectiveness of Server Blocks
    end
end

%CRAH Properties %%%%%%%%%%%%%%%%%%%%%%%%%%%%%%%
Cac=(CRAHCFMold/60*0.3048^3*1.242*1005); % Initial CRAH Flow Capacity (W/K)
```

```

Cacnew=(CRAHCFMnew/60*0.3048^3*1.242*1005); % Steady State CRAH Flow Capacity (W/K)
UACR=3789; % Initial Thermal Conductance (W/K)
ECR=1-exp(-UACR/Cac); % Effectiveness of CRAH Heat Exchange
CCR=236815; % Thermal Capacitance (J/K)

%CRAH Fan Power
QfCold=2654; % Initial CRAH Fan Power (W)
QfC=2654; % CRAH FAN Power (W/K)
%%%%%%%%%%%%%%%%%%%%%%%%%%%%%%%%%%%%%%%%%%%%%%%%%%%%%%%%%%%%%%%%%%%%%%%%
%CRAH second block Properties %%%%%%%%%%%%%%%%%%%%%%%%%%%%%%%%%%%%%%%%%%%%%%%%%%%%%%%%%%%%%%%%%%%%%%%%%
UACR2=149; % Initial Thermal Conductance (W/K)
ECR2=1-exp(-UACR2/Cac); % Effectiveness of CRAH Heat Exchange
CCR2=152151; % Thermal Capacitance (J/K)

%%%%%%%%%%%%%%%%%%%%%%%%%%%%%%%%%%%%%%%%%%%%%%%%%%%%%%%%%%%%%%%%%%%%%%%%

%Plenum Properties %%%%%%%%%%%%%%%%%%%%%%%%%%%%%%%%%%%%%%%%%%%%%%%%%%%%%%%%%%%%%%%%%%%%%%%%%
CPL=1506729; % Thermal Capacitance (J/K)
if CASE==1 % Rack Shutdown Experiment
UAPL=904; % Thermal Conductance (W/K)
elseif CASE==2 % Chilled Water Shutdown Experiment
UAPL=904; % Thermal Conductance (W/K)
elseif CASE==3 % CRAH Fan Failure Experiment
UAPL=927; % Thermal Conductance (W/K)
elseif CASE==4 % Decreasing CRAH Air Flow
UAPL=694; % Thermal Conductance (W/K)
elseif CASE==5 % Increasing CRAH Air Flow
UAPL=904; % Thermal Conductance (W/K)
end

QPL=0; % Heat Generation in Plenum Block (W)

%%%%%%%%%%%%%%%%%%%%%%%%%%%%%%%%%%%%%%%%%%%%%%%%%%%%%%%%%%%%%%%%%%%%%%%%

% Room Air Capacitance %%%%%%%%%%%%%%%%%%%%%%%%%%%%%%%%%%%%%%%%%%%%%%%%%%%%%%%%%%%%%%%%%%%%%%%%%
Croom=190000*1; % Thermal Capacitance (J/K)
r_hotaisle=0.063; % Ratio of Hot Aisle to Room Volume (-)
CMh=r_hotaisle*Croom; % Hot Aisle Thermal Capacitance (J/K)
CMc=(1-r_hotaisle)*Croom; % Cold Aisle Thermal Capacitance (J/K)
for j=1:s
Cin(j)=CMc/s; % Server Air Inlet Zone Thermal Capacitance (J/K)
end

%%%%%%%%%%%%%%%%%%%%%%%%%%%%%%%%%%%%%%%%%%%%%%%%%%%%%%%%%%%%%%%%%%%%%%%%

% Calculation of Initial Condition %%%%%%%%%%%%%%%%%%%%%%%%%%%%%%%%%%%%%%%%%%%%%%%%%%%%%%%%%%%%%%%%%%%%%%%%%

Tcold=Ttold; % Initial CRAH exit air temperature (C)
Tmold=Ttold+(sum(sum(Qold))+sum(Qfold))/Cac; % Initial Mixed Room Air Temperature
Tmnew=Ttnew+(sum(sum(Q))+sum(Qf))/Cacnew; % Initial Mixed Room Air Temperature

for j=1:s
Tinold(j,1)=DT1t(j,1)+Ttold; % Initial Server Inlet Air Temperature (C)
F(j,1)=1-(Tinold(j)-Ttold)/(Tmold-Ttold); % Initial Capture Index based on experimental
data
end

if CASE==4 || CASE==5 % This statement is for CRAH Air Flow Change
Cases
for j=1:s
Tinnew(j,1)=DT1tnew(j,1)+Ttnew; % New Server Inlet Air Temperature (C)
Fnew(j,1)=1-(Tinnew(j)-Ttnew)/(Tmnew-Ttnew); % New Capture Index based on experimental data
end
Catnew=dot(Fnew,Ca); % Steady State Tile Air Flow Capacity (W/K)
Calnew=Cacnew-Catnew; % Steady State Leakage Flow Capacity (W/K)
lknew=Calnew/Cacnew; % Steady State Leakage Rate
end

Cas=sum(Ca); % Initial Server Air Flow Capacity (W/K)
Cat=dot(F,Ca); % Initial Tile Air Flow Capacity (W/K)

```

```

Car=Ca.*(1-F); % Initial Recirculation Air Flow Capacity per Server (W/K)
CaRZ=transpose(Car)*RS+0.000000001; % Initial Recirculation Air Flow Capacity per Recirculation
Path (W/K)

% Recirculation Zone Properties %%%%%%%%%%%%%%%%%%%%%%%%%%%%%%%%%%%%%%%%%%%%%%%%%%%%%%%%%%%%%%%%%%%%%%%%%%
F_C=1; % Correction Factor for CR
F_UA=1; % Correction Factor for UA

CRbl=2664832;
UARbl=937;

CR= F_C*CRbl; % Thermal Capacitance (J/K)
UAR=F_UA*UARbl*CaRZ/Cas; % Thermal Conductance (W/K)

for r=1:rz
    CR_new(r,1)=CR(r,1); % New Thermal Capacitance (J/K)
    UAR_new(r,1)=UAR(r,1); % New Thermal Conductance (W/K)
    QR(r,1)=0; % Heat Generation in Recirculation Paths (W)
end

% Initial Temperatures at the inlet and exit of server blocks (C)
for j=1:s
    Told(j,1)=Tinold(j);
    Told(j,2)=Told(j,1)+Qold(j,1)/Ca(j);
    Told(j,3)=Told(j,2)+(Qold(j,2)+Qfold(j))/Ca(j);
    Teold(j)=Told(j,3)+Qold(j,3)/Ca(j);
end
% Initial server block temperatures (C)
for j=1:s
    for k=1:b
        TBold(j,k)=Told(j,k)+Qold(j,k)/Ca(j)/E(j,k);
    end
end

Txold=dot(Ca,Teold)/Cas; % Initial Mixed Server Exit Air Temperature (C)

Cal=Cac-Cat; % Initial Leakage Flow Capacity (W/K)
lk=Cal/Cac; % Initial Leakage Rate

QCRold=(-sum(sum(Qold))-sum(Qfold))-QfCold; % Initial CRAH Cooling Capacity (W)
QCR=(-sum(sum(Q))-sum(Qf))-QfC; % CRAH Cooling Capacity (W)

QCR2old=0; % Initial CRAH Cooling Capacity (W)
QCR2=0; % CRAH Cooling Capacity (W)

for r=1:rz
    ER(r)=1-exp(-UAR(r)/CaRZ(r)); % Effectiveness of Recirculation Path Heat Exchange
end

for r=1:rz
    TBRold(r)=Tmold+QR(r)/CaRZ(r)/ER(r); % Initial Temperature of Recirculation Path Thermal
    Mass (C)
    TRold(r)=TBRold(r)+(Tmold-TBRold(r))*(1-ER(r)); % Initial Temperature of Recirculation Path
    Air (C)
end

TRSold=RS*transpose(TRold); % Initial Temperature of Recirculation Air into
Servers (C)
ERS=RS*transpose(ER); % Effectiveness of Recirculation Path Heat Exchange
of individual servers

TBCRold=Tmold+QCRold/Cac/ECR; % Initial Temperature of CRAH Thermal
Mass (C)
TCRold=(TBCRold+(Tmold-TBCRold)*(1-ECR)); % Initial Temperature of CRAH exit air in case CW=0
TBCR2old=TCRold+QCR2old/Cac/ECR2; % Initial Temperature of CRAH Thermal
Mass (C)
TCR2old=(TBCR2old+(TCRold-TBCR2old)*(1-ECR2))+QfCold/Cac; % Initial Temperature of CRAH exit
air in case CW=0

```

```

Tcc=Tcold-QfCold/Cac; % Initial Temperature of CRAH exit air
before the CRAH fan (C)
Tcold=CW*(CRC*(TBCR2old+(TCRold-TBCR2old)*(1-ECR2)))+(1-CRC)*(Tcc+QfCold/Cac)+(1-CW)*(TCR2old);
% Initial Temperature of CRAH exit (C)

EPL=1-exp(-UAPL/Cat); % Effectiveness of Plenum Heat Exchange
TBPLold=Tcold+QPL/Cat/EPL; % Initial Temperature of Plenum Thermal Mass (C)
Ttold=Tcold-(Tcold-TBPLold)*EPL; % Initial Temperature of the Tile (C)

% Collection of Initial Temperatures as a Vector
for k=1:b
    Xold((k-1)*s+1:k*s,1)=Told(:,k);
    Xold(s*b+(k-1)*s+1:s*b+k*s,1)=TBold(:,k);
end
Xold(s*b*2+1:s*b*2+s,1)=Teold(:);
Xold(s*b*2+s+1:s*b*2+s+s,1)=TRSold(:);
Xold(s*b*2+s+s+1:s*b*2+s+s+rz,1)=TBRold(:);
Xold(s*b*2+s+s+rz+1,1)=TBPLold;
Xold(s*b*2+s+s+rz+2,1)=TBCRold;
Xold(s*b*2+s+s+rz+3,1)=TCRold;
Xold(s*b*2+s+s+rz+4,1)=Tcold;
Xold(s*b*2+s+s+rz+5,1)=Tmold;
Xold(s*b*2+s+s+rz+6,1)=Ttold;
Xold(s*b*2+s+s+rz+7,1)=Txold;
Xold(s*b*2+s+s+rz+8,1)=TBCR2old;
Xold(s*b*2+s+s+rz+9,1)=TCR2old;

Fold=F;
if CASE==1 % Rack Shutdown Experiment
    Fnew=F; % Capture Index after t>0
elseif CASE==2 % Chilled Water Shutdown Experiment
    Fnew=F; % Capture Index after t>0
elseif CASE==3 % CRAH Fan Failure Experiment
    Fnew=zeros(s,1)+0.000000000000001; % Capture Index after t>0
elseif CASE==4 || CASE==5 % CRAH Flow Air Change
    lk=lknew; % Leakage Rate after t>0
end

% Transient Simulation Starts Here %%%%%%%%%%%%%%%%%%%%%%%%%%%%%%%%%%%%%%%%%%%%%%%%%%%%%%%%%%%%%%%%%%%%%%%%%
AA = zeros(s*b*2+s+s+rz+9,s*b*2+s+s+rz+9); % Matrix created for the transient simulation
time=0; % Initialized Time
for t=1:ndt
    if time>=0 % Changes in the transient simulation happen after the specified
time
        F=Fnew; % New Capture Index
        CW=CWnew; % The chilled water supply into the CRAH unit
    end
    time=time+dt; % Start of counting the time

    tic

    % Recompute flow rates at the room level (Recirculation)
    Cat=dot(F,Ca); % Tile air flow capacity (W/K)
    Cac=Cat/(1-lk); % CRAH air flow capacity (W/K)
    Cal=lk*Cac; % Leakage air flow capacity (W/K) Based on computed
initial value
    Car=Ca.*(1-F); % Recirculation Air Flow Capacity per Server (W/K)
    CaRZ=transpose(Car)*RS+0.000000001; % Recirculation Air Flow Capacity per Recirculation Path
(W/K)
    ECR=1-exp(-UACR/Cac); % Effectiveness of CRAH Heat Exchange
    ECR2=1-exp(-UACR2/Cac); % Effectiveness of CRAH Heat Exchange

CR_new= F_C*CRb1; % Thermal Capacitance (J/K)
UAR_new=F_UA*UARb1*CaRZ/Cas; % Thermal Conductance (W/K)

% Recirculation Zone Properties (if "new" values are different)
for r=1:rz
    CR(r,1)=CR_new(r,1);
    UAR(r,1)=UAR_new(r,1);
end

```

```

for r=1:rz
    ER(r)=1-exp(-UAR(r)/CaRZ(r)); % Effectiveness of Recirculation Path Heat Exchange
end

ERS=RS*transpose(ER); % Effectiveness of Recirculation Path Heat Exchange per Server

EPL=1-exp(-UAPL/Cat); % Effectiveness of Plenum Heat Exchange

%%% Constants of equations %%%%%%%%%%%%%%%%%%%%%%%%%%%%%%%%%%%%%%%%%%%%%%%%%%%%%%%%%%%%%%%%%%%%%%%%%
for j=1:s
    tau_in(j)=Cin(j)/Ca(j);
    A_in(j)=(1-dt/2/tau_in(j))/(1+dt/2/tau_in(j));
    B_in(j)=((1-F(j))*dt/2/tau_in(j))/(1+dt/2/tau_in(j));
    C_in(j)=(F(j)*dt/2/tau_in(j))/(1+dt/2/tau_in(j));
end

for j=1:s
    for k=1:b
        tau(j,k)=Cs(j,k)/E(j,k)/Ca(j);
        A(j,k)=(1-dt/2/tau(j,k))/(1+dt/2/tau(j,k));
        B(j,k)=dt*Q(j,k)/Cs(j,k)/(1+dt/2/tau(j,k));
        C(j,k)=dt/tau(j,k)/(1+dt/2/tau(j,k))/2;
    end
end

for r=1:rz
    tauR(r)=CR(r)/ER(r)/CaRZ(r);
    A_R(r)=(1-dt/2/tauR(r))/(1+dt/2/tauR(r));
    B_R(r)=dt*QR(r)/CR(r)/(1+dt/2/tauR(r));
    C_R(r)=dt/tauR(r)/(1+dt/2/tauR(r))/2;
end

tauPL=CPL/EPL/Cat;
tauPL_2=CPL/UAPL;
A_PL=(1-dt/2/tauPL)/(1+dt/2/tauPL);
B_PL=dt*QPL/CPL/(1+dt/2/tauPL);
C_PL=dt/tauPL/(1+dt/2/tauPL)/2;

tauCR=CCR/ECR/Cac;
A_CR=(1-dt/2/tauCR)/(1+dt/2/tauCR);
B_CR=dt*QCR/CCR/(1+dt/2/tauCR);
C_CR=dt/tauCR/(1+dt/2/tauCR)/2;

tauCR2=CCR2/ECR2/Cac;
A_CR2=(1-dt/2/tauCR2)/(1+dt/2/tauCR2);
B_CR2=dt*QCR2/CCR2/(1+dt/2/tauCR2);
C_CR2=dt/tauCR2/(1+dt/2/tauCR2)/2;

tauM=CMh/(Cas+Cal);
tauML=CMh/(Cal);
tauMS=CMh/(Cas);
A_M=(1-dt/2/tauM)/(1+dt/2/tauM);
A_ML=(dt/4/tauML)/(1+dt/2/tauM);
A_MS=(dt/2/tauMS)/(1+dt/2/tauM);

% Data input into the matrix representing linear systems of equations %%%%
AA(1:s*b,1:s*b)=eye(s*b); % Tjk
AA(s*b+1:s*b*2,s*b+1:s*b*2)=eye(s*b); % TBjk

for j=1:s
    for k=1:b-1
        AA(s*k+j,s*(k-1)+j)=-(1-E(j,k)); % Factor of T(j,k) in T(j,k+1)
    end
end

for j=1:s
    for k=1:b
        AA(s*b+s*(k-1)+j,s*(k-1)+j)=-C(j,k); % Factor of T(j,k) in TB(j,k)
    end
end

```



```

end

for j=1:s
    for k=1:b-1
        AA(s*k+j,s*b+s*(k-1)+j)=-E(j,k);           % Factor of TB(j,k) in T(j,k+1)
    end
end

AA(s*b*2+1:s*b*2+s,s*b*2+1:s*b*2+s)=eye(s);       % Te(j)

for j=1:s
    for k=b
        AA(s*b*2+j,s*(k-1)+j)=- (1-E(j,k));       % Factor of T(j,k=b) in Te(j)
    end
end

for j=1:s
    for k=b
        AA(s*b*2+j,s*b+s*(k-1)+j)=-E(j,k);       % Factor of TB(j,k=b) in Te(j)
    end
end

for j=1:s
    AA(s*b*2+s+j,s*b*2+s+s+rz+5)=- (1-ERS(j));    % Factor of Tm in Tr(j)
end

for j=1:s
    for r=1:rz
        AA(s*b*2+s+j,s*b*2+s+s+r)=-ER(r)*RS(j,r); % Factor of TRB(j,k) in Tr(j)
    end
end

for j=1:s
    AA(s*b*2+s+j,s*b*2+s+j)=1;                     % Factor of Tr(r) in Tr(j)
end

AA(s*b*2+s+s+1:s*b*2+s+s+rz,s*b*2+s+s+1:s*b*2+s+s+rz)=eye(rz); % Factor of TRB(r) in TRB(r)

for r=1:rz
    AA(s*b*2+s+s+r,s*b*2+s+s+rz+5)=-C_R(r);       % Factor of Tm in TRB(r)
end

AA(s*b*2+s+s+rz+1,s*b*2+s+s+rz+1) = 1;           % Factor of TPB in TPB
AA(s*b*2+s+s+rz+1,s*b*2+s+s+rz+4) = -C_PL;       % Factor of Tc in TPB

AA(s*b*2+s+s+rz+2,s*b*2+s+s+rz+2) = 1;           % Factor of TCB in TCB
AA(s*b*2+s+s+rz+2,s*b*2+s+s+rz+5) = -C_CR;       % Factor of Tm in TCB

AA(s*b*2+s+s+rz+8,s*b*2+s+s+rz+8) = 1;           % Factor of TCB2 in TCB2
AA(s*b*2+s+s+rz+8,s*b*2+s+s+rz+3) = -C_CR2;      % Factor of Tcx(TCR) in TCB2

AA(s*b*2+s+s+rz+3,s*b*2+s+s+rz+3) = 1;           % Factor of Tcx in Tcx (TCR)
AA(s*b*2+s+s+rz+3,s*b*2+s+s+rz+2) = -ECR;        % Factor of TCB in Tcx (TCR)
AA(s*b*2+s+s+rz+3,s*b*2+s+s+rz+5) = -(1-ECR);    % Factor of Tm in Tcx (TCR)

AA(s*b*2+s+s+rz+9,s*b*2+s+s+rz+9) = 1;           % Factor of Tcx2 in Tcx2 (TCR2)
AA(s*b*2+s+s+rz+9,s*b*2+s+s+rz+8) = -ECR2;       % Factor of TCB2 in Tcx2 (TCR2)
AA(s*b*2+s+s+rz+9,s*b*2+s+s+rz+3) = -(1-ECR2);   % Factor of Tcx(TCR) in Tcx2 (TCR2)

AA(s*b*2+s+s+rz+4,s*b*2+s+s+rz+4) = 1;           % Factor of Tc in Tc
AA(s*b*2+s+s+rz+4,s*b*2+s+s+rz+9) = -(1-CW);     % Factor of Tcx2(TCR) in Tc

AA(s*b*2+s+s+rz+6,s*b*2+s+s+rz+6) = 1;           % Factor of Tt in Tt
AA(s*b*2+s+s+rz+6,s*b*2+s+s+rz+4) = -(1-EPL);    % Factor of Tc in Tt
AA(s*b*2+s+s+rz+6,s*b*2+s+s+rz+1) = -EPL;        % Factor of TPB in Tt

for j=1:s
    AA(s*b*2+s+s+rz+7,s*b*2+j) = -Ca(j)/Cas;      % Factor of Te(j) in Tx
end
AA(s*b*2+s+s+rz+7,s*b*2+s+s+rz+7) = 1;           % Factor of Tx in Tx

```

```

AA(s*b*2+s+s+rz+5,s*b*2+s+s+rz+5) = 1; % Factor of Tm in Tm
AA(s*b*2+s+s+rz+5,s*b*2+s+s+rz+4) = -A_ML; % Factor of Tc in Tm
AA(s*b*2+s+s+rz+5,s*b*2+s+s+rz+6) = -A_ML; % Factor of Tt in Tm
AA(s*b*2+s+s+rz+5,s*b*2+s+s+rz+7) = -A_MS; % Factor of Tx in Tm

for j=1:s
    AA(j,s*b*2+s+s+rz+6)=-C_in(j); % Factor of Tt in T(j,k)
end
for j=1:s
    AA(j,s*b*2+s+j)=-B_in(j); % Factor of Tr(j) in T(j,k)
end

% Call control function for the return air
Tcs=Tmc+(QCR+QfC)/Cac;
[CRET] = crah_control(Xold(s*b*2+s+s+rz+3,t),Xold(s*b*2+s+s+rz+9,t),Tmc,Tcs,RF);

% Vector V (RHS of the linear system of equations)
V = zeros(s*b*2+s+s+rz+9,1);

for j=1:s
    V(j)=Xold(j,t)*A_in(j)+Xold(s*b*2+s+j,t)*B_in(j)+Xold(s*b*2+s+s+rz+6,t)*C_in(j); % RHS
of Inlet Air Temperature Zone
end

for j=1:s
    V(s*(b-1)+j)=Qf(j)/Ca(j); % RHS of T(j,k=b) equation(s)
end

for j=1:s
    for k=1:b
        V(s*b+(k-1)*s+j)=A(j,k)*Xold(s*b+(k-1)*s+j,t)+B(j,k)+C(j,k)*Xold((k-1)*s+j,t); % RHS of
TB(j,k) equation(s)
    end
end

for r=1:rz
    V(s*b*2+s+s+r)=A_R(r)*Xold(s*b*2+s+s+r,t)+B_R(r)+C_R(r)*Xold(s*b*2+s+s+rz+5,t); % RHS
of T(j,k=b) equation(s)
end

V(s*b*2+s+s+rz+1) = A_PL*Xold(s*b*2+s+s+rz+1,t)+B_PL+C_PL*Xold(s*b*2+s+s+rz+4,t); % TBPL
V(s*b*2+s+s+rz+2) = A_CR*Xold(s*b*2+s+s+rz+2,t)+B_CR*CW+C_CR*Xold(s*b*2+s+s+rz+5,t); % TBCR
V(s*b*2+s+s+rz+3) = 0; %Tcx (TCR)
V(s*b*2+s+s+rz+4) = CW*(CRC*CRET+(1-CRC)*(Tcc-a1*time+a2*(time)^2+QfC/Cac)); %Tc
V(s*b*2+s+s+rz+5) =
A_M*Xold(s*b*2+s+s+rz+5,t)+A_ML*Xold(s*b*2+s+s+rz+6,t)+A_ML*Xold(s*b*2+s+s+rz+4,t)+A_MS*Xold(s*b*
2+s+s+rz+7,t); %Tm

V(s*b*2+s+s+rz+8) = A_CR2*Xold(s*b*2+s+s+rz+8,t)+B_CR2*CW+C_CR2*Xold(s*b*2+s+s+rz+3,t);
%TBCR2
V(s*b*2+s+s+rz+9) = QfC/Cac; %TCR2

T=AA\V; % Solving Linear System of Equations

Xold(:,t+1)=T;

% Recording Redline Temperature Violation Time for each Server
for j=1:s
    if T(j)>=redline && time_redline(j)==0
        time_redline(j,1)=time;
    end
end

toc
end

for j=1:s
    DT(j,:)=Xold(j,:)-Xold(s*b*2+s+s+rz+6,:);
    Tin_comp(j,:)=Xold(j,:);
end

```

```

Ttile_comp(j,:)=Xold(s*b*2+s+s+rz+6,:);
end

for j=1:s
Tin_exp(:,j)=DTexp(:,j)+Ttile_exp(:,1);
end

[stdevDTin,err] =
postprocess(CASE,err,imsize_x,imsize_y,tstamp,Tin_comp,tstamp_exp,Tin_exp,cc,xmin,xtick,xmax,ym
in,ytick,ymax,ndt_exp,dt_exp,dt,s,savefigures);

```

```

function
[Ttold,DT1t,Ttnew,DT1tnew,cc,imsize_x,imsize_y,DTexp,Ttile_exp,err,CRAHCFMold,CRAHCFMnew,ymin,y
max,ytick,xmin,xmax,xtick,dt_exp,ndt_exp,tstamp_exp,dt,ndt,tstamp] = readdata(CASE,s)

```

```

load cc4 % Color code for plotting servers per rack
cc=cc4;
imsize_x=960; % Width of the time axis
imsize_y=720; % Width of the temperature axis

if CASE==1 % Rack Shutdown Experiment
load DTexp_1 % Experimental Data: Server Inlet Air Temperature - Tile Temperature
load Ttile_exp_1 % Experimental Data: Tile Air Temperature
load err_1 % Experimental Uncertainty
CRAHCFMold=6400; % CRAH Flow Rate (CFM)
CRAHCFMnew=6400; % New CRAH Flow Rate (CFM)

% Plotting parameters %%%%%%%%%%%%%%%%%%%%%%%%%%%%%%%%%%%%%%%%%%%%%%%%%%%%%%%%%%%%%%%%%%%%%%%%%%
ymin=10; % Maximum value of vertical axis : Tin-Ttile
ymax=20; % Minimum value of vertical axis : Tin-Ttile
ytick=2; % Vertical axis tick size : Tin-Ttile
xmin=0; % Maximum value of horizontal axis : Tin-Ttile
xmax=2000; % Minimum value of horizontal axis : Tin-Ttile
xtick=400; % Horizontal axis tick size : Tin-Ttile

dt_exp=100; % Experimental time step size (s)
ndt_exp=20; % Experimental number of time steps
tstamp_exp=0:dt_exp:dt_exp*ndt_exp; % Time stamp for experimental data

dt=10; % Computational time step size (s)
ndt=200; % Computational number of time steps
tstamp=0:dt:ndt*dt; % Time stamp for computational data
%%%%%%%%%%%%%%%%%%%%%%%%%%%%%%%%%%%%%%%%%%%%%%%%%%%%%%%%%%%%%%%%%%%%%%%%%

elseif CASE==2 % Chilled Water Shutdown Experiment
load DTexp_2 % Experimental Data: Server Inlet Air Temperature - Tile Temperature
load Ttile_exp_2 % Experimental Data: Tile Air Temperature
load err_2 % Experimental Uncertainty
CRAHCFMold=6400; % CRAH Flow Rate (CFM)
CRAHCFMnew=6400; % New CRAH Flow Rate (CFM)

% Plotting parameters %%%%%%%%%%%%%%%%%%%%%%%%%%%%%%%%%%%%%%%%%%%%%%%%%%%%%%%%%%%%%%%%%%%%%%%%%%
ymin=12; % Maximum value of vertical axis : Tin
ymax=24; % Minimum value of vertical axis : Tin
ytick=2; % Vertical axis tick size : Tin
xmin=0; % Maximum value of horizontal axis : Tin
xmax=400; % Minimum value of horizontal axis : Tin
xtick=50; % Horizontal axis tick size : Tin

dt_exp=30; % Experimental time step size (s)
ndt_exp=12; % Experimental number of time steps
tstamp_exp=0:dt_exp:dt_exp*ndt_exp; % Time stamp for experimental data

dt=1; % Computational time step size (s)
ndt=600; % Computational number of time steps
tstamp=0:dt:ndt*dt; % Time stamp for computational data
%%%%%%%%%%%%%%%%%%%%%%%%%%%%%%%%%%%%%%%%%%%%%%%%%%%%%%%%%%%%%%%%%%%%%%%%%

```

```

elseif CASE==3          % CRAH Fan Failure Experiment
    load DTexp_3         % Experimental Data: Server Inlet Air Temperature - Tile Temperature
    load Ttile_exp_3    % Experimental Data: Tile Air Temperature
    load err_3          % Experimental Uncertainty
    CRAHCFMold=6000*1.1;% CRAH Flow Rate (CFM)
    CRAHCFMnew=1;      % New CRAH Flow Rate (CFM)

    %%%%%%%%%%%%%%%%%%%%%%%%%%%%%%%%%%%%%%%%%%%%%%%%%%%%%%%%%%%%%%%%%%%%%%%%%
    % Fill in CFD data in place of missing experimental data
    %%%%%%%%%%%%%%%%%%%%%%%%%%%%%%%%%%%%%%%%%%%%%%%%%%%%%%%%%%%%%%%%%%%%%%%%%
    sizedata=size(DTexp);
    DTexp=zeros(sizedata(1,1),s);
    DTexp(:,1)=1.172906;
    DTexp(:,2)=1.9323598;
    DTexp(:,3)=DTexp(:,1);
    DTexp(:,4)=DTexp(:,2);
    DTexp(:,5)=-0.26385513;
    DTexp(:,6)=0.52408445;
    DTexp(:,7)=1.9589895;
    DTexp(:,8)=DTexp(:,3);
    DTexp(:,9)=0.85459632;
    DTexp(:,10)=1.2304921;
    DTexp(:,11)=1.8355286;
    DTexp(:,12)=DTexp(:,4);
    DTexp=DTexp_;
    %%%%%%%%%%%%%%%%%%%%%%%%%%%%%%%%%%%%%%%%%%%%%%%%%%%%%%%%%%%%%%%%%%%%%%%%%

    % Plotting parameters %%%%%%%%%%%%%%%%%%%%%%%%%%%%%%%%%%%%%%%%%%%%%%%%%%%%%%%%%%%%%%%%%%%%%%%%%
    ymin=12;           % Maximum value of vertical axis : Tin
    ymax=40;           % Minimum value of vertical axis : Tin
    ytick=4;           % Vertical axis tick size : Tin
    xmin=0;            % Maximum value of horizontal axis : Tin
    xmax=400;          % Minimum value of horizontal axis : Tin
    xtick=50;          % Horizontal axis tick size : Tin

    dt_exp=30;         % Experimental time step size (s)
    ndt_exp=12;        % Experimental number of time steps
    tstamp_exp=0:dt_exp:dt_exp*ndt_exp; % Time stamp for experimental data

    dt=1;              % Computational time step size (s)
    ndt=600;           % Computational number of time steps
    tstamp=0:dt:ndt*dt; % Time stamp for computational data
    %%%%%%%%%%%%%%%%%%%%%%%%%%%%%%%%%%%%%%%%%%%%%%%%%%%%%%%%%%%%%%%%%%%%%%%%%

elseif CASE==4          % Chilled Water Shutdown Experiment
    load DTexp_4         % Experimental Data: Server Inlet Air Temperature - Tile Temperature
    load Ttile_exp_4    % Experimental Data: Tile Air Temperature
    load err_4          % Experimental Uncertainty
    CRAHCFMold=6400;   % CRAH Flow Rate (CFM)
    CRAHCFMnew=4600;   % New CRAH Flow Rate (CFM)

    % Plotting parameters %%%%%%%%%%%%%%%%%%%%%%%%%%%%%%%%%%%%%%%%%%%%%%%%%%%%%%%%%%%%%%%%%%%%%%%%%
    ymin=12;           % Maximum value of vertical axis : Tin
    ymax=24;           % Minimum value of vertical axis : Tin
    ytick=2;           % Vertical axis tick size : Tin
    xmin=0;            % Maximum value of horizontal axis : Tin
    xmax=600;          % Minimum value of horizontal axis : Tin
    xtick=100;         % Horizontal axis tick size : Tin

    dt_exp=20;         % Experimental time step size (s)
    ndt_exp=30;        % Experimental number of time steps
    tstamp_exp=0:dt_exp:dt_exp*ndt_exp; % Time stamp for experimental data

    dt=1;              % Computational time step size (s)
    ndt=1500;          % Computational number of time steps
    tstamp=0:dt:ndt*dt; % Time stamp for computational data
    %%%%%%%%%%%%%%%%%%%%%%%%%%%%%%%%%%%%%%%%%%%%%%%%%%%%%%%%%%%%%%%%%%%%%%%%%

elseif CASE==5          % Chilled Water Shutdown Experiment
    load DTexp_5         % Experimental Data: Server Inlet Air Temperature - Tile Temperature
    load Ttile_exp_5    % Experimental Data: Tile Air Temperature

```

```

load err_5          % Experimental Uncertainty
CRAHCFMold=4600;   % CRAH Flow Rate (CFM)
CRAHCFMnew=6400;  % New CRAH Flow Rate (CFM)

% Plotting parameters %%%%%%%%%%%%%%%%%%%%%%%%%%%%%%%%%%%%%%%%%%%%%%%%%%%%%%%%%%%%%%%%%%%%%%%%%
ymin=12;           % Maximum value of vertical axis : Tin
ymax=24;           % Minimum value of vertical axis : Tin
ytick=2;           % Vertical axis tick size : Tin
xmin=0;            % Maximum value of horizontal axis : Tin
xmax=600;         % Minimum value of horizontal axis : Tin
xtick=100;        % Horizontal axis tick size : Tin

dt_exp=20;         % Experimental time step size (s)
ndt_exp=30;        % Experimental number of time steps
tstamp_exp=0:dt_exp:dt_exp*ndt_exp; % Time stamp for experimental data

dt=1;              % Computational time step size (s)
ndt=1500;         % Computational number of time steps
tstamp=0:dt:ndt*dt; % Time stamp for computational data
%%%%%%%%%%%%%%%%%%%%%%%%%%%%%%%%%%%%%%%%%%%%%%%%%%%%%%%%%%%%%%%%%%%%%%%%

end

% Initial Conditions based on Experimental Data %%%%%%%%%%%%%%%%%%%%%%%%%%%%%%%%%%%%%%%%%%%%%%%%%%%%%%%%%%%%%%%%%%%%%%%%%
Ttold=Ttile_exp(1,1); % Initial Tile Air Temperature (C)
Ttnew=mean(Ttile_exp(ndt_exp,1)); % New Tile Air Temperature (C)

for j=1:s
    DT1t(j,1)=DTexp(1,j); % Initial Server Inlet Air Temperature - Tile Temperature
end
for j=1:s
    DT1tnew(j,1)=mean(DTexp(ndt_exp,j)); % New Server Inlet Air Temperature - Tile Temperature
end
%%%%%%%%%%%%%%%%%%%%%%%%%%%%%%%%%%%%%%%%%%%%%%%%%%%%%%%%%%%%%%%%%%%%%%%%

end

function [CW,CWnew,CRC,Tmc,redline,time_redline,t_flow,RF,Cs,UAs,Ca,Qfold,Qf,a1,a2,Qold,Q] =
inputs(CASE,s,b,dt)

CW=1; % Initial Chilled Water Availability: (1) CW is ON, (0) CW is OFF
CRC=0; % Initial CRAH control : (1) fixed return air temperature, (0) fixed
exit air temperature
Tmc=35; % Return Air Temperature Control Set Point (C)
redline=25; % Redline Temperature for Server Inlet Temperature (C)
time_redline=zeros(s,1); % Vector defined - The recorded simulation time for servers
when their inlet temperature exceeds redline temperature (s)
t_flow=1; % Flow adjustment time after fan speed changes (s)
RF=1-exp((log(0.01)*dt/t_flow)); % Flow adjustment factor to reach 99% of the steady state
flow within adjustment time of t_flow

% Server Properties %%%%%%%%%%%%%%%%%%%%%%%%%%%%%%%%%%%%%%%%%%%%%%%%%%%%%%%%%%%%%%%%%%%%%%%%%
C_S=91250; % Thermal Capacitance (J/K)
UA_S=[122;122;123;121;133;133;138;139;123;121;122;121]; % Thermal Conductance (W/K)
cb(2)=0.45; % Distribution of Thermal Mass in block 2
cb(3)=0.05; % Distribution of Thermal Mass in block 3
cb(1)=1-cb(2)-cb(3); % Distribution of Thermal Mass in block 1
for j=1:s
    for k=1:b
        Cs(j,k)=cb(k)*C_S; % Distributed Thermal Capacitance within
blocks (J/K)
        UAs(j,k)=cb(k)*UA_S(j); % Distributed Thermal Conductance within
blocks (W/K)
    end
end

Ca= [368;368;373;365;414;414;435;437;375;368;373;368]; % Server Flow Capacity (W/K)
Qfold= [259;253;251;253;360;348;354;348;261;272;259;248]; % Initial Server Fan Power (W)
Qf= [259;253;251;253;360;348;354;348;261;272;259;248]; % Server Fan Power (W)

```

```

if CASE==1 % Rack Shutdown Experiment
    CWnew=1; % Chilled Water Supply after t=0 : (1) CW is ON, (0) CW is OFF
    %Constants of polynomial change in the CRAH exit air temperature
    a1=0.002;
    a2=4e-7;
    Qold= [0 3456 0;0 3427 0;0 3437 0; 0 3446 0;0 3466 0;0 3466 0;0 3466 0;0 3437 0;0 3418
0;0 3418 0;0 3398 0;0 3389 0]; % Initial Heating Power of Server Blocks (W)
    Q= [0 0 0;0 0 0;0 0 0;0 0 0;0 0 0;0 0 0;0 0 0;0 0 0;0 0 0;0 0 0;0 0 0]; %
Heating Power of Server Blocks (W)
elseif CASE==2 % Chilled Water Shutdown Experiment
    CWnew=0; % Chilled Water Supply after t=0 : (1) CW is ON, (0) CW is OFF
    %Constants of polynomial change in the CRAH exit air temperature
    a1=0;
    a2=0;
    Qold= [0 1728 0;0 1714 0;0 1718 0;0 1723 0;0 1733 0;0 1733 0;0 1733 0;0 1718 0;0 1709 0;0
1709 0;0 1699 0;0 1694 0]; % Initial Heating Power of Server Blocks (W)
    Q= [0 1728 0;0 1714 0;0 1718 0;0 1723 0;0 1733 0;0 1733 0;0 1733 0;0 1718 0;0 1709 0;0
1709 0;0 1699 0;0 1694 0]; % Heating Power of Server Blocks (W)
elseif CASE==3 % CRAH Fan Failure Experiment
    CWnew=0; % Chilled Water Supply after t=0 : (1) CW is ON, (0) CW is OFF
    %Constants of polynomial change in the CRAH exit air temperature
    a1=0;
    a2=0;
    Qold= [0 2592 0;0 2570 0;0 2578 0;0 2585 0;0 2599 0;0 2599 0;0 2599 0;0 2578 0;0 2563 0;0
2563 0;0 2549 0;0 2542 0]; % Initial Heating Power of Server Blocks (W)
    Q= [0 2592 0;0 2570 0;0 2578 0;0 2585 0;0 2599 0;0 2599 0;0 2599 0;0 2578 0;0 2563 0;0
2563 0;0 2549 0;0 2542 0]; % Heating Power of Server Blocks (W)
elseif CASE==4 || 5 % Decreasing CRAH Air Flow Experiment
    CWnew=1; % Chilled Water Supply after t=0 : (1) CW is ON, (0) CW is OFF
    %Constants of polynomial change in the CRAH exit air temperature
    a1=0;
    a2=0;
    a2=0;
    Qold= [0 2592 0;0 2570 0;0 2578 0;0 2585 0;0 2599 0;0 2599 0;0 2599 0;0 2578 0;0 2563 0;0
2563 0;0 2549 0;0 2542 0]; % Initial Heating Power of Server Blocks (W)
    Q= [0 2592 0;0 2570 0;0 2578 0;0 2585 0;0 2599 0;0 2599 0;0 2599 0;0 2578 0;0 2563 0;0
2563 0;0 2549 0;0 2542 0]; % Heating Power of Server Blocks (W)
else
    printf('Incorrect CASE definition')
    exit
end
end

function [stdevDTin,err] =
postprocess(CASE,err,imgsize_x,imgsize_y,tstamp,Tin_comp,tstamp_exp,Tin_exp,cc,xmin,xtick,xmax,ym
in,ytick,ymax,ndt_exp,dt,s,savefigures)

if CASE==1 || CASE==2 || CASE==4 || CASE==5 % Rack Shutdown Experiment

% Comparison of Corrected Experimental Data Based on Tile Temperature and actual
% Tin-Ttile of experiments.
hold all

figure(1)
hFig = figure(1);
set(hFig, 'Position', [0 0 imgsize_x imgsize_y])
figure(1)
hold on
for j=1:4
plot(tstamp(1,:),Tin_comp(j,:), 'color',cc(j,:), 'LineWidth',3)
end
for j=1:4
plot(tstamp_exp,Tin_exp(1:ndt_exp+1,j), 'o', 'LineWidth',2, 'MarkerEdgeColor',cc(j,:), 'MarkerFaceCol
or',cc(j,:))
end
hold off
% title('Rack 1','FontSize',20)

```

```

text(xmin+xtick*1.1,ymax-0.5*ytick,'Rack-1','FontSize',20)
xlabel('Time, s','FontSize',20)
ylabel('T_{inlet}, \circ C','FontSize',20)
if CASE==4 || CASE==5
    legend('C1-C','C2-C','C3-C','C4-C','C1-E','C2-E','C3-E','C4-E','Location','NorthEast')
else
    legend('C1-C','C2-C','C3-C','C4-C','C1-E','C2-E','C3-E','C4-E','Location','Best')
end
axis([xmin,xmax,ymin,ymax])
set(gca,'XTick',xmin:xtick:xmax,'FontSize',16)
set(gca,'YTick',ymin:ytick:ymax,'FontSize',16)
grid on
if savefigures==1
saveas(hFig,'r1','emf'); %name is a string
end

figure(2)
hFig = figure(2);
set(hFig, 'Position', [0 0 imgsize_x imgsize_y])
hold on
for j=1:4
plot(tstamp(1,:),Tin_comp(j+4,:),'color',cc(j,:),'LineWidth',3)
end
for j=1:4
plot(tstamp_exp,Tin_exp(1:ndt_exp+1,j+4),'o','LineWidth',2,'MarkerEdgeColor',cc(j,:),'MarkerFaceColor',cc(j,:))
end
hold off
% title('Rack 2','FontSize',20)
text(xmin+xtick*1.1,ymax-0.5*ytick,'Rack-2','FontSize',20)
xlabel('Time, s','FontSize',20)
ylabel('T_{inlet}, \circ C','FontSize',20)
if CASE==4 || CASE==5
    legend('C1-C','C2-C','C3-C','C4-C','C1-E','C2-E','C3-E','C4-E','Location','NorthEast')
else
    legend('C1-C','C2-C','C3-C','C4-C','C1-E','C2-E','C3-E','C4-E','Location','Best')
end
axis([xmin,xmax,ymin,ymax])
set(gca,'XTick',xmin:xtick:xmax,'FontSize',16)
set(gca,'YTick',ymin:ytick:ymax,'FontSize',16)
grid on
if savefigures==1
saveas(hFig,'r2','emf'); %name is a string
end

figure(3)
hFig = figure(3);
set(hFig, 'Position', [0 0 imgsize_x imgsize_y])
hold on
for j=1:4
plot(tstamp(1,:),Tin_comp(j+8,:),'color',cc(j,:),'LineWidth',3)
end
for j=1:4
plot(tstamp_exp,Tin_exp(1:ndt_exp+1,j+8),'o','LineWidth',2,'MarkerEdgeColor',cc(j,:),'MarkerFaceColor',cc(j,:))
end
hold off
% title('Rack 3','FontSize',20)
text(xmin+xtick*1.1,ymax-0.5*ytick,'Rack-3','FontSize',20)
xlabel('Time, s','FontSize',20)
ylabel('T_{inlet}, \circ C','FontSize',20)
if CASE==4 || CASE==5
    legend('C1-C','C2-C','C3-C','C4-C','C1-E','C2-E','C3-E','C4-E','Location','NorthEast')
else
    legend('C1-C','C2-C','C3-C','C4-C','C1-E','C2-E','C3-E','C4-E','Location','Best')
end
axis([xmin,xmax,ymin,ymax])
set(gca,'XTick',xmin:xtick:xmax,'FontSize',16)
set(gca,'YTick',ymin:ytick:ymax,'FontSize',16)
grid on
if savefigures==1

```

```

saveas(hFig,'r3','emf'); %name is a string
end

Tin_exp_comparison_=transpose(Tin_exp);
for j=1:ndt_exp+1
    Tin_exp_comparison(:,j)=Tin_exp_comparison(:,j);
    Tin_comp_comparison(:,j)=Tin_comp(:,(j-1)*dt_exp/dt+1);
end

mTexp=mean(mean(Tin_exp_comparison));
mTcomp=mean(mean(Tin_comp_comparison));

Tin_exp_n=Tin_exp_comparison-mTexp;
Tin_comp_n=Tin_comp_comparison-mTcomp;

for j=1:ndt_exp
    Tin_exp_v((j-1)*s+1:(j-1)*s+s,1)=Tin_exp_comparison(:,j);
    Tin_comp_v((j-1)*s+1:(j-1)*s+s,1)=Tin_comp_comparison(:,j);
end

DTin=(Tin_comp_v-Tin_exp_v);
stdevDTin=sqrt((dot(DTin,DTin')/(s*ndt_exp)));

figure(10)
hFig = figure(10);
set(hFig, 'Position', [0 0 imgsize_x imgsize_x])
axis([ymin,ymax,ymin,ymax])
set(gca, 'XTick', ymin:ytick:ymax, 'FontSize',16)
set(gca, 'YTick', ymin:ytick:ymax, 'FontSize',16)

hline = refline([1 0]);
set(hline, 'LineWidth',3, 'Color','k')

hold on
text(ymin+ytick,ymax-1.5*ytick,['\sigma=' num2str(stdevDTin,2) '\circ C'],'FontSize',20)

for j=1:4

scatter(Tin_exp_comparison(j,:),Tin_comp_comparison(j,:),80,'o','LineWidth',1,'MarkerEdgeColor','k','MarkerFaceColor','w')

scatter(Tin_exp_comparison(j+4,:),Tin_comp_comparison(j+4,:),80,'o','LineWidth',1,'MarkerEdgeColor','b','MarkerFaceColor','w')

scatter(Tin_exp_comparison(j+8,:),Tin_comp_comparison(j+8,:),80,'o','LineWidth',1,'MarkerEdgeColor','r','MarkerFaceColor','w')

end

hold off
xlabel('T_{inlet} - Experimental, \circ C','FontSize',20)
ylabel('T_{inlet} - Computed, \circ C','FontSize',20)
leg=legend('45\circ', 'R1', 'R2', 'R3');
set(leg, 'Location', 'SouthEast')
grid on
set(gca, 'FontSize',16);
if savefigures==1
saveas(hFig,'compare','emf'); %name is a string
end

for t=1:ndt_exp+1
err(t,:)=err(1,:);
end

figure(11); % Server Exit Air Temperature Comparison
hFig = figure(11);
set(hFig, 'Position', [0 0 imgsize_x imgsize_y])
axis([xmin,xmax,ymin,ymax])

```



```

set(gca,'XTick',xmin:xtick:xmax,'FontSize',16)
set(gca,'YTick',ymin:ytick:ymax,'FontSize',16)

hold on
for k=1:4
    plot(tstamp, Tin_comp(k,:), 'color',cc(k,:), 'LineWidth',3)
end
for k=1:4
h=errorbar(tstamp_exp,Tin_exp(1:ndt_exp+1,k),err(:,k), 'o', 'color',cc(k,:));
set(h, 'LineWidth', 1.5, 'MarkerSize', 8, 'MarkerFaceColor', 'w', 'MarkerEdgeColor', cc(k,:));
end
hold off
% title('Rack-1','FontSize',20)
text(xmin+xtick*1.1,ymax-0.5*ytick, 'Rack-1', 'FontSize',20)
xlabel('Time (s)', 'FontSize',20)
ylabel('T_{a-in} (\circC)', 'FontSize',20)
if CASE==4 || CASE==5
    legend('C1-C', 'C2-C', 'C3-C', 'C4-C', 'C1-E', 'C2-E', 'C3-E', 'C4-E', 'Location', 'NorthEast')
else
    legend('C1-C', 'C2-C', 'C3-C', 'C4-C', 'C1-E', 'C2-E', 'C3-E', 'C4-E', 'Location', 'Best')
end
grid on
if savefigures==1
saveas(hFig, 'rlerr', 'emf'); %name is a string
end

figure(12); % Server Exit Air Temperature Comparison
hFig = figure(12);
set(hFig, 'Position', [0 0 imgsize_x imgsize_y])
axis([xmin,xmax,ymin,ymax])
set(gca,'XTick',xmin:xtick:xmax,'FontSize',16)
set(gca,'YTick',ymin:ytick:ymax,'FontSize',16)

hold on
for k=1:4
    plot(tstamp, Tin_comp(k+4,:), 'color',cc(k,:), 'LineWidth',3)
end
for k=1:4
h=errorbar(tstamp_exp,Tin_exp(1:ndt_exp+1,k+4),err(:,k+4), 'o', 'color',cc(k,:));
set(h, 'LineWidth', 1.5, 'MarkerSize', 8, 'MarkerFaceColor', 'w', 'MarkerEdgeColor', cc(k,:));
end
hold off
% title('Rack-2','FontSize',20)
text(xmin+xtick*1.1,ymax-0.5*ytick, 'Rack-2', 'FontSize',20)
xlabel('Time (s)', 'FontSize',20)
ylabel('T_{a-in} (\circC)', 'FontSize',20)
if CASE==4 || CASE==5
    legend('C1-C', 'C2-C', 'C3-C', 'C4-C', 'C1-E', 'C2-E', 'C3-E', 'C4-E', 'Location', 'NorthEast')
else
    legend('C1-C', 'C2-C', 'C3-C', 'C4-C', 'C1-E', 'C2-E', 'C3-E', 'C4-E', 'Location', 'Best')
end
grid on
if savefigures==1
saveas(hFig, 'r2err', 'emf'); %name is a string
end

figure(13); % Server Exit Air Temperature Comparison
hFig = figure(13);
set(hFig, 'Position', [0 0 imgsize_x imgsize_y])
axis([xmin,xmax,ymin,ymax])
set(gca,'XTick',xmin:xtick:xmax,'FontSize',16)
set(gca,'YTick',ymin:ytick:ymax,'FontSize',16)

hold on
for k=1:4
    plot(tstamp, Tin_comp(k+8,:), 'color',cc(k,:), 'LineWidth',3)
end
for k=1:4

```

```

h=errorbar(tstamp_exp,Tin_exp(1:ndt_exp+1,k+8),err(:,k+8),'o','color',cc(k,:));
set(h, 'LineWidth', 1.5, 'MarkerSize', 8, 'MarkerFaceColor', 'w', 'MarkerEdgeColor', cc(k,:));
end
hold off
% title('Rack-3','FontSize',20)
text(xmin+xtick*1.1,ymax-0.5*ytick,'Rack-3','FontSize',20)
xlabel('Time (s)','FontSize',20)
ylabel('T_{a-in} (\circ C)','FontSize',20)
if CASE==4 || CASE==5
    legend('C1-C','C2-C','C3-C','C4-C','C1-E','C2-E','C3-E','C4-E','Location','NorthEast')
else
    legend('C1-C','C2-C','C3-C','C4-C','C1-E','C2-E','C3-E','C4-E','Location','Best')
end
grid on
if savefigures==1
saveas(hFig,'r3err','emf'); %name is a string
end

elseif CASE==3 % CRAH Fan Failure Experiment
% Comparison of Corrected Experimental Data Based on Tile Temperature and actual
% Tin-Ttile of experiments.
hold all

figure(1)
hFig = figure(1);
set(hFig, 'Position', [0 0 imgsize_x imgsize_y])
figure(1)
hold on
for j=3:4
plot(tstamp(1,:),Tin_comp(j,:), 'color',cc(j,:), 'LineWidth',3)
end
for j=3:4
plot(tstamp_exp,Tin_exp(:,j), 'o', 'LineWidth',2, 'MarkerEdgeColor',cc(j,:), 'MarkerFaceColor',cc(j,:))
end
hold off
% title('Rack 1','FontSize',20)
text(xmin+xtick*1.1,ymax-0.5*ytick,'Rack-1','FontSize',20)
xlabel('Time, s','FontSize',20)
ylabel('T_{inlet}, \circ C','FontSize',20)
legend('C3-C','C4-C','C3-E','C4-E','Location','SouthEast')
axis([xmin,xmax,ymin,ymax])
set(gca, 'XTick',xmin:xtick:xmax, 'FontSize',16)
set(gca, 'YTick',ymin:ytick:ymax, 'FontSize',16)
grid on
if savefigures==1
saveas(hFig,'r1','emf'); %name is a string
end

figure(2)
hFig = figure(2);
set(hFig, 'Position', [0 0 imgsize_x imgsize_y])
hold on
for j=4:4
plot(tstamp(1,:),Tin_comp(j+4,:), 'color',cc(j,:), 'LineWidth',3)
end
for j=4:4
plot(tstamp_exp,Tin_exp(:,j+4), 'o', 'LineWidth',2, 'MarkerEdgeColor',cc(j,:), 'MarkerFaceColor',cc(j,:))
end
hold off
% title('Rack 2','FontSize',20)
text(xmin+xtick*1.1,ymax-0.5*ytick,'Rack-2','FontSize',20)
xlabel('Time, s','FontSize',20)
ylabel('T_{inlet}, \circ C','FontSize',20)
legend('C4-C','C4-E','Location','SouthEast')
axis([xmin,xmax,ymin,ymax])
set(gca, 'XTick',xmin:xtick:xmax, 'FontSize',16)
set(gca, 'YTick',ymin:ytick:ymax, 'FontSize',16)
grid on
if savefigures==1

```

```

saveas(hFig,'r2','emf'); %name is a string
end

figure(3)
hFig = figure(3);
set(hFig, 'Position', [0 0 imgsize_x imgsize_y])
hold on
for j=4:4
plot(tstamp(1,:),Tin_comp(j+8,:), 'color',cc(j,:), 'LineWidth',3)
end
for j=4:4
plot(tstamp_exp,Tin_exp(:,j+8), 'o', 'LineWidth',2, 'MarkerEdgeColor',cc(j,:), 'MarkerFaceColor',cc(j
,:))
end
hold off
% title('Rack 3','FontSize',20)
text(xmin+xtick*1.1,ymax-0.5*ytick, 'Rack-3', 'FontSize',20)
xlabel('Time, s','FontSize',20)
ylabel('T_{inlet}, \circ C','FontSize',20)
legend('C4-C', 'C4-E', 'Location', 'SouthEast')
axis([xmin,xmax,ymin,ymax])
set(gca, 'XTick', xmin:xtick:xmax, 'FontSize',16)
set(gca, 'YTick', ymin:ytick:ymax, 'FontSize',16)
grid on
if savefigures==1
saveas(hFig,'r3','emf'); %name is a string
end

Tin_exp_comparison=transpose(Tin_exp);
for j=1:ndt_exp+1
Tin_comp_comparison(:,j)=Tin_comp(:,(j-1)*dt_exp/dt+1);
end

% Only include 4 data points into comparison
Tin_exp_comparison_=[Tin_exp_comparison(3,:);Tin_exp_comparison(4,:);Tin_exp_comparison(8,:);Tin
_exp_comparison(12,:)];
clear Tin_exp_comparison
Tin_exp_comparison = Tin_exp_comparison_;

Tin_comp_comparison_=[Tin_comp_comparison(3,:);Tin_comp_comparison(4,:);Tin_comp_comparison(8,:);
Tin_comp_comparison(12,:)];
clear Tin_comp_comparison
Tin_comp_comparison = Tin_comp_comparison_;
%%%%%%%%%%%%%%%%%%%%%%%%%%%%%%%%%%%%%%%%%%%%%%%%%%%%%%%%%%%%%%%%%%%%%%%%

mTexp=mean(mean(Tin_exp_comparison));
mTcomp=mean(mean(Tin_comp_comparison));

Tin_exp_n=Tin_exp_comparison-mTexp;
Tin_comp_n=Tin_comp_comparison-mTcomp;

s=4;
for j=1:ndt_exp
Tin_exp_v((j-1)*s+1:(j-1)*s+s,1)=Tin_exp_comparison(:,j);
Tin_comp_v((j-1)*s+1:(j-1)*s+s,1)=Tin_comp_comparison(:,j);
end

DTin=(Tin_comp_v-Tin_exp_v);
stdevDTin=sqrt((dot(DTin,DTin')/(s*ndt_exp)));

figure(7)
hFig = figure(7);
set(hFig, 'Position', [0 0 imgsize_x imgsize_x])
axis([ymin,ymax,ymin,ymax])
set(gca, 'XTick', ymin:ytick:ymax, 'FontSize',16)
set(gca, 'YTick', ymin:ytick:ymax, 'FontSize',16)

hline = reffline([1 0]);

```

```

set(hline,'LineWidth',3,'Color','k')

hold on
text(ymin+ytick,ymax-1.5*ytick,['\sigma=' num2str(stdevDTin,2) '\circ C'],'FontSize',20)

scatter(Tin_exp_comparison(1,:),Tin_comp_comparison(1,:),80,'o','LineWidth',1,'MarkerEdgeColor','k','MarkerFaceColor','w')

scatter(Tin_exp_comparison(2,:),Tin_comp_comparison(2,:),80,'o','LineWidth',1,'MarkerEdgeColor','g','MarkerFaceColor','w')

scatter(Tin_exp_comparison(3,:),Tin_comp_comparison(3,:),80,'o','LineWidth',1,'MarkerEdgeColor','b','MarkerFaceColor','w')

scatter(Tin_exp_comparison(4,:),Tin_comp_comparison(4,:),80,'o','LineWidth',1,'MarkerEdgeColor','r','MarkerFaceColor','w')

hold off
xlabel('T_{inlet} - Experimental, \circ C','FontSize',20)
ylabel('T_{inlet} - Computed, \circ C','FontSize',20)
leg=legend('45\circ C','R1C3','R1C4','R2C4','R3C4');
set(leg,'Location','SouthEast')
grid on
set(gca,'FontSize',16);
if savefigures==1
saveas(hFig,'compare','emf'); %name is a string
end

for t=1:ndt_exp+1
err(t,:)=err(1,:);
end

figure(11); % Server Exit Air Temperature Comparison
hFig = figure(11);
set(hFig, 'Position', [0 0 imgsize_x imgsize_y])
axis([xmin,xmax,ymin,ymax])
set(gca,'XTick',xmin:xtick:xmax,'FontSize',16)
set(gca,'YTick',ymin:ytick:ymax,'FontSize',16)

hold on
for k=1:2
plot(tstamp, Tin_comp(k+2,:), 'color',cc(k+2,:), 'LineWidth',3)
end
for k=1:2
h=errorbar(tstamp_exp,Tin_exp(:,k+2),err(:,k), 'o','color',cc(k+2,:));
set(h, 'LineWidth', 1.5, 'MarkerSize', 8, 'MarkerFaceColor', 'w', 'MarkerEdgeColor', cc(k+2,:));
end
hold off
% title('Rack-1','FontSize',20)
text(xmin+xtick*1.1,ymax-0.5*ytick,'Rack-1','FontSize',20)
xlabel('Time (s)','FontSize',20)
ylabel('T_{a-in} (\circ C)','FontSize',20)
legend('C3-C','C4-C','C3-E','C4-E','Location','SouthEast')
grid on

hline = reffline([0 8+max(Tin_comp(:,1))]);
set(hline,'LineStyle','--','LineWidth',3,'Color','k')

if savefigures==1
saveas(hFig,'rlerr','emf'); %name is a string
end

figure(12); % Server Exit Air Temperature Comparison
hFig = figure(12);
set(hFig, 'Position', [0 0 imgsize_x imgsize_y])
axis([xmin,xmax,ymin,ymax])
set(gca,'XTick',xmin:xtick:xmax,'FontSize',16)
set(gca,'YTick',ymin:ytick:ymax,'FontSize',16)

```

```

hold on
for k=1:1
    plot(tstamp, Tin_comp(k+7,:), 'color', cc(k+3,:), 'LineWidth', 3)
end
for k=1:1
h=errorbar(tstamp_exp, Tin_exp(:,k+7), err(:,k+2), 'o', 'color', cc(k+3,:));
set(h, 'LineWidth', 1.5, 'MarkerSize', 8, 'MarkerFaceColor', 'w', 'MarkerEdgeColor', cc(k+3,:));
end
hold off
% title('Rack-2', 'FontSize', 20)
text(xmin+xtick*1.1, ymax-0.5*ytick, 'Rack-2', 'FontSize', 20)
xlabel('Time (s)', 'FontSize', 20)
ylabel('T_{a-in} (\circC)', 'FontSize', 20)
legend('C4-C', 'C4-E', 'Location', 'SouthEast')
grid on

hline = reline([0 8+max(Tin_comp(:,1))]);
set(hline, 'LineStyle', '--', 'LineWidth', 3, 'Color', 'k')

if savefigures==1
saveas(hFig, 'r2err', 'emf'); %name is a string
end

figure(13); % Server Exit Air Temperature Comparison
hFig = figure(13);
set(hFig, 'Position', [0 0 imgsize_x imgsize_y])
axis([xmin, xmax, ymin, ymax])
set(gca, 'XTick', xmin:xtick:xmax, 'FontSize', 16)
set(gca, 'YTick', ymin:ytick:ymax, 'FontSize', 16)

hold on
for k=1:1
    plot(tstamp, Tin_comp(k+11,:), 'color', cc(k+3,:), 'LineWidth', 3)
end
for k=1:1
h=errorbar(tstamp_exp, Tin_exp(:,k+11), err(:,k+3), 'o', 'color', cc(k+3,:));
set(h, 'LineWidth', 1.5, 'MarkerSize', 8, 'MarkerFaceColor', 'w', 'MarkerEdgeColor', cc(k+3,:));
end
hold off
% title('Rack-3', 'FontSize', 20)
text(xmin+xtick*1.1, ymax-0.5*ytick, 'Rack-3', 'FontSize', 20)
xlabel('Time (s)', 'FontSize', 20)
ylabel('T_{a-in} (\circC)', 'FontSize', 20)
legend('C4-C', 'C4-E', 'Location', 'SouthEast')
grid on

hline = reline([0 8+max(Tin_comp(:,1))]);
set(hline, 'LineStyle', '--', 'LineWidth', 3, 'Color', 'k')

if savefigures==1
saveas(hFig, 'r3err', 'emf'); %name is a string
end

end

end

```

# Appendix-E: MATLAB Codes for the Hybrid-Lumped Capacitance Model (CRAH Fan Failure and CW Interruption Tests in Quadrant Data Center)

```

clear all; close all; clc;
CASE=1;      % (1) Rack Shutdown
             % (2) Chilled Water Shutdown
             % (3) Fan Failure
             % (4) Decreased Air Flow
             % (5) Increased Air Flow
savefigures=0; % (0) Does not save figures
              % (1) Saves figures to the directory

% Physical properties of the Room and Racks %%%%%%%%%%%%%%%%%%%%%%%%%%%%%%%
b=3;        % number of blocks in the server
s=60;       % number of servers
rz=1;       % number of recirculation zones
sr=6;       % number of servers per rack
nr=s/sr;    % number of racks
%%%%%%%%%%%%%%%%%%%%%%%%%%%%%%%%%%%%%%%%%%%%%%%%%%%%%%%%%%%%%%%%%%%%%%%%%%%%%%

% Assignment of recirculation path/zone to server j %%%%%%%%%%%%%%%%%%%%%%%%%
for j=1:s
    rzassign(j,1)=1;
end

% if RS(j,k)=1 Server j is part of recirculation zone k
% Based on the numbering of servers assign servers to recirculation zones
for j=1:s
    for r=1:rz
        if r==rzassign(j,1)
            RS(j,r)=1;
        else
            RS(j,r)=0;
        end
    end
end
%%%%%%%%%%%%%%%%%%%%%%%%%%%%%%%%%%%%%%%%%%%%%%%%%%%%%%%%%%%%%%%%%%%%%%%%%%%%%%

% This function loads the experimental data and the plotting
% parameters specific to various cases depending on the definition of CASE
[Ttold,DT1t,Ttnew,DT1tnew,cc,imshow_x,imshow_y,DTcfd,Ttile_cfd,CRAHCFMold,...
    CRAHCFMnew,ymin,ymax,ytick,xmin,xmax,xtick,dt_exp,ndt_exp,tstamp_exp,dt,ndt,tstamp]...
    = readdata(CASE,s);

% Model Inputs for Servers and CRAH Controls %%%%%%%%%%%%%%%%%%%%%%%%%%%%%%%
% This function loads case dependent model inputs for servers and CRAH controls
[CW,CWnew,CRC,Tmc,redline,time_redline,t_flow,RF,Cs,UAs,Ca,Qfold,Qf,a1,a2,Qold,Q] ...
    = inputs(CASE,s,b,dt);

for j=1:s
    for k=1:b
        E(j,k)=1-exp(-UAs(j,k)/Ca(j)); % Effectiveness of Server Blocks
    end
end

%CRAH Properties %%%%%%%%%%%%%%%%%%%%%%%%%%%%%%%
Cac=(CRAHCFMold/60*0.3048^3*1.225*1005); % Initial CRAH Flow Capacity (W/K)
Cacnew=(CRAHCFMnew/60*0.3048^3*1.225*1005); % Steady State CRAH Flow Capacity (W/K)
UACR=3789*2; % Initial Thermal Conductance (W/K)
ECR=1-exp(-UACR/Cac); % Effectiveness of CRAH Heat Exchange
CCR=236815*2; % Thermal Capacitance (J/K)

```

```

%CRAH Fan Power
QfCold=2654*2;          % Initial CRAH Fan Power (W)
QfC=2654*2;           % CRAH FAN Power (W/K)
%%%%%%%%%%%%%%%%%%%%%%%%%%%%%%%%%%%%%%%%%%%%%%%%%%%%%%%%%%%%%%%%%%%%%%%%
%CRAH second block Properties %%%%%%%%%
UACR2=149*2;          % Initial Thermal Conductance (W/K)
ECR2=1-exp(-UACR2/Cac); % Effectiveness of CRAH Heat Exchange
CCR2=152151*2;       % Thermal Capacitance (J/K)
%%%%%%%%%%%%%%%%%%%%%%%%%%%%%%%%%%%%%%%%%%%%%%%%%%%%%%%%%%%%%%%%%%%%%%%%

%Plenum Properties %%%%%%%%%
CPL=1872143;         % Thermal Capacitance (J/K)
UAPL= 1232;         % Thermal Conductance (W/K)
QPL=0;              % Heat Generation in Plenum Block (W)
%%%%%%%%%%%%%%%%%%%%%%%%%%%%%%%%%%%%%%%%%%%%%%%%%%%%%%%%%%%%%%%%%%%%%%%%

% Room Air Capacitance %%%%%%%%%
Croom=157365*1;      % Thermal Capacitance (J/K)
r_hotaisle=0.13;    % Ratio of Hot Aisle to Room Volume (-)
CMh=r_hotaisle*Croom; % Hot Aisle Thermal Capacitance (J/K)
CMc=(1-r_hotaisle)*Croom; % Cold Aisle Thermal Capacitance (J/K)
for j=1:s
    Cin(j)=CMc/s; % Server Air Inlet Zone Thermal Capacitance (J/K)
end

%%%%%%%%%%%%%%%%%%%%%%%%%%%%%%%%%%%%%%%%%%%%%%%%%%%%%%%%%%%%%%%%%%%%%%%%

% Calculation of Initial Condition %%%%%%%%%

Tcold=Ttold; % Initial CRAH exit air temperature (C)
Tmold=Ttold+(sum(sum(Qold))+sum(Qfold))/Cac; % Initial Mixed Room Air Temperature
Tmnew=Ttnew+(sum(sum(Q))+sum(Qf))/Cacnew; % Initial Mixed Room Air Temperature

for j=1:s
    Tinold(j,1)=DTlt(j,1)+Ttold; % Initial Server Inlet Air Temperature (C)
    F(j,1)=1-(Tinold(j)-Ttold)/(Tmold-Ttold); % Initial Capture Index based on experimental
data
end

if CASE==4 || CASE==5 % This statement is for CRAH Air Flow Change
Cases
for j=1:s
    Tinnew(j,1)=DTltnew(j,1)+Ttnew; % New Server Inlet Air Temperature (C)
    Fnew(j,1)=1-(Tinnew(j)-Ttnew)/(Tmnew-Ttnew); % New Capture Index based on experimental data
end
Catnew=dot(Fnew,Ca); % Steady State Tile Air Flow Capacity (W/K)
Calnew=Cacnew-Catnew; % Steady State Leakage Flow Capacity (W/K)
lknew=Calnew/Cacnew; % Steady State Leakage Rate
end

Cas=sum(Ca); % Initial Server Air Flow Capacity (W/K)
Cat=dot(F,Ca); % Initial Tile Air Flow Capacity (W/K)
Car=Ca.*(1-F); % Initial Recirculation Air Flow Capacity per Server (W/K)
CaRZ=transpose(Car)*RS+0.00000001; % Initial Recirculation Air Flow Capacity per Recirculation
Path (W/K)

% Recirculation Zone Properties %%%%%%%%%
F_C=1; % Correction Factor for CR
F_UA=1; % Correction Factor for UA

if CASE==1 % Rack Shutdown Experiment
CR= F_C*1953279; % Thermal Capacitance (J/K)
UAR=F_UA*152; % Thermal Conductance (W/K)
elseif CASE==2 % Chilled Water Shutdown Experiment
CR= F_C*1953279; % Thermal Capacitance (J/K)
UAR=F_UA*152; % Thermal Conductance (W/K)
elseif CASE==3 % CRAH Fan Failure Experiment
CR= F_C*1953279; % Thermal Capacitance (J/K)
UAR=F_UA*411; % Thermal Conductance (W/K)
elseif CASE==4 % Decreasing CRAH Air Flow
CR= F_C*1953279; % Thermal Capacitance (J/K)

```

```

UAR=F_UA*271;          % Thermal Conductance (W/K)
elseif CASE==5        % Increasing CRAH Air Flow
CR= F_C*1953279;      % Thermal Capacitance (J/K)
UAR=F_UA*152;         % Thermal Conductance (W/K)
end

for r=1:rz
CR_new(r,1)=CR(r,1); % New Thermal Capacitance (J/K)
UAR_new(r,1)=UAR(r,1); % New Thermal Conductance (W/K)
QR(r,1)=0;           % Heat Generation in Recirculation Paths (W)
end

% Initial Temperatures at the inlet and exit of server blocks (C)
for j=1:s
Told(j,1)=Tinold(j);
Told(j,2)=Told(j,1)+Qold(j,1)/Ca(j);
Told(j,3)=Told(j,2)+(Qold(j,2)+Qfold(j))/Ca(j);
Teold(j)=Told(j,3)+Qold(j,3)/Ca(j);
end
% Initial server block temperatures (C)
for j=1:s
for k=1:b
TBold(j,k)=Told(j,k)+Qold(j,k)/Ca(j)/E(j,k);
end
end

Txold=dot(Ca,Teold)/Cas; % Initial Mixed Server Exit Air Temperature (C)

Cal=Cac-Cat; % Initial Leakage Flow Capacity (W/K)
lk=Cal/Cac; % Initial Leakage Rate

QCRold=(-sum(sum(Qold))-sum(Qfold))-QfCold; % Initial CRAH Cooling Capacity (W)
QCR=(-sum(sum(Q))-sum(Qf))-QfC; % CRAH Cooling Capacity (W)

QCR2old=0; % Initial CRAH Cooling Capacity (W)
QCR2=0; % CRAH Cooling Capacity (W)

for r=1:rz
ER(r)=1-exp(-UAR(r)/CaRZ(r)); % Effectiveness of Recirculation Path Heat Exchange
end

for r=1:rz
TBRold(r)=Tmold+QR(r)/CaRZ(r)/ER(r); % Initial Temperature of Recirculation Path Thermal
Mass (C)
TRold(r)=TBRold(r)+(Tmold-TBRold(r))*(1-ER(r)); % Initial Temperature of Recirculation Path
Air (C)
end

TRSold=RS*transpose(TRold); % Initial Temperature of Recirculation Air into
Servers (C)
ERS=RS*transpose(ER); % Effectiveness of Recirculation Path Heat Exchange
of individual servers

TBCRold=Tmold+QCRold/Cac/ECR; % Initial Temperature of CRAH Thermal
Mass (C)
TCRold=(TBCRold+(Tmold-TBCRold)*(1-ECR)); % Initial Temperature of CRAH exit air in case CW=0
TBCR2old=TCRold+QCR2old/Cac/ECR2; % Initial Temperature of CRAH Thermal
Mass (C)
TCR2old=(TBCR2old+(TCRold-TBCR2old)*(1-ECR2))+QfCold/Cac; % Initial Temperature of CRAH exit
air in case CW=0

Tcc=Tcold-QfCold/Cac; % Initial Temperature of CRAH exit air
before the CRAH fan (C)
Tcold=CW*(CRC*(TBCR2old+(TCRold-TBCR2old)*(1-ECR2))+(1-CRC)*(Tcc+QfCold/Cac))+(1-CW)*(TCR2old);
% Initial Temperature of CRAH exit (C)

EPL=1-exp(-UAPL/Cat); % Effectiveness of Plenum Heat Exchange
TBPLold=Tcold+QPL/Cat/EPL; % Initial Temperature of Plenum Thermal Mass (C)
Ttold=Tcold-(Tcold-TBPLold)*EPL; % Initial Temperature of the Tile (C)

```



```

% Collection of Initial Temperatures as a Vector
for k=1:b
    Xold((k-1)*s+1:k*s,1)=Told(:,k);
    Xold(s*b+(k-1)*s+1:s*b+k*s,1)=Tbold(:,k);
end
Xold(s*b*2+1:s*b*2+s,1)=Teold(:);
Xold(s*b*2+s+1:s*b*2+s+s,1)=TRSold(:);
Xold(s*b*2+s+s+1:s*b*2+s+s+rz,1)=TBRold(:);
Xold(s*b*2+s+s+rz+1,1)=TBPLold;
Xold(s*b*2+s+s+rz+2,1)=TBRCold;
Xold(s*b*2+s+s+rz+3,1)=TCRold;
Xold(s*b*2+s+s+rz+4,1)=Tcold;
Xold(s*b*2+s+s+rz+5,1)=Tmold;
Xold(s*b*2+s+s+rz+6,1)=Ttold;
Xold(s*b*2+s+s+rz+7,1)=Txold;
Xold(s*b*2+s+s+rz+8,1)=TBCR2old;
Xold(s*b*2+s+s+rz+9,1)=TCR2old;

Fold=F;
if CASE==1 % Rack Shutdown Experiment
    Fnew=F; % Capture Index after t>0
elseif CASE==2 % Chilled Water Shutdown Experiment
    Fnew=F; % Capture Index after t>0
elseif CASE==3 % CRAH Fan Failure Experiment
    Fnew=zeros(s,1)+0.00000000000001; % Capture Index after t>0
elseif CASE==4 || CASE==5 % CRAH Flow Air Change
    lk=lknew; % Leakage Rate after t>0
end

% Transient Simulation Starts Here %%%%%%%%%%%%%%%%%%%%%%%%%%%%%%%%%%%%%%%%%%%%%%%%%%%%%%%%%%%%%%%%%%%%%%%%%
AA = zeros(s*b*2+s+s+rz+9,s*b*2+s+s+rz+9); % Matrix created for the transient simulation
time=0; % Initialized Time
for t=1:ndt
    if time>=0 % Changes in the transient simulation happen after the specified
time
        F=Fnew; % New Capture Index
        CW=CWnew; % The chilled water supply into the CRAH unit
    end
    time=time+dt; % Start of counting the time

    tic

    % Recompute flow rates at the room level (Recirculation)
    Cat=dot(F,Ca); % Tile air flow capacity (W/K)
    Cac=Cat/(1-lk); % CRAH air flow capacity (W/K)
    Cal=lk*Cac; % Leakage air flow capacity (W/K) Based on computed
initial value
    Car=Ca.*(1-F); % Recirculation Air Flow Capacity per Server (W/K)
    CaRZ=transpose(Car)*RS+0.000000001; % Recirculation Air Flow Capacity per Recirculation Path
(W/K)
    ECR=1-exp(-UACR/Cac); % Effectiveness of CRAH Heat Exchange
    ECR2=1-exp(-UACR2/Cac); % Effectiveness of CRAH Heat Exchange

    % Recirculation Zone Properties (if "new" values are different)
    for r=1:rz
        CR(r,1)=CR_new(r,1);
        UAR(r,1)=UAR_new(r,1);
    end

    for r=1:rz
        ER(r)=1-exp(-UAR(r)/CaRZ(r)); % Effectiveness of Recirculation Path Heat Exchange
    end

    ERS=RS*transpose(ER); % Effectiveness of Recirculation Path Heat Exchange per Server

    EPL=1-exp(-UAPL/Cat); % Effectiveness of Plenum Heat Exchange

%% Constants of equations %%%%%%%%%%%%%%%%%%%%%%%%%%%%%%%%%%%%%%%%%%%%%%%%%%%%%%%%%%%%%%%%%%%%%%%%%
for j=1:s
    tau_in(j)=Cin(j)/Ca(j);

```

```

A_in(j)=(1-dt/2/tau_in(j))/(1+dt/2/tau_in(j));
B_in(j)=((1-F(j))*dt/2/tau_in(j))/(1+dt/2/tau_in(j));
C_in(j)=(F(j)*dt/2/tau_in(j))/(1+dt/2/tau_in(j));
end

for j=1:s
    for k=1:b
        tau(j,k)= Cs(j,k)/E(j,k)/Ca(j);
        A(j,k)= (1-dt/2/tau(j,k)) / (1+dt/2/tau(j,k));
        B(j,k)= dt*Q(j,k)/Cs(j,k) / (1+dt/2/tau(j,k));
        C(j,k)= dt/tau(j,k) / (1+dt/2/tau(j,k))/2;
    end
end

for r=1:rz
    tauR(r)= CR(r)/ER(r)/CaRZ(r);
    A_R(r)=(1-dt/2/tauR(r)) / (1+dt/2/tauR(r));
    B_R(r)=dt*QR(r)/CR(r) / (1+dt/2/tauR(r));
    C_R(r)=dt/tauR(r) / (1+dt/2/tauR(r))/2;
end

tauPL= CPL/EPL/Cat;
tauPL_2= CPL/UAPL;
A_PL=(1-dt/2/tauPL) / (1+dt/2/tauPL);
B_PL=dt*QPL/CPL / (1+dt/2/tauPL);
C_PL=dt/tauPL / (1+dt/2/tauPL)/2;

tauCR= CCR/ECR/Cac;
A_CR=(1-dt/2/tauCR) / (1+dt/2/tauCR);
B_CR=dt*QCR/CCR / (1+dt/2/tauCR);
C_CR=dt/tauCR / (1+dt/2/tauCR)/2;

tauCR2= CCR2/ECR2/Cac;
A_CR2=(1-dt/2/tauCR2) / (1+dt/2/tauCR2);
B_CR2=dt*QCR2/CCR2 / (1+dt/2/tauCR2);
C_CR2=dt/tauCR2 / (1+dt/2/tauCR2)/2;

tauM= CMh/(Cas+Cal);
tauML=CMh/(Cal);
tauMS=CMh/(Cas);
A_M=(1-dt/2/tauM) / (1+dt/2/tauM);
A_ML=(dt/4/tauML) / (1+dt/2/tauM);
A_MS=(dt/2/tauMS) / (1+dt/2/tauM);

% Data input into the matrix representing linear systems of equations %%%
AA(1:s*b,1:s*b)=eye(s*b); % Tjk
AA(s*b+1:s*b*2,s*b+1:s*b*2)=eye(s*b); % TBjk

for j=1:s
    for k=1:b-1
        AA(s*k+j,s*(k-1)+j)=- (1-E(j,k)); % Factor of T(j,k) in T(j,k+1)
    end
end

for j=1:s
    for k=1:b
        AA(s*b+s*(k-1)+j,s*(k-1)+j)=-C(j,k); % Factor of T(j,k) in TB(j,k)
    end
end

for j=1:s
    for k=1:b-1
        AA(s*k+j,s*b+s*(k-1)+j)=-E(j,k); % Factor of TB(j,k) in T(j,k+1)
    end
end

AA(s*b*2+1:s*b*2+s,s*b*2+1:s*b*2+s)=eye(s); % Te(j)

for j=1:s
    for k=b

```

```

        AA(s*b*2+j,s*(k-1)+j)=- (1-E(j,k));           % Factor of T(j,k=b) in Te(j)
    end
end

for j=1:s
    for k=b
        AA(s*b*2+j,s*b+s*(k-1)+j)=-E(j,k);           % Factor of TB(j,k=b) in Te(j)
    end
end

for j=1:s
    AA(s*b*2+s+j,s*b*2+s+s+rz+5)=- (1-ERS(j));       % Factor of Tm in Tr(j)
end

for j=1:s
    for r=1:rz
        AA(s*b*2+s+j,s*b*2+s+s+r)=-ER(r)*RS(j,r);    % Factor of TRB(j,k) in Tr(j)
    end
end

for j=1:s
    AA(s*b*2+s+j,s*b*2+s+j)=1;                         % Factor of Tr(r) in Tr(j)
end

AA(s*b*2+s+s+1:s*b*2+s+s+rz,s*b*2+s+s+1:s*b*2+s+s+rz)=eye(rz); % Factor of TRB(r) in TRB(r)

for r=1:rz
    AA(s*b*2+s+s+r,s*b*2+s+s+rz+5)=-C_R(r);          % Factor of Tm in TRB(r)
end

AA(s*b*2+s+s+rz+1,s*b*2+s+s+rz+1) = 1;               % Factor of TPB in TPB
AA(s*b*2+s+s+rz+1,s*b*2+s+s+rz+4) = -C_PL;          % Factor of Tc in TPB

AA(s*b*2+s+s+rz+2,s*b*2+s+s+rz+2) = 1;               % Factor of TCB in TCB
AA(s*b*2+s+s+rz+2,s*b*2+s+s+rz+5) = -C_CR;          % Factor of Tm in TCB

AA(s*b*2+s+s+rz+8,s*b*2+s+s+rz+8) = 1;               % Factor of TCB2 in TCB2
AA(s*b*2+s+s+rz+8,s*b*2+s+s+rz+3) = -C_CR2;         % Factor of Tcx(TCR) in TCB2

AA(s*b*2+s+s+rz+3,s*b*2+s+s+rz+3) = 1;               % Factor of Tcx in Tcx
AA(s*b*2+s+s+rz+3,s*b*2+s+s+rz+2) = -ECR;           % Factor of TCB in Tcx
AA(s*b*2+s+s+rz+3,s*b*2+s+s+rz+5) = -(1-ECR);       % Factor of Tm in Tcx

AA(s*b*2+s+s+rz+9,s*b*2+s+s+rz+9) = 1;               % Factor of Tcx2 in Tcx2 (TCR2)
AA(s*b*2+s+s+rz+9,s*b*2+s+s+rz+8) = -ECR2;          % Factor of TCB2 in Tcx2 (TCR2)
AA(s*b*2+s+s+rz+9,s*b*2+s+s+rz+3) = -(1-ECR2);     % Factor of Tcx(TCR) in Tcx2 (TCR2)

AA(s*b*2+s+s+rz+4,s*b*2+s+s+rz+4) = 1;               % Factor of Tc in Tc
AA(s*b*2+s+s+rz+4,s*b*2+s+s+rz+9) = -(1-CW);        % Factor of Tcx2(TCR) in Tc

AA(s*b*2+s+s+rz+6,s*b*2+s+s+rz+6) = 1;               % Factor of Tt in Tt
AA(s*b*2+s+s+rz+6,s*b*2+s+s+rz+4) = -(1-EPL);       % Factor of Tc in Tt
AA(s*b*2+s+s+rz+6,s*b*2+s+s+rz+1) = -EPL;           % Factor of TPB in Tt

for j=1:s
    AA(s*b*2+s+s+rz+7,s*b*2+j) = -Ca(j)/Cas;         % Factor of Te(j) in Tx
end
AA(s*b*2+s+s+rz+7,s*b*2+s+s+rz+7) = 1; % Factor of Tx in Tx

AA(s*b*2+s+s+rz+5,s*b*2+s+s+rz+5) = 1;               % Factor of Tm in Tm
AA(s*b*2+s+s+rz+5,s*b*2+s+s+rz+4) = -A_ML;          % Factor of Tc in Tm
AA(s*b*2+s+s+rz+5,s*b*2+s+s+rz+6) = -A_ML;          % Factor of Tt in Tm
AA(s*b*2+s+s+rz+5,s*b*2+s+s+rz+7) = -A_MS;          % Factor of Tx in Tm

for j=1:s
    AA(j,s*b*2+s+s+rz+6)=-C_in(j); % Factor of Tt in T(j,k)
end
for j=1:s
    AA(j,s*b*2+s+j)=-B_in(j); % Factor of Tr(j) in T(j,k)
end

```

```

% Call control function for the return air
Tcs=Tmc+(QCR+QfC)/Cac;
[CRET] = crah_control(Xold(s*b*2+s+s+rz+3,t),Xold(s*b*2+s+s+rz+9,t),Tmc,Tcs,RF);

% Vector V (RHS of the linear system of equations)
V = zeros(s*b*2+s+s+rz+9,1);

for j=1:s
    V(j)=Xold(j,t)*A_in(j)+Xold(s*b*2+s+j,t)*B_in(j)+Xold(s*b*2+s+s+rz+6,t)*C_in(j); % RHS
of Inlet Air Temperature Zone
end

for j=1:s
    V(s*(b-1)+j)=Qf(j)/Ca(j); % RHS of T(j,k=b) equation(s)
end

for j=1:s
    for k=1:b
        V(s*b+(k-1)*s+j)=A(j,k)*Xold(s*b+(k-1)*s+j,t)+B(j,k)+C(j,k)*Xold((k-1)*s+j,t); % RHS of
TB(j,k) equation(s)
    end
end

for r=1:rz
    V(s*b*2+s+s+r)=A_R(r)*Xold(s*b*2+s+s+r,t)+B_R(r)+C_R(r)*Xold(s*b*2+s+s+rz+5,t); % RHS
of T(j,k=b) equation(s)
end

V(s*b*2+s+s+rz+1) = A_PL*Xold(s*b*2+s+s+rz+1,t)+B_PL+C_PL*Xold(s*b*2+s+s+rz+4,t); % TBPL
V(s*b*2+s+s+rz+2) = A_CR*Xold(s*b*2+s+s+rz+2,t)+B_CR*CW+C_CR*Xold(s*b*2+s+s+rz+5,t); % TBCR
V(s*b*2+s+s+rz+3) = 0; %Tcx
V(s*b*2+s+s+rz+4) = CW*(CRC*CRET+(1-CRC)*(Tcc-a1*time+a2*(time)^2+QfC/Cac)); %Tc
V(s*b*2+s+s+rz+5) =
A_M*Xold(s*b*2+s+s+rz+5,t)+A_ML*Xold(s*b*2+s+s+rz+6,t)+A_ML*Xold(s*b*2+s+s+rz+4,t)+A_MS*Xold(s*b*
2+s+s+rz+7,t); %Tm

V(s*b*2+s+s+rz+8) = A_CR2*Xold(s*b*2+s+s+rz+8,t)+B_CR2*CW+C_CR2*Xold(s*b*2+s+s+rz+3,t);
%TBCR2
V(s*b*2+s+s+rz+9) = QfC/Cac; %TCR2

T=AA\V; % Solving Linear System of Equations

Xold(:,t+1)=T;

% Recording Redline Temperature Violation Time for each Server
for j=1:s
    if T(j)>=redline && time_redline(j)==0
        time_redline(j,1)=time;
    end
end

toc
end

for j=1:s
    DT(j,:)=Xold(j,:)-Xold(s*b*2+s+s+rz+6,:);
    Tin_comp(j,:)=Xold(j,:);
    Ttile_comp(j,:)=Xold(s*b*2+s+s+rz+6,:);
end

postprocess(imgsize_x,imgsize_y,tstamp,Tin_comp,cc,xmin,xtick,xmax,ymin,ytick,ymax,nr,sr,savefigu
res);
if savefigures==1
close all
end

```

```

function
[Ttold,DT1t,Ttnew,DT1tnew,cc,imsize_x,imsize_y,DTcfd,Ttile_cfd,CRAHCFMold,CRAHCFMnew,ymin,ymax,
ytick,xmin,xmax,xtick,dt_exp,ndt_exp,tstamp_exp,dt,ndt,tstamp] = readdata(CASE,s)

    load cc6          % Color code for plotting servers per rack
    cc=cc6;
    imsize_x=960;    % Width of the time axis
    imsize_y=720;    % Width of the temperature axis
    load DTcfd       % Experimental Data: Server Inlet Air Temperature - Tile Temperature
    load Ttile_cfd   % Experimental Data: Tile Air Temperature

if CASE==1          % Rack Shutdown Experiment
    CRAHCFMold=15567; % CRAH Flow Rate (CFM)
    CRAHCFMnew=15567; % New CRAH Flow Rate (CFM)

    % Plotting parameters %%%%%%%%%%%%%%%%%%%%%%%%%%%%%%%%%%%%%%%%%%%%%%%%%%%%%%%%%%%%%%%%%%%%%%%%%
    ymin=16;         % Maximum value of vertical axis : Tin-Ttile
    ymax=30;         % Minimum value of vertical axis : Tin-Ttile
    ytick=2;         % Vertical axis tick size : Tin-Ttile
    xmin=0;          % Maximum value of horizontal axis : Tin-Ttile
    xmax=2000;       % Minimum value of horizontal axis : Tin-Ttile
    xtick=200;       % Horizontal axis tick size : Tin-Ttile

    dt_exp=100;      % Experimental time step size (s)
    ndt_exp=20;      % Experimental number of time steps
    tstamp_exp=0:dt_exp:dt_exp*ndt_exp; % Time stamp for experimental data

    dt=10;           % Computational time step size (s)
    ndt=200;         % Computational number of time steps
    tstamp=0:dt:ndt*dt; % Time stamp for computational data
    %%%%%%%%%%%%%%%%%%%%%%%%%%%%%%%%%%%%%%%%%%%%%%%%%%%%%%%%%%%%%%%%%%%%%%%%%

elseif CASE==2      % Chilled Water Shutdown Experiment
    CRAHCFMold=15567; % CRAH Flow Rate (CFM)
    CRAHCFMnew=15567; % New CRAH Flow Rate (CFM)

    % Plotting parameters %%%%%%%%%%%%%%%%%%%%%%%%%%%%%%%%%%%%%%%%%%%%%%%%%%%%%%%%%%%%%%%%%%%%%%%%%
    ymin=15;         % Maximum value of vertical axis : Tin
    ymax=55;         % Minimum value of vertical axis : Tin
    ytick=5;         % Vertical axis tick size : Tin
    xmin=0;          % Maximum value of horizontal axis : Tin
    xmax=600;        % Minimum value of horizontal axis : Tin
    xtick=100;       % Horizontal axis tick size : Tin

    dt_exp=30;       % Experimental time step size (s)
    ndt_exp=12;      % Experimental number of time steps
    tstamp_exp=0:dt_exp:dt_exp*ndt_exp; % Time stamp for experimental data

    dt=1;            % Computational time step size (s)
    ndt=1200;        % Computational number of time steps
    tstamp=0:dt:ndt*dt; % Time stamp for computational data
    %%%%%%%%%%%%%%%%%%%%%%%%%%%%%%%%%%%%%%%%%%%%%%%%%%%%%%%%%%%%%%%%%%%%%%%%%

elseif CASE==3      % CRAH Fan Failure Experiment
    CRAHCFMold=15567;% CRAH Flow Rate (CFM)
    CRAHCFMnew=1;    % New CRAH Flow Rate (CFM)

    % Plotting parameters %%%%%%%%%%%%%%%%%%%%%%%%%%%%%%%%%%%%%%%%%%%%%%%%%%%%%%%%%%%%%%%%%%%%%%%%%
    ymin=15;         % Maximum value of vertical axis : Tin
    ymax=55;         % Minimum value of vertical axis : Tin
    ytick=5;         % Vertical axis tick size : Tin
    xmin=0;          % Maximum value of horizontal axis : Tin
    xmax=300;        % Minimum value of horizontal axis : Tin
    xtick=50;        % Horizontal axis tick size : Tin

    dt_exp=30;       % Experimental time step size (s)
    ndt_exp=12;      % Experimental number of time steps
    tstamp_exp=0:dt_exp:dt_exp*ndt_exp; % Time stamp for experimental data

    dt=1;            % Computational time step size (s)

```

```

ndt=900; % Computational number of time steps
tstamp=0:dt:ndt*dt; % Time stamp for computational data
%%%%%%%%%%%%%%%%%%%%%%%%%%%%%%%%%%%%%%%%%%%%%%%%%%%%%%%%%%%%%%%%%%%%%%%%

elseif CASE==4 % Chilled Water Shutdown Experiment
CRAHCFMold=15567; % CRAH Flow Rate (CFM)
CRAHCFMnew=15567/2; % New CRAH Flow Rate (CFM)
load DTcfdnew % Experimental Data: Server Inlet Air Temperature - Tile Temperature

% Plotting parameters %%%%%%%%%%%%%%%%%%%%%%%%%%%%%%%%%%%%%%%%%%%%%%%%%%%%%%%%%%%%%%%%%%%%%%%%%
ymin=15; % Maximum value of vertical axis : Tin
ymax=55; % Minimum value of vertical axis : Tin
ytick=5; % Vertical axis tick size : Tin
xmin=0; % Maximum value of horizontal axis : Tin
xmax=300; % Minimum value of horizontal axis : Tin
xtick=50; % Horizontal axis tick size : Tin

dt_exp=30; % Experimental time step size (s)
ndt_exp=12; % Experimental number of time steps
tstamp_exp=0:dt_exp:dt_exp*ndt_exp; % Time stamp for experimental data

dt=1; % Computational time step size (s)
ndt=900; % Computational number of time steps
tstamp=0:dt:ndt*dt; % Time stamp for computational data
%%%%%%%%%%%%%%%%%%%%%%%%%%%%%%%%%%%%%%%%%%%%%%%%%%%%%%%%%%%%%%%%%%%%%%%%

elseif CASE==5 % Chilled Water Shutdown Experiment
CRAHCFMold=15567/2; % CRAH Flow Rate (CFM)
CRAHCFMnew=15567; % New CRAH Flow Rate (CFM)

% Plotting parameters %%%%%%%%%%%%%%%%%%%%%%%%%%%%%%%%%%%%%%%%%%%%%%%%%%%%%%%%%%%%%%%%%%%%%%%%%
ymin=15; % Maximum value of vertical axis : Tin
ymax=55; % Minimum value of vertical axis : Tin
ytick=5; % Vertical axis tick size : Tin
xmin=0; % Maximum value of horizontal axis : Tin
xmax=300; % Minimum value of horizontal axis : Tin
xtick=50; % Horizontal axis tick size : Tin

dt_exp=30; % Experimental time step size (s)
ndt_exp=12; % Experimental number of time steps
tstamp_exp=0:dt_exp:dt_exp*ndt_exp; % Time stamp for experimental data

dt=1; % Computational time step size (s)
ndt=900; % Computational number of time steps
tstamp=0:dt:ndt*dt; % Time stamp for computational data
%%%%%%%%%%%%%%%%%%%%%%%%%%%%%%%%%%%%%%%%%%%%%%%%%%%%%%%%%%%%%%%%%%%%%%%%

end

% Initial Conditions based on Experimental Data %%%%%%%%%%%%%%%%%%%%%%%%%%%%%%%%%%%%%%%%%%%%%%%%%%%%%%%%%%%%%%%%%%%%%%%%%
Ttold=Ttile_cfd; % Initial Tile Air Temperature (C)
Ttnew=Ttold; % New Tile Air Temperature (C)

for j=1:s
DT1t(j,1)=DTcfd(j,1); % Initial Server Inlet Air Temperature - Tile Temperature
end
if CASE==4 || CASE==5 % Rack Shutdown Experiment

DT1tnew(:,1)=DTcfdnew(:,1); % New Server Inlet Air Temperature - Tile Temperature
else
DT1tnew(:,1)=DTcfd(:,1); % New Server Inlet Air Temperature - Tile Temperature
end
%%%%%%%%%%%%%%%%%%%%%%%%%%%%%%%%%%%%%%%%%%%%%%%%%%%%%%%%%%%%%%%%%%%%%%%%

end

```

```

function [CW,CWnew,CRC,Tmc,redline,time_redline,t_flow,RF,Cs,UAs,Ca,Qfold,Qf,a1,a2,Qold,Q] =
inputs(CASE,s,b,dt)

CW=1;          % Initial Chilled Water Availability: (1) CW is ON, (0) CW is OFF
CRC=0;        % Initial CRAH control                : (1) fixed return air temperature, (0) fixed
exit air temperature
Tmc=35;       % Return Air Temperature Control Set Point (C)
redline=25;   % Redline Temperature for Server Inlet Temperature (C)
time_redline=zeros(s,1); % Vector defined - The recorded simulation time for servers
when their inlet temperature exceeds redline temperature (s)
t_flow=1;     % Flow adjustment time after fan speed changes (s)
RF=1-exp((log(0.01)*dt/t_flow)); % Flow adjustment factor to reach 99% of the steady state
flow within adjustment time of t_flow

% Server Properties %%%%%%%%%%%%%%%%%%%%%%%%%%%%%%%%%%%%%%%%%%%%%%%%%%%%%%%%%%%%%%%%%%%%%%%%%%
C_S=60000;    % Thermal Capacitance (J/K)
UA_S=84*2.5; % Thermal Conductance (W/K)
cb(2)=0.45;   % Distribution of Thermal Mass in block 2
cb(3)=0.05;   % Distribution of Thermal Mass in block 3
cb(1)=1-cb(2)-cb(3); % Distribution of Thermal Mass in block 1
for j=1:s
    for k=1:b
        Cs(j,k)=cb(k)*C_S; % Distributed Thermal Capacitance within
blocks (J/K)
        UAs(j,k)=cb(k)*UA_S; % Distributed Thermal Conductance within
blocks (W/K)
    end
    Ca(j,1)= 201; % Server Flow Capacity (W/K)
    Qfold(j,1)=0; % Initial Server Fan Power (W)
    Qf(j,1)=0; % Server Fan Power (W)
end

if CASE==1 % Rack Shutdown Experiment
    CWnew=1; % Chilled Water Supply after t=0 : (1) CW is ON, (0) CW is OFF
    %Constants of polynomial change in the CRAH exit air temperature
    a1=0;
    a2=0;
    for j=1:s
        Qold(j,:)= [0 2035 0]; % Initial Heating Power of Server Blocks (W)
        Q(j,:)= [0 0 0]; % Heating Power of Server Blocks (W)
    end
elseif CASE==2 % Chilled Water Shutdown Experiment
    CWnew=0; % Chilled Water Supply after t=0 : (1) CW is ON, (0) CW is OFF
    %Constants of polynomial change in the CRAH exit air temperature
    a1=0;
    a2=0;
    for j=1:s
        Qold(j,:)= [0 2035 0]; % Initial Heating Power of Server Blocks (W)
        Q(j,:)= [0 2035 0]; % Heating Power of Server Blocks (W)
    end
elseif CASE==3 % CRAH Fan Failure Experiment
    CWnew=0; % Chilled Water Supply after t=0 : (1) CW is ON, (0) CW is OFF
    %Constants of polynomial change in the CRAH exit air temperature
    a1=0;
    a2=0;
    for j=1:s
        Qold(j,:)= [0 2035 0]*1; % Initial Heating Power of Server Blocks (W)
        Q(j,:)= [0 2035 0]*1; % Heating Power of Server Blocks (W)
    end
elseif CASE==4 || 5 % Decreasing CRAH Air Flow Experiment
    CWnew=1; % Chilled Water Supply after t=0 : (1) CW is ON, (0) CW is OFF
    %Constants of polynomial change in the CRAH exit air temperature
    a1=0;
    a2=0;
    for j=1:s
        Qold(j,:)= [0 2035 0]*1; % Initial Heating Power of Server Blocks (W)
        Q(j,:)= [0 2035 0]*1; % Heating Power of Server Blocks (W)
    end
end
end
end

```

```

function [] =
postprocess(imgsize_x,imgsize_y,tstamp,Tin_comp,cc,xmin,xtick,xmax,ymin,ytick,ymax,nr,sr,savefigu
res)

for k=1:nr

% Server Inlet Air Temperatures
hold all
figure(k)
hFig = figure(k);
set(hFig, 'Position', [0 0 imgsize_x imgsize_y])
figure(k)
hold on
for j=1:sr
plot(tstamp(1,:),Tin_comp((k-1)*sr+j,:), 'color',cc(j,:), 'LineWidth',3)
end
hold off
title(['Rack' int2str(k)] , 'FontSize',20)
xlabel('Time, s', 'FontSize',20)
ylabel('T_{inlet}, \circ C', 'FontSize',20)
legend('C1-C', 'C2-C', 'C3-C', 'C4-C', 'C5-C', 'C6-C', 'Location', 'SouthEast')
axis([xmin,xmax,ymin,ymax])
set(gca, 'XTick',xmin:xtick:xmax, 'FontSize',16)
set(gca, 'YTick',ymin:ytick:ymax, 'FontSize',16)
grid on
hline = reline([0 8+max(Tin_comp(:,1))]);
set(hline, 'LineStyle', '--', 'LineWidth',3, 'Color', 'k')

if savefigures==1
saveas(hFig,['rack' int2str(k)], 'emf'); %name is a string
end
end
end

```



## Appendix-F: Method of Determining Recirculation Path Thermal Characteristics for Multiple Paths

Consider a server of face area  $A_f$  with an average face velocity  $V_f$ . If we visualize a conduit of the same cross-sectional area conveying the recirculated air flow to the inlet of the servers emanating from the exhaust, the velocity of the recirculated air in this conduit,  $V_r$ , can be approximated by

$$V_r = V_f(1 - \psi_j). \quad (\text{F.1})$$

Assuming that the conduit has a constant rectangular cross section area but allowed to distort at a certain aspect ratio,  $\gamma$ , as defined in Figure 6.3.

$$b/W = \gamma. \quad (\text{F.2})$$

For the distorted conduit, the hydraulic diameter,  $D_h$ , can be defined as

$$D_h = 4A_f / P = 2W\gamma / (1 + \gamma), \quad (\text{F.3})$$

where the perimeter,  $P$ , and the  $A_f$  can be defined as

$$P = 2W(1 + \gamma), \quad (\text{F.4})$$

$$A_f = \gamma W^2. \quad (\text{F.5})$$

Along this conduit, energy transfer between the room thermal mass and the recirculated air is assumed to happen along the width,  $W$ , of the cross-section area. The thermal conductance of the heat transfer surface can be related to the conduit dimensions by,

$$UA = UWL, \tag{F.6}$$

where L is the length of the conduit, and U is the heat transfer coefficient. Overall heat transfer coefficient U can be assumed to be given by a relationship of the form (Incropera & DeWitt, 2007),

$$U = \frac{kNu}{D_h} = 0.023 \frac{k}{D_h} \text{Re}^{0.8} \text{Pr}^{1/3}. \tag{F.7}$$

There are two dimensions, conduit length, L, and width, W, that need to be determined to make a closure for this approach. For a data center with the exposed surface area,  $A_R$ , a practical rule for the characteristic length can be as follows,

$$L = \sqrt{A_R}. \tag{F.8}$$

## Appendix-G: Conjugate Heat Transfer Model of the CRAH Heat Exchanger

The transient heat transfer problem of the CRAH heat exchanger following an interruption of chilled water can be solved more rigorously through the solution of the conjugate heat transfer problem between the thermal masses of still (or very slowly moving) water and the metal body of the heat exchanger (aluminum fins and copper tubes). Unsteady heat balance equations for the metal and the water thermal masses are respectively as,

$$C_m \frac{dT_m}{dt} = \dot{C}_a \varepsilon_a (T_{a-in} - T_m) + (UA)_w (T_w - T_m), \quad (G.1)$$

$$C_w \frac{dT_w}{dt} = (UA)_w (T_m - T_w) - \dot{Q}_C. \quad (G.2)$$

$T_m$  and  $T_w$  are uniform temperatures of the heat exchanger metal and water, while  $C_m$  ( $\sim 112\text{kJ/K}$ ) and  $C_w$  ( $\sim 124\text{kJ/K}$ ) are the thermal capacitances of these components based on the dimensional measurements.  $\dot{Q}_C$ , which is forced to be zero during a water interruption, represents the room heat load including the heat dissipated by the server heaters, server fans and CRAH fans.

During steady state operation and for the known dimensions of the CRAH tubes convective heat transfer coefficient (and thermal conductance  $(UA)_w \sim 29\text{kW/K}$ ) on the water side can be computed using the Gnielinski correlation (Incropera & DeWitt, 2007),

$$Nu = \frac{f / 8 (\text{Re}_D - 1000) \text{Pr}}{1 + 127 \sqrt{f / 8 (\text{Pr}^{2/3} - 1)}}, \quad (G.3)$$

which is for turbulent flows of  $\text{Re}_D$  between  $3 \times 10^3$  and  $5 \times 10^6$ .

The  $(UA)_a$  ( $\sim 3.8\text{kW/K}$ ) on the air side between air and metal surface can be estimated through Equation 6.26, which is assumed to remain constant at constant CRAH air flow rate.

The chilled water flow during an interruption can be considered laminar with velocities representing typical water displacement due to leaking water. For laminar flow and uniform surface heat flux, the Nusselt number asymptotes to 4.36 at low velocities (Incropera & DeWitt, 2007). The resultant  $(UA)_w$  ( $\sim 1.7\text{kW/K}$ ) is present between the water and metal thermal masses after a typical chilled water interruption scenario.

The abovementioned approach assumes a uniform temperature of water body during the transient event. However, after the interruption of chilled water with minute amount of flow, both the temperature and the velocity are expected to have profiles. Velocity profile for laminar flow is

$$\frac{u}{\bar{u}} = 2 \left[ 1 - \left( \frac{r}{R} \right)^2 \right]. \quad (\text{G.4})$$

For the constant heat rate solution, a normalized temperature profile inside the tube can be expressed as (Kays et al., 2002)

$$\frac{T - T_m}{\bar{T} - T_m} = \frac{24}{11} \left[ \frac{3}{4} + \frac{\bar{r}^4}{4} - \bar{r}^2 \right], \quad (\text{G.5})$$

where  $T_m$  and  $\bar{T}$  respectively are the surface (metal) temperature and the mixed mean temperature of the water inside a cylindrical pipe with a normalized radius  $\bar{r} = r/R$ . Explicitly, the mass weighted average temperature  $\bar{T} - T_m$  and average temperature of the water body inside a pipe  $\bar{T}_w - T_m$  are defined as

$$\bar{T} - T_m = \frac{\int_0^R u(T - T_m) r dr}{\bar{u} \pi R^2} \text{ and} \quad (\text{G.6})$$

$$\bar{T}_w - T_m = \frac{\int_0^R (T - T_m) r dr}{\pi R^2}, \quad (\text{G.7})$$

which can be integrated using the definition in Equation G.5. Their ratio gives,

$$\frac{\bar{T} - T_m}{\bar{T}_w - T_m} = \frac{\int_0^R \frac{u}{\bar{u}} (T - T_m) r dr}{\int_0^R (T - T_m) r dr} = 1.375. \quad (\text{G.8})$$

This can be reduced to the form of

$$\dot{Q}_w = (T_m - \bar{T})(UA)_w = (T_m - \bar{T}_w)(1.375 \times (UA)_w), \quad (\text{G.9})$$

which means that the actual heat transfer inside a tube with a non-uniform temperature profile is a factor of 1.375 higher than the heat transfer inside an assumed uniform body temperature at  $\bar{T}_w$ .

Therefore, a corrected UA value for the water side (during an interruption) can be used as an even further refinement.

$$(UA)_{w-corr} = 1.375 (UA)_w, \quad (\text{G.10})$$

The differential equations (G.1 and G.2) are incorporated into the model as a verification tool for the simple approach. The results for the chilled water interruption case obtained by these approaches are given in Figure G.1. The simple approach results in Figure G.2 are in reasonable agreement with the more detailed modeling approach. Hence, due to its practicality, the simpler approach is proposed and used in the simulation results presented in this study.

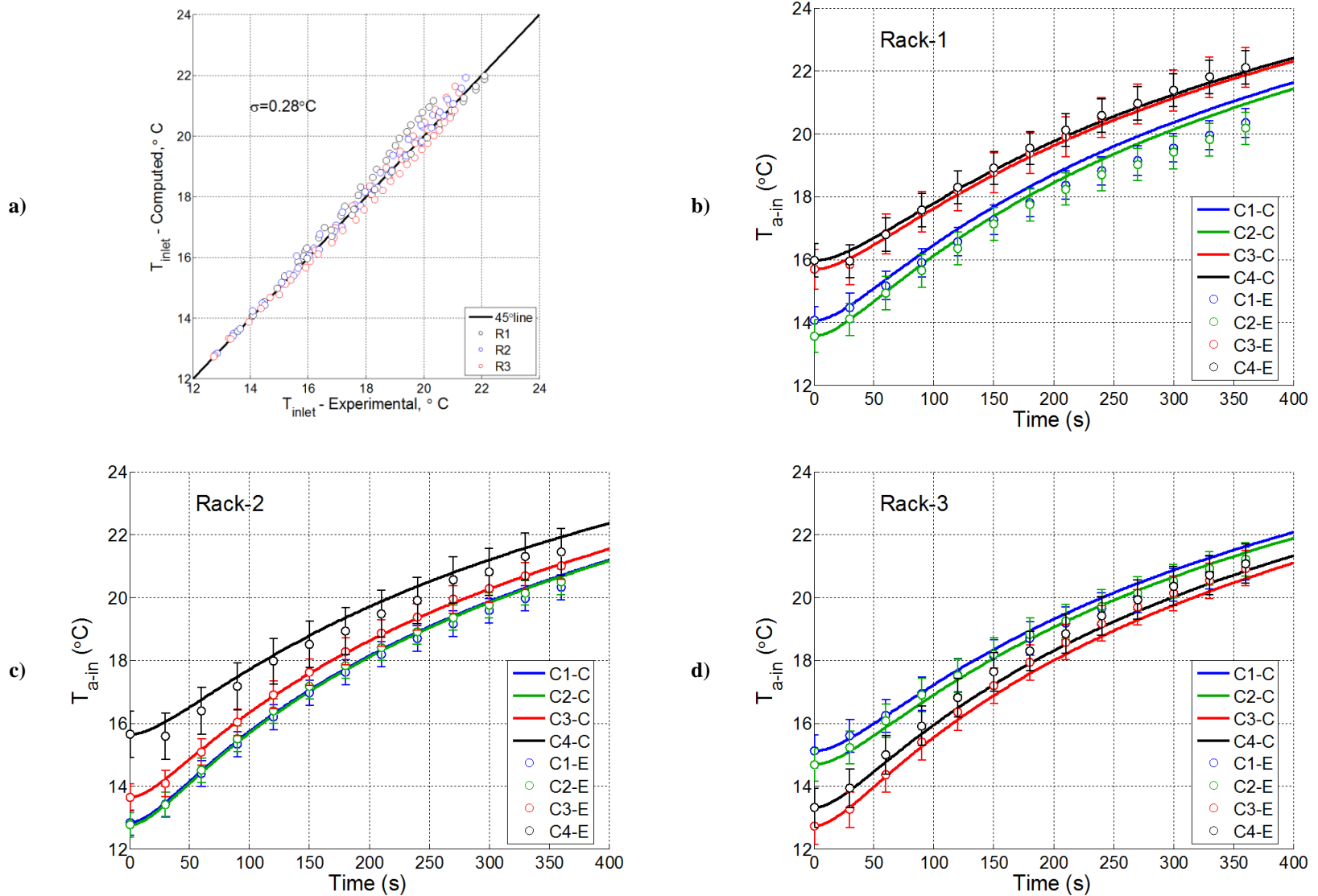


**Figure G.1: Comparison of server inlet air temperature for CRAH Chilled Water Interruption Experiment with Conjugate CRAH Heat Exchanger:**

**Model vs. experiment. a) 4 racks b) Rack1 c) Rack2 d) Rack3**

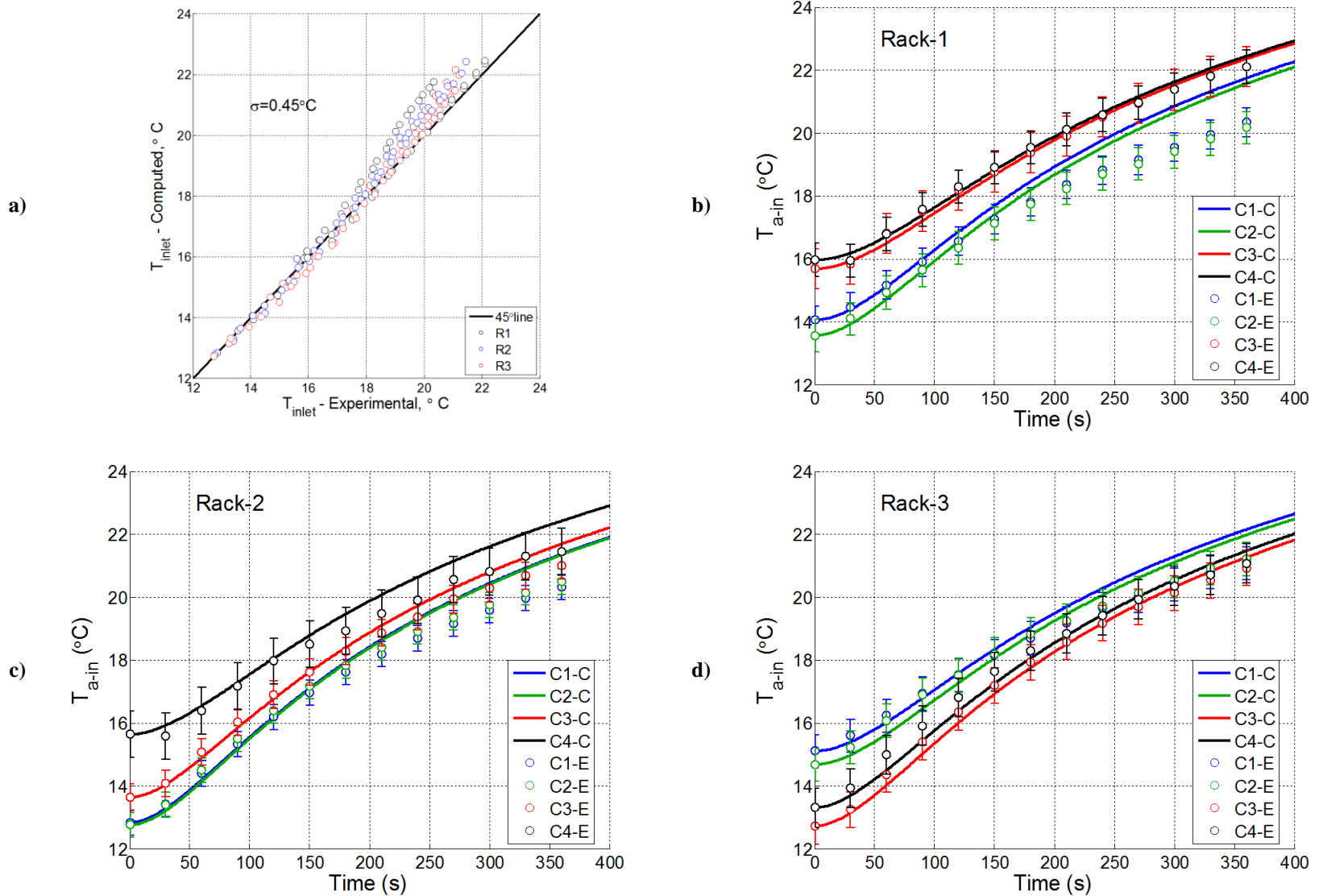


Figure G.2: Comparison of server inlet air temperature for CRAH Chilled Water Interruption Experiment with Simple CRAH Heat Exchanger Model:

Model vs. experiment. a) 4 racks b) Rack1 c) Rack2 d) Rack3

## Appendix-H: CFD as an Alternative to Conduit Approach for Room Thermal Characterization

Required input data for the Hybrid Lumped-Capacitance Model may not be available for data centers that are insufficiently instrumented or are in design phase. Steady state CFD simulations can be used to obtain the server inlet temperatures and to construct flow field in the Hybrid Model through capture indices. After constructing the flow field, the sole purpose of the hypothetical conduit approach was to obtain thermal conductance ( $UA_r$ ) value for the recirculation path and the approach would still be applicable as described in Chapter 6. In other words, CFD-based inlet temperature data can still be used in the absence of measurements to utilize the conduit approach.

An alternative to the conduit approach to estimate  $UA_r$  could be based on a second run of steady state CFD simulation with isothermal enclosure boundary condition ( $T_{en}$ ). Equations H.1 through H.3 show the set of equations for the proposed method.

$$\dot{Q}_{en} = \varepsilon_r \dot{C}_s (T_m - T_{en}), \quad (\text{H.1})$$

$$NTU_{en} = -\ln(1 - \varepsilon_r), \quad (\text{H.2})$$

$$UA_{en} = \dot{C}_s NTU_{en}. \quad (\text{H.3})$$

$UA_{en}$  obtained by the second CFD simulation is driven by the maximum potential recirculation air flow of  $\dot{C}_s$ .  $UA_r$  can be approximated by apportioning the  $UA_{en}$  by the ratio of the actual recirculated air flow to the total server air flow rate,



$$UA_r = UA_{en} \frac{\dot{C}_r}{\dot{C}_s}, \quad (\text{H.4})$$

Similar procedure can be applied for the calculation of the plenum thermal conductance, which can be summarized with the equations below.

$$\dot{Q}_{pl} = \varepsilon_{pl} \dot{C}_c (T_c - T_{pl}), \quad (\text{H.6})$$

$$NTU_{pl} = -\ln(1 - \varepsilon_{pl}), \quad (\text{H.7})$$

$$UA_{pl} = \dot{C}_c NTU_{pl}. \quad (\text{H.8})$$

The proposed method typically gives resultant thermal conductance values that are relatively higher than the UA values based on conduit approach. Hence, the results are less conservative for failure scenarios leading to temperature predictions that are lower than previous predictions with an error less than 1°C within the time frame of interest. The following figures show the results obtained for the set of experiments conducted in the research lab.

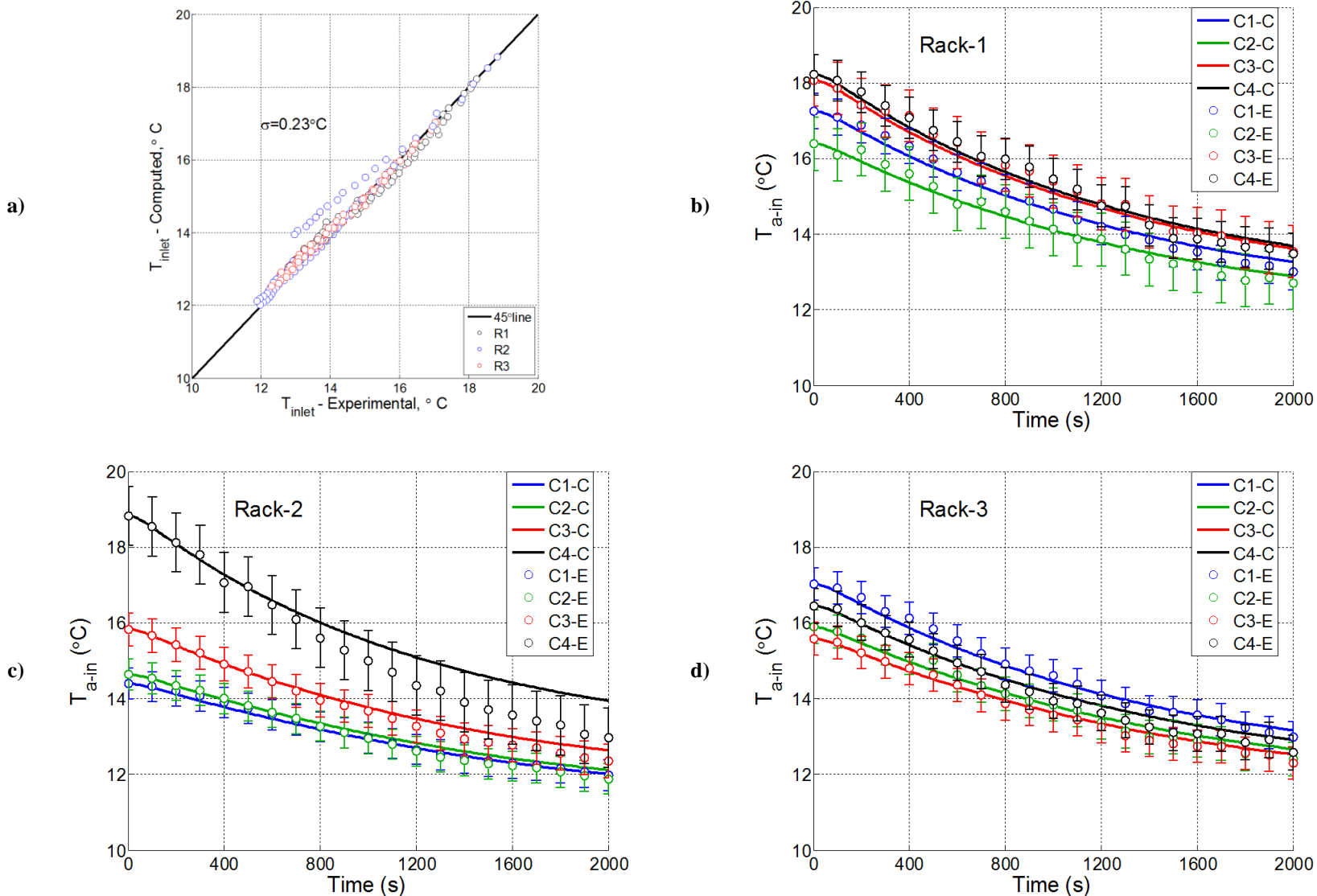


**Figure H.1: Comparison of server inlet air temperature for Rack Shutdown Experiment with single path for the recirculated flow and UA obtained from CFD: Model vs. experiment. a) 4 racks b) Rack1 c) Rack2 d) Rack3**

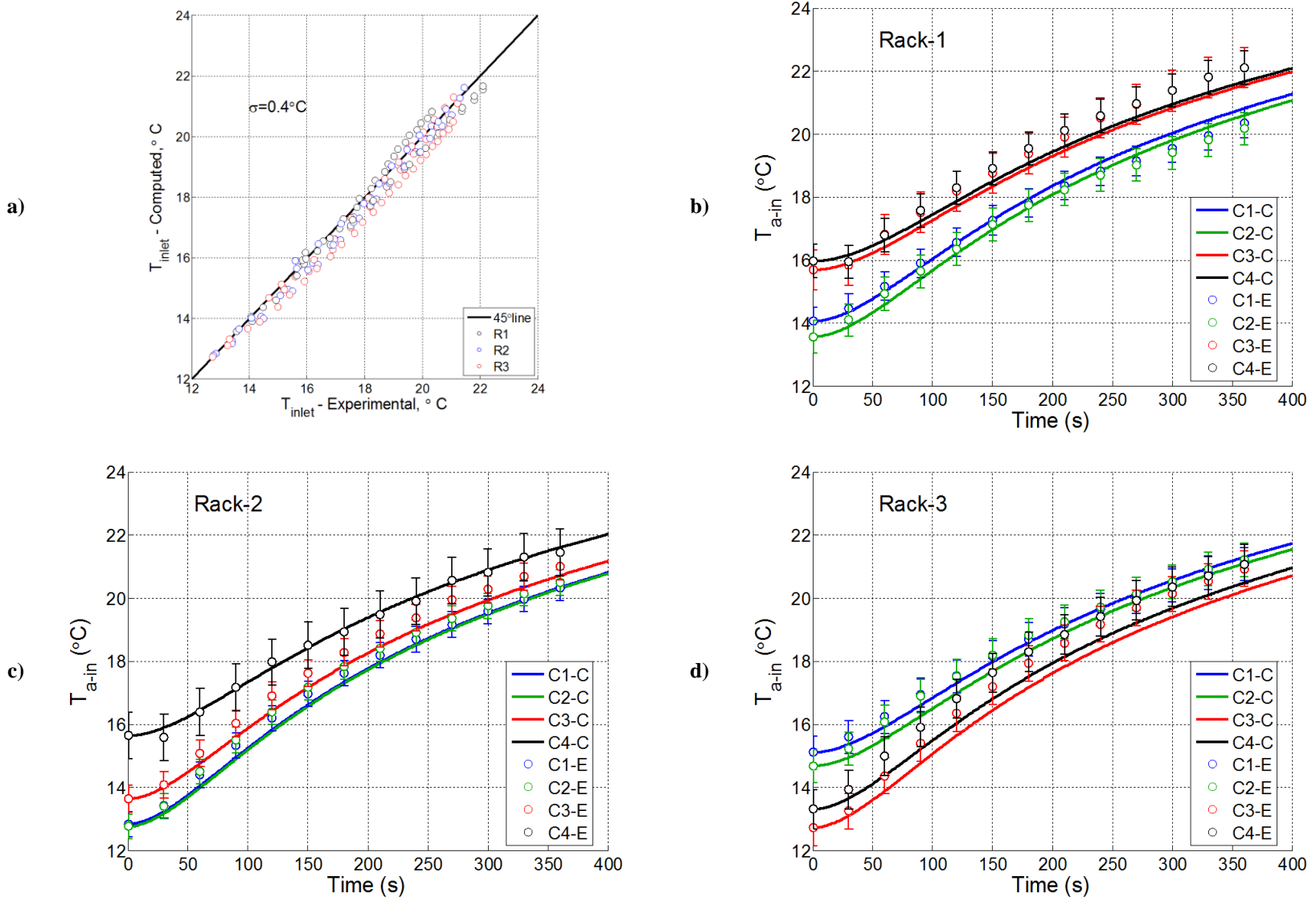


**Figure H.2: Comparison of server inlet air temperature for CRAH Chilled Water Interruption Experiment with single path for the recirculated flow and UA obtained from CFD: Model vs. experiment. a) 4 racks b) Rack1 c) Rack2 d) Rack3**

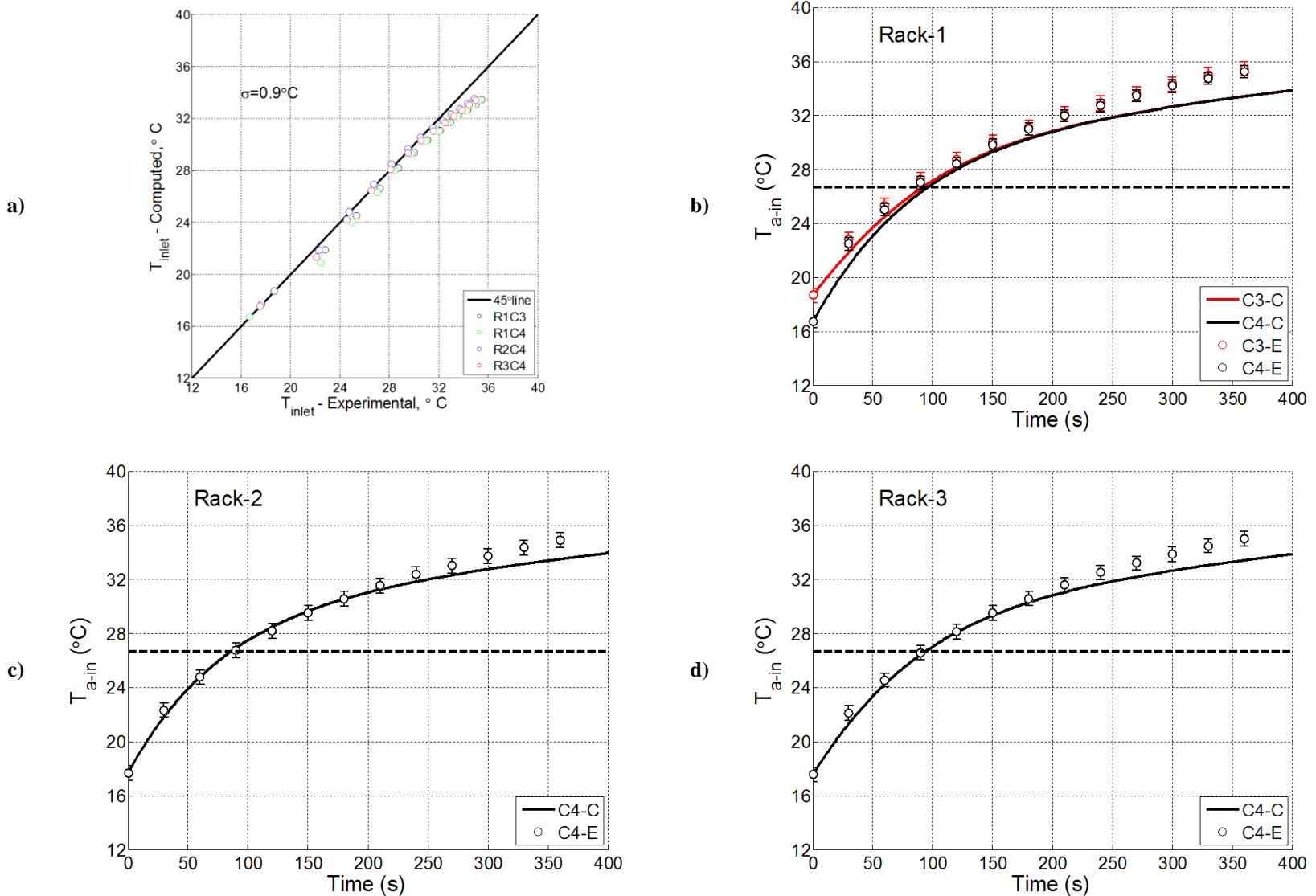


**Figure H.3: Comparison of server inlet air temperature for CRAH Fan Failure Experiment with single path for the recirculated flow and UA obtained from CFD: Model vs. experiment. a) 4 racks b) Rack1 c) Rack2 d) Rack3**

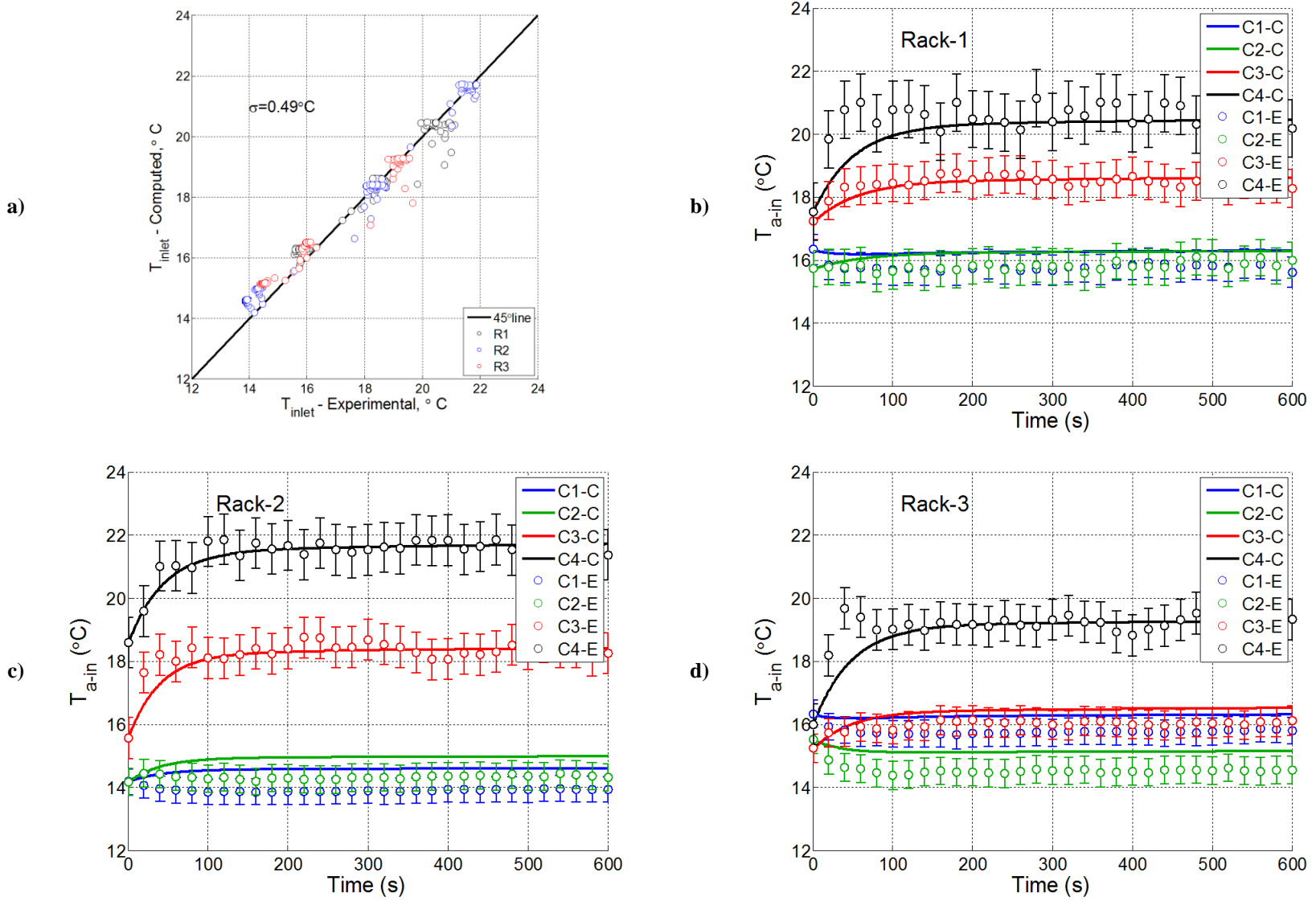


**Figure H.4: Comparison of server inlet air temperature for Decreased CRAH Air Flow Rate Experiment with single path for the recirculated flow and UA obtained from CFD: Model vs. experiment. a) 4 racks b) Rack1 c) Rack2 d) Rack3**

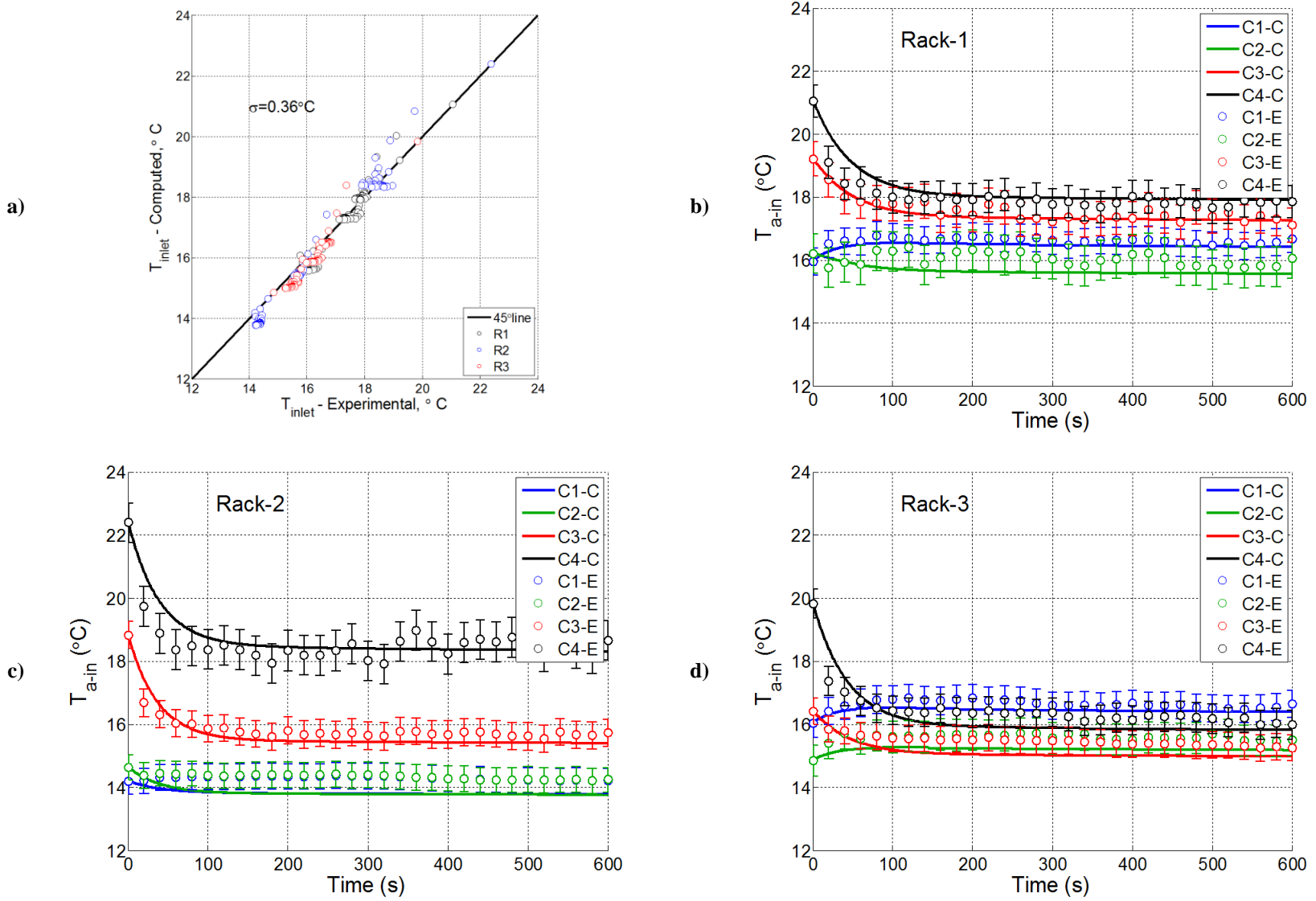


**Figure H.5: Comparison of server inlet air temperature for Increased CRAH Air Flow Rate Experiment with single path for the recirculated flow and UA obtained from CFD: Model vs. experiment. a) 4 racks b) Rack1 c) Rack2 d) Rack3**

## Appendix-I: Transient Experimental Data

### *Rack Shutdown - Server Inlet Air Temperature (°C)*

Time (s)	R1C1	R1C2	R1C3	R1C4	R2C1	R2C2	R2C3	R2C4	R3C1	R3C2	R3C3	R3C4
0	17.3	16.4	18.1	18.2	14.4	14.6	15.8	18.8	17.0	15.9	15.6	16.5
100	17.1	16.1	17.9	18.1	14.3	14.5	15.7	18.5	16.9	15.8	15.5	16.4
200	16.9	16.2	17.4	17.8	14.2	14.4	15.4	18.1	16.7	15.6	15.2	16.0
300	16.6	15.8	17.3	17.4	14.1	14.2	15.2	17.8	16.3	15.3	15.0	15.7
400	16.3	15.6	17.1	17.1	13.9	14.0	14.9	17.1	16.1	15.1	14.8	15.6
500	16.0	15.3	16.6	16.8	13.7	13.8	14.7	17.0	15.8	15.0	14.6	15.3
600	15.6	14.8	16.4	16.4	13.6	13.6	14.5	16.5	15.5	14.6	14.4	14.9
700	15.4	14.9	16.0	16.1	13.4	13.5	14.2	16.1	15.2	14.4	14.1	14.7
800	15.1	14.6	15.8	16.0	13.3	13.3	14.0	15.6	14.9	14.1	13.9	14.4
900	14.9	14.3	15.7	15.8	13.1	13.1	13.8	15.3	14.7	13.9	13.7	14.2
1000	14.7	14.1	15.4	15.5	13.0	13.0	13.7	15.0	14.6	13.8	13.6	13.9
1100	14.4	13.9	15.1	15.2	12.8	12.8	13.5	14.7	14.4	13.7	13.4	13.9
1200	14.2	13.9	14.8	14.8	12.7	12.6	13.3	14.4	14.1	13.4	13.3	13.6
1300	14.0	13.6	14.8	14.7	12.5	12.5	13.1	14.2	13.9	13.2	13.0	13.4
1400	13.8	13.3	14.3	14.2	12.4	12.4	12.9	13.9	13.7	13.0	12.9	13.3
1500	13.6	13.2	14.1	13.9	12.4	12.3	12.8	13.7	13.6	13.0	12.8	13.1
1600	13.5	13.2	14.0	13.9	12.3	12.2	12.8	13.6	13.6	12.9	12.7	13.1
1700	13.2	12.9	14.0	13.8	12.2	12.2	12.7	13.4	13.4	12.8	12.7	13.1
1800	13.2	12.8	13.8	13.7	12.2	12.1	12.6	13.3	13.2	12.5	12.6	12.8
1900	13.2	12.9	13.6	13.6	12.1	12.0	12.4	13.1	13.1	12.5	12.5	12.9
2000	13.0	12.7	13.5	13.5	12.0	11.9	12.4	13.0	13.0	12.4	12.3	12.6

*Chilled Water Failure - Server Inlet Air Temperature (°C)*

<b>Time (s)</b>	<b>R1C1</b>	<b>R1C2</b>	<b>R1C3</b>	<b>R1C4</b>	<b>R2C1</b>	<b>R2C2</b>	<b>R2C3</b>	<b>R2C4</b>	<b>R3C1</b>	<b>R3C2</b>	<b>R3C3</b>	<b>R3C4</b>
<b>0</b>	14.1	13.6	15.7	16.0	12.8	12.8	13.6	15.6	15.1	14.7	12.7	13.3
<b>30</b>	14.5	14.1	15.8	15.9	13.4	13.4	14.1	15.6	15.6	15.2	13.2	13.9
<b>60</b>	15.2	14.9	16.8	16.8	14.4	14.5	15.1	16.4	16.2	16.1	14.4	15.0
<b>90</b>	15.9	15.6	17.5	17.6	15.3	15.5	16.0	17.2	16.9	16.9	15.4	15.9
<b>120</b>	16.6	16.4	18.2	18.3	16.2	16.4	16.9	18.0	17.5	17.5	16.3	16.8
<b>150</b>	17.3	17.1	18.8	18.9	17.0	17.2	17.6	18.5	18.1	18.2	17.2	17.6
<b>180</b>	17.8	17.7	19.4	19.5	17.6	17.8	18.3	18.9	18.7	18.8	17.9	18.3
<b>210</b>	18.4	18.2	19.9	20.1	18.2	18.4	18.9	19.5	19.2	19.2	18.6	18.9
<b>240</b>	18.8	18.7	20.5	20.6	18.7	18.9	19.4	19.9	19.6	19.7	19.2	19.4
<b>270</b>	19.1	19.0	20.9	21.0	19.2	19.4	19.9	20.6	20.0	20.1	19.7	19.9
<b>300</b>	19.6	19.4	21.4	21.4	19.6	19.8	20.3	20.8	20.4	20.5	20.1	20.4
<b>330</b>	20.0	19.8	21.8	21.8	20.0	20.1	20.7	21.3	20.8	20.9	20.5	20.7
<b>360</b>	20.3	20.2	22.1	22.1	20.3	20.5	21.0	21.5	21.1	21.2	20.9	21.1



*CRAH Fan Failure - Server Inlet Air Temperature (°C)*

<b>Time (s)</b>	<b>R1C3</b>	<b>R1C4</b>	<b>R2C4</b>	<b>R3C4</b>
<b>0</b>	18.7	16.7	17.7	17.6
<b>30</b>	22.8	22.5	22.3	22.1
<b>60</b>	25.3	25.0	24.7	24.5
<b>90</b>	27.2	27.0	26.7	26.6
<b>120</b>	28.7	28.4	28.2	28.1
<b>150</b>	30.0	29.8	29.5	29.5
<b>180</b>	31.1	31.0	30.5	30.6
<b>210</b>	32.1	32.0	31.5	31.6
<b>240</b>	32.9	32.7	32.4	32.5
<b>270</b>	33.6	33.5	33.0	33.2
<b>300</b>	34.3	34.2	33.7	33.9
<b>330</b>	35.0	34.7	34.4	34.5
<b>360</b>	35.5	35.2	34.9	35.0

*CRAH Air Flow Decrease - Server Inlet Air Temperature (°C)*

<b>Time (s)</b>	<b>R1C1</b>	<b>R1C2</b>	<b>R1C3</b>	<b>R1C4</b>	<b>R2C1</b>	<b>R2C2</b>	<b>R2C3</b>	<b>R2C4</b>	<b>R3C1</b>	<b>R3C2</b>	<b>R3C3</b>	<b>R3C4</b>
<b>0</b>	16.3	15.7	17.2	17.5	14.2	14.2	15.6	18.6	16.3	15.5	15.2	16.0
<b>20</b>	15.8	15.8	17.9	19.8	14.1	14.5	17.7	19.6	15.9	14.9	15.7	18.2
<b>40</b>	15.7	15.8	18.3	20.8	14.0	14.4	18.2	21.0	15.8	14.6	15.8	19.7
<b>60</b>	15.8	15.8	18.3	21.0	13.9	14.3	18.0	21.0	15.7	14.6	15.9	19.4
<b>80</b>	15.7	15.6	18.4	20.3	13.9	14.3	18.4	21.0	15.7	14.5	15.9	19.0
<b>100</b>	15.7	15.7	18.4	20.8	13.9	14.3	18.1	21.8	15.7	14.4	15.8	19.0
<b>120</b>	15.7	15.8	18.4	20.8	13.9	14.3	18.1	21.9	15.7	14.4	16.0	19.2
<b>140</b>	15.7	15.6	18.5	20.6	13.9	14.3	18.2	21.4	15.7	14.5	15.9	19.0
<b>160</b>	15.7	15.7	18.7	20.1	13.9	14.2	18.4	21.7	15.7	14.5	16.1	19.2
<b>180</b>	15.7	15.7	18.8	21.0	13.9	14.3	18.2	21.6	15.7	14.5	16.1	19.2
<b>200</b>	15.7	15.8	18.5	20.5	13.9	14.3	18.4	21.7	15.7	14.5	16.1	19.2
<b>220</b>	15.9	15.9	18.7	20.5	13.9	14.3	18.8	21.4	15.7	14.5	16.0	19.1
<b>240</b>	15.7	15.7	18.7	20.4	13.9	14.2	18.7	21.7	15.7	14.4	16.0	19.3
<b>260</b>	15.7	15.8	18.7	20.1	13.9	14.2	18.4	21.5	15.7	14.5	16.1	19.1
<b>280</b>	15.7	15.9	18.5	21.1	13.9	14.3	18.4	21.4	15.7	14.6	16.1	19.1
<b>300</b>	15.7	15.8	18.6	20.4	13.9	14.3	18.7	21.5	15.7	14.5	16.0	19.3
<b>320</b>	15.8	15.8	18.3	20.8	13.9	14.3	18.5	21.6	15.8	14.5	16.0	19.5
<b>340</b>	15.8	15.6	18.5	20.6	13.9	14.3	18.4	21.6	15.8	14.6	16.1	19.3
<b>360</b>	15.7	15.7	18.5	21.0	13.9	14.3	18.3	21.8	15.8	14.5	16.1	19.2

*CRAH Air Flow Increase - Server Inlet Air Temperature (°C)*

Time (s)	R1C1	R1C2	R1C3	R1C4	R2C1	R2C2	R2C3	R2C4	R3C1	R3C2	R3C3	R3C4
0	16.0	16.2	19.2	21.1	14.2	14.6	18.8	22.4	16.0	14.8	16.4	19.8
20	16.5	15.8	18.5	19.1	14.2	14.4	16.7	19.7	16.4	15.4	15.9	17.4
40	16.6	15.9	18.0	18.4	14.3	14.4	16.3	18.9	16.6	15.7	15.8	17.0
60	16.6	15.9	17.9	18.5	14.3	14.4	16.0	18.4	16.7	15.5	15.6	16.7
80	16.8	16.3	17.8	18.1	14.3	14.4	16.0	18.5	16.8	15.6	15.6	16.5
100	16.7	16.3	17.8	18.0	14.3	14.4	15.9	18.4	16.8	15.6	15.6	16.4
120	16.7	16.4	17.8	17.9	14.3	14.4	15.9	18.5	16.8	15.6	15.5	16.4
140	16.6	15.9	17.9	18.0	14.3	14.4	15.8	18.4	16.8	15.6	15.6	16.4
160	16.7	16.1	17.4	18.0	14.4	14.4	15.7	18.2	16.7	15.7	15.5	16.5
180	16.7	16.3	17.6	17.9	14.4	14.4	15.6	17.9	16.8	15.7	15.5	16.4
200	16.7	16.3	17.4	17.9	14.3	14.4	15.8	18.3	16.8	15.7	15.5	16.3
220	16.7	16.3	17.8	18.0	14.3	14.4	15.7	18.2	16.8	15.6	15.6	16.4
240	16.7	16.2	17.7	18.1	14.4	14.4	15.7	18.2	16.8	15.6	15.5	16.4
260	16.7	16.3	17.3	17.8	14.4	14.4	15.7	18.3	16.7	15.7	15.5	16.4
280	16.7	16.0	17.3	17.9	14.4	14.4	15.7	18.5	16.7	15.7	15.5	16.3
300	16.6	16.0	17.2	17.8	14.4	14.4	15.6	18.0	16.6	15.6	15.5	16.4
320	16.5	15.9	17.4	17.9	14.4	14.4	15.6	17.9	16.6	15.7	15.5	16.2
340	16.6	15.8	17.3	17.7	14.3	14.4	15.8	18.6	16.6	15.7	15.4	16.1
360	16.6	16.0	17.3	17.7	14.3	14.3	15.8	19.0	16.6	15.5	15.4	16.1

## References

- Abdelmaksoud, W., Dang, T. Q., Khalifa, H.E., Elhadidi, B., Schmidt, R., and Iyengar, M., 2010, “Experimental and Computational Study of Perforated Floor Tile in Data Centers”, *Proceedings of the Intersociety Conference on Thermal Phenomena (ITHERM)*, Las Vegas, USA.
- Abdelmaksoud, W., 2012, Experimental and Numerical Investigations of the Thermal Environment in Air-cooled Data Centers, PhD Dissertation, Syracuse University, NY.
- Amemiya, Y., Hamann, H., Schappert, M., Van Kessel, T., Iyengar, M., O’Boyle, M. and Shen, J., 2007, “Comparison of experimental temperature results with numerical modeling predictions of a real-world compact data center facility”, *Proceedings of ASME InterPack Conference 2007*, July, pp. 871-876.
- ANSYS Fluent, 2009, “User’s Guide,” Release 12.0.
- ASHRAE, 2008a, “ASHRAE Environmental Guidelines for Datacom Equipment: Expanding the Recommended Environmental Envelope,” Atlanta: American Society of Heating, Refrigerating and Air-Conditioning Engineers, Inc.
- ASHRAE, 2008b, “High Density Data Centers: Case Studies and Best Practices,” Atlanta: American Society of Heating, Refrigerating and Air-Conditioning Engineers, Inc.

ASHRAE, 2012, *Thermal Guidelines for Data Processing Environments*, 3<sup>rd</sup> Edition, Atlanta:  
American Society of Heating, Refrigerating and Air-Conditioning Engineers, Inc.

Ayoub, R., Indukuri, K.R., Rosing, T.S., 2010, “Energy Efficient Proactive Thermal Management in Memory Subsystem”, *International Symposium on Low Power Electronics and Design*, pp.195-200.

Bash, C.E., Patel, C.D. and Sharma, R.K., 2006, “Dynamic Thermal Management of Air Cooled Data Centers”, 2006, The Tenth Intersociety Conference on Thermal and Thermomechanical Phenomena in Electronics Systems, IThERM '06, pp. 452-459.

Basman, E and Khalifa, E.H., 2005, “Application of proper orthogonal decomposition to indoor airflows”, *ASHRAE Transactions*, Volume.111, pp. 625-634.

Bautista, L., Sharma, R., 2007, “Analysis of Environmental Data in Data Centers”, *HP Reports*, HPL-2007-98.

Bhopte, S., Schmidt, R., Agonafer, D., and Sammaika, B., 2006, “Optimization of Data Center Room Layout to Minimize Rack Inlet Air Temperature”. *Journal of Electronic Packaging*. Volume 128, Issue 4, pp.380-387.

Boucher, T.D., Auslander, D.M., Cullen, E.B., Chandrakant, D.P., and Federspiel, C.C., 2006, “Viability of Dynamic Cooling Control in a Data Center Environment,” *ASME Journal of Electronic Packaging*, June, Vol. 128 pp.137-144.

Cengel, Y. and Ghajar, A., 2010, *Heat and Mass Transfer: Fundamentals and Applications*, 4th Edition, McGrawHill.

Chen, K., Auslander, D.M., Bash, C.E., Patel, C.D., 2006a, “Local Temperature Control in Data Center Cooling: Part I, Correlation Matrix” *HP Reports*, HPL-2006-42.

Chen, K., Auslander, D.M., Bash, C.E., Patel, C.D., 2006b, “Local Temperature Control in Data Center Cooling: Part II, Statistical Analysis” *HP Reports*, HPL-2006-43.

Choi, J., Kim, Y., Sivasubramaniam, A., Srebric, J., Wang, Q. and Lee, J., 2007, “Modeling and Managing Thermal Profiles of Rack-mounted Servers with ThermoStat”, *13th International Symposium on High Performance Computer Architecture, HPCA 2007*.

Demetriou, D.W., 2012, Thermally aware, energy-based techniques for improving data center energy efficiency, PhD Dissertation, Syracuse University, NY.

Demetriou, D. W., and Khalifa, H. E., 2011, “Energy Optimization of Air-Cooled Data Centers,” *Journal of Thermal Science and Engineering Applications*, 2(4) , 041005.

Elhadidi, B., Khalifa, H.E., 2005, “Application of Proper Orthogonal Decomposition to Indoor Airflows”. *ASHRAE Transactions*. Volume 111, Issue 1, pp.625-634.

Ferreira, A.P., Mosse, D. and Oh, J.C., 2007, “Thermal Faults Modeling using a RC model with an Application to Web Farms”, *19<sup>th</sup> Euromicro Conference on Real-Time Systems (ECRTS'07)*, pp.113-124.

Ghosh, R., Kumar, P., Sundaralingam, V., Joshi, Y., 2011, “Experimental Characterization of Transient Temperature Evolution in a Data Center Facility”, *22nd International Symposium on Transport Phenomena*.

Gondipalli, S., Ibrahim, M., Bhopte, S., Sammakia, B., Murray, B., Ghose, K., 2010, Numerical Modeling of Data Center with Transient Boundary Conditions, *12th IEEE Intersociety Conference on Thermal and Thermomechanical Phenomena in Electronic Systems (ITherm)*, pp.1-7.

Heath, T., Centeno, A.P., George, P., Ramos, L., Jaluria, Y. and Bianchini R., 2006, “Mercury and Freon: Temperature Emulation and Management for Server Systems”, *Proceedings of the 12th international conference on Architectural support for programming languages and operating systems, ASPLOS'06*, pp.106-116.

Ibrahim, M., Gondipalli, S., Bhopte, S., Sammakia, B., Murray, B. and Ghose, K., 2010, “Numerical Modeling Approach to Dynamic Data Center Cooling”, *12th IEEE Intersociety Conference on Thermal and Thermomechanical Phenomena in Electronic Systems (ITherm)*, pp.1-7.

Ibrahim, M., Bhopte, S., Sammakia, B., Murray, B., Iyengar, M., and Schmidt, R., 2011, "Effect of Transient Boundary Conditions and Detailed Thermal Modeling of Data Center Rooms", *IEEE Transactions on Components, Packaging and Manufacturing Technology*, Volume 2 , Issue 2, pp. 300 - 310.

Ibrahim, M., Shrivastava, S., Sammakia, B. and Ghose K., 2012, "Thermal Mass Characterization of a Server at Different Fan Speeds", *13<sup>th</sup> IEEE Intersociety Conference on Thermal and Thermomechanical Phenomena in Electronic Systems (ITherm)*, pp.457-465.

Incropera, F.P., Dewitt, D.P., Bergman, T.L. and Lavine, A.S., 2007, *Fundamentals of Heat and Mass Transfer*, 6th ed., Wiley.

Karki, K., Radmehr, A., and Patankar, S., 2003, "Use of Computational Fluid Dynamics for Calculating Flow Rates through Perforated Tiles in Raised-Floor Data Center." *HVAC&R Research*, 9(2), pp. 153-166.

Kays, W.M., Crawford, M.E. and Weigand B., 2002, *Convective Heat and Mass Transfer*, 4th ed., McGraw-Hill.

Khankari, K., 2009, "Rack Enclosures: A Crucial Link in Airflow Management in Data Centers," *ASHRAE Journal*, August, pp. 48 - 51.



- Khankari, K., 2010, "Thermal Mass Availability for Cooling Data Centers during Power Shutdown", *ASHRAE Transactions*, Volume 116, Part 2.
- Khankari, K., 2011, "Rate of Heating Analysis of Data Centers during Power Shutdown", *ASHRAE Transactions*, Volume 117, Part 1.
- Koomey, J., 2011, "Growth in Data Center Electricity Use 2005 to 2010," A Report by Analytical Press, completed at the request of The New York Times.
- Le, K., Bianchini, R., Nguyen, T.D., Zhang, J., Meng, J. and Jaluria, Y., 2010, "Cost-Aware Virtual Machine Placement in Cloud Computing Systems", *Technical Report DCS-TR-680, Dept. of Computer Science, Rutgers University*, November.
- Lee, E.K., Kulkarni, I., Pompili, D., Parashar, M., 2012, "Proactive thermal management in green datacenters", *The Journal of Supercomputing*, Volume 60, Number 2, pp. 165-195.
- Marshall, L., 2010, "Transient CRAC Failure Analysis". *Applied Math Modeling Inc. White Paper*.
- Marwah, M., Sharma, R., Patnaik, D., Ramakrishnan, N., 2009, "Sustainable Operation and Management of Data Center Chillers using Temporal Data Mining", *Proceedings of ACM Conference on Knowledge Discovery and Data Mining*.

Marwah, M., Sharma, R., Bash, C., 2010, “Thermal Anomaly Prediction in Data Centers”, *12th IEEE Intersociety Conference on Thermal and Thermomechanical Phenomena in Electronic Systems (ITherm)*, pp.1-7.

Nelson, G.M., 2007, Development of an Experimentally-Validated Compact Model of a Server Rack, Master’s Thesis, Georgia Institute of Technology, GA.

Parolini, L., Sinopoli, B., Krogh, B.H., 2009, “A Unified Thermal-Computational Approach to Data Center Energy Management”, *Proceedings of ACM International Workshop on Feedback Control Implementation and Design in Comp. Sys. and Networks*.

Qihong, N., 2008, Experimentally Validated Multiscale Thermal Modeling of Electric Cabinets, PhD Dissertation, Georgia Institute of Technology, GA.

Rambo, J. and Joshi, Y., 2003, “Multi-scale Modeling of High Power Density Data Centers”, *ASME 2003 International Electronic Packaging Technical Conference and Exhibition (InterPACK2003)*, July 6–11, 2003 , Maui, Hawaii, USA, pp. 521-527.

Rambo, J., 2006, Reduced Order Modeling of Multiscale Turbulent Convection: Application to Data Center Thermal Management, PhD Dissertation, Georgia Institute of Technology, GA.

- Samadiani, E., Joshi, Y., 2010, “Multi-parameter model reduction in multi-scale convective systems”, *International Journal of Heat and Mass Transfer*, Volume 53, Issues 9–10, April 2010, pp. 2193–2205.
- Schmidt, R., Karki, K., Kelkar, K., Radmehr, A., and Patankar, S., 2001, “Measurements and Predictions of the Flow Distribution through Perforated Tiles in raised Floor Data Centers,” *Proceedings of ASME InterPACK*, Kauai, HI, July 8 - 13.
- Schmidt, R., Karki, K., and Pantankar, S., 2004, “Raised-floor Data Center: Perforated Tile Flow Rates for Various Tile Layouts”, *Proceedings of IEEE ITherm*, Las Vegas, NV, June 1 – 4.
- Shah, A.J., Bash, C.E., Breen, T.J., Walsh, E.J., Punch, J., 2010a, “From chip to cooling tower data center modeling: Part I Influence of server inlet temperature and temperature rise across cabinet” *12th IEEE Intersociety Conference on Thermal and Thermomechanical Phenomena in Electronic Systems (ITherm)*, pp. 1-10.
- Shah, A.J., Bash, C.E., Breen, T.J., Walsh, E.J., Punch, J., 2010b, “From chip to cooling tower data center modeling: Part II Influence of chip temperature control philosophy” *12th IEEE Intersociety Conference on Thermal and Thermomechanical Phenomena in Electronic Systems (ITherm)*, pp. 1-7.

Sharma, R.K., Bash, C.E., Patel, C.D., Friedrich, R.J. and Chase, J.S., 2005, “Balance of Power - Dynamic Thermal Management for Internet Data Centers”, *Internet Computing IEEE*, Volume 9 , Issue 1, pp. 42-49.

Shields, S.P., 2009, Dynamic Thermal Response of the Data Center to Cooling Loss During Facility Power Failure, Master’s Thesis, Georgia Institute of Technology, GA.

Smith, J. F., Abdelmaksoud, W., Erden, H., Dannenhoffer, J. F., Dang, T.Q., Khalifa, H.E., Schmidt, R., and Iyengar, M., 2011. “Design of Simulated Server Racks for Data Center Research”, *Proceedings of ASME InterPACK*, Portland, OR, July 6 – 8.

Tate Access Floors, Inc., [www.tateinc.com](http://www.tateinc.com)

Tavoularis, S., 2005. *Measurement in Fluid Mechanics*. Cambridge University Press, Cambridge, UK.

Tolia, N., Wang, Z., Ranganathan, P., Bash, C., Marwah, M. and Zhu, X., 2009, “Unified Thermal and Power Management in Server Enclosures”, *Proceedings of the ASME/ InterPACK '09*.

United States Environmental Protection Agency. August 2, 2007. *Report to Congress on Server and Data Center Energy Efficiency, Public Law*. pp.109-431.

VanGilder, W., Schmidt, R., 2005. "Air flow Uniformity through Perforated Tiles in a Raised-Floor Data Center", *Proceedings of IPACK2005*, San Francisco, California, USA.

VanGilder, J. and Shrivastava, S., 2007, "Capture Index: An Airflow-Based Rack Cooling Performance Index," *ASHRAE Transactions*, Vol. 113(1), pp. 126 - 136.

Viewpoint Systems, 2009. *VDAQ: Variable Data Acquisition System Installation and Operaiton Manual*. Version 4.0

Wang, Z., Bash, C., Tolia, N., Marwah, M., Zhu, X. and Ranganathan, P., 2009, "Optimal Fan Speed Control for Thermal Management of Servers", *Proceedings of the ASME/ InterPACK '09*.

Wang, Z., Tolia, N. and Bash, C., 2010, "Opportunities and Challenges to Unify Workload, Power, and Cooling Management in Data Centers", *ACM International Workshop on Feedback Control Implementation and Design in Comp. Sys. and Networks*.

Zhang, X., VanGilder, J., Iyengar, M., and Schmidt, R., 2008. "Effect of Rack Modeling Detail on the Numerical Results of a Data Center Test Cell". *Proceeding of the 11th IEEE ITherm Conference*, Orlando, FL, USA.

## Hamza Salih Erden

211 Lafayette Rd. Apt. 300, Syracuse, NY 13205, (315)-395-7457 salisherden@gmail.com

**Education:** Ph.D., Mechanical & Aerospace Engineering, Syracuse University, August 2013

**Dissertation:** “Experimental and Analytical Investigation of the Transient Thermal Response of Air Cooled Data Centers”

**Advisor:** Dr. H. Ezzat Khalifa

M.Sc., Mechanical and Aerospace Engineering, Syracuse University, May 2009

**Capstone:** “Energy Analysis of Dedicated Outdoor Air Systems Based on Distributed Environmental Control in Multi-zone Buildings”

**Advisor:** Dr. H. Ezzat Khalifa

B.Sc., Mechanical Engineering, Istanbul Technical University, June 2007

**Capstone:** “Design of Air Conditioning System Using Chilled Beams”

**Advisor:** Dr. F. Taner Ozkaynak

**Experience:** Syracuse University, Teaching Assistant, January 2008 – Spring 2013

*Conducted recitations, held lectures in the absence of the faculty, prepared quizzes and graded homeworks for undergraduate courses.*

MAE 355: Heat and Mass Transfer, Spring 2008-09 / 2010-13

MAE 341: Fluid Mechanics, Fall 2008-09/2012

ECS 222: Dynamics, Spring 2008

Syracuse University, Research Assistant, Fall 2010-11, Spring 2011-12, Summer 2008-13

*Conducted research on Experimental Investigation and Transient Modeling of Thermal Environment in Air Cooled Data Centers; Thermodynamic Modeling, Energy and Economic Assessment of Data Centers and Cogeneration Systems; Dedicated Outdoor Air Systems based on Distributed Environmental Control in Multi-zone Buildings.*

**Journals:** Erden, H.S. and Khalifa, H.E. (2012). "Energy and environmental assessment of on-site power and cooling for data centers," HVAC&R Research, Vol. 18(1-2), pp. 51-66.

**Conferences:** Erden, H. S., Khalifa, H.E. and Schmidt, R., (2013). “Transient Thermal Response of Servers Through Air Temperature Measurements”, Proceedings of the ASME InterPACK, Burlingame, CA, July 16-18, 2013.

Erden, H. S., Khalifa, H.E. and Schmidt, R., (2013). “Room-Level Transient CFD Modeling of Rack Shutdown”, Proceedings of the ASME InterPACK, Burlingame, CA, July 16-18, 2013.

Ringham, D.C., Rice, D.J., Granetz, B.S., Erden, H. S., Khalifa, H.E. and Schmidt, R., (2013). “Assessment of the Energy Performance of Cogeneration Systems for Powering and

Cooling Data Centers”, Proceedings of the ASME InterPACK, Burlingame, CA, July 16-18, 2013.

Smith, J.F., Abdelmaksoud, W.A., Erden, H.S., Dannenhoffer, J.F., Dang, Q.T., Khalifa, H.E., Schmidt, R.R., Iyengar, M. Design of Simulated Server Racks for Data Center Research, InterPACK 2011, July 6-8th, 2011

Erden, H. S. and H. E. Khalifa, On-Site Power Generation for Data Centers, Proceedings of IAQVEC 2010, September 16th, 2010

Erden, H. S. and H. E. Khalifa, Energy Analysis of Dedicated Outdoor Air Systems Based on Distributed Environmental Control in Multi-zone Buildings, Proceedings of Healthy Buildings 2009, September 15th, 2009

**Presentations:** Granetz, B.S., Erden, H. S., D. C. Ringham, D.J. Rice and H. E. Khalifa, Seasonal Energy Assessment of the Syracuse/IBM Cogeneration Green Data Center, poster in 12th Annual Symposium on Environmental and Energy Systems, presented by the Syracuse Center of Excellence, October 11th, 2012

Erden, H. S. and H. E. Khalifa, Assessment of Cogeneration for Data Centers, Thousand Islands Energy Research Forum, November 11-13th, 2011

Erden, H. S., D. C. Ringham, L. M. Graham, B. S. Granetz and H. E. Khalifa, Energy, Environmental and Economic Analysis of On-Site Power Generation for Data Centers, poster in 11th Annual Symposium on Environmental and Energy Systems, presented by the Syracuse Center of Excellence, September 22th, 2011

Erden, H. S. and H. E. Khalifa, Annual Energy Consumption Analysis of Dedicated Outdoor Air Systems, poster in 8th Annual Syracuse Symposium on Environmental and Energy Systems, presented by the Syracuse Center of Excellence, September 29th, 2008

**Skills:** Programming: Matlab, Fortran, EES

CFD: Ansys Fluent

Thermodynamic Modeling: TRNSYS

Experiment: Thermocouples, Hot wire anemometry

Languages English: Fluent / German: Intermediate / Turkish: Native

**Awards:** Ph.D. Poster Award, Syracuse CoE Annual Symposium, Oct 2012

Graduate Student Grant, Syracuse University, Fall 2007

High Honor List, Istanbul Technical University, June 2007

**Affiliations:** Student Member, ASHRAE, 2008-present

Student Member, ASME, 2008-present

President, Turkish Student Association, Syracuse University, 2011-2013